ABSTRACT

THE ELECTRON CAPTURE DECAY SCHEMES OF Bi^{203} AND Bi^{204}

By

James Burke Cross

The electron capture decay schemes of Bi^{203} and Bi^{204} have been investigated by high-resolution γ-ray spectroscopy in an effort to acquire information about their nuclear structure and properties.

Such γ-ray spectroscopic techniques as Ge(Li) singles, Ge(Li)-NaI(Tl) coincidence, and Ge(Li)-Ge(Li) multiparameter, 2-dimensional coincidence techniques have been utilized to identify the many new γ rays in $Bi^{203,204}$ and to determine the coincidence (cascade) relationships of these γ rays. Several computer programs which are useful in handling data from complex decay schemes are presented.

Two hundred and ten (210) γ rays have been assigned to the electron capture decay of 11.2-hour Bi^{204}. Sixty (60) γ rays (accounting for >90% of the total γ-ray intensity) have been incorporated in a decay scheme having 31 levels with energies of 0, 899.2, 1273.9, 1562.8, 1817.3, 2065.1, 2185.4, 2257.9, 2385.8, 2434.0, 2480.0, 2506.8, 2919.5, 2928.5, 3029.0, 3092.0, 3104.9, 3170.0, 3215.0, 3232.0, 3637.8, 3768.4, 3782.0, 3814.4, 3826.2, 3842.2, 3875.7, 3996.1, 4080.5, 4165.5, and 4249.6 keV. A secondary decay scheme was proposed; γ-ray transitions in this decay scheme are placed solely on the basis of precise energy sums and weak coincidence data. One hundred and forty-

seven (147) γ rays have been associated with the electron capture decay of 11.7-hour Bi^{203}. Twenty-six (26) levels accommodating 51 γ rays (accounting for >80% of the total γ-ray intensity) have been placed at 0, 126.4, 186.4, 820.2, 825.2, 866.5, 896.9, 1033.6, 1160.8, 1547.6, 1641.6, 1802.4, 2033.8, 2184.0, 2387.8, 2568.9, 2620.5, 2667.8, 2713.4, 2748.7, 2753.4, 2793.7, 2821.1, 2964.4, 3016.9, and 3045.2 keV. A secondary decay scheme with transitions placed solely on the basis of energy sums and weak coincidence data was also proposed.

Limits on the spin and parity assignments of the nuclear states investigated are made on the basis of log ft values, relative γ intensities to states of known spin and parity, and transition multipolarities (for those transitions where internal conversion-electron intensities were available).

A brief survey of and comparison with previously reported scattering reaction data is presented for Pb^{203} and Pb^{204}. Nuclear shell-model level spacings in the vicinity of Z=82 and N=121 are discussed. Possible shell-model transitions associated with the electron capture decay of $Bi^{203,204}$ are suggested. Probable dominant configurations of 8 low-lying levels in Pb^{203} are offered in simple shell- and collective-model terminology. Finally, a summary of the previous theoretical calculations on Pb^{204} is made along with suggestions for a theoretical re-evaluation of these lead isotopes.

THE ELECTRON CAPTURE DECAY SCHEMES OF Bi^{203} AND Bi^{204}

By

James Burke Cross

A THESIS

Submitted to
Michigan State University
in partial fulfillment of the requirements
for the degree of

DOCTOR OF PHILOSPHY

Department of Chemistry

1970

ACKNOWLEDGEMENTS

I earnestly wish to thank Dr. Wm. C. McHarris for proposing this area of study. In addition, his expert guidance, encouragement, and patience during the experimental work and in the thesis preparation are greatly appreciated. Without his constant interest and enthusiasm the sheer magnitude of the project might have become overwhelming.

Working in close cooperation with our group, Dr. W. H. Kelly, Physics Department, must receive my heartfelt thanks. His invaluable help on several computer programs relieved me of a great deal of drudgery connected with relatively routine calculations.

Dr. H. G. Blosser, Mr. H. Hilbert, and Dr. W. P. Johnson assisted with the maintainance and operation of the Michigan State University Sector-Focused Cyclotron which was used to prepare the radioactive sources for this investigation.

Dr. D. B. Beery, Mr. J. Black, Mr. W. B. Chaffee, Mr. R. E. Doebler, Mr. R. E. Eppley, Mr. G. C. Geisler, Mr. R. Goles, Mr. K. Kosanke, and Mr. R. Todd have provided stimulating discussions and advice throughout the data acquisition and analysis.

Mr. and Mrs. W. Merritt, Miss T. Arnette, and the Michigan State cyclotron computer staff have also aided greatly in the data acquisition and evaluation through the use of the XDS Sigma-7 Cyclotron Computer.

I also want to thank the Department of Physics for the

outstanding cooperation they have extended to me. Without their physical and financial aid this project could never have been successful.

Our secretary Mrs. I. Samra typed portions of this thesis.

I thank the U.S. Army for allowing me to return to school to complete this degree.

I acknowledge the financial assistance of the National Science Foundation, U.S. Atomic Energy Commission, and Michigan State University.

Finally, I thank my wife Karen for her encouragement, inspiration, perspiration, and understanding during the course of this study.

TABLE OF CONTENTS

Chapter

Page

LIST OF TABLES

LIST OF FIGURES

Figure

Page

CHAPTER I

INTRODUCTION

Nuclear models, abundant as they are with empirical parameters, provide a significant measure of our understanding of nuclear structure. Since these nuclear models are at least partially based upon experimental data, any increase in the quality and/or quantity of experimental results can greatly aid in the testing of the appropriate theoretical model. Moreover, while experimental observations are a necessary test of theory, they can also function as stimuli for preparation of improved models. The investigations included in this thesis are therefore intended to extend and improve significantly the information acquired from the radioactive decay of Bi^{203} and Bi^{204} through high-resolution gamma-ray spectroscopy, thereby aiding in the task of understanding something of the inner structure of these nuclei and in the development of more sophisticated nuclear theory. For a more complete appreciation of and insight into the experimental results found in this thesis a consideration of the Pb isotope systematics in general and Pb^{203} and Pb^{204} in particular is essential.

1.1. General Survey of Pb Isotope Systematics

Unlike the transuranium isotopes which are far removed from the "magic" closed shells and hence spheroidal rather then spherical in shape, the nuclei in the vicinity of the doubly closed nuclide Pb^{208} are nearly spherical, and the nuclear shell model should work very well in predicting and describing the properties of individual levels in nearby nuclei. Since these nuclei are strongly stabilized in spherical shapes, the collective modes of excitation would be expected to appear at higher energies than for most nuclei; the lower levels then should be interpreted quite well as single-particle or few-particle states. This treatment has been done for several varied and reasonably successful calculations; these will be discussed later in this thesis when a correlation between the experimental data and the theoretical predictions is proposed.

Unlike other regions of the Chart of Nuclides, the lead-bismuth region of interest (Figure 1) indicates deceptively simple modes of decay. For example, since there is virtually a total absence of appreciable alpha decay, one is relieved of the difficulties of resolving the genetic relationships. The predominant reason for this lack of alpha decay is that the large binding energy per nucleon associated with the closed shells makes the energy available for alpha decay so small as practically to eliminate this as mode of decay. Consequently, the lead and bismuth isotopes having $N<126$ have particularly low alpha-decay energies; in fact, with the possible exception of Pb^{204} for which an alpha group of 2.6 MeV and 1.4×10^{17} year (y) half-life ($t_{\frac{1}{2}}$) [Ri58] has been reported, no alpha activity

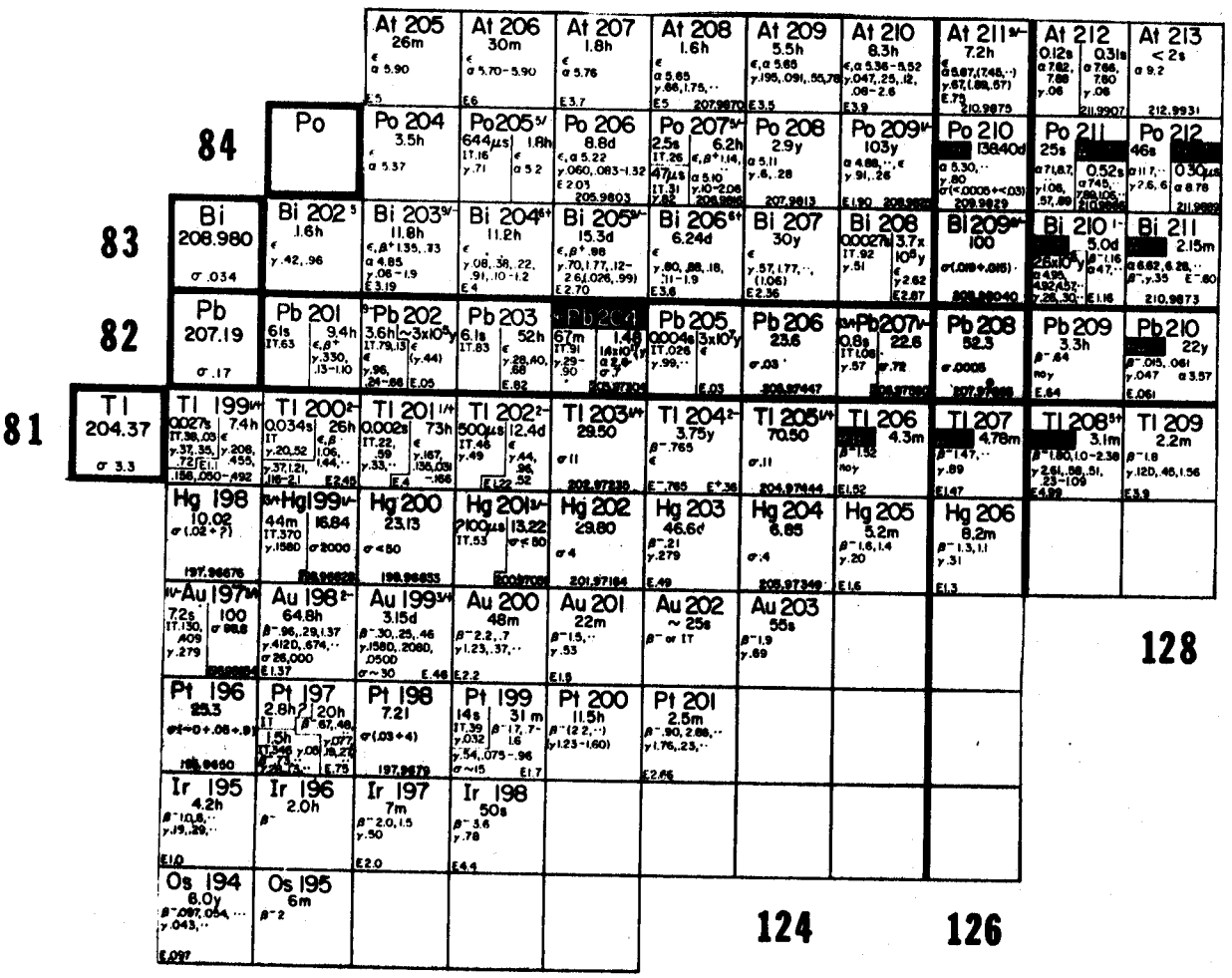

Fig. 1. Portion of the Chart of Nuclides, including the lead-bismuth region of interest in this thesis. Taken from the Chart of Nuclides compiled by the Knolls Atomic Power Laboratory, Ninth Edition.

has been detected in the low mass (A<210) Pb isotopes (until very light masses (A≈190) are reached). The light Bi isotopes having A=198-201 (and also the very low A) show a slight alpha branching, while Bi^{203} and Bi^{209} have long half-life alpha activities. In these light odd-mass bismuth isotopes Bi^{203} has a 10^{-5}%, 4.85 MeV alpha group [Du52]; Bi^{201}, a 0.003%, 5.5 MeV alpha group; and Bi^{199} has a 0.01%, 5.54 MeV group [Ne50]. None at all has been reported for the even-mass Bi^{202} and Bi^{200} isotopes.

Since the nuclei in this region are neutron deficient, the principal mode of decay is by orbital electron capture (ε). As was implied, however, the systematics and decay schemes of these nuclei are not simple at all. Table 1 shows the progress to date in deciphering the light lead isotopes from Pb^{207} to Pb^{203}, including the isomeric decays. The references included are both published literature data and unpublished results from the investigations at the Michigan State University. The reference(s) given is generally the most recent or thorough but not the sole reference from which the information was obtained. An outstanding reference for a survey background of the lead-bismuth region is the excellent review by Hyde, Perlman, and Seaborg [Hy64]; this review was used as a point of departure for a study of this region. Included in this region is the highly interesting doubly closed shell nucleus Pb^{208}. Being closed at both Z=82 and N=126 major shells, one would expect Pb^{208} to be particularly stable, and in truth such is indeed the case, even to the point of being the end product of the 4n naturally occurring radioactive decay chain. As one or more neutrons are removed to produce the lighter, neutron-deficient lead isotopes, the spectra

Table 1. Summary of the present state of knowledge of transitions and levels in some of the light lead isotopes

	Bi^{207} [A155]	Bi^{206} [Ve63]	Bi^{205} [Ko70]	Bi^{204} [Present]	Bi^{203} [Present]
$t_{\frac{1}{2}}$	27 y	6.4 d	15.3 d	12 h	12 h
Q_{EC} (MeV)	2.40 ±0.04	3.7	2.67	4.4	≈3.2
No. of known transitions	5	28+	100+	210	147
No. placed in level scheme	5	28	85	60	51
No. of known levels	5	21	34	30	25
No. of well-characterized levels	5	>14	>29	>25	>21

	Pb^{207m} [Mc53]	Pb^{206m} [A153,A154]	Pb^{205m} [St60a]	Pb^{204m} [He56]	Pb^{203m} [Do68]
$t_{\frac{1}{2}}$	0.8 s	145 μs	4.5 ms	67.5 m	6.1 s
Excited-state energy (keV)	1633.1	2200.3	1013.8	2185.7	825.2
No. of known transitions	2	8	6	6	3

Table 1. (continued)

No. placed in level scheme	2	8	6	6	3
No. of known levels	3	6	4	5	3
No. of well-characterized levels	3	6	4	5	3

become increasingly complex due to single or multiple hole-hole interactions and configuration mixing, thus providing exciting candidates for a detailed test of the theoretical interparticle force concepts of heavy spherical nuclei.

The first complication, the existence of nuclear isomerism, is found in practically all of the light lead isotopes. Recalling that the N=126 closed shell is obtained in the spherical shell model by the $i_{13/2}$ state being lowered by spin-orbit coupling to lie among the low-spin, odd-parity states from the fifth oscillator level, i.e. $p_{1/2}$, $p_{3/2}$, $f_{5/2}$, $f_{7/2}$, and $h_{9/2}$, one would expect to find near-lying levels having large spin differences, hence producing nuclear isomerism. The odd-mass lead isotopes range from the single-hole $i_{13/2}$ Pb^{207m} to much more complicated configurations, but in all cases they have even parity and one $i_{13/2}$ hole. The even-even lead isomers are unique in that no other even-even isomers are known; in these even-even lead isotopes each metastable isomer is composed of one $i_{13/2}$ hole, but here each is coupled to an odd number of odd-parity holes to produce odd-parity states. Since the other even-even lead isotope levels are even parity, this coupled with the large spin differences gives rise to the nuclear isomerism.

1.2. Lead Level Schemes

Following this general survey of the lead systematics, I now return to examine briefly the work which has been done and needs yet to be done on the other lead isotopes leading up to the complex level schemes of Pb^{204} and Pb^{203}. A truly comprehensive treatment of these nuclides is naturally beyond the scope of this thesis, but even this abbreviated discussion serves to illustrate the reasons for interest in this region of nuclides.

1.2.1. Pb^{208} Level Scheme

Pb^{208}, being closed at both the Z=82 and N=126 major shells, is stable, having no low-lying excited states. Consequently, the Pb^{208} nucleus would be expected to be very stiff towards collective vibrations [Hy64], and no states due to these vibrations are expected to fall less than several MeV. The best evidence for this unusual rigidity is seen in the energy of its first excited state. The first excited state at 2615 keV is greater than the energy of any yet reported first excited state of nuclei with mass greater than 40 atomic mass units (amu). Indeed, the first excited level is a 3- octupole oscillation state of the core [La60], not a proton excitation state as was once proposed [Tr58].

The level scheme for this isotope is also unique for an even-even nucleus in that the two lowest-lying states do not have the usual 2+ and 4+ character. The lowest levels of Pb^{208} and their spins and parities are 0 (0+), 2615 (3-), 3198 (5-), 3475 (4-), and 3700 (5-) keV [E154]. For a more impressive discussion of Pb^{208}, including the preparation and description of its levels, in terms of

complex particle-hole shell model configurations, one should turn to the excellent background reference of Hyde, Perlman, and Seaborg [Hy64].

1.2.2. Pb^{207} Level Scheme

The excited Pb^{207} levels (Figure 2), as revealed [A155] by the electron capture decay of Bi^{207}, make a classic example of a nucleus which satisfies the pure Single-Particle Model. The states in Pb^{207}, differing by only one neutron form the stable Pb^{208} core, should correspond directly to single neutron holes moving in the Pb^{208} core. From simple shell model predictions one would anticipate a $p_{1/2}$ ground state with $f_{5/2}$, $p_{3/2}$, $i_{13/2}$, $f_{7/2}$, and $h_{9/2}$ excited states; these states corresponding to the 570-, 870-, 1634-, and 2035-keV levels in Pb^{207}. Indeed, this is exactly what was found empirically, although the $h_{9/2}$ level at 3.47 MeV is not populated by the Bi^{207} decay because of the energetics of the situation. These levels behave reasonably well as single-hole states, the isomeric $M4$ (1064 keV, $i_{13/2} \rightarrow f_{5/2}$) transition rate being fairly close to that predicted by the Weisskopf estimate [We51]. The fact that the 570-keV transition to the ground state is abnormally fast for a neutron transition can be explained [Pr56] by a slight collective effect in the spherical nucleus.

1.2.3. Pb^{206} Level Scheme

In contrast to the simple Pb^{207} scheme, the Pb^{206} level scheme (Figure 3) is quite complex, since Pb^{206} is two neutrons from the doubly closed Pb^{208}. Nevertheless, there is a fundamental simplicity to the level scheme in that most of the known levels are

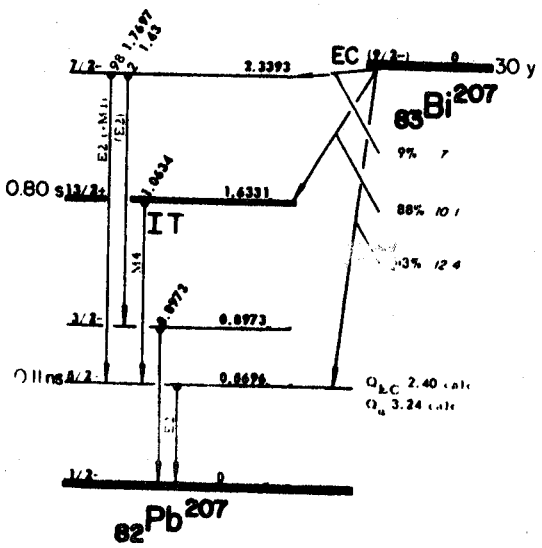

Fig. 2. Pb^{207} Level Scheme [A155]

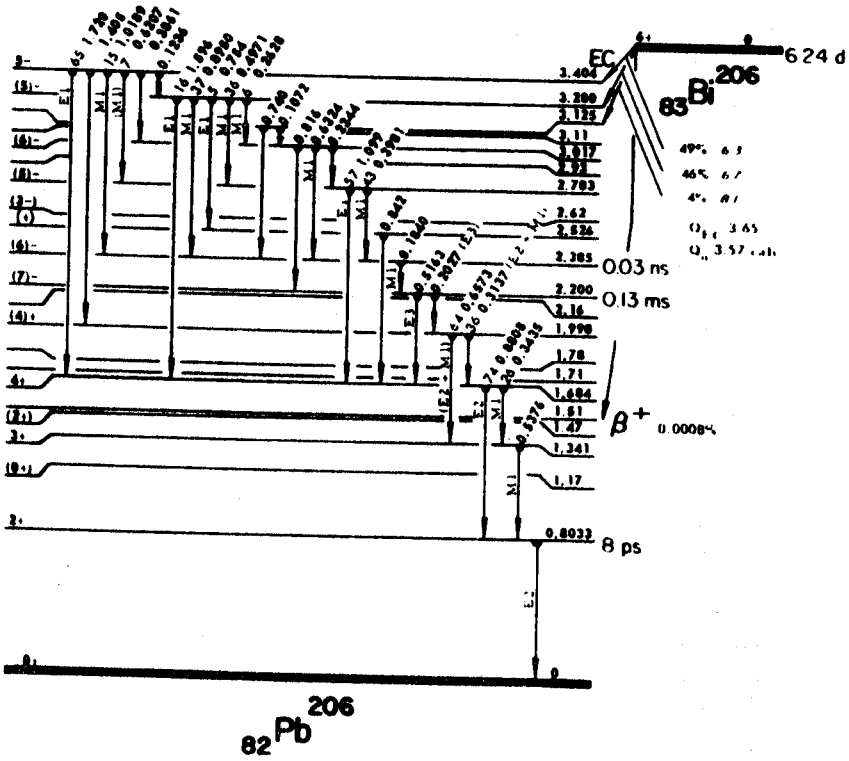

Fig. 3. Pb^{206} Level Scheme [Ve63]

derivatives of the single particle (hole) states in Pb^{207}. An odd-odd nucleus, Bi^{206} has a decay energy of 3.7 MeV and consequently populates many high-lying states of varying complexity. The most comprehensive decay scheme to date was proposed in 1954 by Alburger and Pryce [A154], who successfully placed 27 of the 28 transitions found and assigned many multipolarities from conversion coefficients, thereby well characterizing the Pb^{206} levels. Some small improvements have been made, but essentially the decay scheme must be considered complete. Using the well-placed levels in Pb^{206}, several shell model calculations have been made on this isotope [Pr52,Tr58,Ke57]. The energy of any state of Pb^{206} in these calculations is actually the result of three contributions:

1) the sum of the energies of the two corresponding single-hole states in Pb^{207},
2) the hole-hole interaction energy,

and

3) the configuration mixing between states having the same spins and parities.

These calculations vary widely in the degree of their sophistication, ranging from interactions involving complex potentials with added exchange forces to a simple delta-force interaction between the two holes. This technique, however, is useful only when collective modes of motion are small and when the energy needed for excitation of the core nucleons is so large that it does not influence the low-lying states of the isotope. The first type potential, represented by the calculations of True and Ford [Tr58], indicates excellent agreement with the expermental Pb^{206} levels, but only after assuming some collective enhancement

of a number of the gamma-ray transition probabilities, even to the extent that two levels had to be characterized as vibrational states. Other simple calculations, such as those devised by Kisslinger and Sorenson [Ki60], based upon treating the residual two-nucleon interaction as a BCS [Ba57] superconductivity pairing force plus a long range pairing force, also lead to at least qualitatively good results. The major advantage of the latter is its applicability to many of the lighter lead isotopes, whereas the True and Ford exact calculations become horrendously cumbersome. Since the Kissinger and Sorenson results are at least qualitatively correct for Pb^{206}, one would expect at least qualitative validity for their predicted levels in the lighter lead nuclei.

1.2.4. Pb^{205} Level Scheme

As one moves to Pb^{205}, three neutrons removed from the N= 126 closed shell, the situation becomes very much more complicated. Numerous elaborate investigations of Bi^{205} decay have been reported, including detailed coincidence studies [Sc61,He61] and the extensive conversion-electron spectroscopy of Vegors, Heath, and Proctor [Ve63]. The latter, by studying the half-lives of the transitions so as to distinquish between the 6.4-day (d) Bi^{206} and the 15.3-d Bi^{205} transitions, were able to find 42 new transitions, bringing the total number of observed transitions to 83. Using extensive NaI(Tl) gamma-gamma coincidence measurements, they were able to extend the number of known levels in Pb^{205} from 13 to 22. Perhaps the latest and most thorough investigation of Pb^{205} is the soon-to-be-published work of

Kosanke, McHarris, and Kelly [Ko70] at Michigan State University. Using high-resolution gamma spectroscopy and Ge(Li)-Ge(Li) coincidence experiments, they have made significant changes and improvements in the Pb^{205} decay scheme (Figure 4).

Pb^{205} is distinquished from the other lead isotopes in this region by several peculiar characteristics. Just as one would expect, there is a 13/2+ isomeric state at 1014.0 keV; however, its half-life is just 4.5 milliseconds (ms). This occurs because it is not an *M*4 isomer ($i_{13/2} \rightarrow f_{5/2}$) any longer; rather three-particle 9/2- and 7/2- states now lie between the isomer and the 5/2- ground state. Consequently, *M*2 and *M*3 transitions complete with the 1014-keV *M*4's half-life. Second, there is a low-lying first excited state at 2.3 keV. Since there are numerous high-lying levels which populate both the ground and first excited state the spectrum is abundant with doublets of peaks differing by 2.3 keV. Although seen in the conversion-electron spectra, it is hopeless to resolve them with NaI(Tl) detectors, but with the advent of high-resolution Ge(Li) detectors they can be resolved.

Similar to Pb^{206}, shell model calculations on Pb^{205} have been made by True [Tr61], Pryce [Pr56], and Kisslinger and Sorenson [Ki60]. Despite the success of predicting that the 9/2- and 7/2- levels would lie below the 13/2- state, the results of these calculations are not at all convincing. In attempting to fit the energy spacings, much less the transition probabilities, True found it necessary to modify his original calculations (which used a singlet-even potential with a Gaussian shape) into calculations using

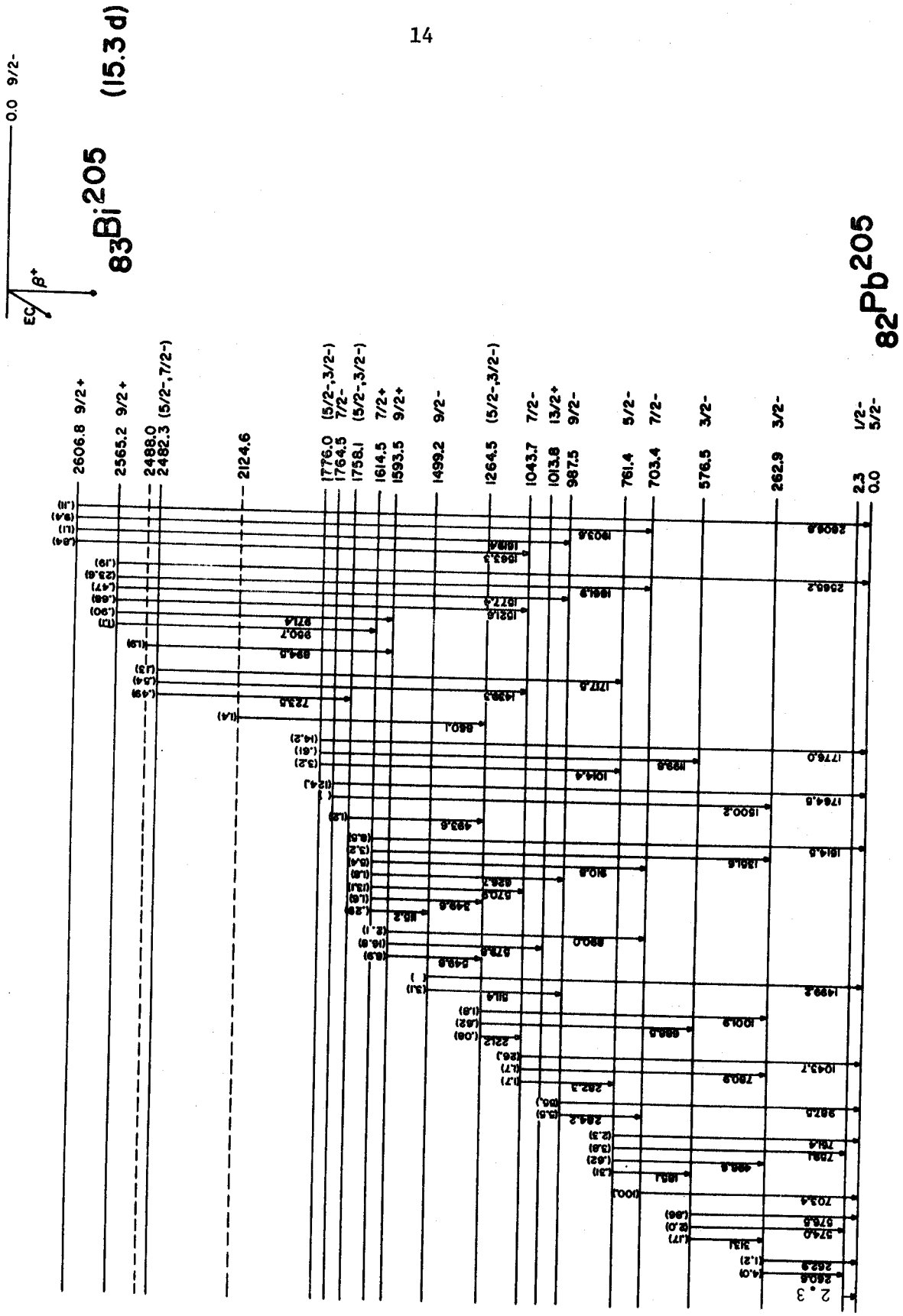

Fig. 4. Pb^{205} Level Scheme [Ko70]

a singlet-even potential of three-quarters the original value plus a weak coupling to the nuclear surface. The monumental failure of all the calculations has been in failing to predict the 1/2- state to lie so close to the ground state. Surprisingly, the semi-empirical calculations of Pryce come closer than do the more complex, sophisticated calculations.

1.2.5. Pb^{204} Level Scheme

If one were to remove four neutrons from the Pb^{208} N=126 closed shell, it would be expected that the complexity of Pb^{204} should be still greater than Pb^{205} and Pb^{206}, because the nucleon-nucleon interactions and the configuration mixing will be greatly increased. The ground state of Pb^{204} is stable, occurring in 1.48% isotopic abundance in natural lead. Since Pb^{204} is not the product of any naturally occurring radioactive decay chain, Pb^{204} content can be used as a guide for the primeval lead content in any natural lead sample. The level scheme of this nucleus is also of great interest in furthering our understanding of the shell model predictions near the Pb^{208} double closed shell.

As previously mentioned, Pb^{204} has been reported to have a measurable half-life for alpha decay. Using nuclear emulsions with enriched Pb^{204}, Riezler and Kauw [Ri58] observed an alpha group of 2.6 MeV and a half-life of 1.4×10^{17} y.

The excited states of Pb^{204} are populated, and hence revealed, by the gamma-ray cascades from the 66.9 minute (m) isomeric 2186-keV Pb^{204m} and also by the 11.5-h electron capture decay of Bi^{204}. An upper limit of 0.6% positron feeding has been reported

[Fr56], while the present data indicate a much smaller upper limit, <0.1%. The existing experimental work was incomplete and sketchy at best, and many published results are seriously questioned by the work in this thesis. The investigation of Pb^{204} has been essentially a two-step procedure, first determining the isomeric decay and second the Bi^{204} decay, but most of the past work has centered upon the Pb^{204m} isomeric decay.

1.2.5.A. Pb^{204m} Isomeric Decay

The 66.9-m Pb^{204m} isomer has been made by the following reactions:

$$Tl^{203}(d,n)Pb^{204m}$$

$$Tl^{205}(d,3n)Pb^{204m}$$

$$Pb^{204}(n,n')Pb^{204m}$$

$$Pb^{204}(d,2n)Bi^{204}\xrightarrow{\varepsilon}Pb^{204m}$$

References to this early Pb^{204m} work are given in reference [Ho53]. The early work limited the mass assignment to Pb^{204} or Pb^{205} but favored the Pb^{204}. The final mass assignment was made certain by the mass separator experiments of Thulin [Th54]. This was of extreme interest at the time because Pb^{204m} was the first even-even isotope found to have a long-lived isomeric state. Unlike the Bi^{204} decay, the Pb^{204m} isomeric decay has been well-investigated, beginning with Sunyar et al. [Su50] in 1950. The conversion-electron spectroscopy, electron-electron, and gamma-gamma [Kr54,Kr55] prompt- and delayed-coincidence data indicate the 912-, 375-, and 899-keV gammas are in cascade. Fritsch [Fr56] found the Pb^{204m} decay scheme

somewhat more complex; by separating the Pb^{204m} from Bi^{204} and examining the electron spectrum in a high-resolution permanent-magnet spectrograph, he found a 289.5-keV gamma ray and a 621.7-keV transition with the K/L and $L_1/L_2/L_3$ ratios expected of an $E5$ transition. Based upon this, he concluded that a new 4+ level was located below the 2186-keV 9- level, causing the 2186-keV level to be depopulated by a 622-keV gamma to a 1563-keV level, which in turn is depopulated by the 289-keV gamma to the well-established 1274-keV level. These same conclusions were reached and confirmed by Stockendal et al. [St58,St60]. The final Pb^{204m} decay scheme to date is seen in Figure 5.

The excellent angular correlation experiments of Krohn and Raboy [Kr55,Hu56] established the 9-4-2-0 spin sequence seen in this figure, but in doing so it was found necessary to assume multipole mixing in the gamma transitions. The 912-keV $E5$ gamma was determined to have 1% $M6$ admixture, and the 375-keV $E2$ gamma to have 1/2% admixture of $M3$. Additional work [He56] revised this figure downward but still found it necessary to assume some multipole admixtures in these transitions.

No significant change in the Pb^{204m} decay seen here has been suggested by the present work, although an interesting peculiarity with the 912-keV transition will be mentioned shortly.

1.2.5.B. Electron Capture Decay of Bi^{204}

Bi^{204}, an odd-odd nucleus, has an estimated [Fr56] decay energy of 4.4 MeV and populates states in Pb^{204} almost up to this energy. Depending on whose calculations you choose, not only are

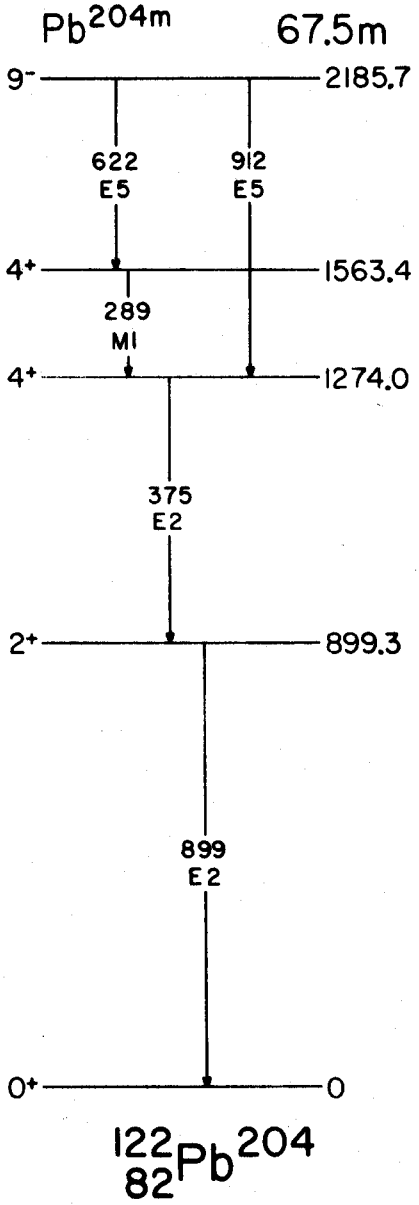

Fig. 5. Pb^{204m} Decay Scheme [Fr58]

there 70 to 80 four-particle (hole) states available for population, but collective effects and levels become more important for this nucleus than for the heavier Pb isotopes. For example, consider the Pb^{204m} levels, the only levels previously known with certainty. The 899.2-keV 2+ state cannot be reconciled with any four-particle predictions and appears to be a quadrupole vibrational state. The next two excited states, at 1274 and 1563 keV (both 4+) also present similar difficulties. Nearly all the gamma-ray cascades from the high-lying states pass through the 1274-keV state, while comparatively little goes through the 1563-keV state. This is also seen in the (p,t) experiments performed at Yale University by Holland [Ho67,Ho69]. Although both are 4+ states, their internal structure must obviously be very different.

Because the Bi^{204} decay is so complicated, clean, impurity-free sources are imperative. In past investigations the sources were prepared by cyclotron bombardments of Pb or Tl targets, enriched electromagnetically separated targets being much to ones advantage. Some of the reactions used were:

$$Pb^{204}(p,n)Bi^{204}$$

$$Pb^{204}(d,2n)Bi^{204}$$

$$Tl^{203}(\alpha,3n)Bi^{204}$$

Since the Pb^{204} and Tl^{203} isotopes are ordinarily not available in high isotopic purity, other Bi isotope impurities are necessarily prepared simultaneously. The common contaminants, in order of decreasing effective quantities, are the 6.4-d Bi^{206}, 15.3-d Bi^{205}, and 27-y Bi^{207}. Since Bi^{203} has a half-life nearly identical to

Bi^{204}, it was necessary to eliminate it entirely by using a cyclotron beam just below the threshold energy for its production.

Some of the characteristics of the Bi^{204} decay are perhaps of small but significant importance at this point. The half-life of the Bi^{204} decay has been measured to be about 11.5 hours (h), with small variations by different research groups, as seen in Table 2.

While many people have investigated the Bi^{204} decay, the two most detailed studies were independently undertaken in the 1950's by Fritsch and Hollander [Fr56,Fr58] at Berkeley and by Stockendal et al. [St58], at the Noble Institute in Stockholm. Since only very high resolution gives any degree of significant data, both groups relied entirely upon high-resolution conversion-electron spectra obtained from permanent-magnet spectrographs with energy resolutions of 0.2% (Fritsch) and 0.1% (Stockendal). In addition, both groups performed gamma-gamma coincidence experiments to a limited extent using NaI(Tl) detectors. Using these data plus scintillation gamma-ray spectra, electron-electron coincidence spectroscopy, and a numerical analysis of energy sums, Fritsch and Hollander concluded that the decay was so complex that they could not hope to construct a Pb^{204} level scheme with any degree of confidence. Consequently, they published essentially just a list of electron energies. From over 150 conversion electrons they made assignments for some 67 transitions and listed them in three confidence groups.

Stockendal et al. found many of the same transitions and did publish a very preliminary decay scheme but emphasized that only the levels populated by the Pb^{204m} decay are known with any assurance.

Table 2. Experimental half-lives for Bi^{204} decay

Principal Investigator	Bi^{204} Half-life (h)
Fritsch[a]	11.0±0.5
Perlman[b]	12±1
Wertheim[c]	11.6±0.2
Stockendal[d]	11.22±0.10

[a]Reference [Fr58]

[b]Reference [Pe47]

[c]Reference [We56]

[d]Reference [St60]

Based upon the previous Bi^{204} work, several conclusions have been reached:

1) the first and second excited states lie high and correspond to the 2+ and 4+ levels at 899.2 and 1273.9 keV, respectively,
2) all gamma cascades pass through the 899.2-keV 2+ level with little or no direct feeding to the ground state,
3) about 10% of the Bi^{204} decay proceeds through the 9- isomeric state,

and 4) a large number of populated levels lie above 2 MeV.

A preliminary re-examination [Gr66] in the MSU laboratory (indeed, the one which prompted the present investigation) using Ge(Li) detectors showed Bi^{204} to be very complex. In the present investigation, upon once again re-examining the Bi^{204} gamma-ray spectrum, using improved high-resolution Ge(Li) gamma-ray spectroscopy, it was found that the Bi^{204} decay was even more complex than previously believed. So complex, in fact, that the previous NaI(Tl) gamma-ray and Ge(Li) work (especially coincidence studies) must be considered as having relatively little worth, with exception of the known Pb^{204m} states, and that the decay scheme was debatable, if not incorrect.

While shell model calculations are to be an integral part of this thesis, the discussion of these will be deferred to a section devoted entirely to the comparison of experimental data to the Pb^{204} shell model calculations.

The present investigation involving standard high-resolution Ge(Li) spectroscopy single and coincidence experiments has been successful in placing many new levels in Pb^{204} as well as making significant changes in the previous decay scheme, and in the process in characterizing more than 200 gamma-rays. With such a wealth of transitions, one can make only limited use of energy sums and differences because of the high probability of accidental agreements. Also NaI(Tl) vs. Ge(Li) gamma-gamma coincidence experiments are of little use because of the complex Compton backgrounds and gating difficulties in such a complex spectrum. This leaves Ge(Li) vs. Ge(Li) gamma-gamma coincidence and double escape spectrometers as the necessary tools.

Even upon the completion of these high-powered spectroscopic techniques it was concluded that it may not be sufficient to establish a completely unambiguous level scheme for Pb^{204}. A great need for preliminary scattering data was seen; this was provided by a study of the $Pb^{206}(p,t)Pb^{204}$ reaction which, having a tendency to pluck out coupled-neutron states, appears to yield a basic framework of levels in Pb^{204} [Ho69].

1.2.6. Pb^{203} Level Scheme

Removing yet one more neutron from Pb^{204} (i.e. five neutrons removed from the N=126 closed shell), one finally reaches the last isotope of interest in this thesis, Pb^{203}. The Pb^{203} isotope

exists in two isomeric forms; the ground state, which decays by ε to the excited states of Tl^{203} with a half-life of 52 h, and a 6.1-second isomeric state (Pb^{203m}) at 825.1 keV. The study of Bi^{203} thus becomes essentially a three-step process, the determination of the decay of Pb^{203}, then Pb^{203m}, and finally the Bi^{203} decay.

1.2.6.A. Pb^{203} Decay Scheme

Indeed, one would not be absolutely forced to study the Pb^{203} decay scheme before studying the others, as the half-life is long enough to allow separation of its peaks from theirs on this basis alone. This, coupled with the realization that the decay scheme is fantastically simple (Figure 6) compared to the $Bi^{204,205,206}$ schemes, led me to make no attempt to improve upon any previously reported data.

The Pb^{203} isotope has been produced by a number of different reactions on Tl^{203} and Pb^{204} using protons, deuterons, and neutrons [Pb53], or as a long-lived product of Pb^{203m} and Bi^{203} which can be prepared by yet other reactions. The experimental and theoretical characteristics of the decay have been well-established by a horde of investigations [St60,Pb53,Wa54,Wa58,Su61,Pr54,Va54,Pe60] utilizing a variety of experimental techniques.

1.2.6.B. Pb^{203m} Decay

The 6.1-s [As57] isomeric state at 825.1 keV was first discovered by Hopkins [Ho52], who mistakenly assigned it to Pb^{202}; in 1955, Fischer [Fi55] correctly reassigned it to Pb^{203} on the basis of excitation function studies. The next decade saw numerous investigations [St60,Fr56,St56,Pe61] on the Pb^{203m} decay using primarily conversion-electron and NaI(Tl) spectrometers. These studies report

a single transition of 825 keV from a 13/2+ state to the 5/2- Pb^{203} ground state, similar to other odd-mass Pb isomers. As the *M*4 reduced transition probability was abnormally large, Stockendal suggested [St60] that there is a likely possibility that the 13/2+ state is partially de-excited by an unobserved 5-keV *M*2 to a 9/2- level at 820.1 keV (which is also populated in the ε decay of Bi^{203}). This possibility was confirmed by the work of R. Doebler et al. [Do68], who showed that the 820.1-keV transition is definitely present in the Pb^{203m} decay, thus implying the presence of the 5-keV transition. At the same time their work solved the difficulty of the abnormally large *M*4 reduced matrix element. The present decay scheme for Pb^{203m} is shown in Figure 6, along with the Pb^{203} decay scheme.

1.2.6.C. Bi^{203} Decay Scheme

Any comprehensive study of Bi^{203} is necessarily complicated by the fact that Bi^{203} and Bi^{204} have nearly identical half-lives (≈12 h). A simple method to prepare clean Bi^{204}sources (to be described later in section 2.1.) involves a $(p,3n)$ reaction on nearly pure Pb^{206} by keeping the beam energy just below the threshold for the $(p,4n)$ reaction (which produces the Bi^{203}); but Bi^{203} sources prepared at the required energies invariably contain considerable amounts of other Bi isotopes, most tragically, Bi^{204}. Because there are so many gamma rays of both Bi^{203} and Bi^{204}, the Bi^{203} can be studied only after a thorough investigation of Bi^{204} has been completed.

Several unrelated characteristics of the Bi^{203} decay should be mentioned at this point. The half-life of Bi^{203}, unlike the decay

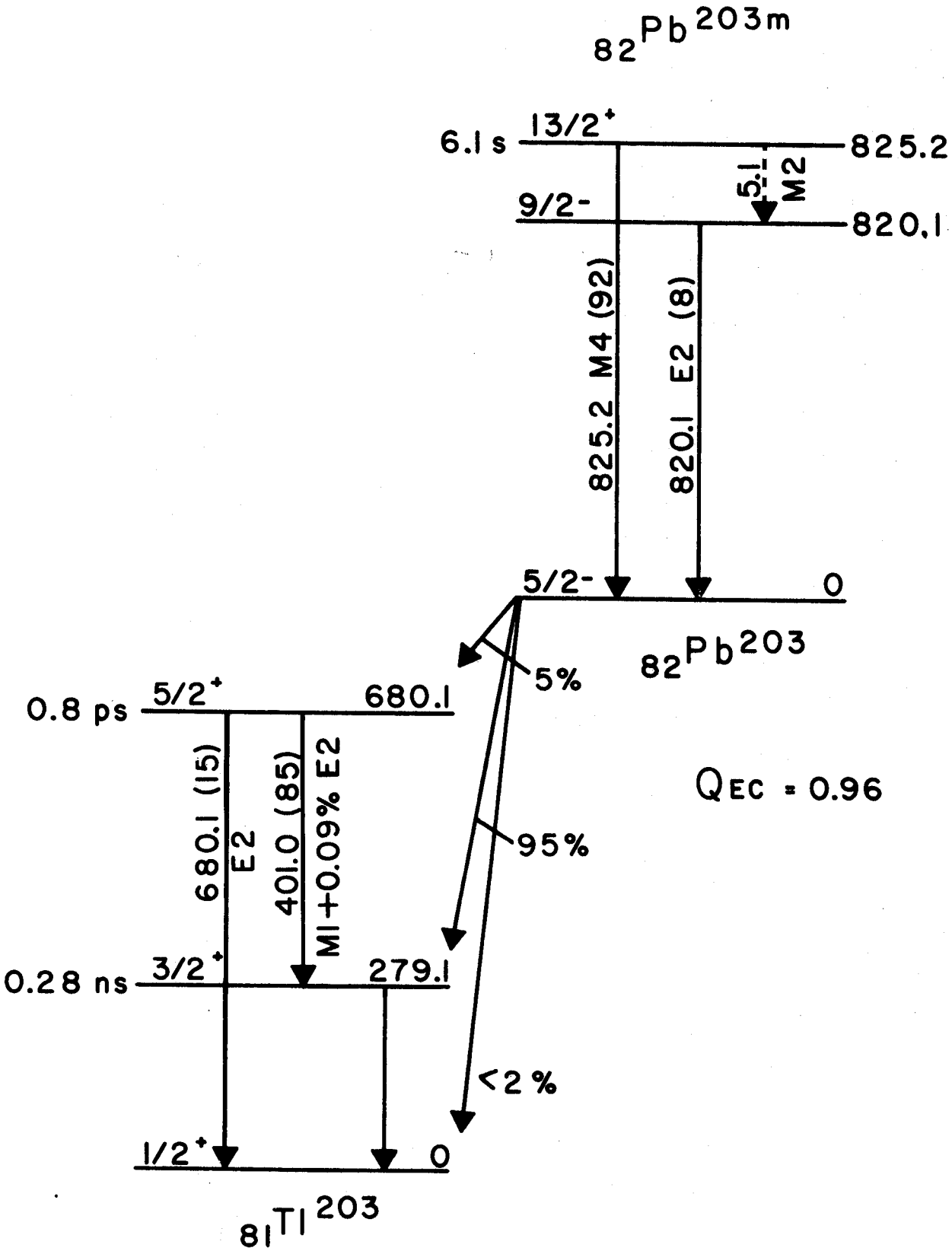

Fig. 6. Pb^{203m} [Do68] and Pb^{203} [Pe60] Decay Schemes

itself, has been well investigated. Table 3 shows the half-life values listed in the literature to date. In addition to the half-life for Bi^{203}, Bergström et al. [Be61] have reported a half-life of 75±3 ns for the 126.4-keV state. The isotope has a small (1 part in 10^7) but measurable alpha branching, as was mentioned in section 1.1. Finally, atomic beam resonance has shown [Li59] that the ground state spin of Bi^{203} is 9/2, which agrees with the 9/2 spin found in Bi^{205} and Bi^{207}, where the 83rd proton is in the $h_{9/2}$ shell model orbital and the neutrons are paired to zero.

With approximately [Vi66] 3.2 MeV of decay energy and the additional levels and collective behavior introduced because Pb^{203} is five neutron holes away from the doubly closed shells of Pb^{208}, one would expect roughly the same complexity for the Bi^{203} decay as for Bi^{204}.

Several investigators, Novakov et al. [No58], Fritsch [Fr56], and Stockendal [St60], have studied the Bi^{203} decay using conversion-electron and scintillation spectrometers and by gamma-gamma and electron-gamma coincidence experiments. The results of these experiments are discussed in Chapter III where the data from these experiments and the present work are compared. As if the decay were not complicated enough already, Bi^{203} also decays partially by positron emission, two β^+ groups with end-point energies of 1.34 and 0.74 MeV having been reported [Kr54]. Fortunately, the positron intensity is low, only about 0.014 positions found for every 825.1-keV gamma.

What was presented about the calculations for Pb^{204} might

Table 3. Experimental half-lives for Bi^{203} decay

Principal Investigator	Bi^{203} Half-life (h)
Fritsch[a]	11.5±1.0
Neumann[b]	12.0±1.0
Stockendal[c]	12.3±0.7
Stockendal[d]	11.76±0.05

[a]Reference [Fr58]

[b]Reference [Ne50]

[c]Reference [St56]

[d]Reference [St60]

be repeated with added emphasis for Pb^{203}. However, more exact calculations are not likely to be forthcoming until a better decay scheme and other experimental data are available. Perhaps the results of this thesis will prompt new, more detailed and comprehensive calculations on this isotope.

Once again this investigation involved the use of high-resolution Ge(Li) spectroscopy singles and coincidence experiments, and the Bi^{203} decay was found to be complex. With these techniques, many new levels and characteristics of Bi^{203} have been uncovered. The comments made in the section on Bi^{204} decay concerning the validity of certain coincidence experiments and the use of energy sums hold equally true for the Bi^{203} decay as well and therefore will not be regurgitated here.

The decay schemes proposed in this thesis, Figures 22 and 31, indicate monumental changes from previously reported decay schemes. As good as they are, they have pressed the "state of the art" to its practical limit. The primary weakness lies in the coincidence data for the very weak and/or high energy transitions. Just as this work has greatly improved upon previous investigations, some day new advances in detector systems, electronics, and computer analysis techniques may show that even this decay scheme has major inconsistencies and anomalies. In lieu of that day, the decay schemes produced by this investigation represent the ultimate in present day gamma-ray spectroscopy.

In addition to the references cited in the review above, several excellent reviews of the lead-bismuth region should be noted

here. Bergström and Andersson [Be61] have published a very comprehensive review article on "Nuclear Energy Levels and Multipole Transitions in the Lead Region" which covers in more detail information on the lead isotopes. Kinsey [Kn57], in "Nuclear Reactions, Levels, and Spectra of Heavy Nuclei", has discussed energy levels in the nuclei of lead and bismuth. Finally, Elliott and Lane [El57] have discussed the shell model interpretations of the level systems of these nuclei in their "The Nuclear Shell Model".

CHAPTER II

EXPERIMENTAL APPARATUS AND TECHNIQUES

During the construction of the electron capture (ε) decay schemes of Bi^{204} and Bi^{203} and throughout this investigation I have utilized both standard and new techniques of gamma-ray spectroscopy. This chapter describes briefly, though thoroughly, the general techniques and apparatus used in the data acquisition and analysis. Section 2.1. deals with the specifics of the radioactive isotope production for Bi^{204} and Bi^{203}. Section 2.2. describes the nuclear spectroscopy apparatus in current use at Michigan State University. Section 2.3. surveys the methods of data analysis used during this investigation. Section 2.4. describes two valuable FORTRAN computer programs useful in the construction of complex decay schemes. Section 2.5. completes the chapter by outlining two spectrum plotting routines which were written to reduce drastically the time involved in preparing spectra for theses and publications.

2.1. Source Preparation

The radioactive Bi^{204} and Bi^{203} sources used in previous studies of these nuclides were prepared by bombarding Pb^{206} and natural Tl by protons and He^3, respectively, at a variety of energies. These sources, however, were highly contaminated with $Bi^{205,206,207}$ activities, making accurate energy and intensity calculations of the complex Bi^{204} spectra nearly impossible. Using the Michigan State University sector-focused cyclotron [B161], a number of reactions were investigated to determine the optimum target isotope, beam particle, and beam energy which would give the cleanest, most contaminant free Bi^{204} source. The one contaminant which must absolutely be avoided is Bi^{203}, since its half-life is nearly identical to that of Bi^{204}, thus making it inseparable solely on the basis of half-life differences. Consequently, any study of Bi^{204} requires that Bi^{203} be either well-known in advance or that it not be present at all in the Bi^{204} source.

The reactions which were tested are listed and discussed below. Although the Tl attempts were nearly abortive, they are included here for descriptive completeness.

2.1.1. Tl Targets

Several sources were prepared using both natural Tl (70.5% Tl^{205}, 29.5% Tl^{203}) and 99.9% Tl^{203} separated isotope as the target and He^3 as the projectile. Table 4 shows the Q values for preparing Bi^{203} and Bi^{204} from the different reactions of He^3 on Tl. Choosing a He^3 energy of 27-28 MeV, one would expect to produce Bi^{204} with

Table 4. Q values for $Tl^{203,205}(He^3,xn)$ reactions

Reaction	Q values (MeV)[†]
$Tl^{203}(He^3,2n)Bi^{204}$	- 6.3
$Tl^{203}(He^3,3n)Bi^{203}$	-13.3
$Tl^{205}(He^3,4n)Bi^{204}$	-20.5
$Tl^{205}(He^3,5n)Bi^{203}$	-27.5

[†]Calculated from experimental masses listed in reference [My65].

a minimum of Bi^{203} from the first reaction. It was hoped that this energy would be high enough to make the $Tl^{203}(He^3,3n)$ cross section quite small and thus produce little, if any, Bi^{203}. Such was apparently not the case, since the samples contained, in addition to Bi^{204}, relatively large activities of Bi^{203}, Bi^{205}, and Bi^{206}. Other work in the MSU laboratory has also indicated that the He^3-induced reactions may not be as clean as the proton-induced ones. Based upon this, plus the present attempts, the Tl was discarded as a possible target source for Bi^{204} production.

2.1.2. Pb Targets

The useable Bi^{204} sources were prepared by bombarding 97.2% Pb^{206} separated isotope obtained from Isotopes Division, Oak Ridge National Laboratory (in the form of $Pb(NO_3)_2$) with a 27-30 MeV proton beam from the MSU cyclotron. Previous experiments at Michigan State University had chosen 27 MeV as the best proton energy based upon the Q values of the competing reactions, but I found that at 27 MeV significant amounts of Bi^{205} and Bi^{206} were also produced, thus obscuring many of the high energy peaks (>1.00 MeV). Using Figure 7, which depicts the empirical cross sections for protons on Pb^{206}, I calculate that at ≈27 MeV about 43% of the radioactive source should be Bi^{205}, but if the proton energy is raised to 30 MeV only about 26% of the source should be Bi^{205}. The large difference in half-lives between Bi^{205} and Bi^{204} make this (30 MeV protons) an excellent method to produce clean Bi^{204} sources. Consequently, most sources for this study were prepared by bombarding Pb^{206} separated isotope

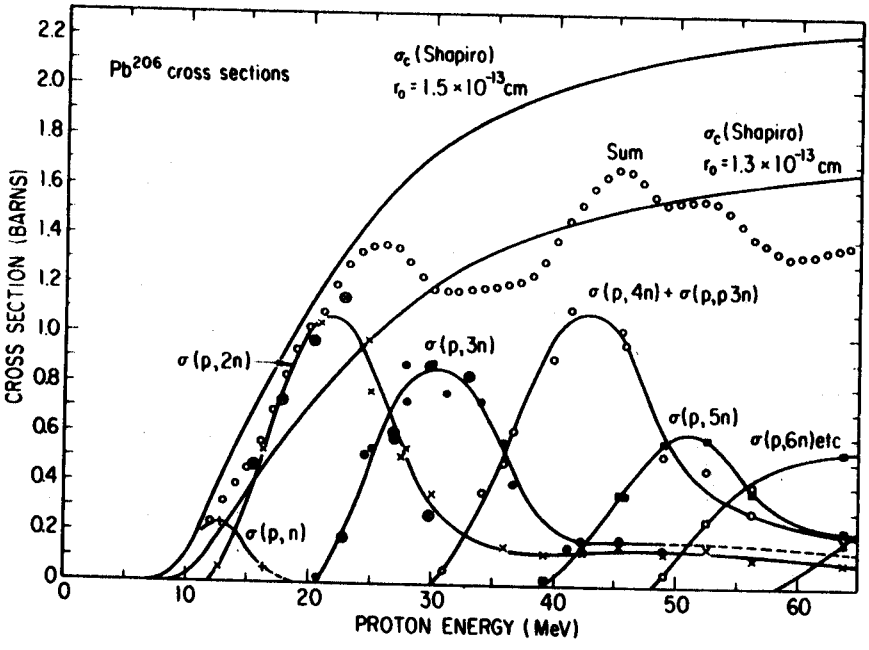

Fig. 7. Excitation curves of Bell and Skarsgard [Be56] showing the measured (p,xn) cross sections of Pb^{206} as a function of proton energy.

with 30 MeV protons.

The useable Bi^{203} sources were prepared similarly by bombarding 97.2% Pb^{206} ($Pb(NO_3)_2$) separated isotope with a 40-45 MeV proton beam from the MSU cyclotron. In determining the optimum energy for the $Pb^{206}(p,4n)$ reaction, excitation functions (comparing Bi^{203} to Bi^{204} production) were run on Pb^{206} from 30-40 MeV. This is shown in Figure 8 along with the equivalent excitation function from work published by Bell and Skarsgard [Be56]. The two are quite comparable, and on the basis of this a proton energy of ≃40 MeV was chosen. At this energy, while the $Bi^{205,206}$ impurities are seen, they are not significant. The unavoidable major impurity was Bi^{204}, but since the photon energies and intensities for Bi^{204} were well-known fron the first portion of this study, it was easy to eliminate these peaks from consideration. In one run with 45 MeV protons some Bi^{202} (hence Pb^{202m}) was produced by the $(p,5n)$ reaction, but this was not troublesome as most runs were performed with 40 MeV p.

Typically several small crystals were crushed, bombarded with the 30-45 MeV protons at ≃1 μA for ≃1 1/2-2 hrs (often behind several mils of aluminum absorber), allowed to decay for 8-12 hours to let any short-lived contaminants decay away, and then counted for 3-5 half-lives, additional quantities of source being added with passing time so as to keep a relatively constant counting rate. It was found that samples prepared and counted in this manner were relatively clean with small amounts of Bi^{205} ($t_{\frac{1}{2}}$=15.3 d) and Bi^{206} ($t_{\frac{1}{2}}$=6.4 d) impurities. The Bi^{206} impurities are seen weakly in the low energy

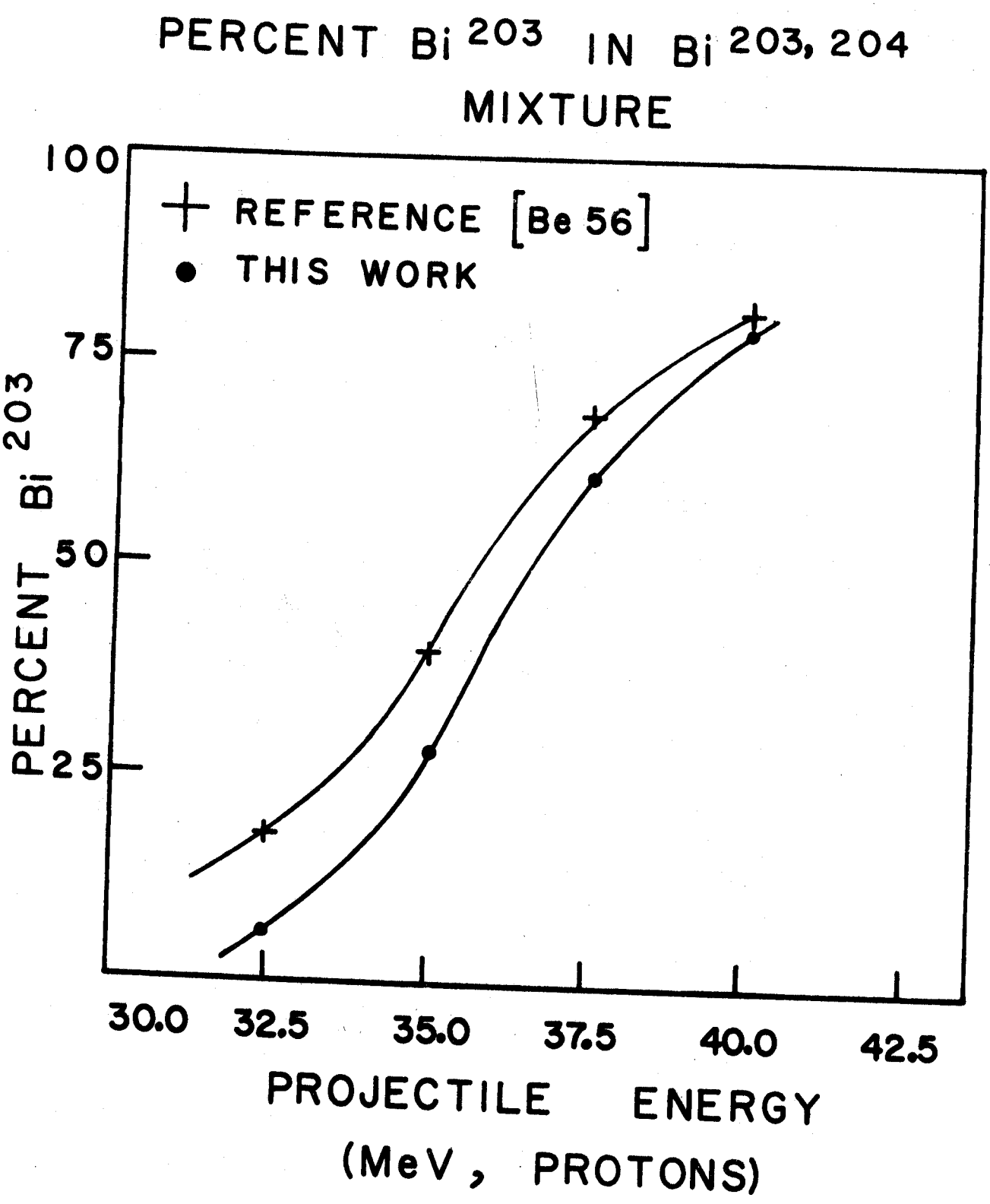

Fig. 8. Curves showing percent Bi^{203} in a $Bi^{203,204}$ mixture as a function of the projectile (proton) energy on a Pb^{206} target.

region (<1 MeV), while the Bi^{205} is seen weakly in the high energy region (>1 MeV). In neither region was the impurity large enough to cause any undue problems in determining the Bi^{204} or Bi^{203} full energy peaks. A chemical separation was found to be unnecessary, thereby making the preparation of the Bi^{204} and Bi^{203} radioactive sources a simple, easily handled process.

2.2. The Gamma-Ray Spectrometer

Recent progress in gamma-ray detector technology, resulting in greatly improved Ge(Li) detectors (both in efficiency and resolution), impressive performances in amplifier-preamplifier systems, faster and more stable analog-to-digital converters (ADC's), and larger memory analyzers has increased data accumulation of gamma-ray spectra, and more importantly, the quality of these data is improving. At this time the laboratory at MSU is impressively equipped with a large complement of Ge(Li) and Si(Li) detectors, culminating in a 3.6%, 1.9-keV (FWHM at 1.33 MeV) Ge(Li) detector, practically the ultimate in Ge(Li) detector technology.

2.2.1. Singles Experiments

The basic components of the gamma-ray singles spectrometer used in this study were:

a) two Ge(Li) detectors, cooled to liquid nitrogen temperature (77° K), possessing resolutions of 2.4 keV and 1.9 keV (FWHM at 1.33 MeV) and efficiencies of 2.5% and 3.6%, respectively,

b) a room temperature FET preamplifier and high voltage supply,

c) a pulse shaping amplifier with DC offset and pole zero compensation,

and d) a data read out system.

No single component can be classified as the weakest link, but when gamma ray energies >2 MeV were measured, the number of

channels in the MCA was often the weakest link. On the other hand, low detector efficiency could often fail to reveal full energy peaks of low intensity gamma rays. In addition, detector resolution may have obscured small peaks within ±0.5 keV of larger peaks. A careful balance of counting rate was important since low counting rate can produce broadened peaks due to long term instability of the electronics, yet high counting rates can cause pulse pileup, which also broadens the peak. Throughout the present study these Ge(Li) detectors were used for all singles gamma-ray energy and intensity measurements.

2.2.2. Coincidence Experiments

Singles experiments are useful in determining the energies and intensities of the gamma-ray transitions of the radioactive nuclides observed but tell one nothing about the structure and composition of the nuclei involved. This information is generally revealed in gamma-ray spectroscopy by a variety of coincidence experiments. These include anti- (revealing direct, ground-state transitions), prompt- (revealing cascade transitions), delayed- (revealing transitions in cascade with states having a measurable lifetime), and 511-511-gamma- (revealing double escape peaks and β^+ fed peaks) coincidence experiments. These coincidence techniques and their usefulness to the present study are described in the following sections.

2.2.2.A. NaI(Tl) Split Annulus-Ge(Li) Spectrometer

One of the most useful pieces of apparatus in the MSU nuclear spectroscopy laboratory has been the 8"×8" NaI(Tl) split-annulus. Reference [Au67] suggests several useful applications of the annulus vs. Ge(Li) gamma-ray spectrometers. In the present

study the 511-511-gamma triple coincidence configuration was found to be extremely useful in determining double escape peaks. The Ge(Li) gamma-ray detector and the radioactive sources were placed inside the annulus. If, when a primary photon interacts with the Ge(Li) detector, two 511-keV anniliation photons are able to escape collection, then each 511-keV photon has a high probability of being collected by either side of the NaI(Tl) annulus surrounding the detector. Requiring a 511-511-gamma coincidence between the halves of the annulus and the Ge(Li) detector, the relative intensity of the weak (E_γ-1022.0)-keV photon (double escape peak) in the spectra is increased. In this configuration it is possible to obtain significant increases in the intensity of the double escape peaks, thus allowing easy identification of these peaks and their subsequent removal from consideration in the singles spectra. More will be said of this technique in Chapter III.

2.2.2.B. Multiparameter Ge(Li)-Ge(Li) Spectrometer

One of the more useful techniques implemented at the MSU laboratory, under the code names EVENT and EVENT RECOVERY [Mi68], is a computerized multiparameter coincidence system. In the past, conventional coincidence experiments were performed by recording signals from one of the Ge(Li) detectors only if certain coincidence requirements are satisfied. Separate coincidence experiments were required for each individual peak or gate set on the pulse height analyzers. The conventional coincidence set-up required two NaI(Tl) or Ge(Li) detectors, a collection of associated electronics, and considerable time to assemble the apparatus. The only change necessary from one run to the next was changing the peak selected by the single channel

pulse height analyzer. For the decay of Bi^{204}, for example, having >200 gamma rays, this would involve years of labor, computer, and cyclotron beam time (to prepare the many required Bi^{204} sources).

One method to prevent such massive duplication and repetition of efforts is to record the signals from both detectors following each and every fast coincidence event. Reference to the Annual Report (1969) of the Nuclear Chemistry group gives a more detailed account of such a system [Mc69]. Figure 9 shows a block diagram of the electronics and computer interfacing. Typically, 20 coincidence events per second are recorded on as many 2400-foot, 9-track magnetic tapes as necessary until each tape is filled with about two million events. Data taking in this manner is controlled via teletype under the program EVENT. A computer program, EVENT RECOVERY, was written in order to extract the coincidence spectra from the tapes, the sequence of operations for the recovery of this coincidence data typically being:

1) scan the tape for the integral coincidence spectrum from each detector, labeled *X* and *Y* respectively,
2) choose peak gates from one side, say *X* detector,

and

3) analyze the resulting coincidence spectra (noting that each of these spectra has the same gain).

Applications of this multiparameter coincidence spectrometer have greatly increased the efficiency of decay scheme studies at Michigan State. In addition to the Ge(Li) multiparameter spectrometer used in this investigation, future developments of this

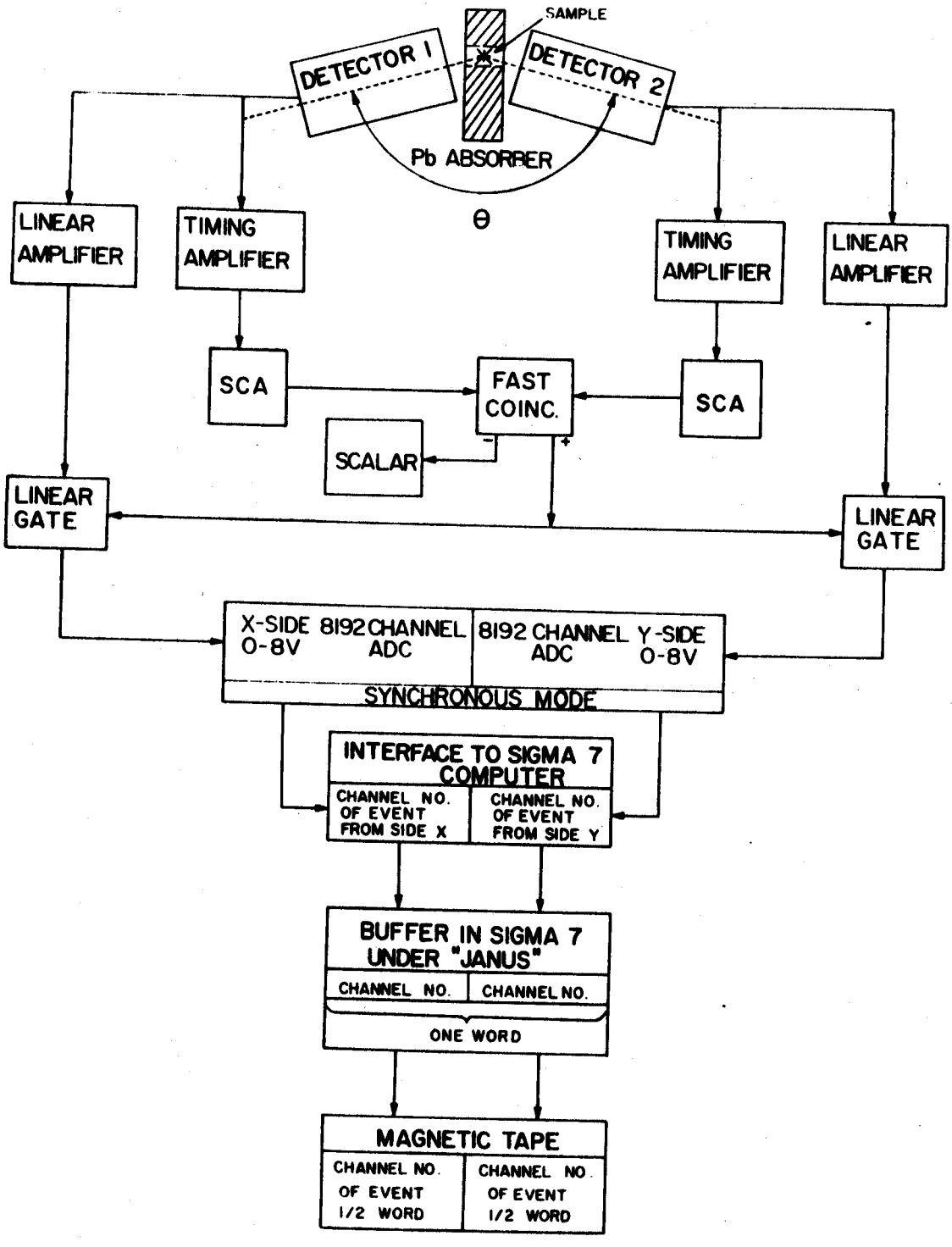

Fig. 9. Block diagram of the electronics used for collecting multiparameter γ-ray spectra with the Sigma-7 computer.

system may include triple-, anti-, and delayed-coincidence experiments. A possibility not previously proposed is to use this multiparameter system to study widely different half-lives of many different radioactive species occurring in the same sample. By recording time on one side and the events from a single Ge(Li) detector on the other, one could obtain accurate half-life measurements for short-lived to moderate-lived components by gating on any time interval desired. A previous weakness of the system, difficult on-line monitoring of total coincidence events, has recently been corrected by allowing EVENT to run under TOOTSIE [Ba67], a two-dimensional machine language program used primarily for recording data from scattering experiments. Without this extremely powerful tool the present study would have obviously been impossible.

2.3. Data Analysis

The rapid advances in experimental nuclear spectroscopy such as precise, high energy cyclotrons for source production, better resolution in Ge(Li) detectors, and large multichannel analyzers, have resulted in a vast increase in the rate of data acquisition. With this rapid increase in data accumulation, the task of data analysis has been monumental. Most of the data analysis in this investigation was performed on the MSU cyclotron laboratory XDS Sigma-7 computer utilizing FORTRAN programs written or adapted for it [Mc70]. Following is a brief but thorough discussion of the gamma-ray energy and intensity measurements, and the analysis of the gamma-gamma coincidence spectra.

2.3.1. Gamma Energy and Intensity Measurements

The centroids and areas of the photon peaks in a spectrum were found following the subtraction of various order interpolated backgrounds. The computations were performed with the aid of two of the spectrum analysis routines used in the MSU cyclotron laboratory; MOIRAE (developed by R. Au and G. Berzins at Michigan State University) and SAMPO (developed by J. Routti at University of California, Berkeley).

2.3.1.A. SAMPO Spectrum Analysis Routine

SAMPO is a computerized data analysis routine written by J. Routti and adapted to the Sigma-7 MSU cyclotron computer by T. Arnette and C. Merritt. Control may be maintained either via a scope and switches and/or FORTRAN control cards.

Some of the varied uses of SAMPO ARE:

1) to produce Calcomp or printer plots of the spectrum,

2) to calculate centroids, and consequently energies,

3) to calculate areas and relative intensities,

and 4) to calculate half-life data.

At present this routine is utilized as a separate program, that is without scope control. SAMPO's mathematical evaluation involves an initial shape parameter calibration over the region to be analyzed. Strong, well-resolved singlet peaks should be used in this calibration. The program fits a Gaussian curve to the upper portion of the peak and leading and trailing exponentials to the base of the peak. The shape parameters are stored and a linear interpolation used to get the parameters for any other peak under consideration. Once the shape parameters have been calculated for any given spectrum, they may be reread directly into the program via control cards for subsequent runs, thereby considerably shortening future calculation times. Once the shape calibration has been established, the energy calibration may be calculated. The energy values may be fit to linear or higher order polynomials at the operator's discretion. Similarly, efficiency calibrations may be made by specifying a number of well-spaced peaks and their corrected relative intensities.

The actual analysis portion of SAMPO may be performed under two basic modes:

1) automatic - in which SAMPO subroutines search out all statistically significant peaks, evaluate suitable fitting intervals, and fit the

peak using the shape, energy, and efficiency calibration data.

and 2) controlled - in which the operator directly prescribes a fitting interval, the number and location of peaks to be found in that interval, the fitting then being made under these prescribed conditions.

Figure 10 shows a sample output of a fitted quartet of peaks, with the following values being returned for each peak:

1) exact centroid (and error)
2) energy (and error)
3) area-counts (and error in percent)

and 4) intensity-counts (and error in percent).

Because of other excellent data analysis routines in our laboratory, SAMPO has only recently been put to much advantage. The foremost advantage found to date has been in reducing time required to strip multiplets in complex spectra. SAMPO allows one to strip all the possible multiplets in a single spectrum in the time previously required to strip a single multiplet by hand. An example of the usefulness of the program is seen in Figure 10, depicting the 212-222-keV quartet seen in the Bi^{204} spectrum. The quartet was stripped by indicating the end points used for background and the approximate center channel of each peak in the multiplet. The dots are actual data points, the +'s are SAMPO fitted points, and the *'s are points where the two are identical. Note that the fit is quite excellent. For a set of 4 separate Bi^{204} runs the energy

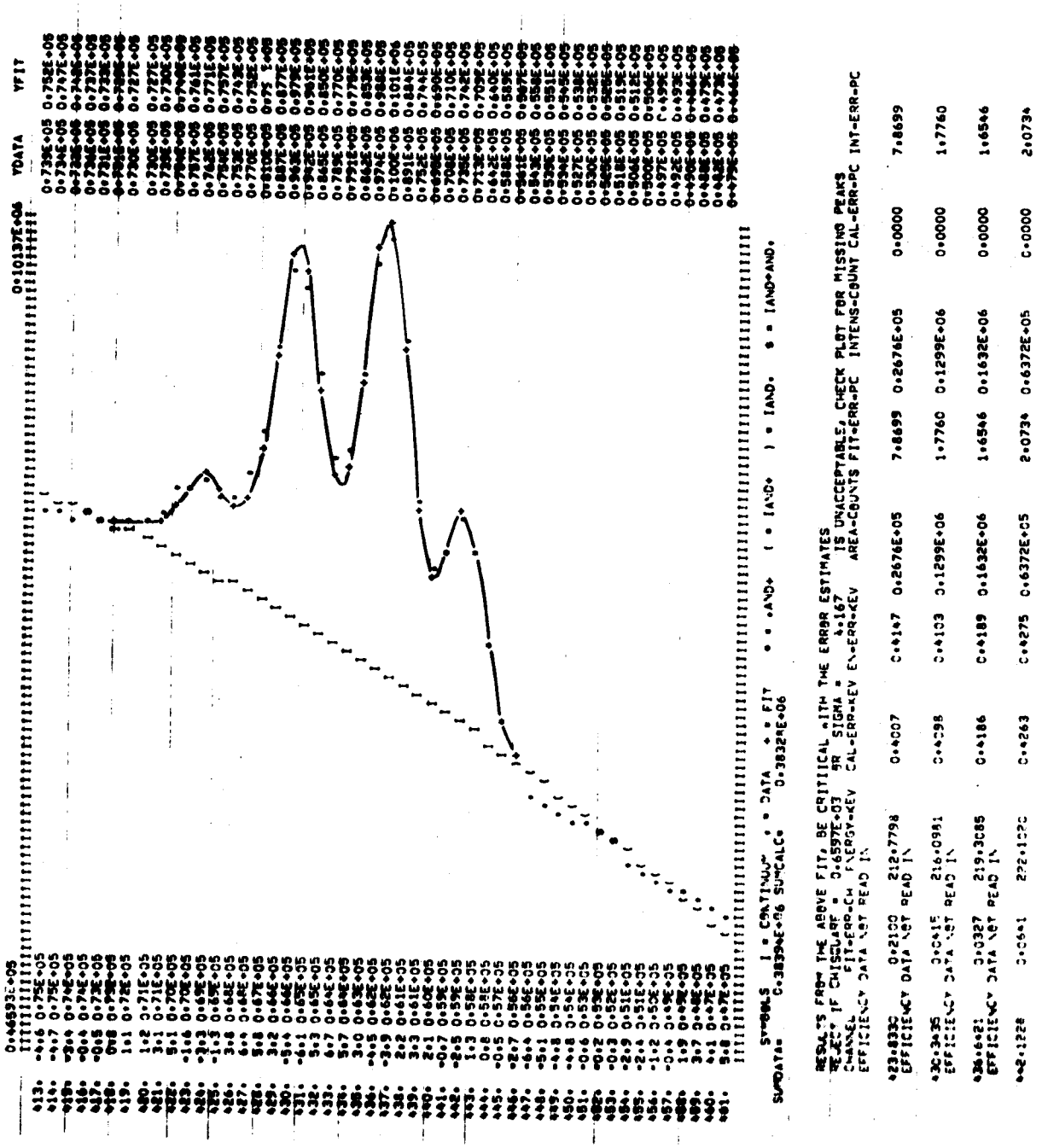

Fig. 10. Photograph of line-printer output from the spectrum analysis routine SAMPO, as run on the Sigma-7 computer. The fit is to a 212-222-keV quartet from the decay of Bi^{204}.

range for the individual peaks in the quartet was about 0.35 keV for each peak and the intensity range within 11%.

2.3.1.B. MOIRAE Spectrum Analysis Routine

MOIRAE, the backbone of the MSU nuclear spectroscopy data analysis system is a FORTRAN program that utilizes a Fairchild 737A live-display scope and sense switches to perform the spectrum analysis. Once the data have been either read in from cards or transferred from an on-line data acquisition program, the switches control the type of display, log or linear, the expansion and shifting of the axes, and various computation routines. Figure 11 shows the display of a portion of the Bi^{204} gamma-ray spectrum. The information at the top gives channel position of the long pointer and the number of counts in that channel, the number of cycles in the log display, the run number, the subroutine presently in use, and the order of the background fit being used. The Compton edge in the center of the display, the Compton of the 375-keV peak, is shown on expanded scales in Figures 12 and 13. In Figure 13, a 4th order fit to the background determined by the set of background points is shown. The sense switches are used to move the tall pointer to the position of points in the spectrum used to calculate the background. The short lines indicate the position of points that have been accepted for the background calculation. Either a set of individual points or regions of points can be used to calculate the background. Figure 13 shows the result of subtracting the background, along with the original spectrum. From this one selects the peak limits, and whether to use the full raw peak or the portion of the peak with

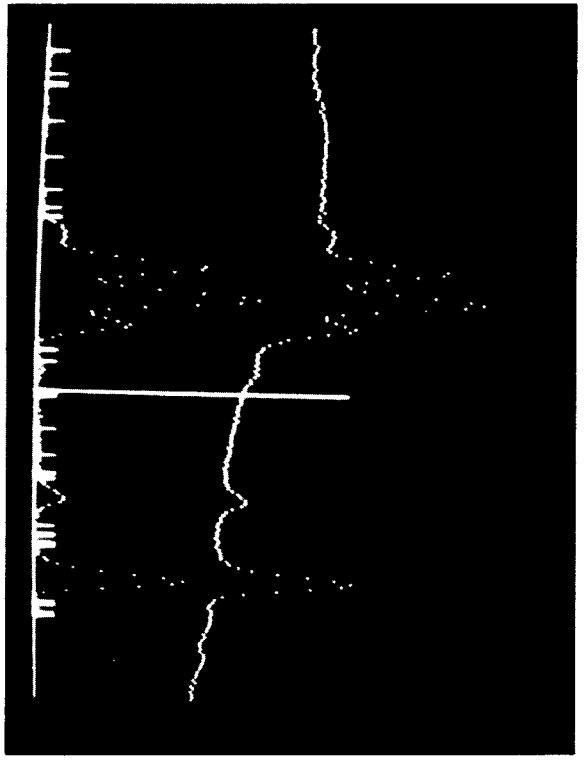

Fig. 13. Display of peaks (including the quartet of Fig. 10.) after the calculated fourth-order background has been subtracted.

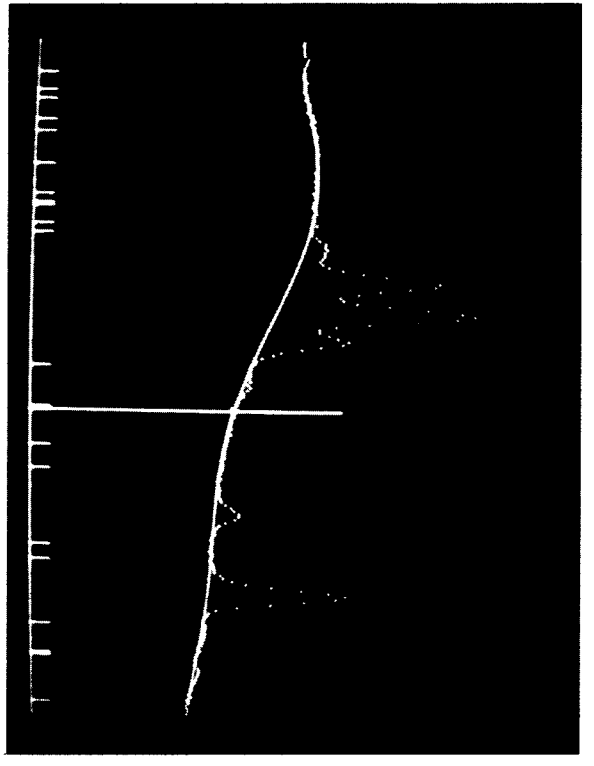

Fig. 12. Expanded view of a fourth-order fit having just been made on Fig. 11.

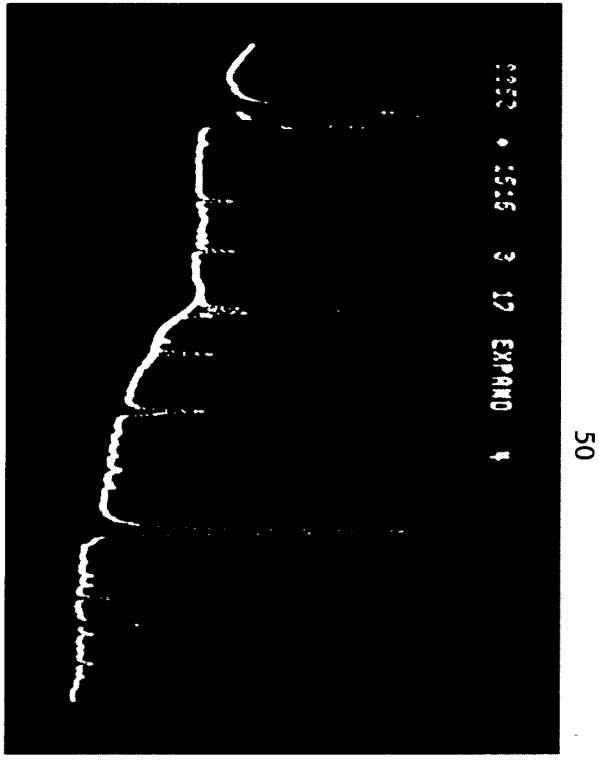

Fig. 11. Oscilloscope display of a portion of the Bi^{204} γ-ray spectrum, as run under the program MOIRAE.

counts greater than one-third maximum to calculate the centroid. :d. The program then finds the centroid, area, sum of raw data and background, and the square root of that sum. This information can be punched on cards, printed, and/or plotted on a Calcomp plotter. Once all the necessary analyses are accumulated, one can have the computer (under the code name MOIRAE $E(I)$) calculate a calibration curve using a least-squares fit to a quadratic equation and calculate the relative intensities from the areas of the peaks.

Naturally, each of these routines, SAMPO and MOIRAE, has distinct advantages and disadvantages. MOIRAE is particularly useful since it allows immediate operator control over such parameters as background order, background points and interval, peak end points, etc. SAMPO, on the other hand, has the distinct advantage of being able to fit multiplet peaks accurately, which MOIRAE is presently unable to do. Conversely, SAMPO is handicapped by a low order (second) background fit, making it difficult to fit peaks accurately in some regions of the spectrum, most notably near a Compton edge. MOIRAE has the added disadvantage of tying up the live-display scope for hours at a time. To alleviate this difficulty, G. Giesler and R. Firestone are presently adapting these analysis programs for a PDP-9 computer so that it can perform the same functions as MOIRAE.

2.3.1.C. Gamma-Ray Energy and Intensity Measurements

The gamma-ray energy measurements were performed by computing a least-squares quadratic calibration equation from the centroid channel numbers of well-known standard gamma-rays and then computing the energies of "unknown" gammas from the centroids and

the standard curve. The energy calibration curves were made from "internal" energy calibration spectra taken by simultaneously counting the unknown and standard calibration sources.

The choice of the standard calibration sources and their employment are important factors in the gamma energy calibrations. Ideally one would like standards which closely "bracket" each unknown gamma, which emit only the gamma rays actually used as standards, and which have a small number of them since their spectral distribution might otherwise obscure photons of interest. However, one must balance these requirements against the need for many good calibration points in order to establish a reliable calibration curve.

The gamma-ray relative intensities were established through the use of a detector efficiency versus gamma energy curve for energies from ≈100 to 3000 keV. A linear relationship between the log of the i^{th} full energy peak (eff_i) and the log of the i^{th} photon energy (E_i) between ≈400 and 3000 keV was observed for each detector. The dependence was incorporated into the MOIRAE $E(I)$ computer program which calculates the energies and relative intensities form the punched MOIRAE cards. In this work the relative areas from 3-6 runs on each of $Bi^{203,204}$ were averaged and then the final relative intensities were calculated from these areas using the MOIRAE $E(I)$ program.

2.3.2. Double and Single Escape Peaks

The detectors used in this study were sufficiently efficient that single escape peaks, peaks differing from full-energy

peaks by 511 keV, were so small that they were undetectable (i.e. no single escape peaks were found for any of the higher intensity peaks). The double escape peaks, having energies 1022.0 keV below the full energy peak, were detectable. A 511-511-gamma coincidence experiment as described earlier was used to determine the double escape peaks. These double escape peaks were also useful in checking the energies of the full energy peaks. However, care must be exercised since recent evidence [Gu68] has suggested that the energy differences need to be corrected by a "field increment effect" factor based upon the detector-source geometry and the electric field in the detector produced by the diode bias voltage. This "field increment effect" is small [Gu68], so it was ignored, the pair-peaks not being used for energy calibrations anyway. An additional method of detecting double and single escape peaks is their lack of Compton edges, but since these peaks are very small and the Bi^{203} and Bi^{204} spectra are so "cluttered" with many peaks, this is definitely not a very useable method.

2.3.3. Gamma-Gamma Coincidence Spectra

In all coincidence spectra recovered from the EVENT RECOVERY multiparameter system there are several sources of the "coincidence" events and peaks:

1) true coincidence events (and peaks),
2) backscatter events (and peaks),
3) chance events (and peaks),
4) cascade events (and peaks) in coincidence with a peak whose Compton lies under the gated region.

and

As only the first (1) is desired, one must do his best to avoid or compensate for the rest. An excellent discussion of backscattering difficulties in coincidence studies has been presented by G. Giesler [Mc69,Gi70]. In these references he shows that a 90° Ge(Li)-Ge(Li) detector configuration is optimum, using a graded lead absorber to shield each detector from the other without absorbing the gamma rays at the same time. Both (2) and (3) can be determined or removed by gating on regions immediately adjacent to the peak, on both low and high sides of the peak. In the EVENT RECOVERY program (used to scan these multiparameter coincidence magnetic tapes) it is possible to subtract immediately weighted spectra taken with adjacent gates as the magnetic tape is scanned. Several examples of this highly effective technique will be illustrated in Chapter III.

2.4. Decay Scheme Construction

2.4.1. DECAY SCHEME Program

The construction of the decay schemes in this thesis have followed relatively standard procedures for decay scheme production, since the great difficulty in these schemes does not lie in their unusual characteristics but rather simply because of the great complexity introduced by an inordinately large number of weak gamma rays. In the present investigation the results include the energies, spins, and parities of the states, the gamma-transition energies and intensities, and the log *ft* values to each state. The methods used to construct a decay scheme are varied and invariably tailored to each individual decay. The location of states can be initially suggested by anti-coincidence data, gamma-energy sums, prompt-coincidence data, delayed-coincidence data, and gamma-ray relative intensity balances or other parameters, but as the number of gamma rays increase this becomes progressively more difficult.

Once the states are determined, however, the beta and gamma transition intensities and the log *ft* values can be determined by a simple (but tedious) sequence of operations. D. Beery has written a FORTRAN computer program, described in reference [Be69], under the code name DECAY SCHEME which does these routine calculations. I found that a major disadvantage of this program was that each time it was to be employed one must calculate the total relative beta feeding to each state due to the populating and depopulating gamma rays, an inconvenience when one is dealing with 25

or more states. The program was consequently modified so that for each of the known states the total relative beta feeding is calculated from card input data. For each well-placed gamma ray, its energy, the level it populates and the level it depopulates, and its conversion coefficient (if known) are input and the resulting total relative beta feeding calculated. If a state has a greater populating than depopulating intensity, a warning flag is output for that state, the relative beta feeding (difference in intensities) is set to zero, and the calculation continued. This minor modification has saved many an hour of labor and exasperation and has been very helpful in a number of other large decay scheme constructions. For a description of DECAY SCHEME it would be worthwhile to see reference [Be69] since it gives a more complete description than I have taken time to give here.

2.4.2. TAKE CARE Program

During any decay scheme preparation one invariably finds oneself taking numerous energy differences between a proposed state and other well-known states hoping to find additional justifying transitions that might confirm that proposed state. When the number of gamma transitions (and hence energy states) is limited this does not seem unusually tedious, but when the number of transitions exceeds 200 and the levels exceed 25, as they do in Pb^{204}, it becomes monumental. Much to my surprise no program was found in this laboratory which alleviated this problem. Therefore, TAKE CARE (see [Cr70] for the derivation of the name) was written to fill this obvious gap.

In spite of its simplicity, it has been of nearly invaluable help in construction of the complex Bi^{204} and Bi^{203} decay schemes. The input parameters consist of the known energy levels, the energies of all the known gamma rays, and control parameters. The program can operate in either or both of two modes, TAKE and/or CARE. In the routine TAKE, all the energy differences between known levels are calculated and compared to the known list of gammas, and any that match within a tolerance set by the control cards are output in a convenient form, illustrated in Figure 14. In the second mode of operation, CARE, the more useful option is excercised, that is, one may "scan" up the existing decay scheme by 1-keV intervals to find those gammas which fit, to within some specifiable tolerance, between the "scanning" level and the existing levels. In this manner one may look at any arbitrary level and find out what known gammas are possibly to be considered as transitions between the unknown level and the known energy levels. Figure 15 shows a portion of the CARE program output from the Bi^{204} study. Since the errors in the energies of the gamma rays are not necessarily uniform over the entire energy range, the tolerances alluded to above can be set independently for two regions, one for the 0-1500-keV region and a separate tolerance for the >1500-keV region.

While this program is simple (yet very useful), it also points up another important aspect of decays involving many gamma rays. Many of the gamma rays appear to be involved in a multitude of possible transitions, thus indicating that, for a large number of gamma rays, placement of levels solely upon precise energy sums is a

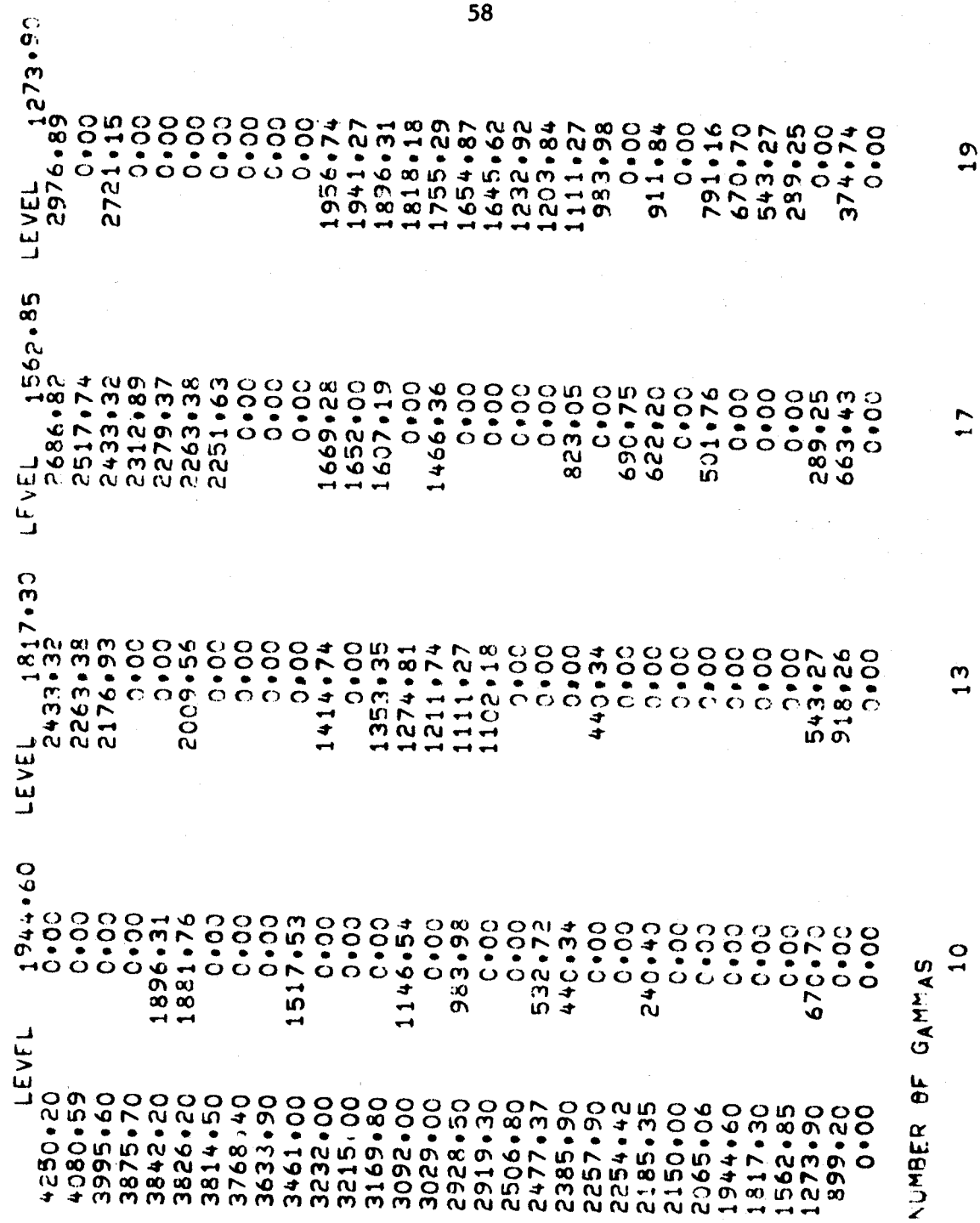

Fig. 14. A portion of the TAKE routine line-printer output from the TAKE CARE program. The energy levels (on the left, in keV) and gamma-ray energies (in keV) are from the present Bi^{204} decay scheme studies. The nonzero energies in the 4 columns to the right of the energy levels correspond to gamma rays whose energies are within a specifiable tolerance (here 1 keV) of the energy difference between the tested level (e.g. "LEVEL 1944.60") and the levels in the left-hand column.

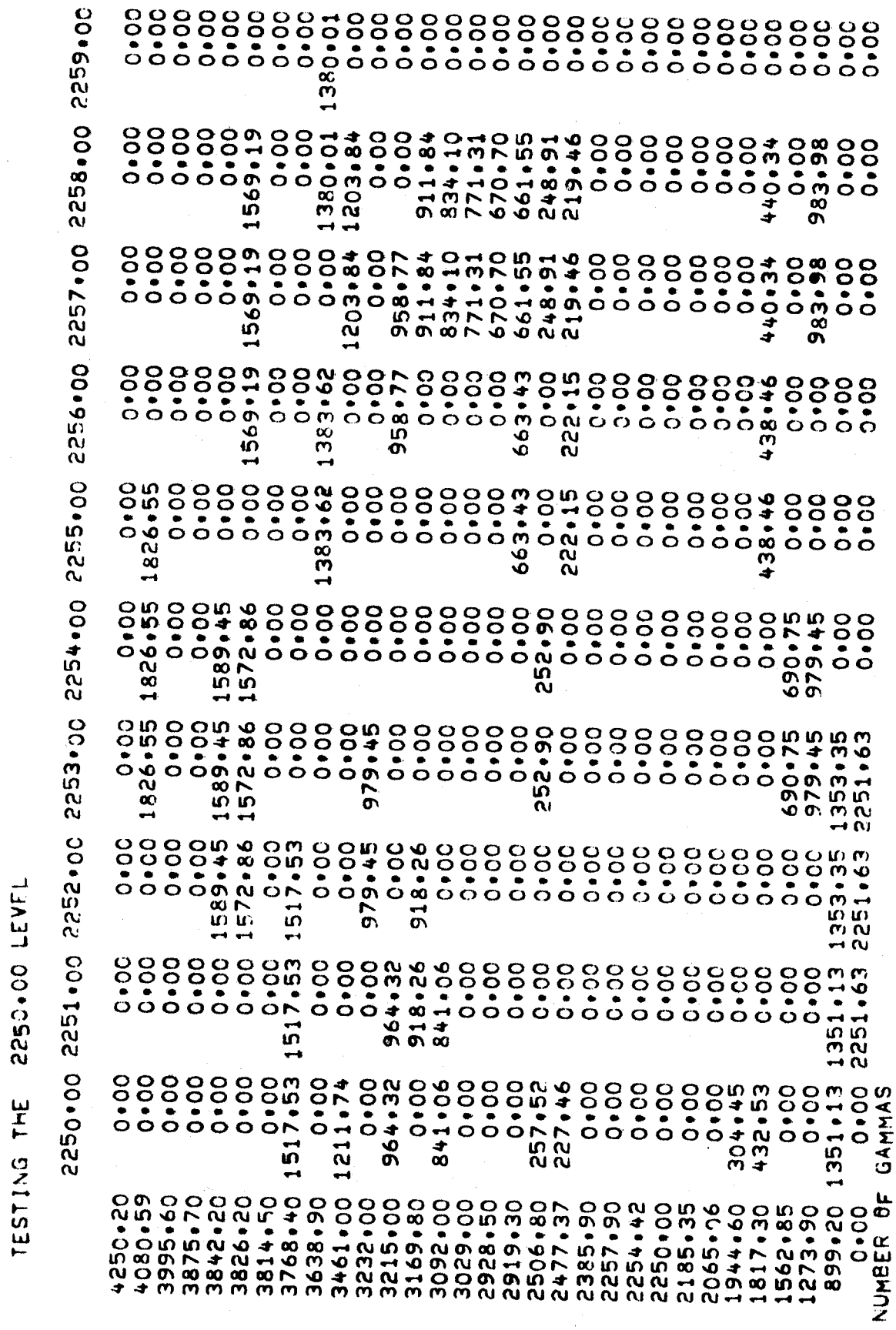

Fig. 15. A portion of the CARE routine line-printer output from the TAKE CARE program. The energy levels and gamma-ray energies are from the Bi^{204} decay scheme studies.

risky if not poor practice. This is well indicated by comparing the decay schemes of this investigation (Figures 22 and 31) with the previously published decay schemes (Figures 17 and 27, respectively), where many levels were based solely upon precise energy sums. It is not so surprising that many of these levels were shown to be incorrectly placed during the present study. A computer listing of the TAKE CARE program (including ample comment cards) can be found in Appendix A.

2.4.3. Auxiliary Programs

The PDP-9 computer in the Nuclear Chemistry group laboratory has been indispensable for excellent data acquisition, but in addition it has proven very useful for performing routine types of numerical calculations. The programs are written in FORTRAN, stored on DECtape, and run under a keyboard monitor system. Each is brought into core via an appropriate teletype command. Most of these programs were written by R. Eppley of the Nuclear Chemistry group; a more complete discussion of each program and the necessary input parameters can be found in reference [Mc69].

1) ARITH - desk top calculator type program,
2) INTEN - calculates and renormalizes gamma-ray intensities from efficiency curves of the detector of interest,
3) PLYFT - a general least-squares program,
4) ICC - used for interpolation of the theoretical internal conversion coefficients from other

published tables,

5) TRIGA - calculates the expected activity of samples submitted to the MSU TRIGA reactor,

and

6) BLACKJACK - just that, the computer plays the operator via teletype, for those moments when it looks as if mother nature is against you.

In the experimental section of this thesis these programs will not always be mentioned by name but they were often used for routine calculations and consequently some mention of them should be made here.

2.5. Plotting Routines

As I neared completion of the $Bi^{203,204}$ projects and began to compile this thesis, I became painfully aware of the time and effort that was soon to be spent in the preparation of many coincidence spectra taken using the Ge(Li)-Ge(Li) multiparameter coincidence system described in section 2.2.2.B. Each spectrum would require plotting the data (in India ink), titling each spectrun, labeling each peak of interest, and finally blocking and titling each finished page of plots. The obvious solution, of course, was to let the Calcomp 565 plotter, interfaced with the Sigma-7 computer, do the entire spectra, <u>including</u> the titles, borders, and peak energy labels. Searching the computer library for such a program, I was astonished to find none that was satisfactory. Remedying this deficit, two plotting routines were written under the code names VALTAVA and COINPLOT. Each of these programs is decsribed in detail below (with listings in the Appendices).

2.5.1. Program VALTAVA

Just as TAKE CARE is a fantastically simple but efficient program for decay scheme work, so VALTAVA is a highly powerful (though simple) answer to our time-consuming drafting problems. (Indeed, the name VALTAVA is Finnish in origin, meaning "powerful".) A FORTRAN listing of the program (with comment cards) can be found in Appendix B.

The data input was kept as simple as feasible so as not to make the program too unwieldly or narrow in scope. These cards are, in order:

1) the title card (containing the desired title for the plot),

2) the crunched data deck (compressed data format, although any data input could be easily adapted to the program),

3) the cards used to label the peaks (one card for each peak, containing the approximate centroid and the energy of the peak),

and 4) a MARK card (billboard card) to separate the individual spectra.

Given these input control cards, the program will (in order) draw a line about the bounds of the entire plot, put tick marks on the base line at 500-channel intervals, put on the title, plot the spectra, put tick marks on the ordinate and the number of counts at each mark, and finally label each peak with the appropriate energy. The program will automatically scale the spectra in a base 10 log plot from 100 counts full scale to 1 million counts full scale, depending upon the magnitude of the largest peak in the spectrum. In addition, care was taken such that two energy labels could never be superimposed, even partially. If two centroids are given such that overlapping of the lettering would occur, the program senses this and will adjust (space) them properly. A sample plot as produced by this program can be found in Figure 21.

2.5.2. Program COINPLOT

Program COINPLOT was actually born out of VALTAVA and an idea to reduce drastically preparation time of coincidence plots.

The input for the program is fantastically simple, a single control card and standard crunch punch data decks. The data input on the control card includes:

1) the size the final plots are to occupy (in inches) on an 8 ½" x 11" page,
2) the number of spectra (N) to be placed in the above area,
3) the number of channels to be plotted from the data deck (default = 4096),

and

4) the starting position of the first plot from the lower left hand corner of the page.

Given this input, COINPLOT will outline an 8½" x 11" page, automatically scale the N spectra for the allowed space, and plot them consecutively. Once again (as in VALTAVA) it will scale each individual plot from 1 to 6 cycles (common log), based upon the largest peak in each spectrum, and put tick marks on each axis. Unlike VALTAVA, it does not plot the characters or label the individual peaks; this is done later with a typewriter. The beauty of this is that the plots can be done with the ballpoint Calcomp pen rather than using the messy India ink. Even so, this was found to yield a good-looking set of coincidence plots at a fraction of cost and labor previously required. Without a doubt this program cut down figure preparation time by (conservatively) at least three weeks. A listing containing detailed comment cards can be found in Appendix C.

Perhaps, I have made this program seem more sophisticated than it really is. On the other hand, simple as it may be, it has

saved literally weeks of work both for the draftsman as well as myself, and as such it certainly deserves mention in this thesis. A sample plot can be seen in either the Bi^{204} or Bi^{203} coincidence spectra sections found in Chapter III. An additional reason for including this program description is that it gives me an opportunity to express a bit of personal philosophy. In the past, certain laboratories and/or publishers have frowned upon the use of computer outputs in published material. The past decade, with the vast information explosion, has seen such an increase in particle and nuclear physics data that unless computer output is freely permitted in such publications, nearly as much time will be spent in preparing material for publication as in doing fundamental research. Programs such as VALTAVA and COINPLOT are, I believe, a step in the right direction.

CHAPTER III

EXPERIMENTAL RESULTS

3.1. Electron Capture Decay Scheme of Bi^{204}

3.1.1. Introduction

As discussed in section 2.1., Bi^{204} has been produced by a number of nuclear reactions involving protons and He^3 at a variety of energies on $Pb^{204,206}$ and Tl isotopes, respectively. Lacking high-purity separated isotope targets and high-resolution cyclotron beam energies, the previous studies [Fr56,St58] of the Bi^{204} decay had to be content with sources which were highly contaminated with $Bi^{205,206,207}$ impurities, making an accurate analysis of the complex Bi^{204} spectrum difficult, if not impossible. Both of these initial attempts utilized high-resolution permanent-magnet spectrometers having energy resolutions of 0.1% [St58] and 0.2% [Fr56]. While both yielded excellent results in the low energy region (<1000 keV), at the same time each suffered the limitation common to most conversion-electron spectroscopy, i.e. the conversion coefficients for low multipole transitions are just too small for many conversion electrons above 1000 keV to be seen. The highest γ transition reported using conversion-electron spectroscopy was only 1140 keV. Using these electron results, Fritsch et al. [Fr58] concluded that the decay scheme was too complex to be constructed from the existing energy and coincidence data. Stockendal et al. [St58], while reaching essentially the same conclusion, did publish

a tentative decay scheme but at the same time emphasized that the only levels and transitions known with complete certainty were the Pb^{204m} levels and γ rays.

Since the decay energy for Bi^{204} has been estimated [Fr56] as 4.4 MeV and the highest previously reported level is at 2478 keV, one certainly would expect to find many states above 2500 keV populated by the Bi^{204} decay. For this reason and because of recent advances in Ge(Li) spectroscopy not formerly available, it was felt that a re-investigation of the Bi^{204} decay might be worthwhile. Some 210 γ rays were identified, this being some 143 more than previously reported. Utilizing the multiparameter coincidence apparatus, many of these were fitted into a radically changed and improved level scheme for Pb^{204}.

3.1.2. Source Preparation

The Bi^{204} sources were prepared by bombarding 97.2% enriched isotope Pb^{206} (as $Pb(NO_3)_2$) with 30 MeV protons from the MSU sector-focused cyclotron for 1-2 h at 1-2 μA. The details of such a production were previously discussed in section 2.1.2. Short-lived contaminants were determined by counting the samples at various times following the bombardment and noting variations in intensities of the peaks. Long-lived contaminants were revealed by allowing the samples to decay for 3-7 days, then determining the remaining impurity peaks. No chemical separations were performed on these sources.

3.1.3. Bi^{204} γ-ray Spectra

3.1.3.A. Singles Spectra

A Ge(Li) detector, mounted in a right angle dip-stick cryostat, was used to determine the energies and intensities of the Bi^{204} γ rays. Typically, the resolution ranged from 2.25 to 2.5 keV FWHM at 1.33 MeV, using a room temperature FET preamplifier, a low-noise RC linear amplifier with DC offset and pole-zero compensation, and a 4096-channel analyzer. This detector had an efficiency of 2.5% compared with 3" x 3" NaI(Tl) detector, using a source-to-detector distance of 10 centimeters (cm). A second Ge(Li) detector, similarly mounted, was used to confirm the energy values of the observed γ rays. This detector had a resolution of 2.0 keV FWHM at 1.33 MeV and a 3.6% efficiency.

The γ-ray energies were determined by comparison with a number of well-known calibration sources, listed in Table 5. The larger peaks were first determined by counting the Bi^{204} sources simultaneously with these standards. The centroid of each standard peak was determined by either SAMPO or MOIRAE (sections 2.3.1.A. and 2.3.1.B.) spectrum analysis routines, the centroids of the peaks being fit to a least-square n^{th} (n=2 commonly) degree curve, which became the calibration curve. The calibration curve was then used, in turn, to determine the energies of the larger unknown Bi^{204} peaks from their centroids. The energies of the weak Bi^{204} γ rays, which are often obscured by the standards, were finally determined by using the now well-known stronger γ rays as internal standards, and applying a similar method. The internal standards of Bi^{204} used in this study

Table 5. γ rays used as energy standards for the $Bi^{204,203}$ decays.

Nuclide	γ-ray energy (keV)	Reference
Ta^{182}	100.104±0.002	a
	152.435±0.003	a
	156.387±0.003	a
	179.393±0.004	a
	264.072±0.009	a
Ce^{139}	165.84±0.03	b
Sc^{46}	889.18±0.10	c
	1120.41±0.10	c
Bi^{207}	569.63±0.003	d
Mn^{54}	834.83±0.04	e,f
Cs^{137}	661.632±0.069	g
Co^{60}	1173.23±0.04	e
	1332.49±0.04	e
Co^{56}	846.782±0.060	f
	1037.851±0.060	f
	1175.085±0.070	f
	1238.290±0.040	f
	1360.219±0.040	f
	1576.561±0.050	f
	1771.33±0.060	f
	2015.33±0.07	f
	2034.90±0.06	f
	2180.17±0.07	f
	2231.60±0.06	f
	2251.15±0.07	f
	2429.28±0.10	f
	2598.52±0.05	f
	3009.9±0.10	h

Table 5. (continued)

	3202.18±0.07	f
Tl^{208}	583.139±0.023	e
	2614.47±0.10	e
Pb^{203}	279.17±0.02	d,i
Y^{88}	1836.13±0.04	e,f

[a]Reference [Gr65]

[b]Reference [Ge65]

[c]Reference [Ra67]

[d]Reference [Ma57]

[e]Reference [Ma68]

[f]Reference [Gu68]

[g]Reference [Wh67]

[h]Reference [Au67a]

[i]Used in the Bi^{203} calibration only.

are shown in Table 6. A γ-ray spectrum of Bi^{204} taken with the 2.5% detector is shown in Figure 16. The 3.6% Ge(Li) detector was not primarily used on the Bi^{204} decay for the simple but understandable reason that it was not purchased until nearly all the Bi^{204} experimental work was completed.

A list of the energies and relative intensities of the γ rays resulting from the decay of Bi^{204} is given in Table 7. The assigned energies are the mean values for 4-6 different measurements taken at varied times and amplifier gains and with each of the two Ge(Li) detectors. The corresponding uncertainties in the energies were: the major calibration peaks, ±0.10 keV; the remaining peaks in the 0-1000-keV region, ±0.15 keV; in the 1000-2000 keV region, ±0.25; and in the 2000-3000-keV region, ±0.5 keV.

The relative peak intensities listed are also averages from several runs, the statistical uncertainties in the intensities being much larger than the uncertainties in the energy determinations, of course. Those peaks having intensities >1% (relative to the 899.2-keV transition) have uncertainties ranging from ±5-15%; the peaks having intensities <1% have uncertainties of ≈15%; and peaks of extremely small intensity (<0.1%) can have uncertainties of up to ≈22%. The relative photopeak efficiency curves (at various distances) for the 2.5% detector were obtained by measuring the relative areas of a standard set of γ-ray sources whose relative intensities are well-known. The results were incorporated in the MOIRAE $E(I)$ computer program, which allows one to get the relative intensities immediately from the relative peak areas of the individual spectrum.

Table 6. Bi^{204} γ-rays used as internal energy standards.

γ-ray energy (keV)	γ-ray energy (keV)
72.80 (K_{α_2} x-ray)†	1043.63
74.97 (K_{α_1} x-ray)†	1111.27
84.8 (K_{β_1} x-ray)†	1211.74
87.3 (K_{β_2} x-ray)†	1274.81
140.80	1414.74
176.17	1524.05
248.91	1645.62
374.74	1703.32
421.55	1925.86
532.72	1941.27
670.70	2263.38
791.16	2517.74
899.15	2566.13
983.98	2686.82
	2837.33

†x-ray notations and energies from reference [Le67].

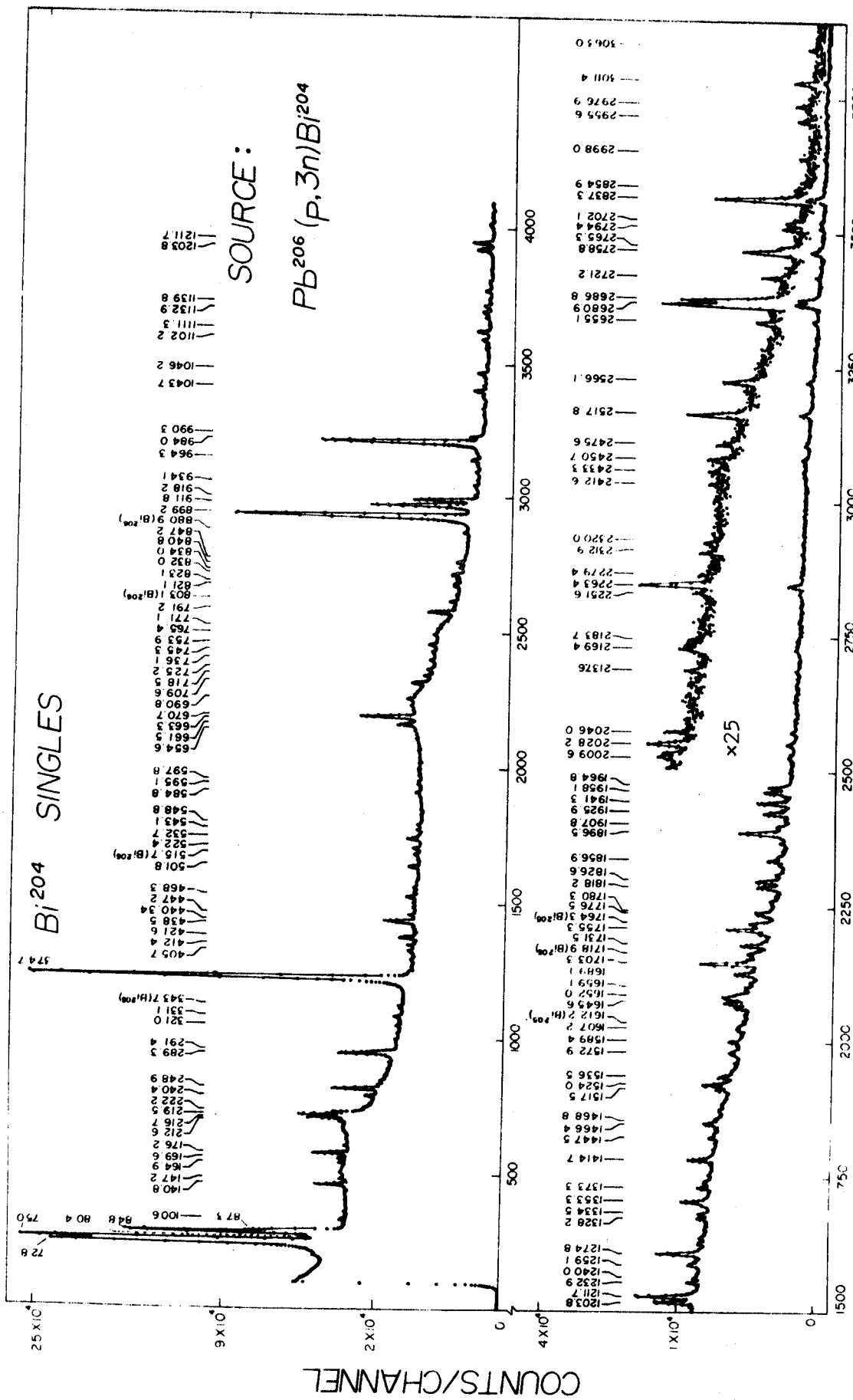

Fig. 16. Bi^{204} singles γ-ray spectrum taken with a 2.5% Ge(Li) detector having a resolution of 2.4 keV FWHM (at 1.33 MeV) in this run.

Table 7. Energies and relative intensities of γ rays present in the ε decay of Bi^{204}.

Measured γ-ray energy(keV)	Relative Intensity	Measured γ-ray energy (keV)	Relative Intensity
80.40	0.32	421.55	1.06
96.54	0.03	432.53	0.05
100.74	0.14	438.46	0.78
109.38	0.04	440.34	2.50
140.80	0.88	447.08	0.46
147.36	0.12	455.92	0.13
164.92	0.11	461.70	0.12
169.83	0.26	468.23	0.50
176.17	1.07	473.50	0.13
212.70	0.34	477.75	0.18
216.11	1.32	501.76	0.88
219.46	2.19	510.67	0.43
222.15	1.00	522.22	0.62
227.46	0.22	532.72	1.30
240.40	0.29	543.27	0.29
248.91	2.04	548.74	0.45
257.50	0.07	585.02	0.31
286.32	0.29	595.13	0.38
289.25	2.75	597.83	0.42
291.35	0.92	604.73	0.22
304.45	0.13	611.88	0.26
320.85	0.14	631.88	0.08
331.07	0.34	654.88	0.13
340.59	0.11	661.55	2.66
374.74	73.74	663.43	0.82
405.82	0.26	670.70	10.73
412.24	0.29	683.39	0.22

Table 7. (continued)

690.75	0.91	1027.59	0.07
709.13	1.44	1037.34	0.39
710.48	1.42	1043.63	1.38
718.43	0.86	1049.04	0.20
725.15	0.97	1056.55	0.18
736.07	0.70	1060.17	0.52
745.23	0.74	1064.22	0.99
753.78	1.03	1092.10	0.10
765.37	0.50	1095.08	0.21
771.31	0.39	1102.18	0.60
791.16	3.39	1111.27	1.62
821.13	0.61	1127.50	0.28
823.05	0.52	1132.89	0.87
827.62	0.51	1139.77	0.63
831.95	0.94	1146.54	0.18
834.10	1.02	1157.66	0.60
841.06	0.25	1167.01	0.22
847.16	0.90	1181.24	0.07
899.15	≡100.00	1198.98	0.24
911.74	13.39	1203.84	2.09
911.96	11.40	1211.74	3.25
918.26	10.67	1232.92	0.46
924.16	0.07	1259.08	0.44
934.13	0.36	1261.71	0.14
950.33	0.16	1274.81	2.79
958.77	0.19	1290.61	0.20
964.32	0.53	1299.21	0.12
979.45	4.35	1328.22	0.39
983.98	58.44	1334.53	0.31
990.34	1.12	1347.93	0.23
1014.19	0.08	1351.13	0.47
1021.93	0.19	1353.35	0.87

Table 7. (continued)

1373.68	0.46	1755.29	1.25
1380.01	0.22	1760.97	0.20
1383.62	0.16	1778.49	0.28
1414.74	1.00	1780.33	0.34
1446.12	0.09	1796.91	0.11
1447.52	0.22	1803.95	0.06
1466.36	0.36	1818.18	0.53
1468.82	0.39	1826.55	0.57
1475.08	0.09	1836.59	0.07
1487.78	0.21	1851.00	0.09
1517.53	0.36	1856.86	0.27
1524.05	0.86	1881.76	0.34
1536.54	0.42	1896.31	1.38
1569.19	0.14	1907.23	0.17
1572.86	0.23	1916.43	0.05
1589.45	0.32	1925.87	0.60
1607.19	0.21	1941.27	0.84
1612.15	0.13	1956.74	0.40
1639.38	0.34	1958.10	0.42
1645.62	0.61	1964.77	0.39
1652.00	0.57	1988.00	0.03
1654.87	0.57	2009.56	0.08
1669.28	0.10	2014.09	0.05
1675.07	0.08	2028.24	0.14
1685.87	0.15	2045.99	0.08
1689.12	0.60	2064.19	0.03
1700.14	0.26	2084.22	0.04
1703.32	2.09	2092.56	0.04
1709.85	0.10	2100.62	0.05
1715.22	0.14	2137.57	0.03
1731.53	0.66	2169.44	0.04
1749.82	0.29	2172.21	0.03

Table 7. (continued)

2176.93	0.05	2686.82	0.31
2183.68	0.03	2721.15	0.03
2251.63	0.04	2758.80	0.10
2263.38	0.31	2765.26	0.02
2279.37	0.04	2794.38	0.02
2312.89	0.07	2802.07	0.02
2325.95	0.04	2837.33	0.25
2433.32	0.03	2854.92	0.02
2450.72	0.05	2864.65	0.01
2472.58	0.04	2898.01	0.01
2475.63	0.03	2947.99	0.01
2517.74	0.21	2955.55	0.02
2566.14	0.10	2976.89	0.02
2655.12	0.05	2990.49	<0.01
2668.24	0.02	3011.36	0.03
2680.93	0.38	3062.99	<0.01

3.1.3.B. Anti-coincidence Spectra

An anti-coincidence spectrum reveals those γ rays which are not in cascades (or very weakly so) and are primarily ε-fed ground-state transitions. Caution! An "anti" experiment is not necessarily a panacea to the elucidation of all direct ground-state transitions. The fact that a γ ray is not enhanced does not mean that the transition does not directly populate the ground state; indeed, it may be in a strong cascade. Conversely, the enhancement of a γ ray in an "anti" does not mean that it is not in cascade with other γ's, or that it goes directly to the ground state. For example, consider a γ ray feeding a long-lived metastable state. In an anti-coincidence experiment this γ ray will be enhanced because the cascade sequence has been effectively broken; even though the populating γ ray is enhanced, it is most definitely not a ground-state transition. Thus, in spite of the fact that a peak is enhanced, one should not accept that γ ray as a direct, non-cascade ground-state transition without further verification.

In the Bi^{204} decay all γ-ray cascades pass through the 899.2-keV state (Figure 17), thus ruling out any possibility of having a γ ray which is not in cascade with another and suggesting that perhaps an "anti" for the Bi^{204} would not be greatly beneficial. Also, the highest γ-ray energy recorded during this study was 3063 keV. This γ ray in cascade with the 899.2 keV of the first excited state would yield a state at 3962 keV, which is approaching the estimated decay energy of 4.4 MeV. However, if any of the high energy states do directly populate the ground state, then one might expect

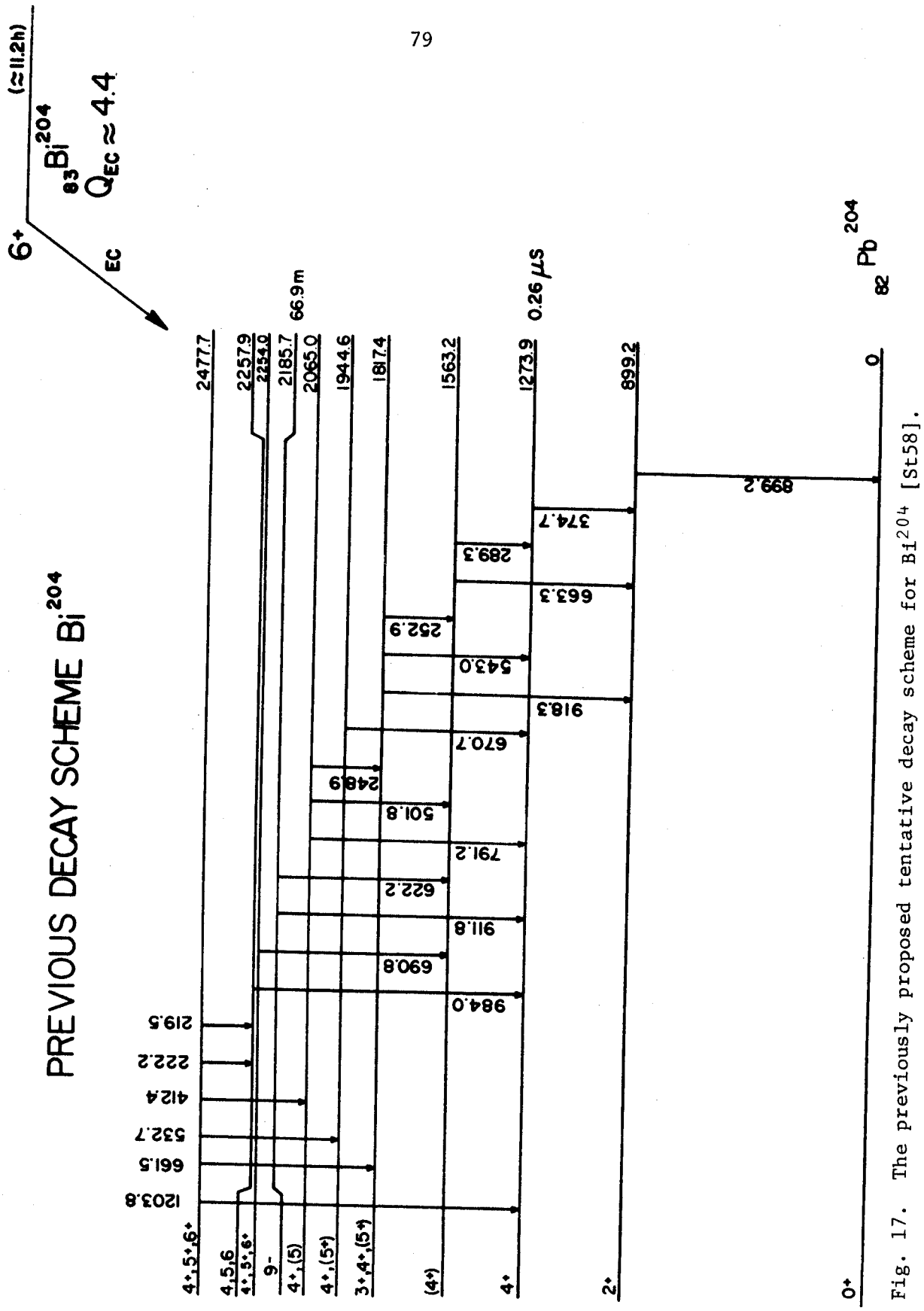

Fig. 17. The previously proposed tentative decay scheme for Bi^{204} [St58].

to see more high energy γ-ray transitions >3 MeV. Finally, a consideration of the spins and parities of Bi^{204} and Pb^{204} lends final support for the argument against an anti-coincidence experiment. The ground state of Bi^{204} is 6+ (determined by atomic beam experiments [Jo58]) and consequently the high-lying populated states of Pb^{204} would be expected to be primarily 5+, 6+, or 7+ states. As the ground state of Pb^{204} is 0+, it would be quite unusual to find direct population from the high-lying states. Based upon these arguments an anti-coincidence experiment was deemed unnecessary. A specialized exception will be discussed in section 3.1.4.F.

3.1.3.C. Double Escape Coincidence Spectra

A most informative but also very time-consuming double escape spectrum was taken early in the investigation using the NaI(Tl) split annulus (section 2.2.2.A.). A block diagram of the necessary electronics and experimental set-up is depicted in Figure 18. Requiring a 511-511-γ triple coincidence between the separate halves of the annulus and the Ge(Li) detector, one finds that the double escape peaks are greatly enhanced in the resulting spectrum. The spectra were calibrated both externally and internally, as well as by using a self-gated singles spectrum. A great problem ensues in trying to obtain enough counts to gain reasonably good statistics in the spectrum. While the experiment lasted nearly a week, gain shifts caused most troublesome difficulties. Figure 19 is such a double escape spectrum, with only the double escape peaks being noted. However, not all the peaks seen in the double escape spectrum are seen in the singles spectrum; only some 11 peaks were actually

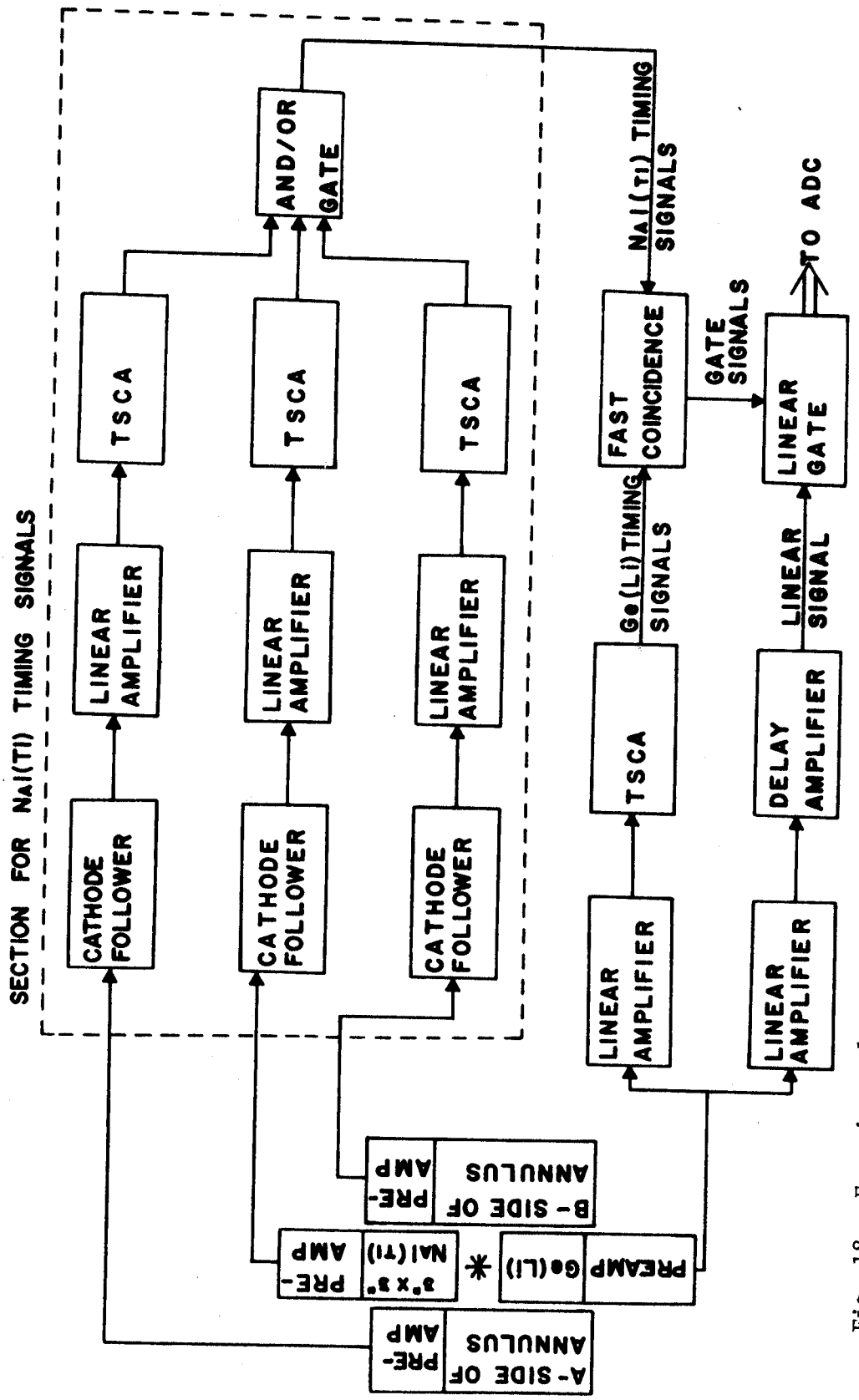

Fig. 18. Experimental setup for recording anti- and double escape (511-511-γ) coincidence spectra. For a 511-511-γ coincidence spectrum the TSCA's are adjusted such that the window falls on the 511-keV region and the linear gate is in the normal mode. For an anti-coincidence spectrum the TSCA's are wide open and the linear gate is in the "anti" mode.

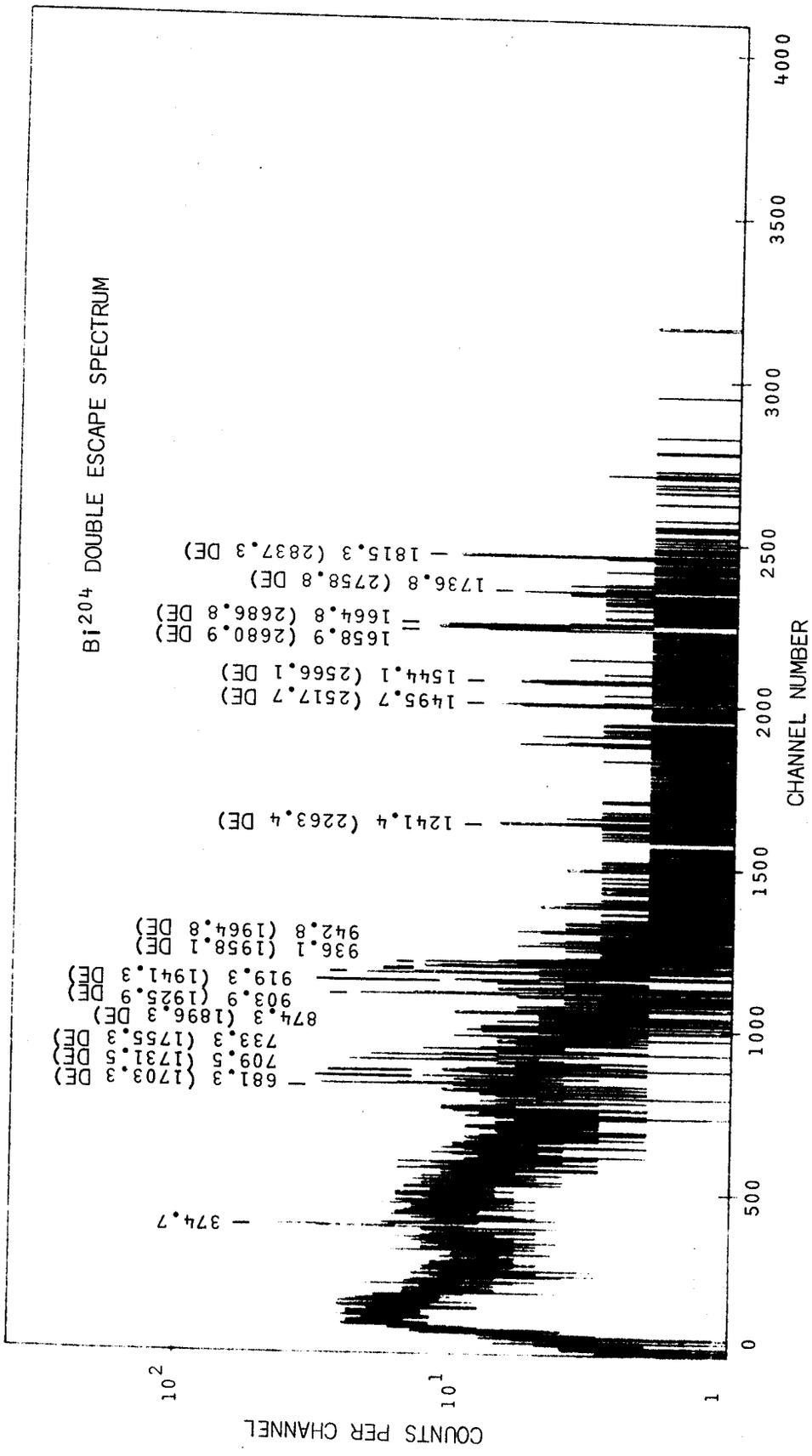

Fig. 19. Bi^{204} double escape spectrum taken with the NaI(Tl) split annulus and a 7 cc Ge(Li) detector having a resolution of about 4 keV (FWHM at 1.33 MeV) in this run.

removed from consideration as double escape γ rays, the remaining being obscured by the much larger photopeaks in the singles spectrum.

3.1.3.D. Prompt Coincidence Spectra

The prompt-coincidence spectra for Bi^{204} were taken utilizing the multiparameter Ge(Li)-Ge(Li) spectrometer described in section 2.2.2.B. A more complete description of the experimental set-up is found in reference [Mi69], including electronics and computer interfacing.

Two high-resolution Ge(Li) detectors were utilized, possessing effeciencies and resolutions of 2.0%, 3.0 keV FWHM (at 1.33 MeV and 2.5%, 2.4 keV FWHM (at 1.33 MeV), respectively. During the 96-h run some 7 million coincidence events were collected on magnetic tapes. These tapes were analyzed and about 2 million events discarded because of gain shifts in one or the other of the detectors. The final resolution in the *X* and *Y* integral coincidence spectra was somewhat poorer, around 4.0 keV (at 1.33 MeV) for each axis; this worsening came about as a result of minor gain shifts and ADC instability during the long run. Even so, the remaining 5 million events gave surprisingly good statistics, even to the point of being able to identify some of the high energy transitions in the gated spectra. Figure 20 shows the *X* and *Y* integral coincidence spectra. During the data recovery (EVENT RECOVERY) gates were set on either (or both) axis and the data displayed from the opposite axis (section 2.2.2.B.). The majority of the data in this thesis were recovered during a period covering almost 6 months, and even at this writing it is almost a certainty that there are useful unanalyzed data "left"

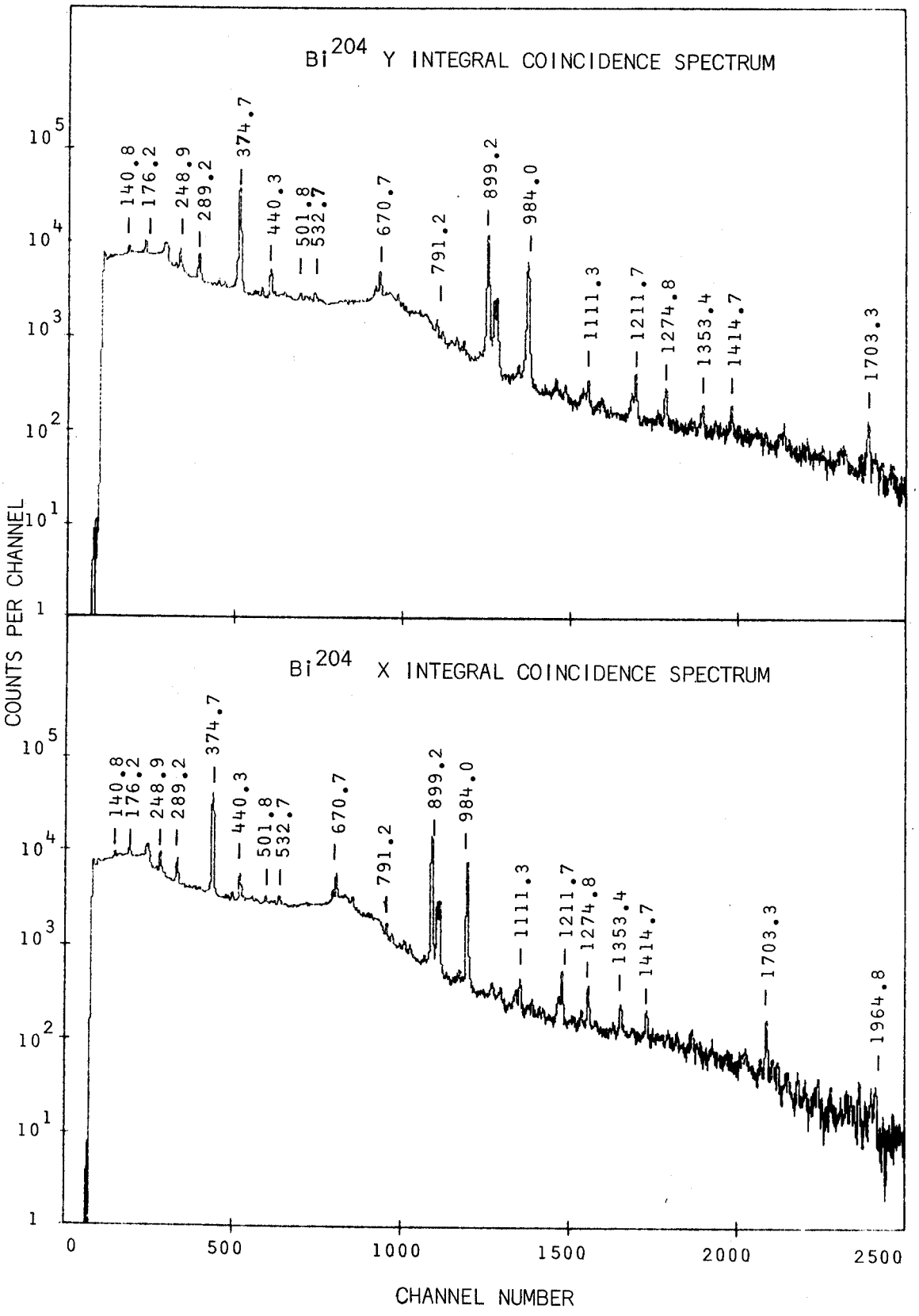

Fig. 20. Bi^{204} integral coincidence spectra taken using the multiparameter Ge(Li)-Ge(Li) spectrometer (section 2.2.2.B.).

on the tape. (This is an outstanding example of how the recent advances in nuclear spectroscopy technology have almost outstripped the techniques of data analysis.)

With only a few exceptions, no intensities were calculated for peaks in each of the Bi^{204} coincidence spectra. With 210 γ rays reported this would have become a monumental project and was discarded as too time consuming in spite of the worth to be gained. The greatest difficulty encountered in the coincidence spectra was the poor statistics for small peaks in the 1200-3000-keV region. The Bi^{204} has many very small peaks in this region, and many could not be distinguished in even the "any" coincidence spectra; hence no spectra produced by gating upon these peaks were found to yield any significant data. Rather than list any individual coincidence spectra here, they will be deferred to a more detailed discussion in section 3.1.4.

The following section, as well as a similar section in the Bi^{203} portion of this chapter, is devoted to the placement of energy levels and γ rays on the basis of γ-γ coincidence spectra. As was mentioned in section 2.3.3., the counts recorded under the multiparameter EVENT program have several origins: true cascade events, chance events, backscatter events, and events from γ rays in coincidence with the underlying Compton backgrounds.

The backscatter peaks have been effectively eliminated by using the 90° Ge(Li)-Ge(Li) detector configuration, the detectors separated by a 1.3 cm graded lead absorber in such a manner as not to absorb the γ rays. An excellent discussion of backscatter problems and γ-γ Compton scattering is found in [Gi70]. Chance events,

as long as they are small in number, also cause little difficulty since they effectively "add" a singles spectrum to the coincidence spectrum and do not affect the enhancement of the cascade peaks to any degree. The major problems in the γ-γ coincidence spectra arise from the underlying Compton background. For example, if one were to gate upon a particular peak, not only are the peak counts above background returned, but also any events in coincidence with the background. One could easily be misled by a spectrum without background subtraction, since peaks in coincidence with the Compton background would often be revealed as peaks in cascade with the gated peak. A decay scheme generated purely from such data would be pure, unadulterated rubbish.

Fortunately, the program EVENT RECOVERY makes provision for subtracting the background from each set of gates. The program subtracts weighted spectra taken with adjacent gates from the spectra obtained with the gates set on the peak of interest. The advantage, of course, is that this subtraction then eliminates the peaks in coincidence with the Compton background, leaving behind a coincidence spectra of the "true" events for that peak.

Figure 21 illustrates the usefulness of this powerful technique. The top spectrum in Figure 21 is the coincidence spectrum obtained by gating upon the 1507-keV peak of the Bi^{203} spectrum. Note that 263.8-, 896.9-, and 820.2-keV peaks are seen in very strong coincidence. However, if we now run a set of gates which also subtracts the background one finds that the 820.2-keV transition has disappeared. This is so because the background of the 1507-keV

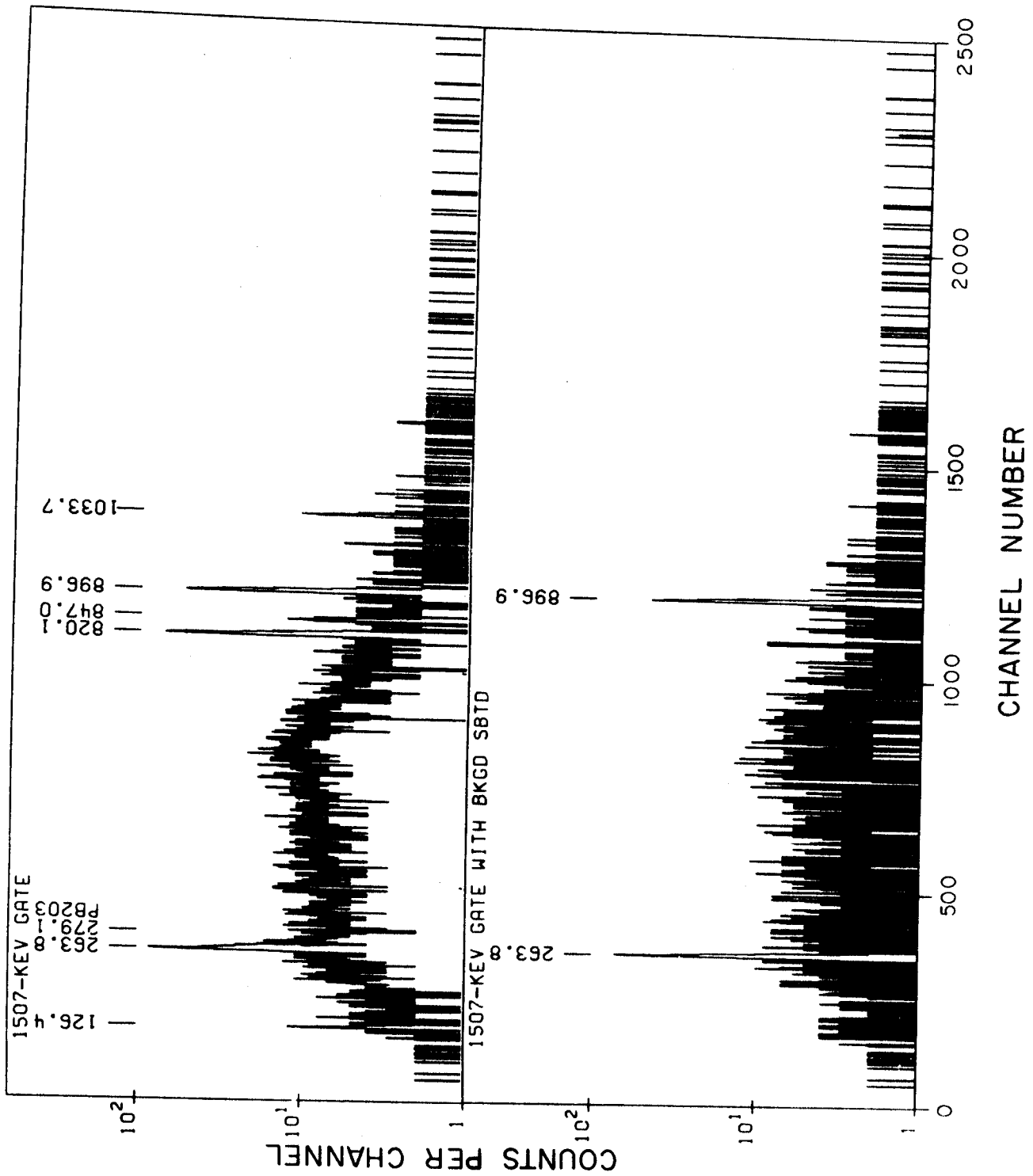

Fig. 21. Two coincidence spectra (from the Bi^{203} decay) illustrating the effectiveness of background subtraction in the EVENT RECOVERY program. (The spectra were prepared using the VALTAVA plotting routine described in section 2.5.1.)

peak contains a good portion of the strong 1847.6- and 1893.3-keV Compton edges. Both 1847.6- and 1893.3-keV transitions are in very strong coincidence with the 820.2-keV γ ray; consequently, the 820.2-keV γ ray appears strongly in the 1507-keV coincidence spectrum. If one were not aware of this problem, he could easily be misled by the "false" coincidence data.

Sections 3.1.4. and 3.2.4., which deal with the construction of the $Pb^{204,203}$ level schemes, contain most of the Pb^{204} and Pb^{203} coincidence plots which have been recovered during the course of this study. All the coincidence plots found in these sections were prepared using the versatile plotting routine, COINPLOT. A label, "XXXX-KEV GATE" indicates that no background has been subtracted, while a label "XXXX-KEV GATE WITH BKGD SBTD" specifies that background has been subtracted. Finally, a label such as "XXXX-KEV BKGD ONLY" specifies a spectrum of the background only for the XXXX-keV peak. Almost all peaks were recovered with and without background subtraction but space limitations preclude including all of them. One last word might be helpful: while all of the coincidence spectra are included, not all will necessarily be referred to explicitly but are included for completeness sake and in hopes that they may facilitate future investigations of these isotopes.

3.1.3.E. Delayed-coincidence Experiments

Only one long-lived state (in addition to Pb^{204m}) has been previously reported [Su50]. This is the 1274-keV state, with a $t_{\frac{1}{2}}$ of 260 ns. The prompt-coincidence experimental apparatus had a resolving time of $\approx$100 ns. Based upon this resolving time and a $t_{\frac{1}{2}}$ of 260 ns

for the 1274-keV state, ≈31% of the counts in the 375-keV prompt-coincidence spectra are true, real coincidence events; the remaining ≈69% are chance. The chance events can then be accounted for easily enough, and the remaining spectrum is the same as a delayed-coincidence spectrum. Consequently, no separate delayed-coincidence experiment was performed. If there are other delayed states present, then I am certainly going to miss them by not performing an anti- or delayed-coincidence experiment, but time considerations require that I forego these. As will be seen in section 3.1.4., >90% of the Bi^{204} decay intensity has been placed in this study and any remaining delayed state will not substantially alter the present data.

3.1.4. Construction of the Pb^{204} Level Scheme

Figure 22 shows schematically the ε decay of Bi^{204} to levels in Pb^{204} as interpreted from my data. These 30 excited states and 60 γ-ray transitions were placed utilizing primarily γ-ray singles and coincidence data, aided by energy sums and intensity balances. This section consists of the specific evidence and the logic used to arrive at this decay scheme for Bi^{204}. Before dashing headlong into an involved discussion of the Bi^{204} "decay scheme logic", however, let me take this brief moment to clarify the purpose of this section.

The preparation of a complicated decay scheme does not follow, as I may have erroneously implied, a hard and fast set of logical steps. Rather, one attempts to assimilate as much experimental data as humanly feasible and then allow these data to gestate or incubate until a pattern, seed, or idea seems to blossom and grow. There is no, as I rapidly discovered, "easy" way to construct a level

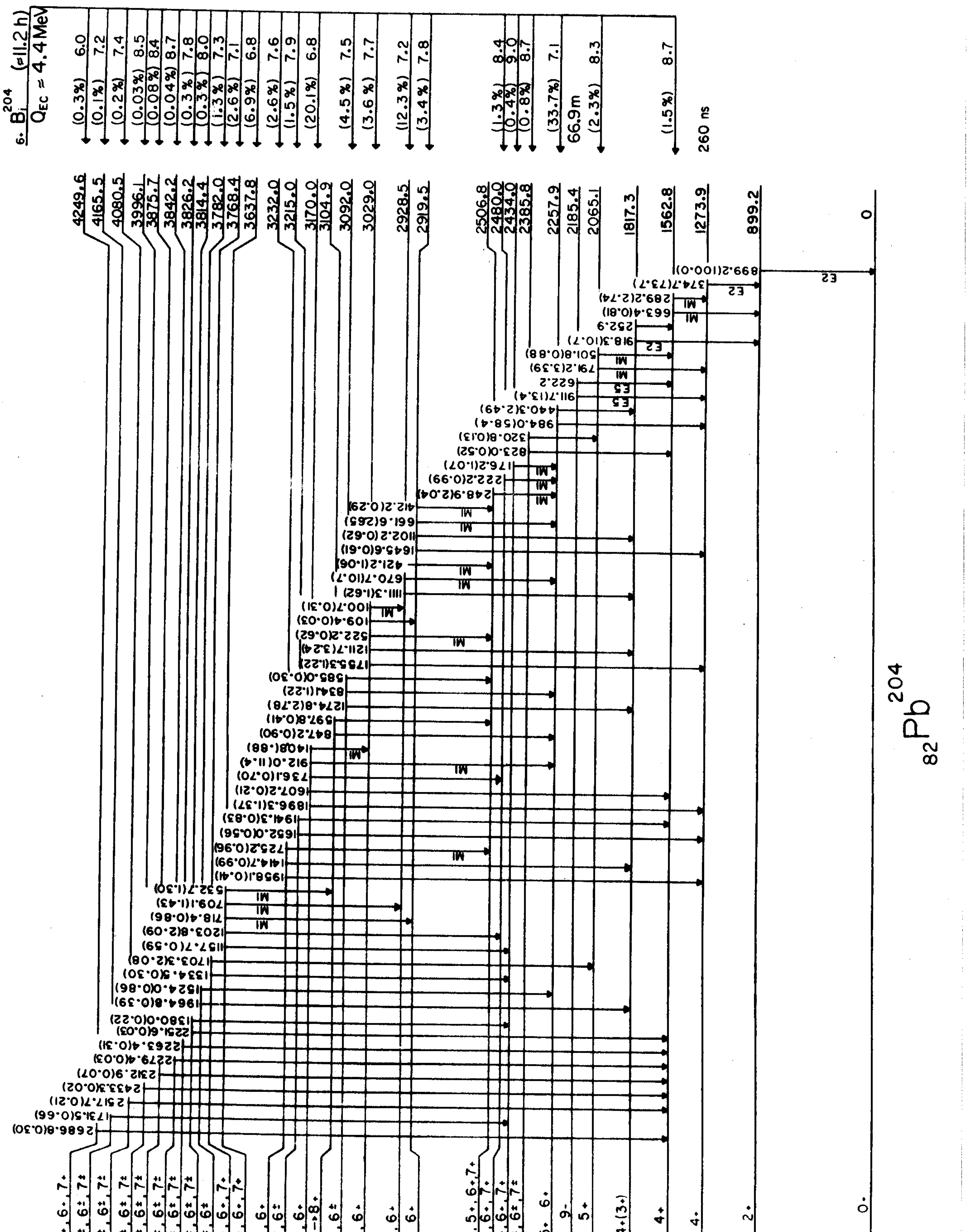

Fig. 22. The ε decay scheme of Bi^{204} proposed by the present study. All transitions were placed using coincidence data alone, without the use of energy sums.

scheme. Consequently, the sequence of steps ("decay scheme logic") which I present in this section, does not represent, even remotely, the method by which the initial decay scheme was constructed. It does, however, give any future investigations the final reasons for such placements as I have made, thereby making future assignments or deletions more understandable in light of my present decay scheme.

Before returning to the level assignments, I also want to look momentarily at the peculiarities of the Bi^{204} decay. Indeed, it is not a "typical" decay at all (though I defy making such a definition). Foremost, inasmuch as the ground states of Bi^{204} and Pb^{204} are 6+ and 0+, respectively, one would expect no direct feeding to the Pb^{204} ground state, as this would have to be a "super"-forbidden transition. Indeed then, everything (i.e., all γ-ray cascades) passes through the 899.2-keV first excited state. The most insidious difficulty, though, is aptly seen in the Bi^{204} γ-ray singles spectrum (Figure 16). Looking at this spectrum one should note that there are very few strong transitions: only some 30 of the 210 γ rays have intensities >1% of the 899.2-keV transition. This presents no inordinate difficulty for the energy and intensity calibrations, but when γ-γ coincidence spectra are being analyzed this causes monumental headaches (literally as well as figuratively). Because the majority ($\approx$85%) of the Bi^{204} γ rays are <1%, it has been exceedingly difficult to construct an internally consistent decay scheme from the available data. The levels I have placed seem to be reasonably accurate, but I would not be overly surprised if some of the very weak transitions I have placed are later shown to be inconsistent with better future data. With these comments and justifications,

let us turn to the business at hand - elucidating the evidence for placement of the following excited states and transitions.

3.1.4.A. 899.2-keV Level

The 899.2-keV γ ray is by far the most intense transition in the Bi^{204} singles. Even if this level had not been very well-placed in previous Pb^{204m} (and Bi^{204}) decay schemes, I would be forced to postulate this as a ground-state transition. If it were otherwise, one would expect other γ rays of comparable intensity that would de-excite the level fed by the 899.2-keV transition. This placement is also consistent with the even-mass neutron-deficient Pb isotope systematics, as summarized in [Be57], in which one would expect the first excited, high-lying 2+ level to fall between the 961- and 803-keV first excited states of Pb^{202} and Pb^{206}, respectively. While this argument may be a little circular, since Pb^{204} is better known than Pb^{202}, it certainly is not inconsistent with these systematics.

3.1.4.B. 1273.9-keV Level

One of the most intense transitions in the Bi^{204} spectrum is the 374.7-keV peak. This fact, coupled with the 899-keV coincidence spectrum in which the 374.7-keV peak is greatly enhanced, leads me to place the second excited level at 1273.9 keV. This is no great surprise since, again, this γ ray and level have been well-placed by previous Pb^{204m} investigations. Additionally, it is substantiated by the (p,t) work done by E.E. Holland et al. [Ho69] at the Wright Nuclear Structure Laboratory, Yale University, as seen in Figure 23. They see a very strong level at 1274 keV, in good agreement with my 1273.9-keV level.

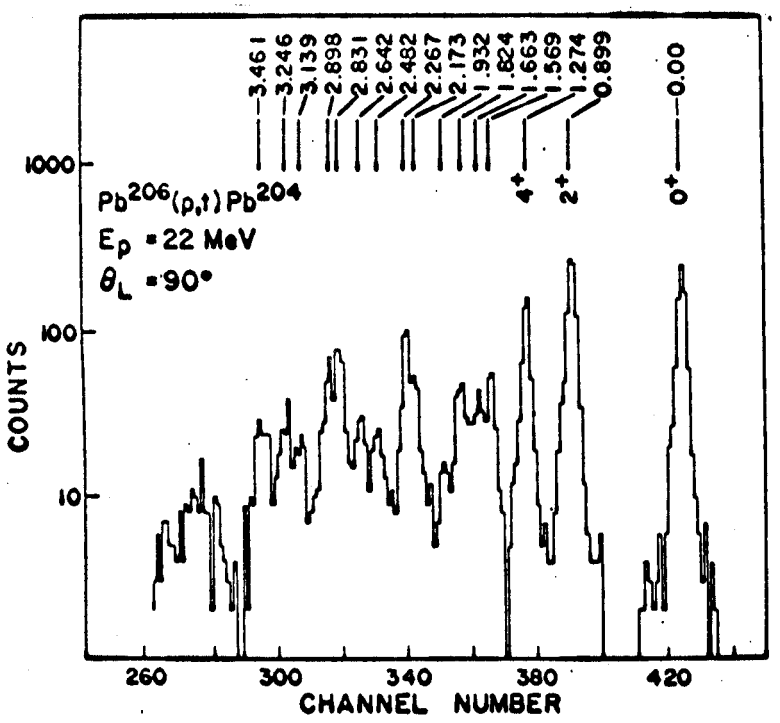

Fig. 23. Triton spectrum of the $Pb^{206}(p,t)Pb^{204}$ reaction obtained at 90° with 22-MeV protons [Ho69].

3.1.4.C. 1562.8-keV Level

Before progressing too far up the level scheme, one word of caution should be noted. When dealing with some 210 γ rays, energy sums (a + b = c and particularly d + e + f = g) have to be taken with the proverbial "grain of salt", since the chance sums number into the thousands. Accurate energy sums between already well-placed levels may have increased validity, but for initial placement of levels they will be of little usefulness.

The level at 1562.8 keV has also been predicted by Fritsch [Fr56] and Stockendal et al. [St58] in their previous investigations. The (p,t) work at Yale also shows a strong level at 1569 keV - quite close agreement considering the poorer resolution in the scattering data. Because the 1273.9-keV state has a measured lifetime of 260 ns, the 375-keV coincidence spectrum (all coincidence spectra referred to are found in Figure 24 at the end of this section) shows the expected strong 899.2-keV peak, but anything feeding the 1273.9-keV level is cut down significantly (coincidence resolving time was 100 ns, killing most of the feeding γ rays). Even so, the 289.2-keV peak is definitely seen. Looking back to the 899-keV coincidence spectrum, I also find the 663.4-keV peak definitely enhanced; thus, if the 663.4-keV γ ray feeds the 899.2-keV state, this would place a level at 1562.6 keV. In light of this evidence, a level is placed at 1562.8 keV, depopulating to each of the first excited states by the forementioned γ rays.

3.1.4.D. 1817.3-keV Level

The Yale (p,t) data indicate an excited state at 1824 keV. The tentative decay scheme advanced by Stockendal (Figure 17) predicts

peaks in the 791-keV coincidence spectrum. Unlike much of the Bi^{204} coincidence data, these coincidence peaks are strongly enhanced and the level placement clear cut. I, therefore, place a level at 2065.1 keV, depopulated by the appropriate γ rays to the 1562.8- and 1273.9-keV states. I also suggest that there is a level at 3768.4 keV, which populates the 2065.1-keV level by the intense 1703.3-keV γ. Admittedly, there might be a transition <100 keV which populates the 2065.1-keV level on which the 1703.3-keV could be placed. Since I have no way of checking this, I assume that this is not the case and assign a level at 3768.4-keV. (Fritsch and Stockendal have reported γ rays of 78, 90, and 92 keV using conversion-electron spectroscopy, but, assuming they are *M*1 transitions, they are not nearly intense enough to account for the 1703.3-keV transition.)

3.1.4.F. 2185.4-keV Level

Little need be said about the 2185.4-keV Pb^{204m} metastable state. It has been well investigated using very precise conversion-electron spectrometers, and the Pb^{204m} decay scheme (Figure 5) has been well discussed. In light of a discussion to be held shortly, I would like to side step a moment to discuss the characteristics of the Pb^{204m} decay. As the 2185.4-keV state has a very long half-life (66.9 m), one should see only the 911.8-, 374.7-, 899.2-keV cascade, and anything populating the state should be cut out by the very short (100 ns) resolving time. Conversely, in any γ cascade populating this state one would not expect to see the 899.2-keV γ ray, which one would expect to see in any γ cascade <u>not</u> involving the 2185.4-keV level. This led me to a flurry of interest, hoping to find a coin-

cidence spectrum which had no trace of the 899.2-keV transition, thus giving me a handle on the γ rays populating Pb^{204m}. However, much to my disgust, most of the coincidence data on the many weak γ rays were sufficiently poor so as to eliminate any hope of unequivocally placing any populating transitions on this basis. Another possible handle to the populating γ's or γ cascades might be a very precise gated anti-coincidence experiment in which any 899- or 375-keV γ is discriminated against. This would effectively stop all Bi^{204} γ's which do not pass through the long-lived Pb^{204m} isomeric state and allow all other γ's to be recorded. Hopefully this will permit me to determine the γ rays feeding the 2185.4-keV state with a high degree of confidence. As of this writing this experiment has not been performed but definitely is in the planning and preparation stage.

3.1.4.G. 2257.9-keV Level

The assignment of this level is perhaps one of the most unambiguous in the decay scheme. The 918-keV spectrum shows (in addition to others) a very strong 440.3-keV coincident transition, and the 440-keV spectrum shows an enhanced 918.3-keV γ as well. No trace of the 440.3-keV γ is found in the coincidence spectra of the other peaks found enhanced in the 918-keV spectrum; the 440.3-keV γ ray therefore directly feeds the 1817.3-keV level. Also, the 375-keV gated coincidence spectrum indicates a very strong 980.4-keV γ in coincidence with the 374.7-keV γ. Considering the intensity (58.4% of 899.2-keV peak), the only consistent choice would be to have the 984.0-keV γ ray feeding the 1273.9-keV state. This leads me to place

a state with a high degree of confidence at 2257.9 keV. The (p,t) data (Figure 23) clearly substantiate this, showing a strongly excited state at 2267 keV.

3.1.4.H. 2385.8-keV Level

Gating upon the 289.2-keV transition in the integral coincidence spectrum, one sees a strong enhancement of the 501.8-, 1652.0-, 164.9-, and 823.0-keV peaks. However, the 1652-, 501-, 164-keV coincidence spectra show no enhancement of the 823.0-keV transition. Based upon this I place the 823.0-keV γ as populating the 1562.8-keV state and depopulating a 2385.8-keV state. In addition, the 320-keV gated spectrum shows a slight enhancement of the 791.2- and 501.8-keV peaks. This, coupled with a precise energy sum, leads me to place a transition between the 2385.8- and 2065.1-keV states. The 320.8-keV transition, being as weak as it is, makes this transition slightly questionable, but nevertheless it appears to be good enough to warrant placement.

3.1.4.I. 2480.0-keV Level

Gating upon the very strong 984.0-keV transition produces a very excellent coincidence spectrum. In this spectrum the 222.1-keV peak is greatly enhanced and easily separated from the rest of the 212-222-keV quartet. The 222-keV coincidence spectrum shows only one strongly enhanced γ ray, at 984.0 keV. Thus, the 222.1-keV γ must directly populate the 2257.9-keV level. The 222-keV spectrum also shows a definite coincidence with the small 1157.7-keV peak, which, if this γ ray were in direct cascade with the 222.1-keV γ, would place a level at 3637.7 keV, in excellent agreement with a 3637.9-keV

level to be proven later. I therefore place a level at 2480.0 keV, depopulated by the 222.1-keV γ and populated by the 1157.7 keV γ. Once again the (p,t) data also confirm this placement with a level at 2482 keV.

3.1.4.J. 2506.8-, 2919.5-, and 2928.5-keV Levels

Each of these levels was placed primarily on the basis of the enhancement of the 248.9-, 661.6-, 670.7-, and 912.0-keV peaks in the 984-keV gated coincidence spectrum. Checking the individual coincidence spectra for each of these peaks assured me that they were not successive cascades but actually directly feeding the 2257.9-keV state. These levels have additional transitions which "lock" these levels into the decay scheme even more firmly, and these are now more thoroughly discussed below.

The 248-keV gated spectrum reveals coincident γ rays of 522.2, 421.6, and 412.2 keV. Each is not in coincidence with another, as may be readily discerned from their individual gated spectra. The 248.9-keV γ feeding the 2257.9-keV level places a level at 2506.8 keV immediately. The 412.2- and 421.6-keV transitions populating this level give rise to additional levels at 2919.5 and 2928.5 keV, these being the same as the levels derived from the 661.6 and 670.7-keV γ's feeding the 2257.9-keV state.

The 918-keV coincidence spectrum adds even further support to these levels in that, among others, there is a strong enhancement of the 1102.2- and 1111.3-keV peaks. These γ rays, if populating the well-known 1817.3-keV state, would suggest levels at 2919.5 and 2928.5 keV. The coincidence data of these γ rays support this assumption.

Therefore, I place levels at 2506.8, 2919.5, and 2928.5 keV with a high degree of certainty.

3.1.4.K. 3029.0- and 3092.0-keV Levels

These levels were initially placed as a consequence of the strong enhancement of the 1211.7- and 1274.8-keV γ's in the 918-keV coincidence spectrum.

The level at 3029.0 keV is additionally supported by a 522.2-keV transition which is seen in the 248-keV gated spectrum. Also, on the basis of only mediocre data, depopulating transitions of 100.7 and 109.4 keV (to 2928.5- and 2919.5-keV states) were placed with only fair confidence. Finally, the 140-keV coincidence spectrum shows an enhancement of the 1211.7-keV peak (and vice versa). If the 140.8-keV γ does indeed populate the 3029.0-keV state, then it must be depopulating the now well-known 3170.0-keV level. To add to this evidence, the 374-keV spectrum shows a weak 1755.3-keV γ ray, which, when added to the 1273.9-keV level, lends even further evidence for the 3029.0-keV state. Under such a barrage of coincidence data and energy sums there appears to be little room for doubt, the 3029.0-keV state most certainly exists.

The 3092.0-keV level in Bi^{204} is almost as firmly rooted as the 3029.0-keV level. The 248-keV coincidence spectrum shows enhanced transitions of 585.0 and 597.8 keV as well as 522.2 keV. If the 585.0-keV transition directly populates the 2506.8-keV state (as the coincidence data indicate), then it is one of the transitions depopulating the 3092.0-keV excited state. Additionally, the 834.1-keV γ is found to be in definite coincidence with the 984.0-keV γ.

I, therefore, place the 834.1-keV γ as depopulating the 3092.0-keV state and feeding the 2257.8-keV state. Once again, like the 3029.0-keV level, the 3092.0-keV excited state (and the transitions from it) does not appear to be in any doubt at all.

3.1.4.L. 3104.9-keV Level

This level is probably one of the least certain levels in Pb^{204} that I have ventured to place. It is based upon the enhancement of the 597.8- and 847.2-keV γ's in the 248- and 984-keV coincidence spectra, respectively. Placing each of these upon its respective level yields a state at 3104.9 keV. Further evidence comes from the 532-keV gated spectrum in which the 847.2- and 597.8-keV transitions are intensified, the latter only weakly. Also, the 532.7-keV peak is increased in each of these (597- and 847-keV) coincidence spectra.

While it is not so firmly entrenched as some of the other levels, I nevertheless place a level in Pb^{204} at 3104.9 keV.

3.1.4.M. 3170.0-keV Level

Without a doubt this is the most interesting level I have placed in Bi^{204} decay scheme, because of its peculiar depopulating transition - the 912.0-keV γ ray. Perhaps I should clarify this impetuous statement.

In all the previous investigations of Bi^{204} and Pb^{204m} decays a ≈911.7-keV transition has been reported. This γ ray has always been placed as depopulating the Pb^{204m} 9-,2185.4-keV metastable state as an *E*5 transition to the 1273.9-keV state. The present Ge(Li) singles spectrum showed no apparent broadening of the initially reported 911.8-keV peak; yet the 984-keV coincidence

spectrum showed a very strong 912.0-keV enhancement. If indeed all of the 911.8-keV "peak" belonged to the *E*5 transition, then no 911.8-keV transition should be seen in any coincidence spectra - yet in the 984-keV spectrum a strong 911.96-keV peak is definitely seen. The only consistent explanation for this phenomenon is that the 911.8-keV "peak" is really a very closely-spaced doublet. Evidence for this can be seen by comparing the "any" coincidence spectra with the Bi^{204} singles. In the singles the 911.8-keV doublet is more intense than the 918.3-keV peak adjacent to it, but in the *X* and *Y* any coincidence spectra the opposite holds true. If the 911.8-keV "peak" were in reality only a single peak, the 911.8-keV transition should have disappeared entirely (except for chance coincidence events).

Searching for further confirmation that the 911.8-keV "peak" is indeed a doublet led me to analyze the peaks in the 984- and 440-keV coincidence spectra. The peaks analyzed in the 984-keV spectrum were at 176.2, 222.1, 248.9, 661.6, 670.7, 912.0, and 1203.8 keV. The intensities of these peaks were normalized to the 670.7-keV transition and are listed in the second column of Table 8. The same set of peaks in the singles spectrum was also normalized to the 670.7-keV γ ray and is listed in the third column. Excellent agreement results, with the exception of the 911.8-keV transition, whose intensity is down by over 1/2 (from 1.53 in the singles to 0.72 in the 984-keV coincidence spectrum). No other coincidence spectrum shows the 911.8-keV "peak" so strongly; yet the intensity is down by 1/2 - the only internally consistent rational is that the 911.8-keV "peak" is really a doublet.

Table 8. Ratios of several γ rays to the 670.7-keV γ in the 984-keV coincidence spectrum and in the Bi^{204} singles spectrum.

γ-ray energy (keV)[a]	Ratio in the 984-keV coincidence spectrum.[b]	Ratio in the Bi^{204} singles spectrum.[c]
176.2	0.60	0.70
222.2	0.36	0.49
248.9	0.96	0.86
661.6	0.20	0.25
670.7	1.0	1.0
911.8	0.72	1.53
1203.8	0.06	0.09

[a] γ-ray energies from the present study.

[b] Ratio of the area of the γ ray in column one to the area of the 670.7-keV γ in the 984-keV coincidence spectrum. (The spectrum was taken using the 2.5% Ge(Li) detector as the display detector.)

[c] Ratio of the area of the γ ray in column one to the area of the 670.7-keV γ in the Bi^{204} singles spectrum. (The singles spectrum was also taken using the 2.5% Ge(Li) detector. As the efficiency curve is identical for both the 984-keV coincidence spectrum and the singles spectrum, I have used relative areas rather than intensities, but this in no way affects the results.)

Yet further evidence comes from examining the 440.3/911.8 area ratios in the 670- and 911-keV coincidence spectra. If the 911.8-keV transition does feed the 2257.9-keV state, the ratios should be identical. Table 9 shows the almost unbelievable results that were obtained. From the data listed in Table 8 I calculate that 46% of the 911.8-keV "peak" belongs to the transition feeding the 2257.9-keV level, while the remaining 54% belongs to the isomeric $E5$ transition. The energies calculated for these respective peaks were 911.96 and 911.73 keV, respectively. This actually makes my new value of 911.73 keV for the $E5$ more compatible with the previously reported values of 911.7 keV for the isomeric transition as in the Pb^{204m} decay.

On the basis of all this evidence, I place a level at 3170.0 keV, depopulating to the 2257.9-keV excited state by a 911.96-keV γ. Two other transitions from the 3170.0-keV state are supported by the coincidence data, a 1896.3-keV γ (to the 1273.9-keV state) and a 1607.2-keV γ ray (to the 1562.8-keV state). As a final fillip, the (p,t) data suggest a level at 3139±25 keV - in fair agreement with my 3170.0-keV state.

3.1.4.N. 3215.0-keV Level

The 289-keV coincidence spectrum shows, among others, a strong enhancement of a 1652.0-keV peak. Inasmuch as the 1652-keV gated coincidence spectrum shows a strong enhancement of only a 289.2-keV γ, I place the 1652.0-keV transition such that it directly feeds the 1562.8-keV excited state, revealing a level lying at 3215.0 keV. The 1941.3-keV γ was placed as depopulating the 3215.0-keV state

Table 9. Ratio of the 440.3-keV γ to the 984.0-keV γ in the 670- and 911-keV coincidence spectra.

γ-ray energy (keV)	Area of γ ray in 670-keV coincidence spectrum†	Area of γ ray in 911-kev coincidence spectrum†
440.3	127	129
984.0	682	632
Ratio of 440.3-keV γ to 984.0-keV γ in the 670-keV coincidence spectrum	0.19	
Ratio of 440.3-keV γ to 984.0-keV γ in the 911-keV coincidence spectrum		0.20

†Both spectra were taken using the same 2.5% Ge(Li) detector as the display detector. Area is given as the number of counts in the peak of interest, as determined by the MOIRAE analysis program.

solely on the basis of its coincidence spectrum, in which only the 374.7-keV transition was enhanced. Even though this level is still slightly shaky, these two transitions appear to be certain enough to support such a placement.

3.1.4.O. 3232.0-keV Level

This level was assigned on the basis of the strong enhancement of the 1414.7-keV γ (along with several others) in the 918-keV coincidence spectrum. Conversely, the 918.3-keV peak was strongly intensified in the 1414-keV gated coincidence spectrum. If the 1414.7-keV transition does indeed feed the 1817.3-keV excited state, then there must be another excited state at 3232.0 keV. Additional evidence is lent by the enhancement of a 1958.1-keV γ in the 374-keV coincidence spectrum (and, of course, the inverse as well) and by the enhancement of a 725.2-keV γ in the 248-keV spectrum (725.2-keV γ feeding the 2506.8-keV level). These transitions can be seen in Figure 24. This, then, appears to be sufficient to postulate a level at 3232.0 keV in Pb^{204}.

3.1.4.P. 3637.8-keV Level

The assignment of the 3637.8-keV state is quite certain. It is based upon several pieces of evidence. The enhancement of the 709.1- and 718.4-keV γ's in the 670- and 661-keV γ coincidence spectra, respectively, together suggest a level at 3637.8 keV. (Conversely, the 661.6- and 670.7-keV transitions are seen in the 709- and 718-keV coincidence spectra.) Additionally, the very strong enhancement of the 1203.8-keV γ in the 176.2-keV spectrum (and vice versa) and the weak increase in the 1157.7-keV transition in the 222-keV gated

spectrum led me to conclude that there is an excited state at 3637.8 keV.

3.1.4.Q. 3782.0-keV Level

Much to my chagrin, this level seems to be still in some doubt, although I personally "feel" (through a marvelously unscientific sense of intuition) that it is correctly placed. It is based solely upon the enhancement of the 984.0-keV γ in the 1524-keV spectrum and of the 918.3-keV γ in the 1964-keV coincidence spectrum. The inverse relationships are present but much weaker (and in more doubt) because of the small intensities of the two γ's involved. Even so, I place a level, with some reservation, at 3782.0 keV.

3.1.4.R. 3814.4-, 3826.2-, 3842.2-, 3875.7-, 3996.1-, 4080.5-, and 4249.6-keV Levels

Most of these levels are placed on the basis of only mediocre coincidence data, and absolute placement must await better coincidence technology. However, the enhancements of the 289.2-keV γ in the 2251-, 2263-, 2279-, 2312-, 2433-, 2517-, and 2686-keV gated coincidence spectra led me to postulate levels at 3814.4, 3826.2, 3842.2, 3875.7, 3996.1, 4080.5, and 4249.6 keV. Surely many of the other high energy γ rays could be similarly placed (i.e. feeding the 1273.9- or 1562.9-keV excited states), but the low efficiency of the detector and low intensity of the γ rays prevented sufficient coincidence evidence to warrant such a conclusion - and thus they were not assigned.

3.1.4.S. 2434.0-keV Level

This level was reserved for the next to last for a very

important, but honest, reason - it was the next to last in being placed. Ever since the coincidence data recovery began, the 1203.8-, 176.2-, and 984.0-keV cascade (see Figure 22) has been nearly a total enigma. From the three coincidence spectra of the cascade members it was immediately obvious that they indeed did form a "chain". Almost immediately (in conjunction with other data) the 984.0-keV transition was placed on the "bottom". The major mystery was whether the 1203.8- or 176.2-keV γ was on "top". The (p,t) scattering data showed a possible level at 3461 keV; as a result I initially placed the 1203.8-keV γ as feeding the well-known 2257.8-keV level, with the 176.2-keV transition then feeding the level at 3461 keV. While this satisfied the (p,t) data, it left me with an internally inconsistent decay scheme and was subsequently discarded. For a long time nothing further could be concluded. Finally, upon careful reexamination I found three enhanced peaks in the 176-keV coincidence spectrum (other than the strong 1203.8- and 984.0-keV γ's) which corresponded to transitions between the 2434.0-keV state and three known excited states, a 736.1-keV γ (from the 3170.0-keV state), a 1334.5-keV γ (from the 3768.4-keV state) and a 1380.0-keV γ (from the 3814.4-keV state). While none of these (except the 1203.8- and 984.0-keV transitions) is very intense or greatly or clearly enhanced, the fact that there are 5 γ's which are transitions between known levels certainly indicates that it is rather safe to place a level at 2434.0 keV.

3.1.4.T. 4165.5-keV Level

A level at 4165.5 keV is placed only on a single piece

of evidence. In the 176-keV coincidence spectrum the 1731.5-keV γ is quite clearly enhanced (conversely, in the 1731-keV spectrum the 176.2-keV γ is enhanced). Since the 1731.5-keV transition cannot be depopulating the 2434.0-keV state, it clearly must be feeding this level. This assumption, in turn, then places a level at 4165.5 keV, since in no other recovered coincidence spectrum did I see the 1731.5-keV transition so clearly enhanced.

3.1.4.U. Comments

Before abandoning this "decay scheme logic" section a few well-chosen words are certainly in order. The construction of the Bi^{204} decay scheme shown in Figure 22 was definitely not a trivial task. The intensities of nearly all the peaks are so low as to make the present coincidence data, as fine as they were, extremely difficult to interpret. The decay scheme for Bi^{204} which I have presented, is the most consistent of which I was able to construct. While most of the levels seem to be quite firmly established, a few of the weak transitions between these levels appear to be slightly questionable. Even so, this decay scheme is a far cry from the previous decay scheme that had been suggested (Figure 17). Note the several changes that have been made. Levels at 2477, 1944, and 2254 keV have not been observed (nor their associated transitions); the 248.7-keV transition between the 1817.3- and 2065.0-keV states has been replaced, the 543.4-keV γ was not found between the 1273.9- and 1817.3-keV levels and was removed; and the 690.8-keV γ was not observed. Placing 60 γ rays (out of 210) in a decay scheme may not, normally, seem like anything to crow about; however, when one considers that

these transitions account for ≈90% of the decay, one is not so concerned about the absolute number of γ rays assigned. The 60 γ rays placed in this section represent only those which can be placed primarily upon coincidence data, energy sums being somewhat risky when one has >200 γ rays. During the course of this study many other transitions and levels were suggested by the coincidence data and energy sums but sufficient evidence was lacking to place these with a high degree of confidence. Figure 25 shows a decay scheme for Bi^{204} with these additional γ rays and excited energy states included. Without further evidence these cannot be placed with unqualified certainty, but the existing evidence seems to indicate that these additional transitions and levels may exist. The placement of those transitions for which there is some coincidence evidence are denoted by a semicircle at the base of the transition, while the rest are placed solely on the basis of energy sums. On the right hand side of the diagram are some possible levels and their associated γ rays which may feed the 2185.4-keV isomeric state. These were obtained by using the TAKE CARE program to scan up the existing decay scheme through the already known states and searching for levels which might be "locked" in by several γ's between the 2185.4-keV and remaining states. While not necessarily adequate, this may lead to states which do indeed feed the 2185.4-keV level. No separate calculations (e.g. external quantum number assignments, and log *ft*'s) will be made for these levels, although one might wish to do so at some later date.

Fig. 24. The γ-γ coincidence spectra from the Bi^{204} decay. The spectra were recovered from the coincidence data stored on magnetic tapes using EVENT data-taking routine. Sample titles of the coincidence spectra and their meanings are found below:

100-KEV GATE: A gated region from which background has <u>not</u> been subtracted;

100-KEV GATE WITH BKGD SBTD: A gated region from which background <u>has</u> been subtracted;

100-KEV BKGD ONLY: Spectrum of the background adjacent to the 100-keV gated region.

Unless otherwise specified, all spectra are displayed from the *X* axis.

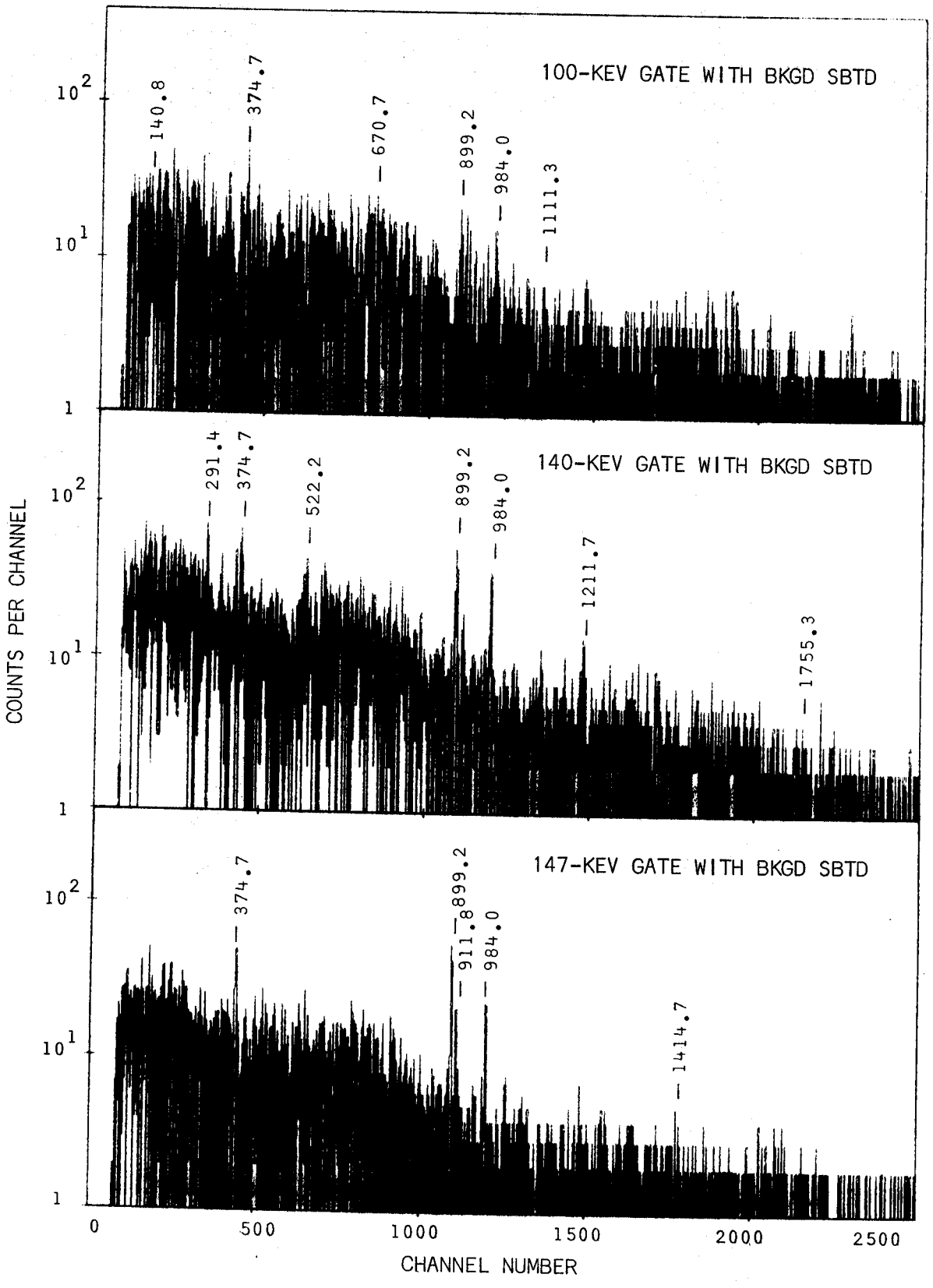

Fig. 24. (continued)

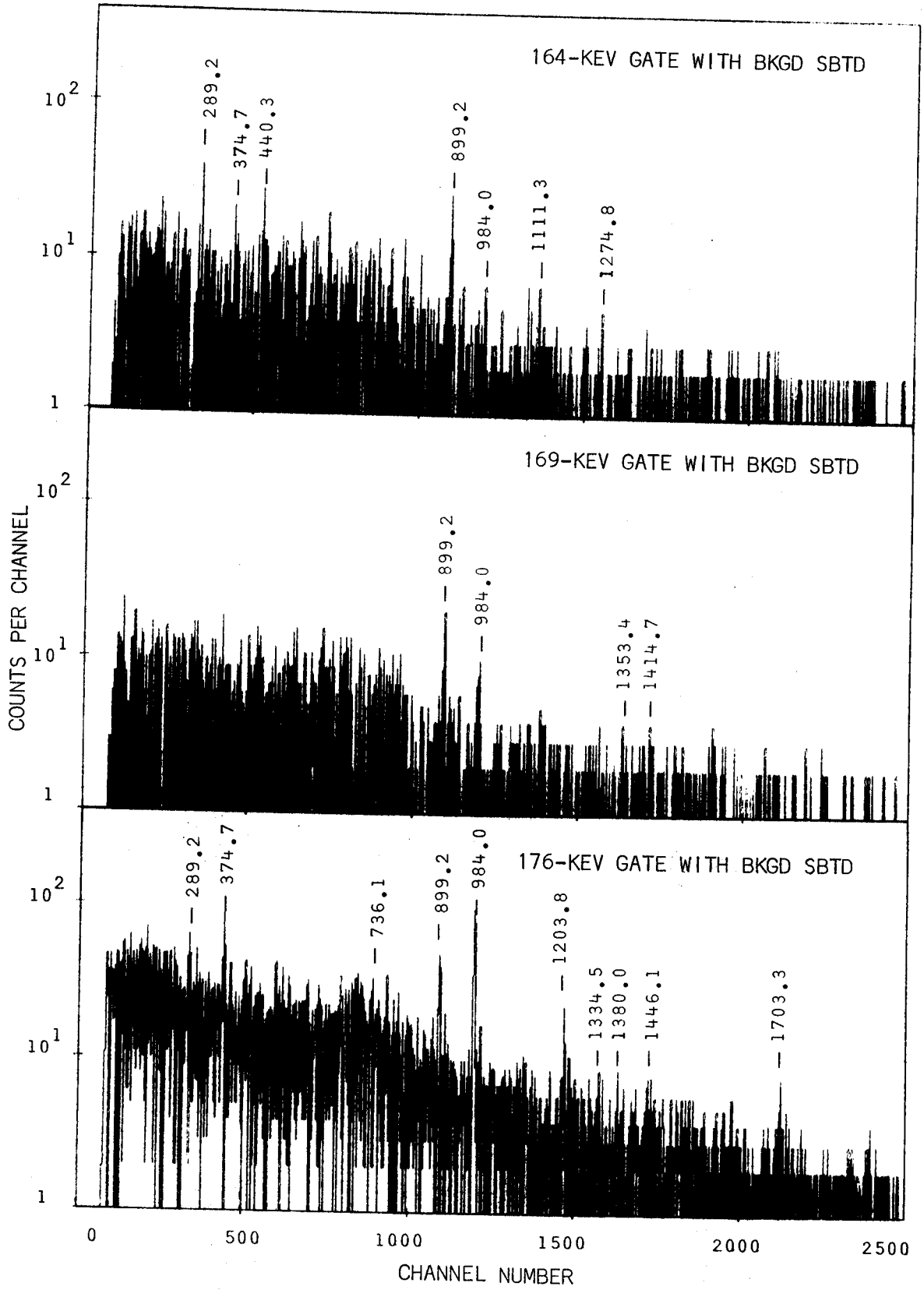

Fig. 24. (continued)

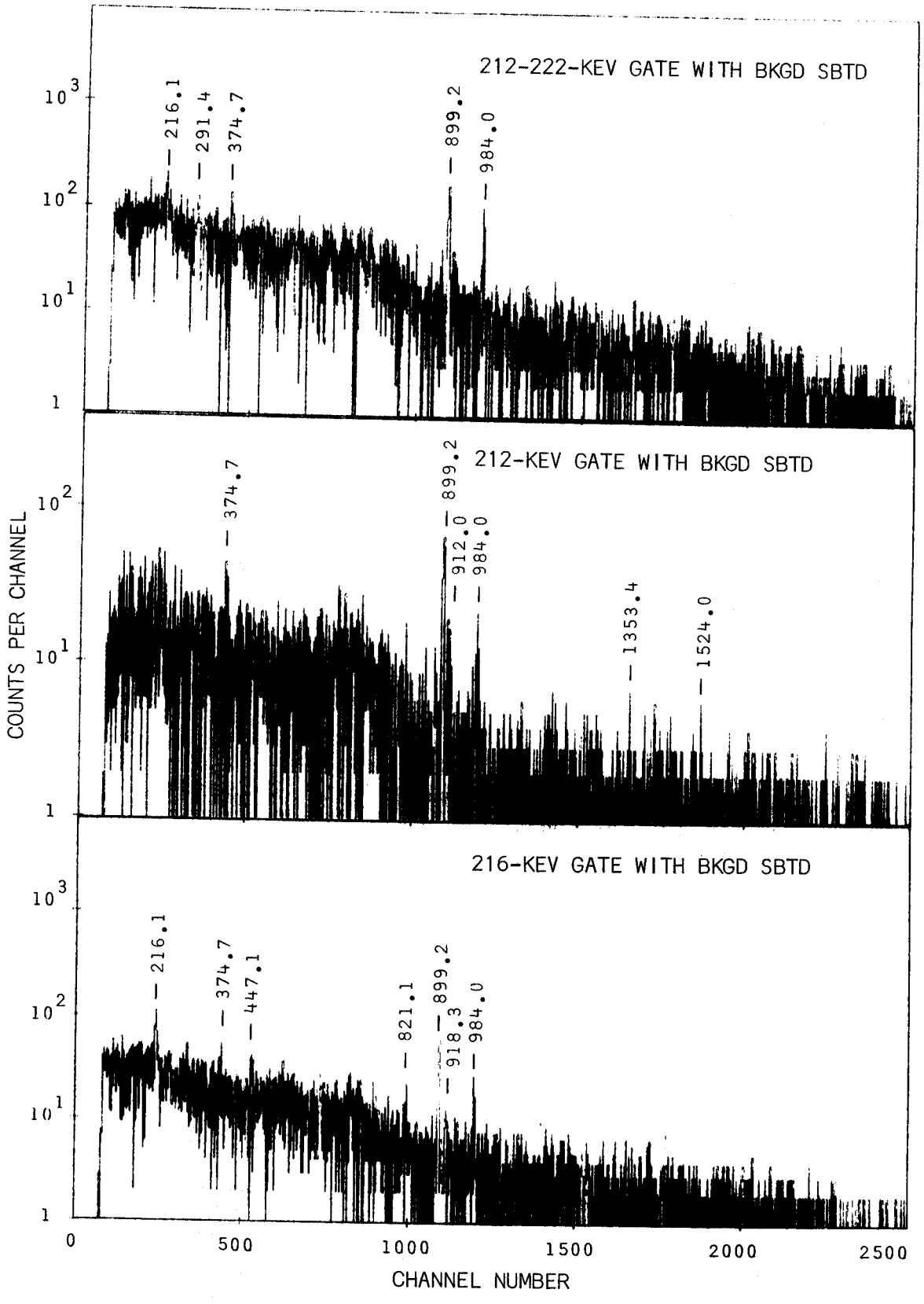

Fig. 24. (continued)

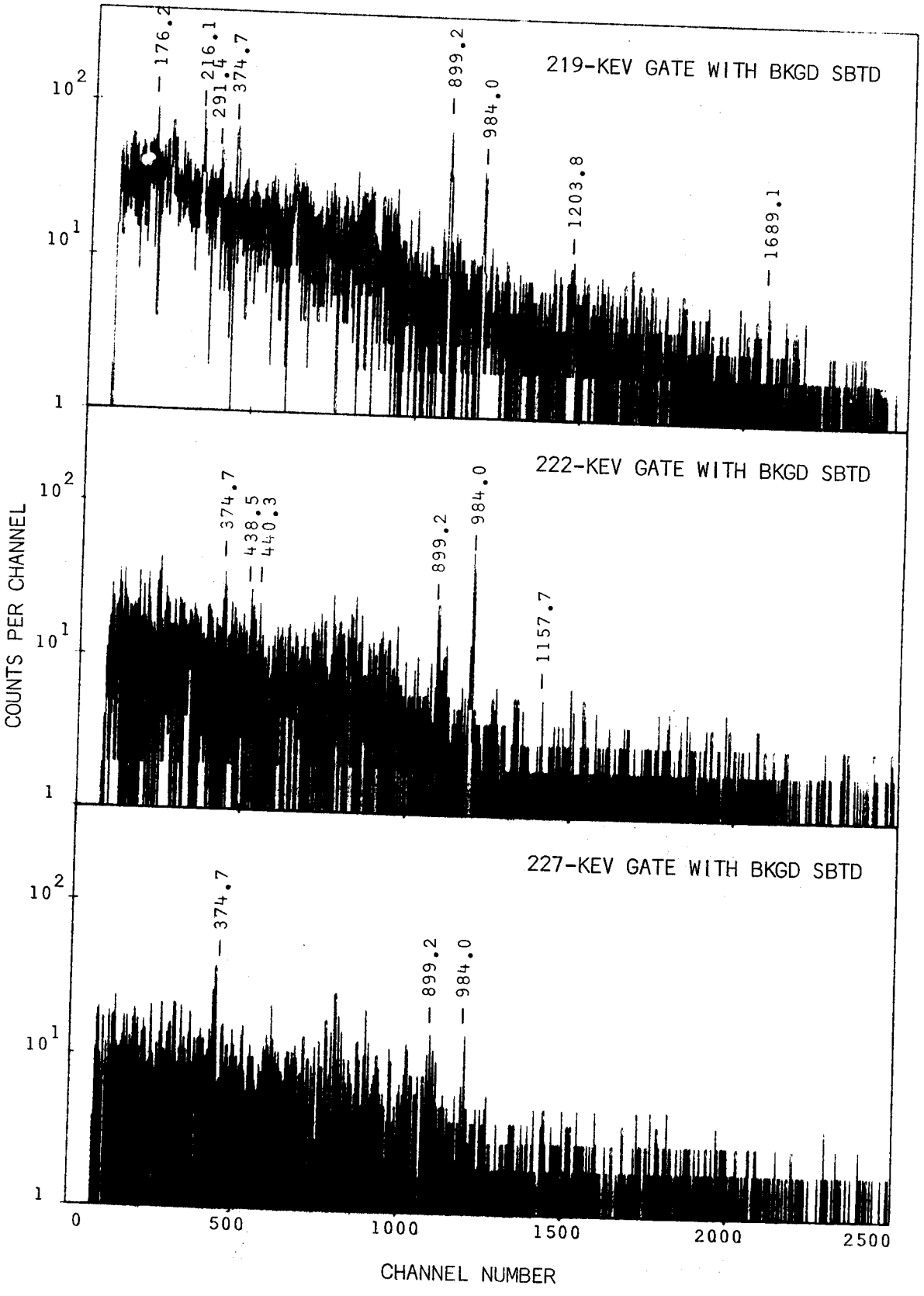

Fig. 24. (continued)

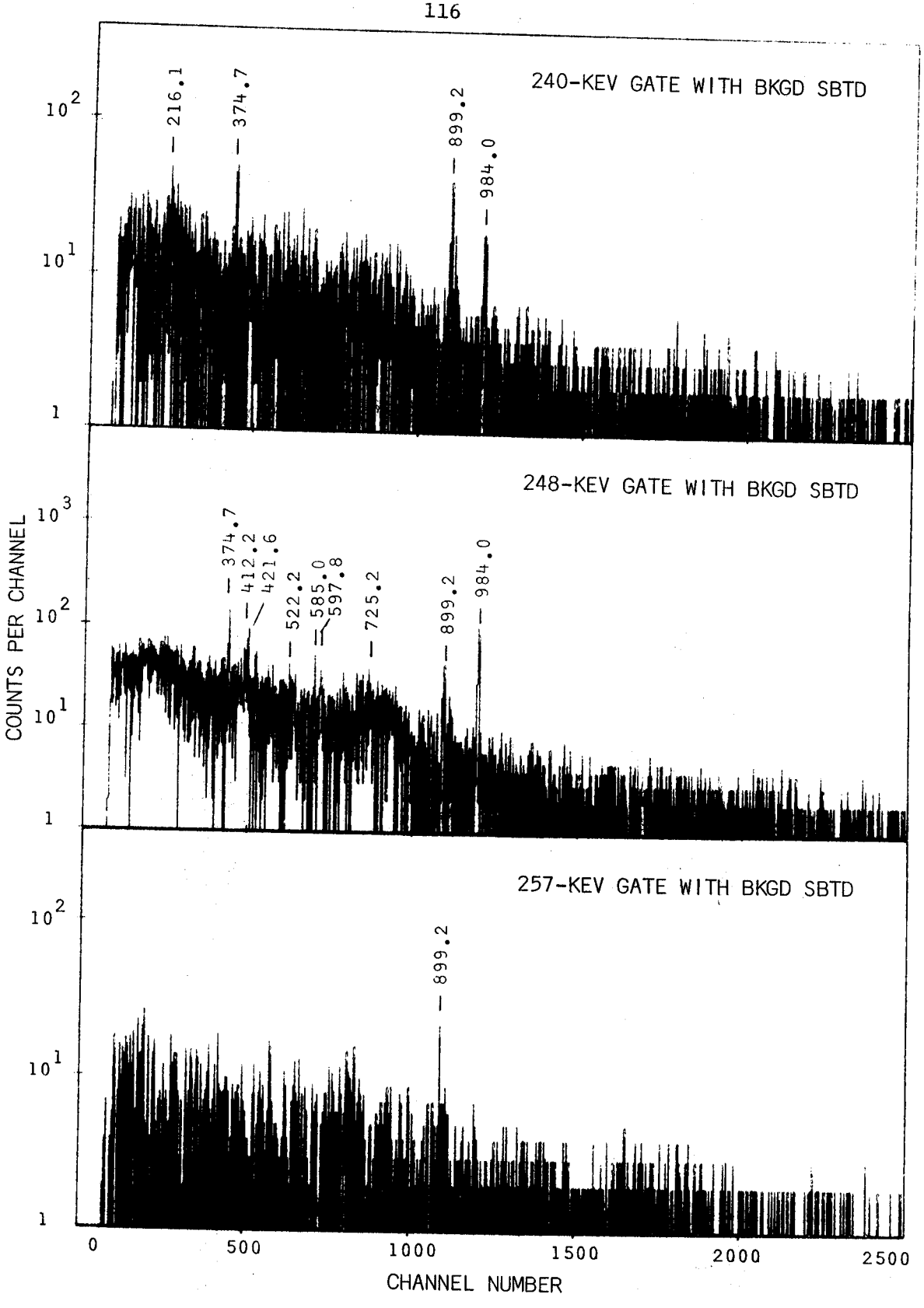

Fig. 24. (continued)

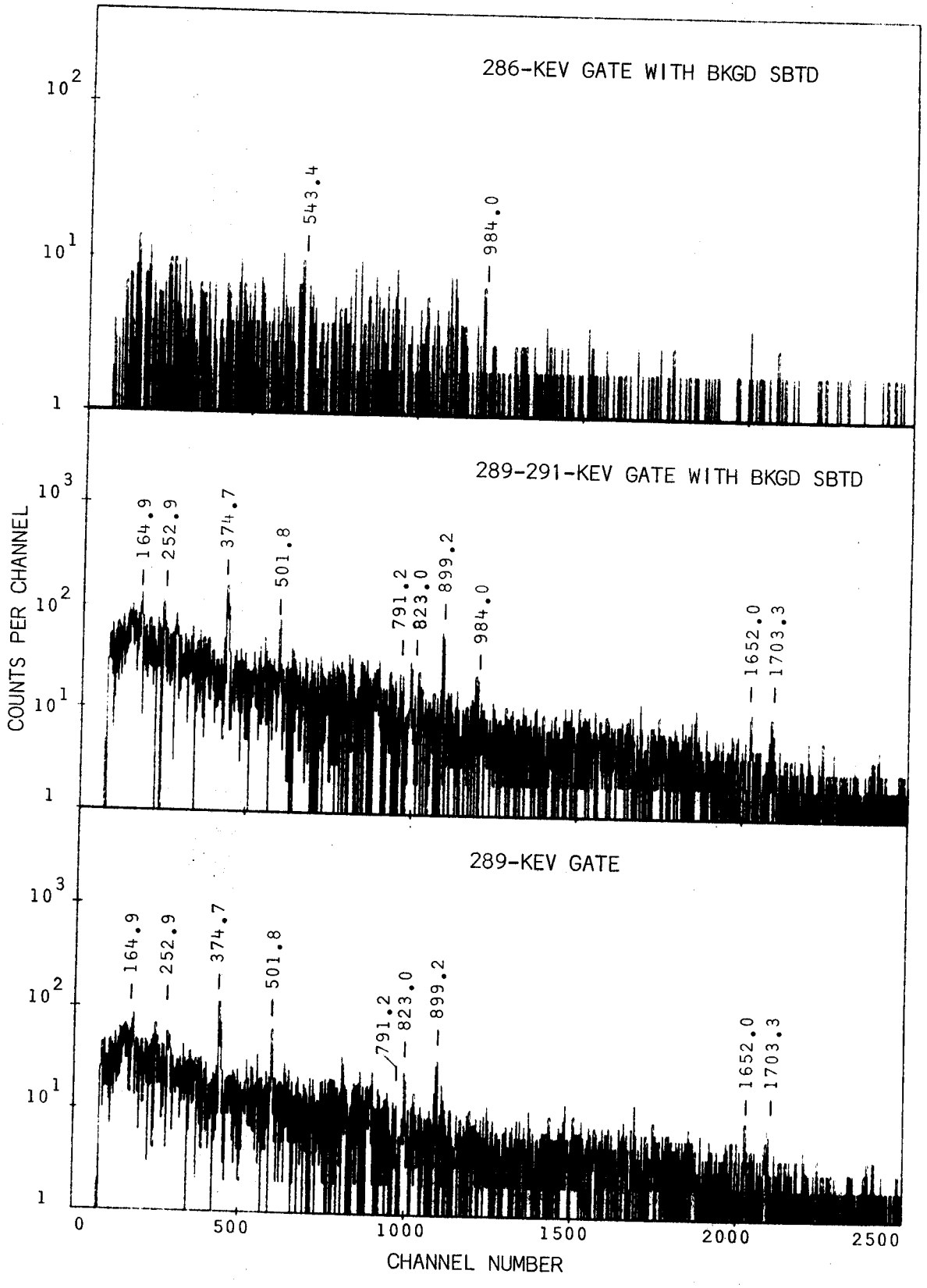

Fig. 24. (continued)

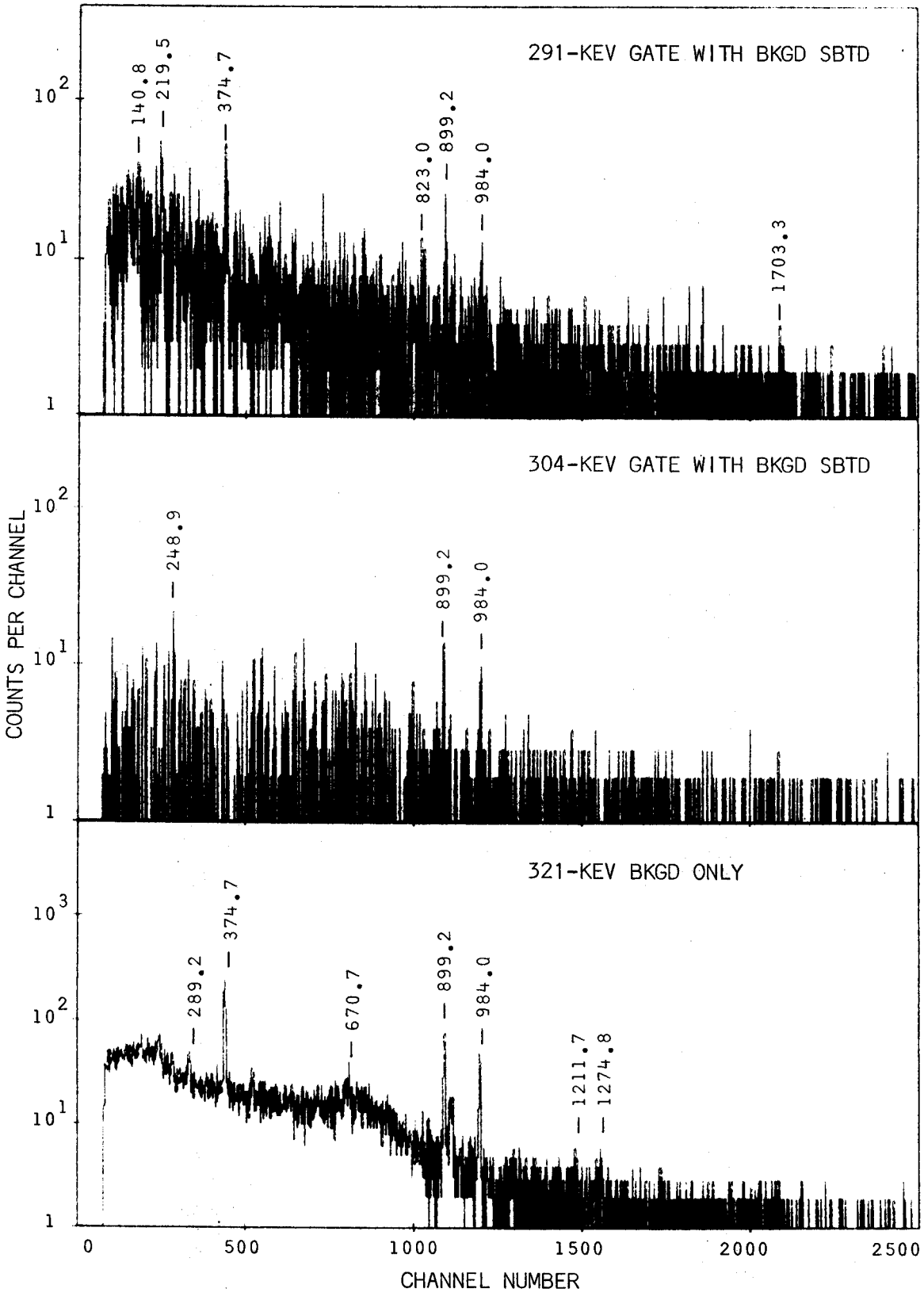

Fig. 24. (continued)

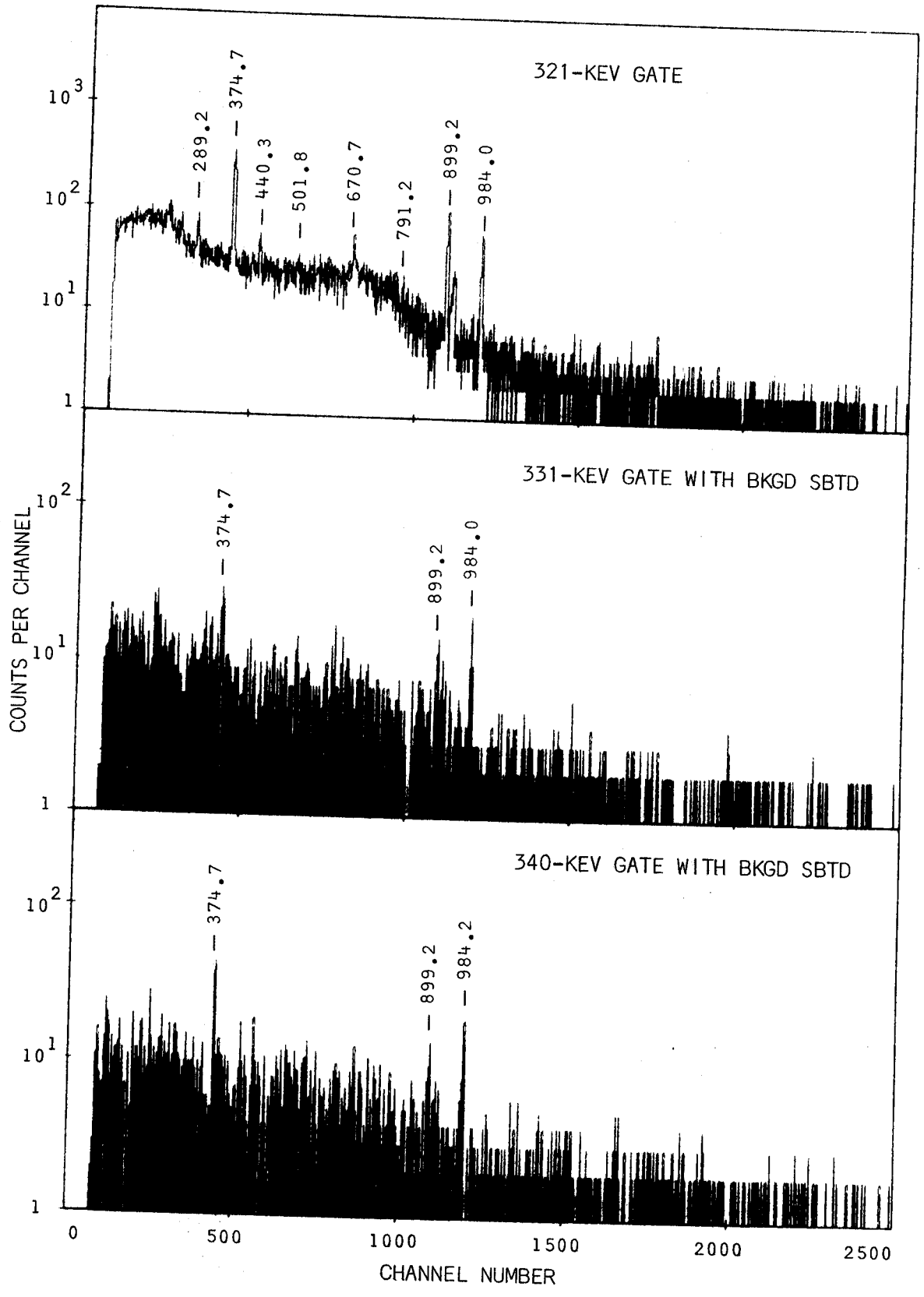

Fig. 24. (continued)

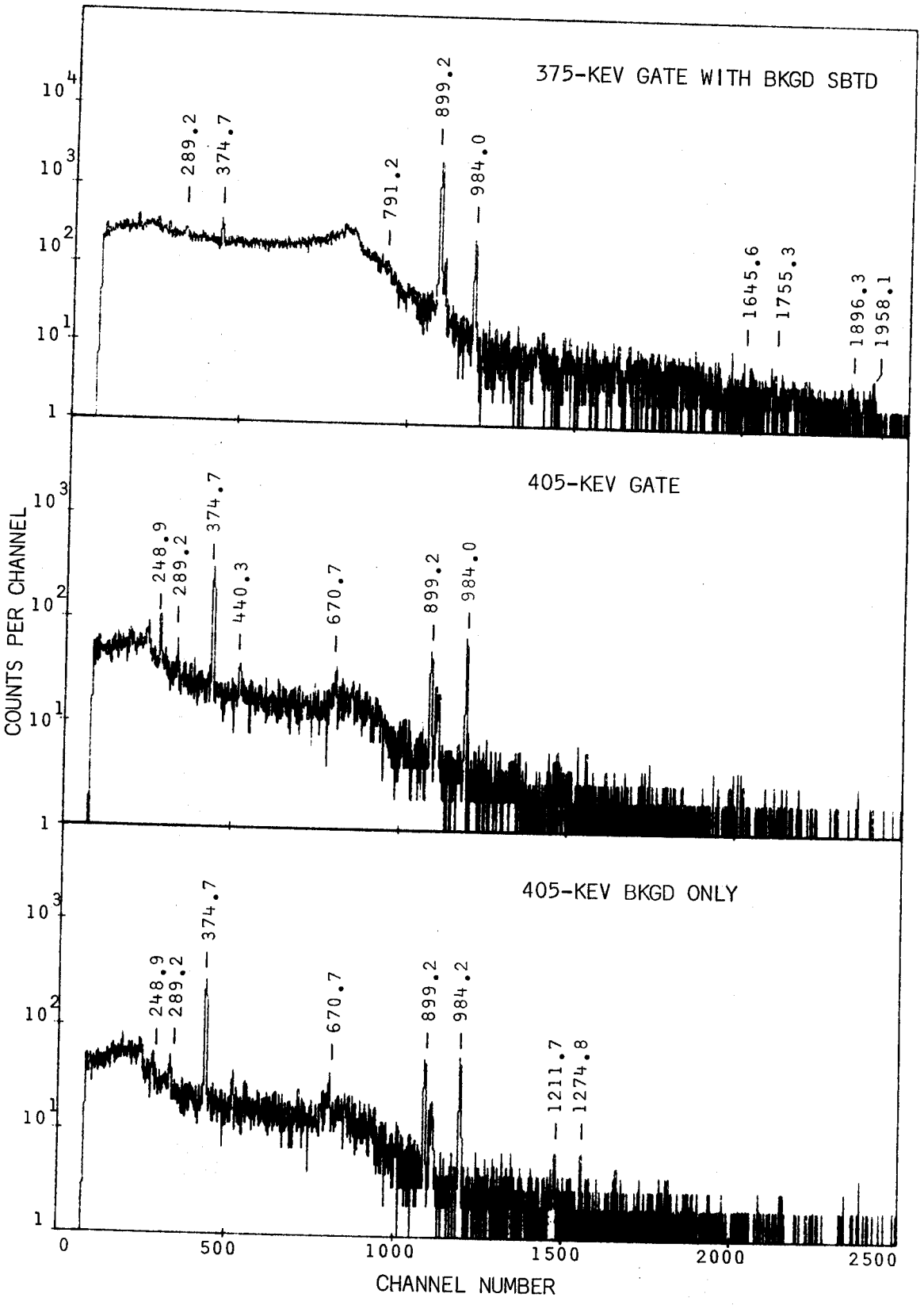

Fig. 24. (continued)

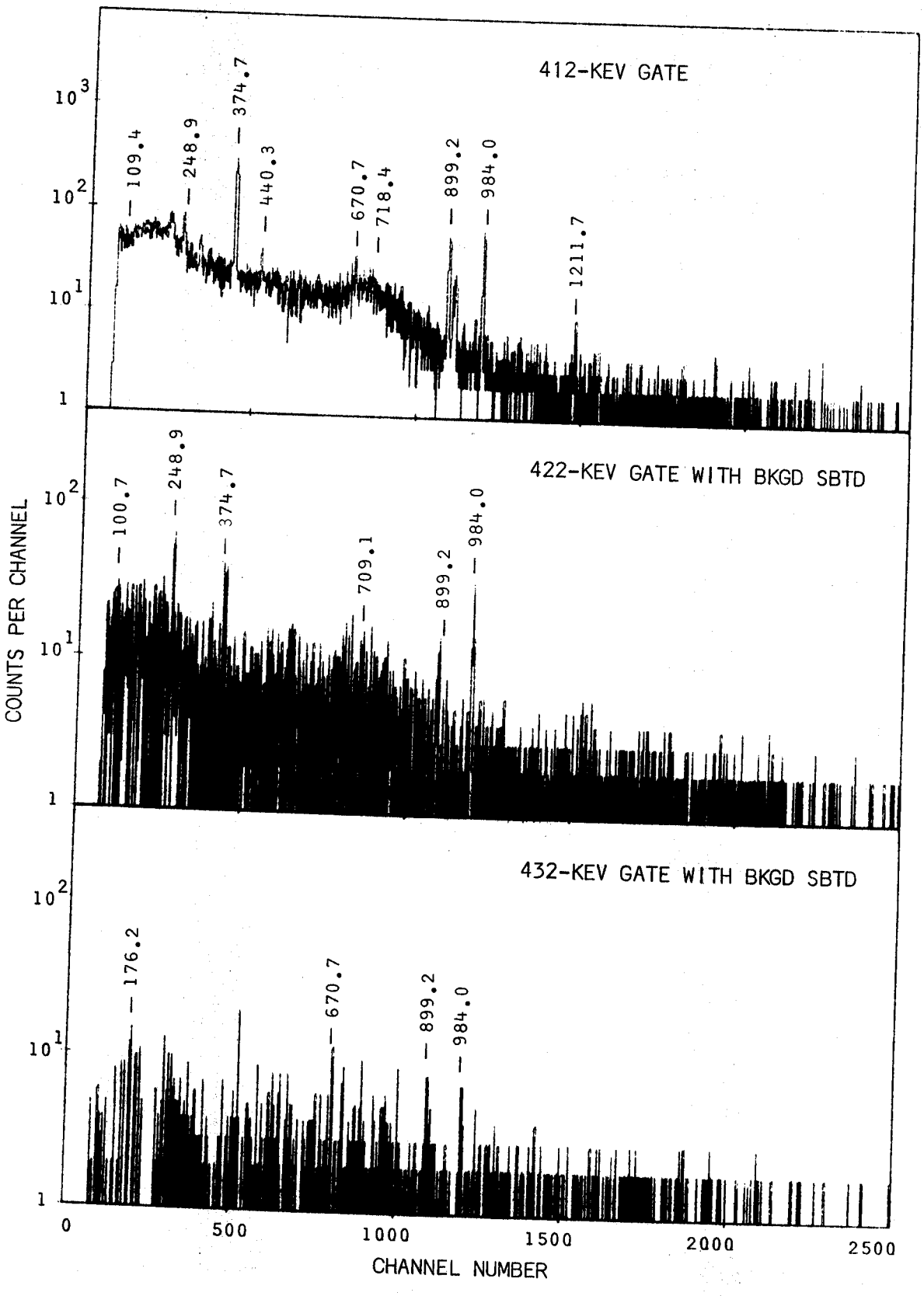

Fig. 24. (continued)

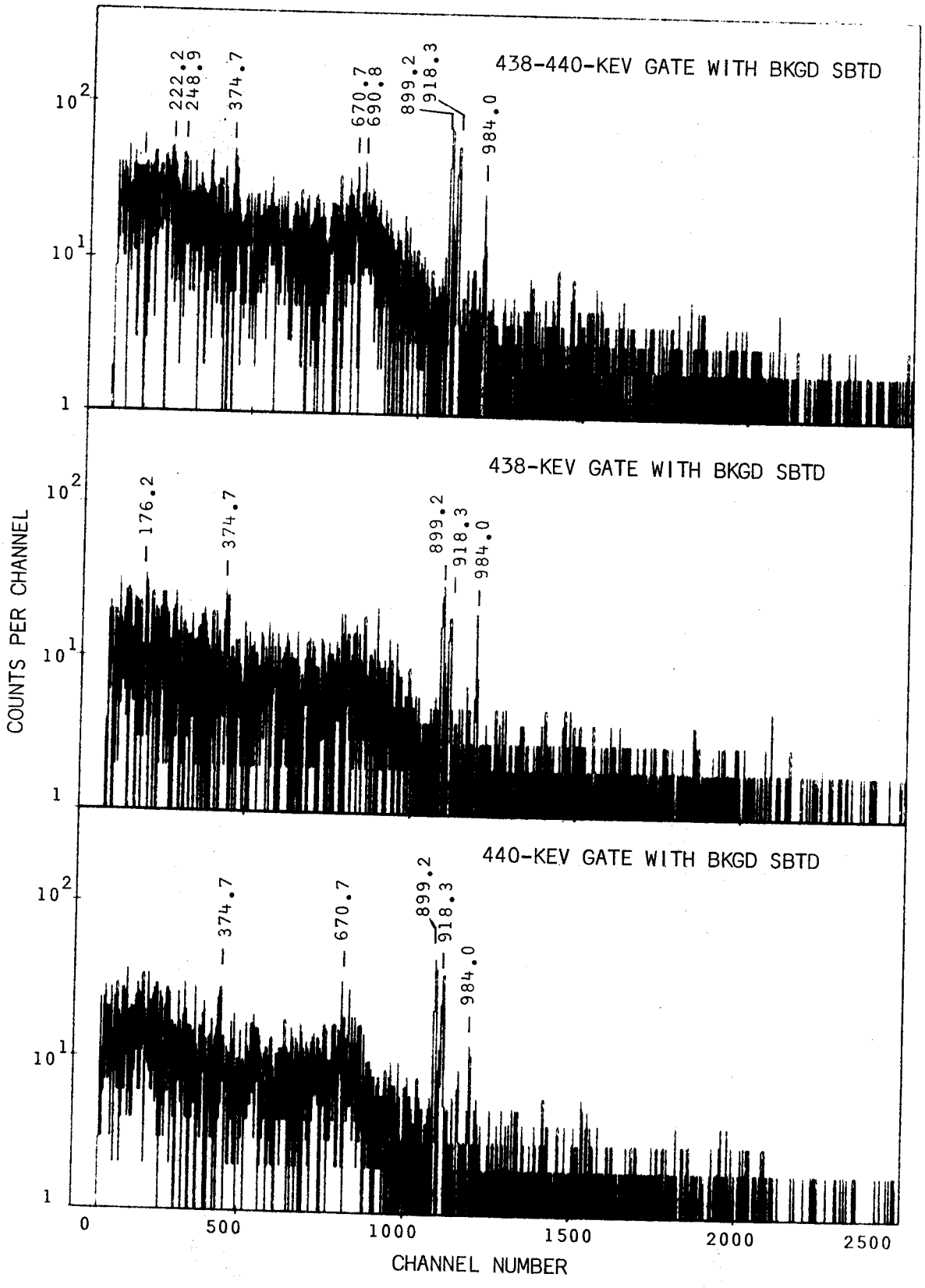

Fig. 24. (continued)

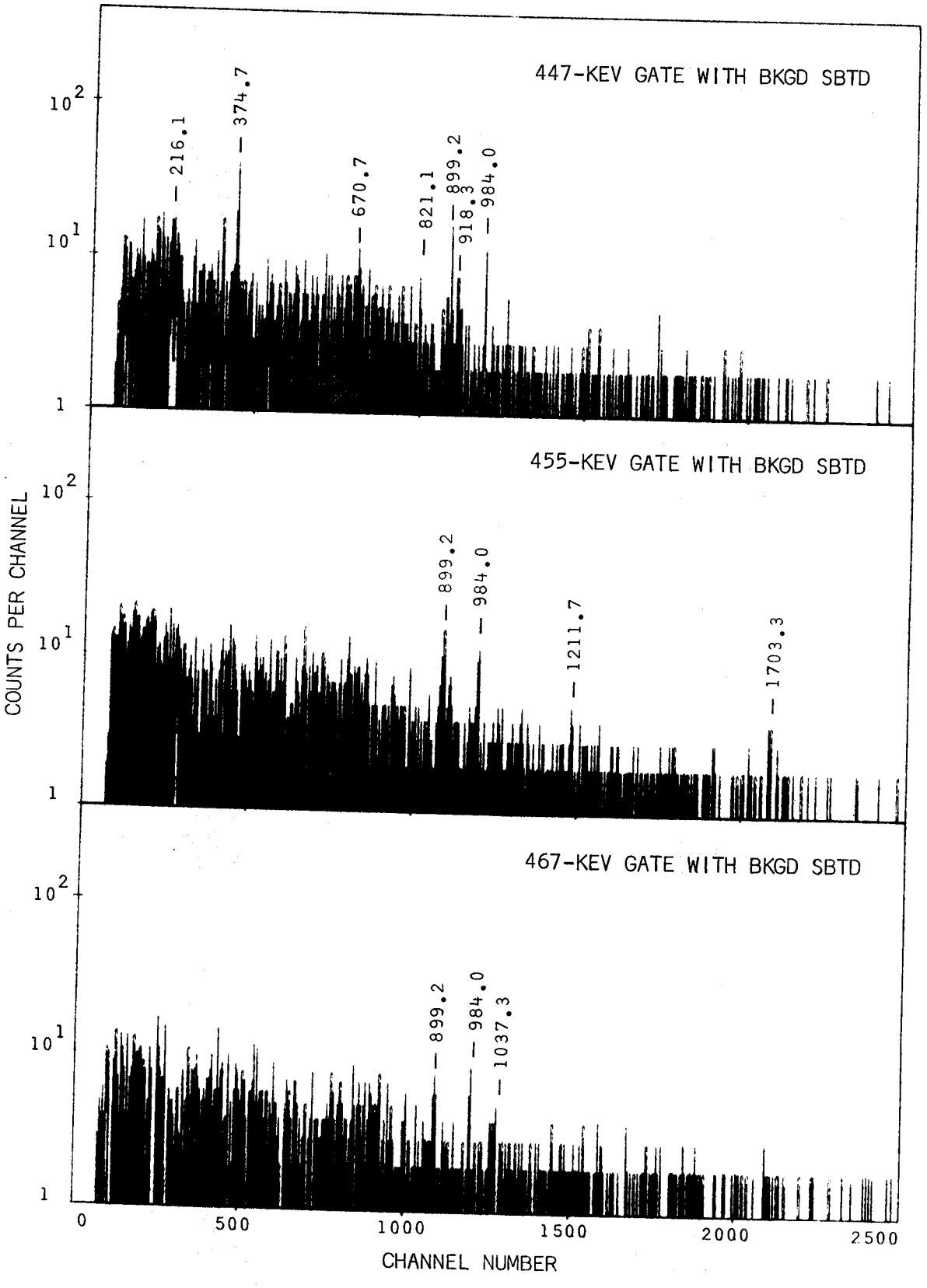

Fig. 24. (continued)

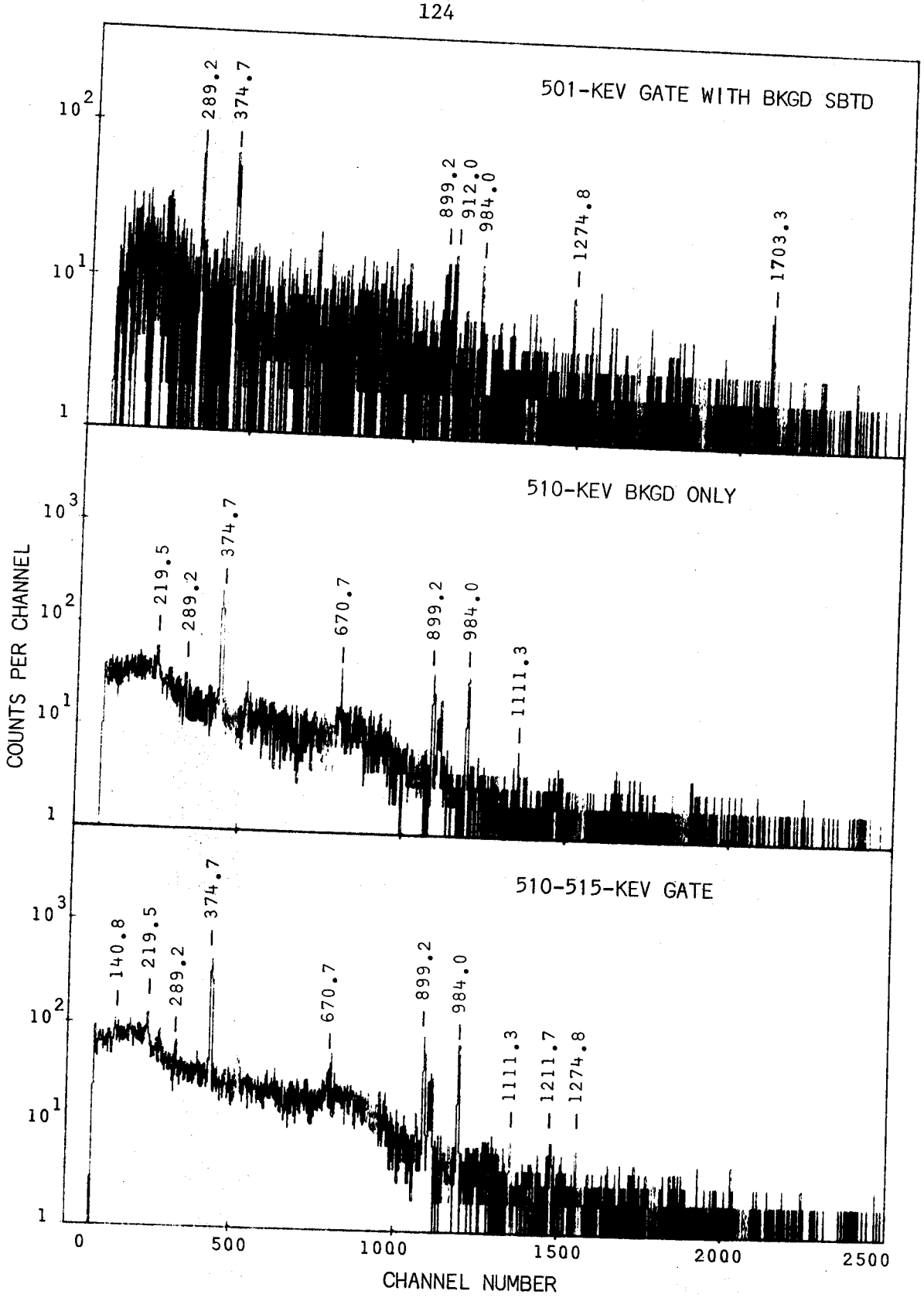

Fig. 24. (continued)

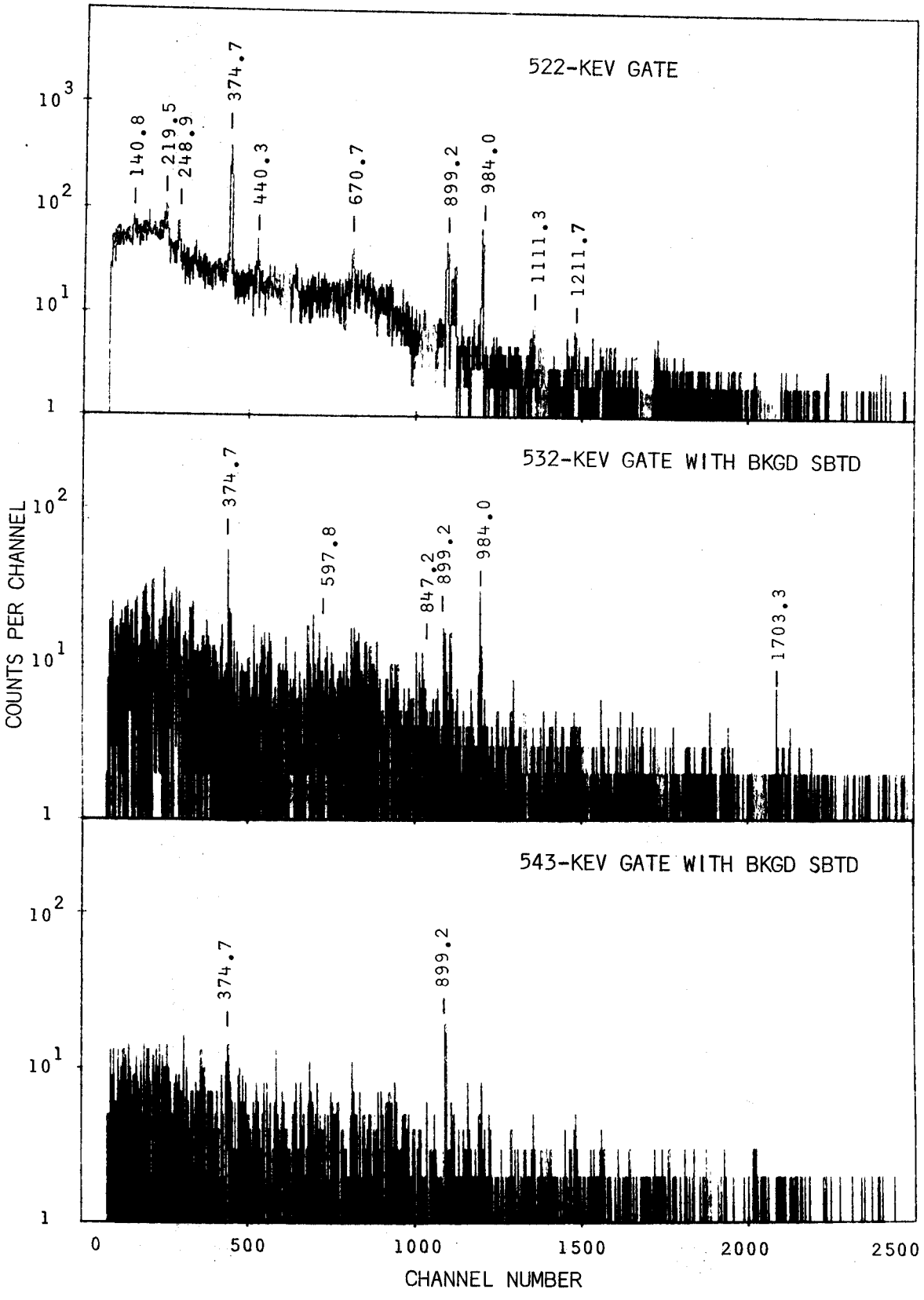

Fig. 24. (continued)

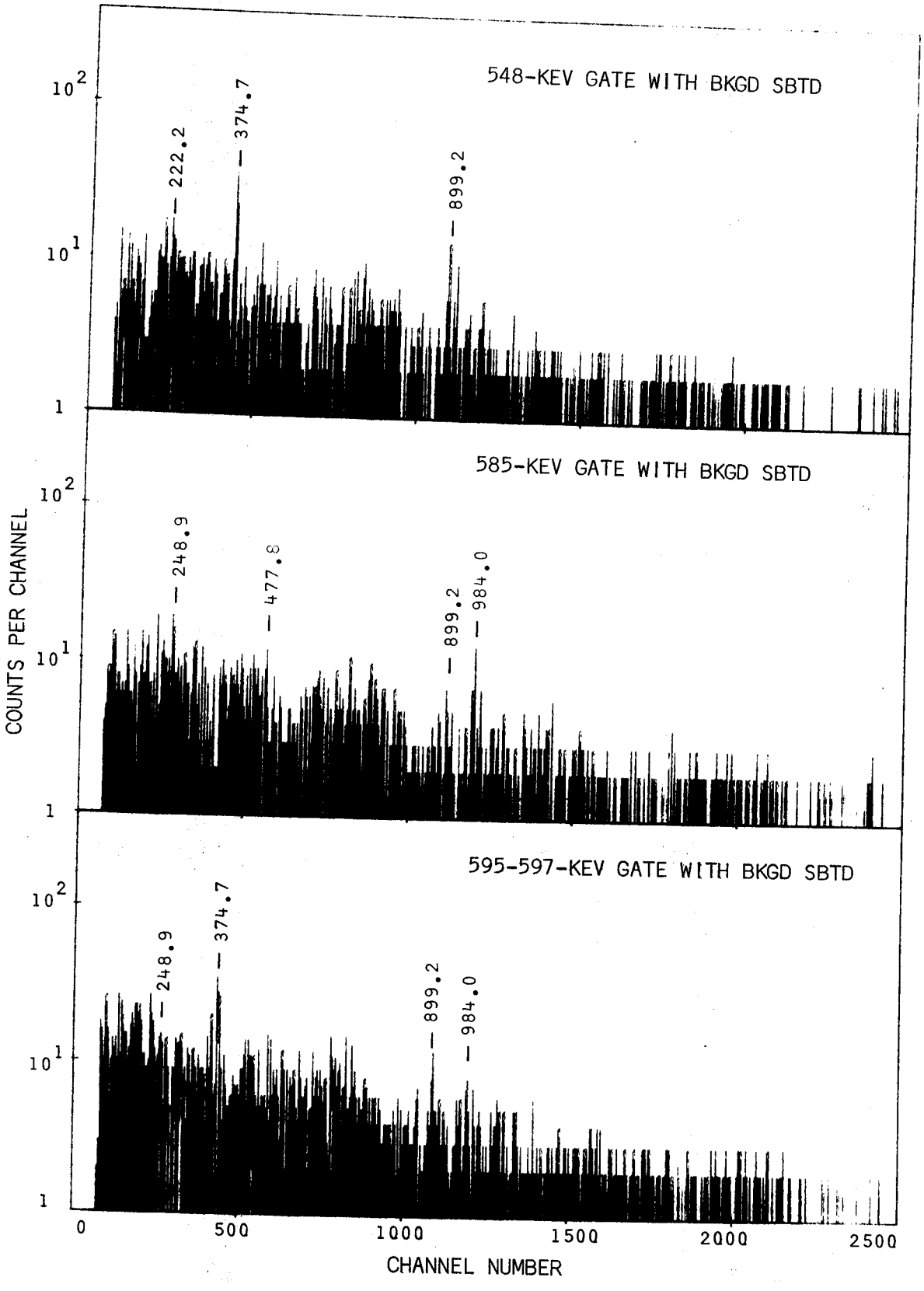

Fig. 24. (continued)

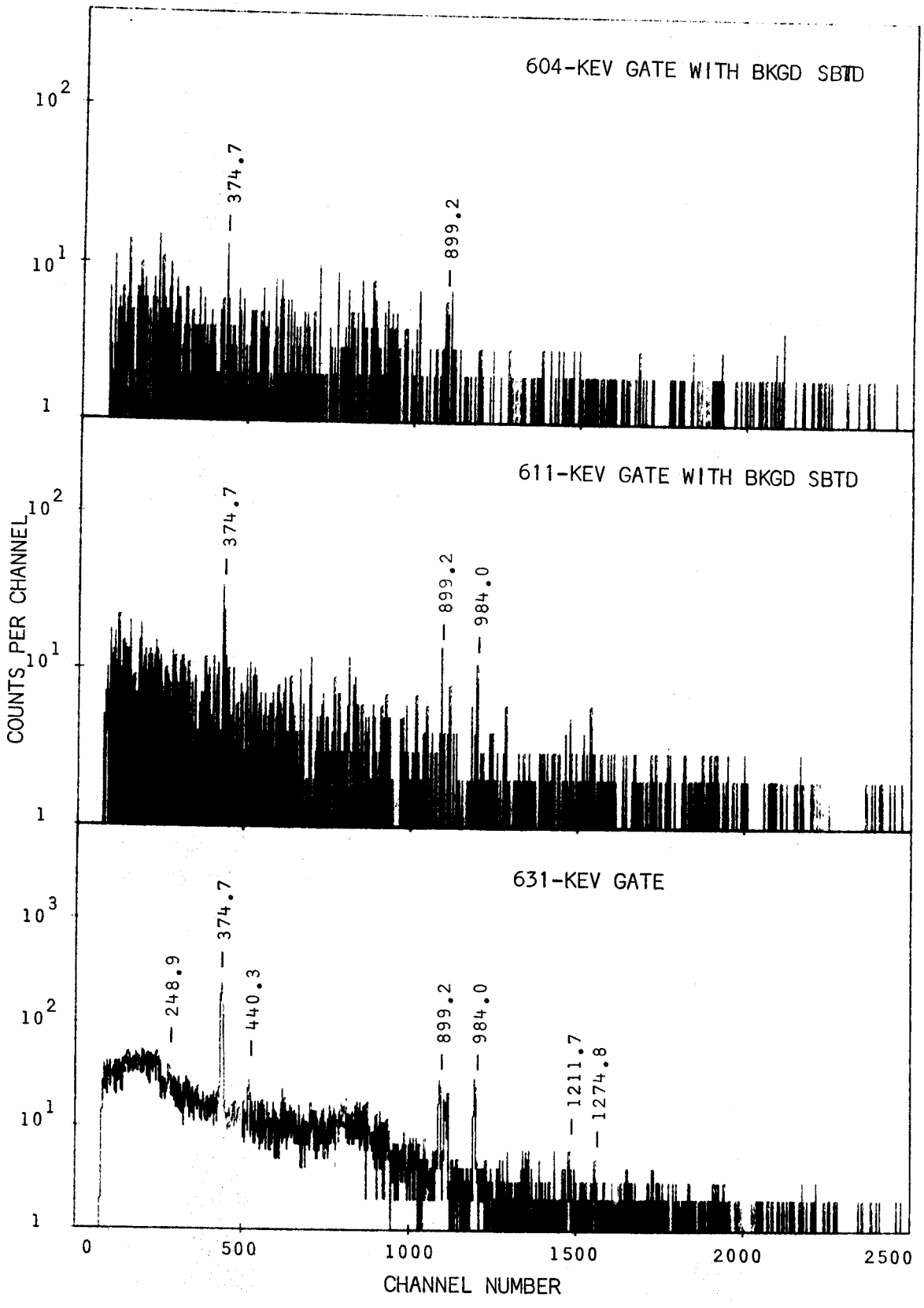

Fig. 24. (continued)

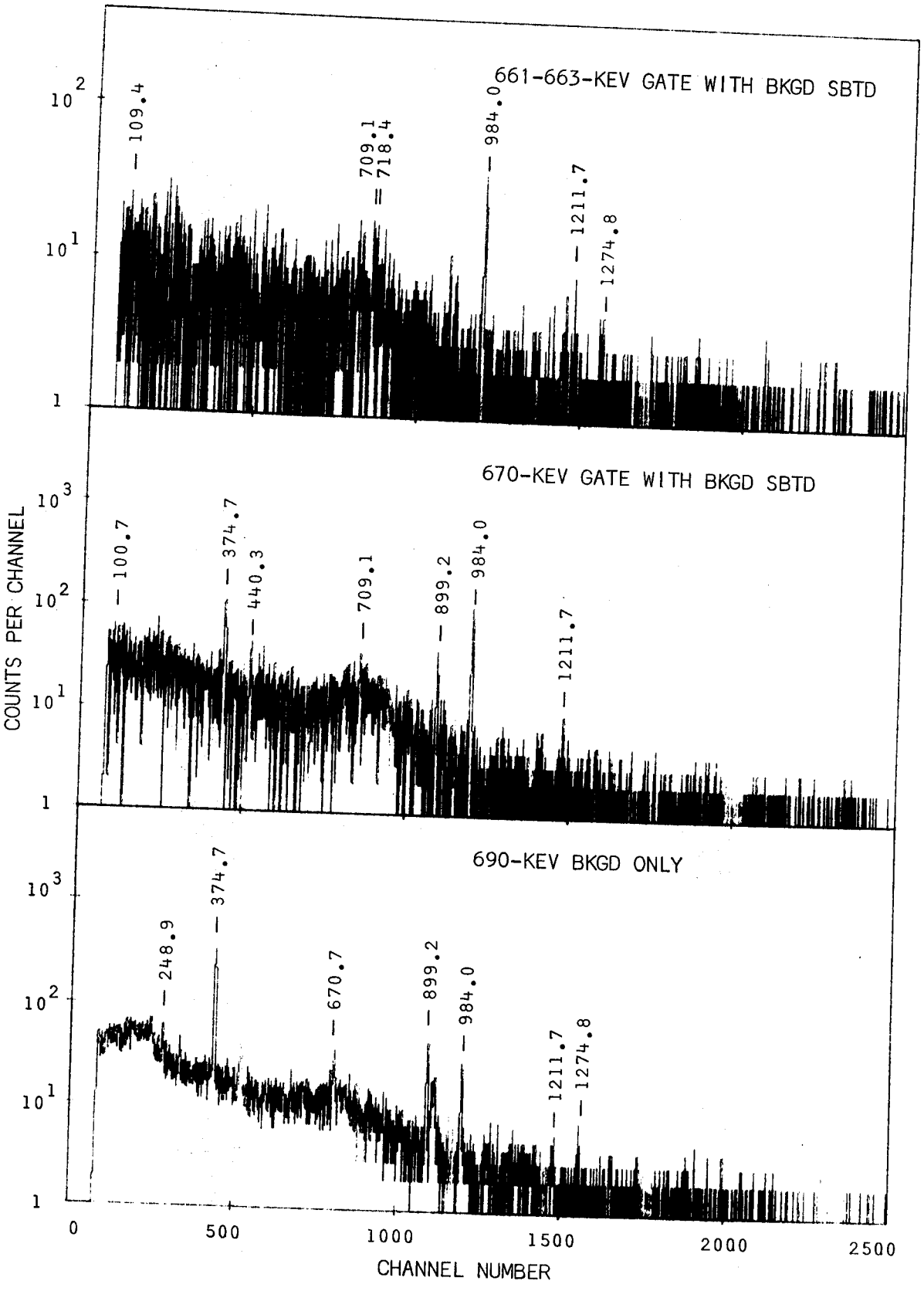

Fig. 24. (continued)

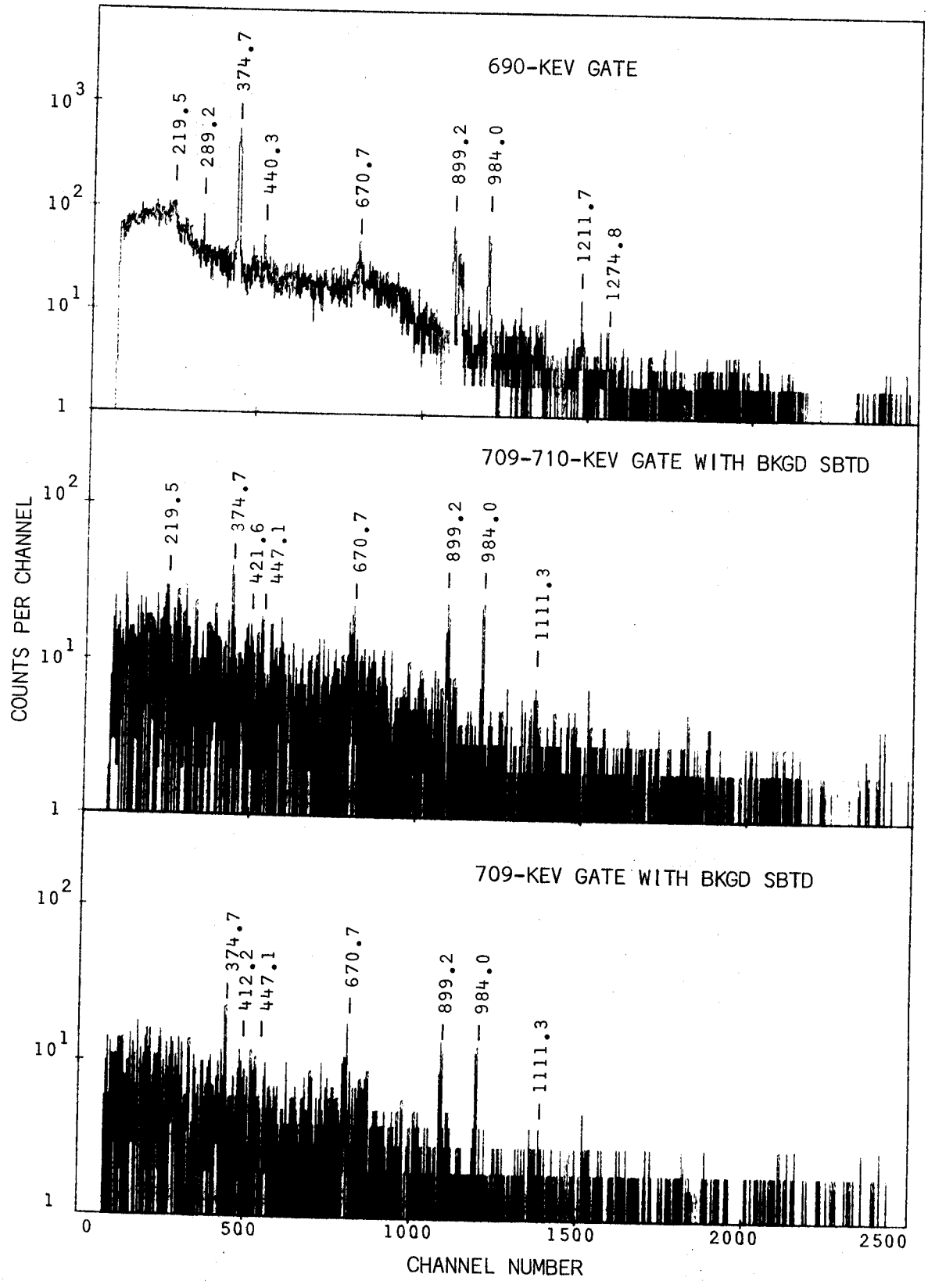

Fig. 24. (continued)

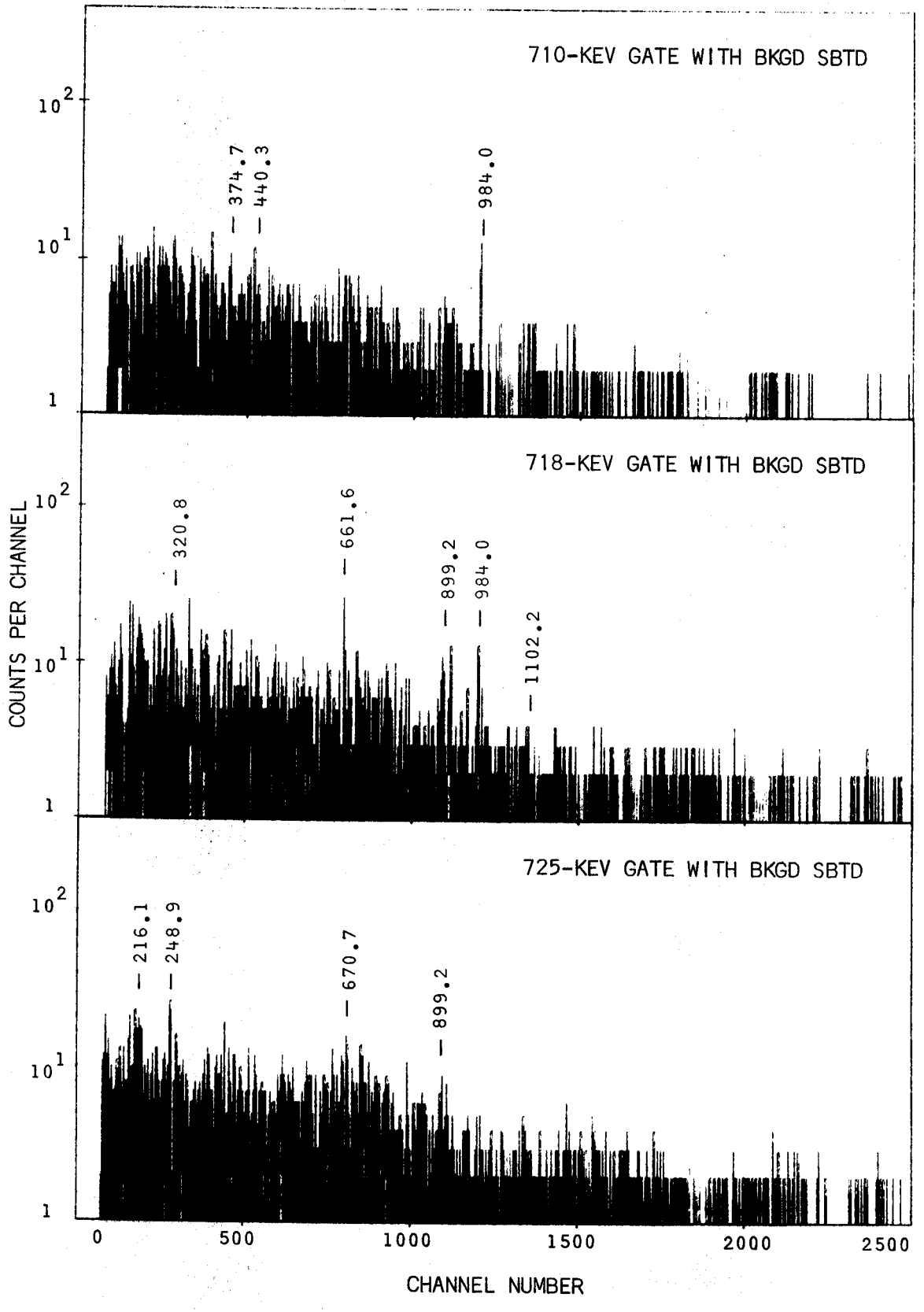

Fig. 24. (continued)

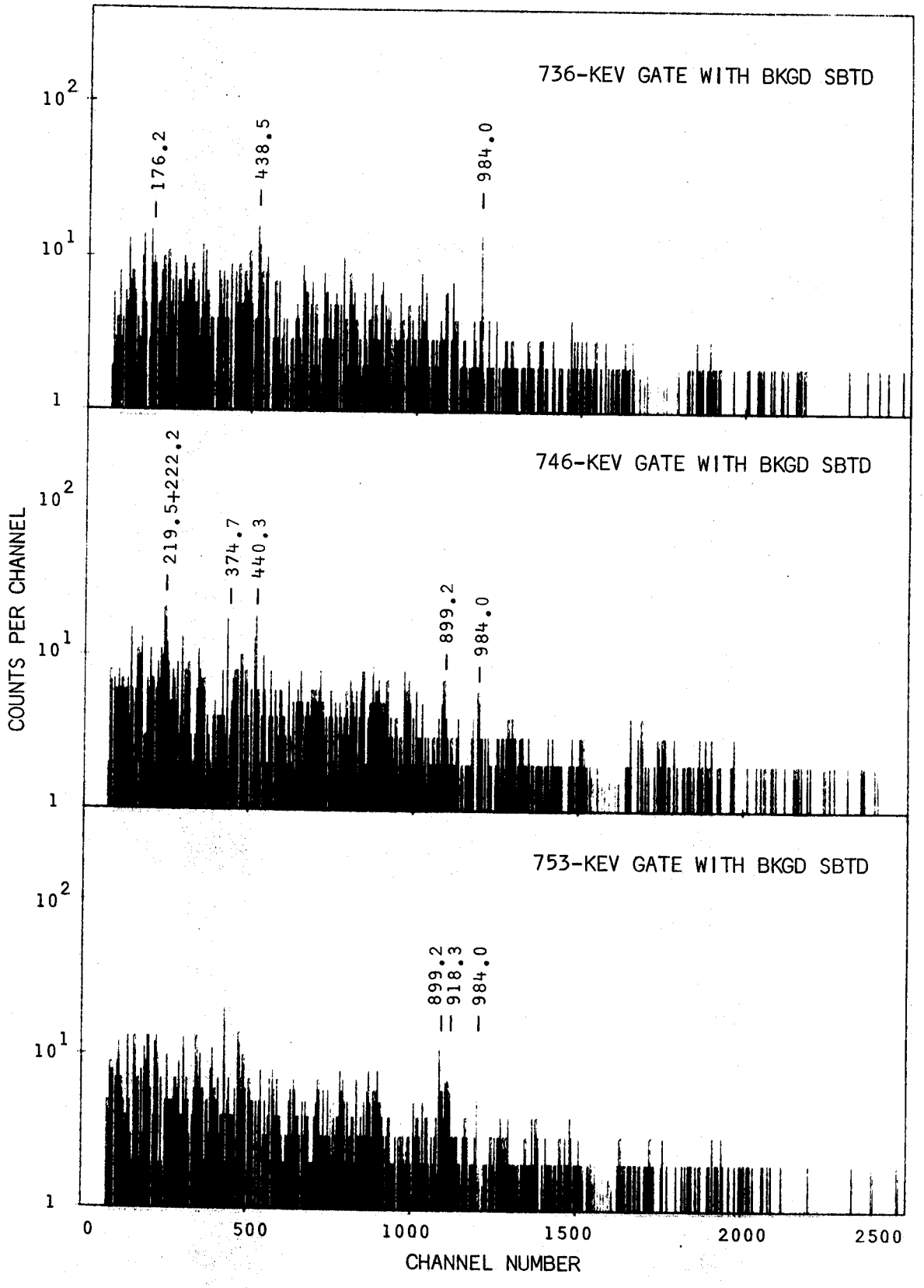

Fig. 24. (continued)

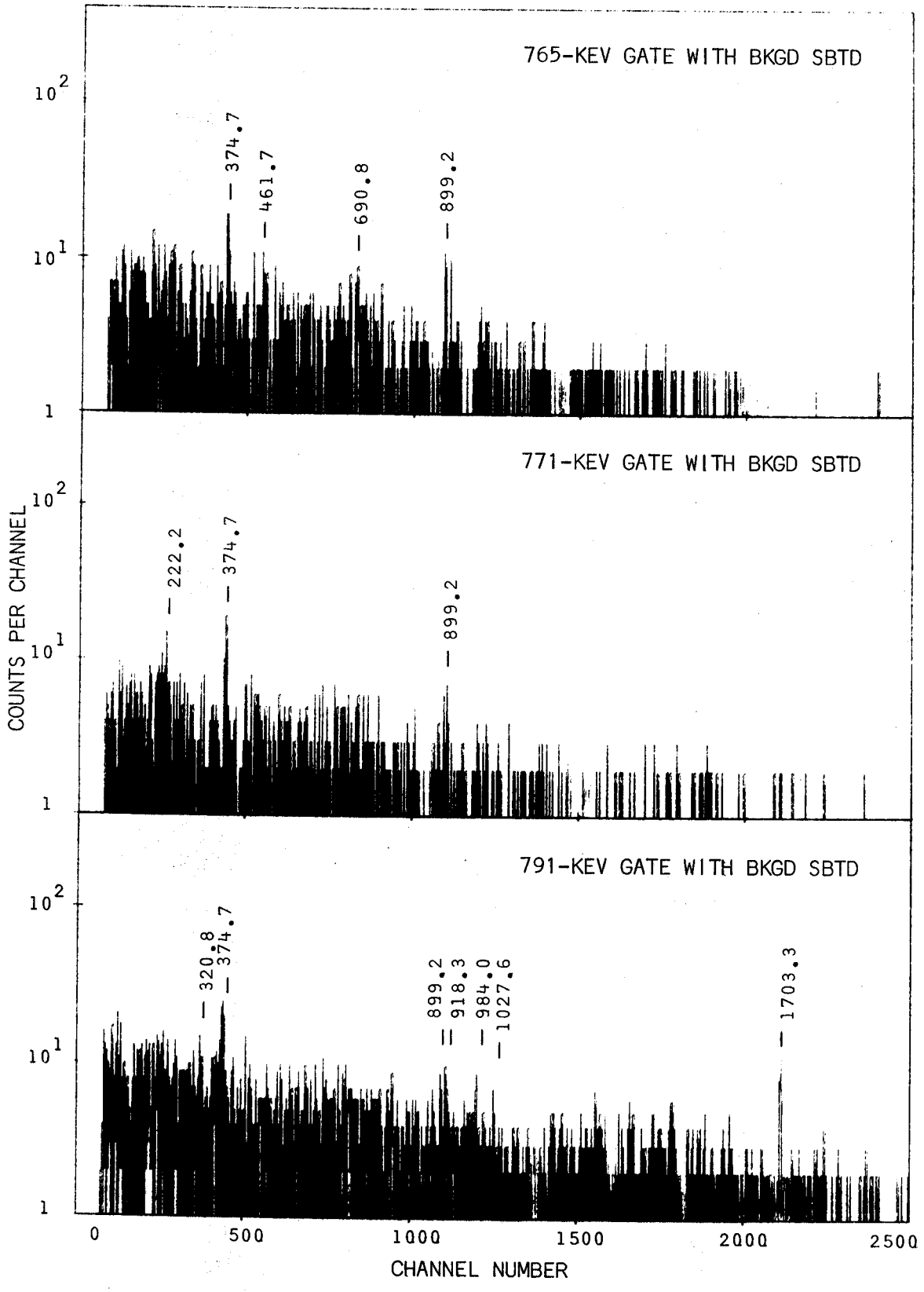

Fig. 24. (continued)

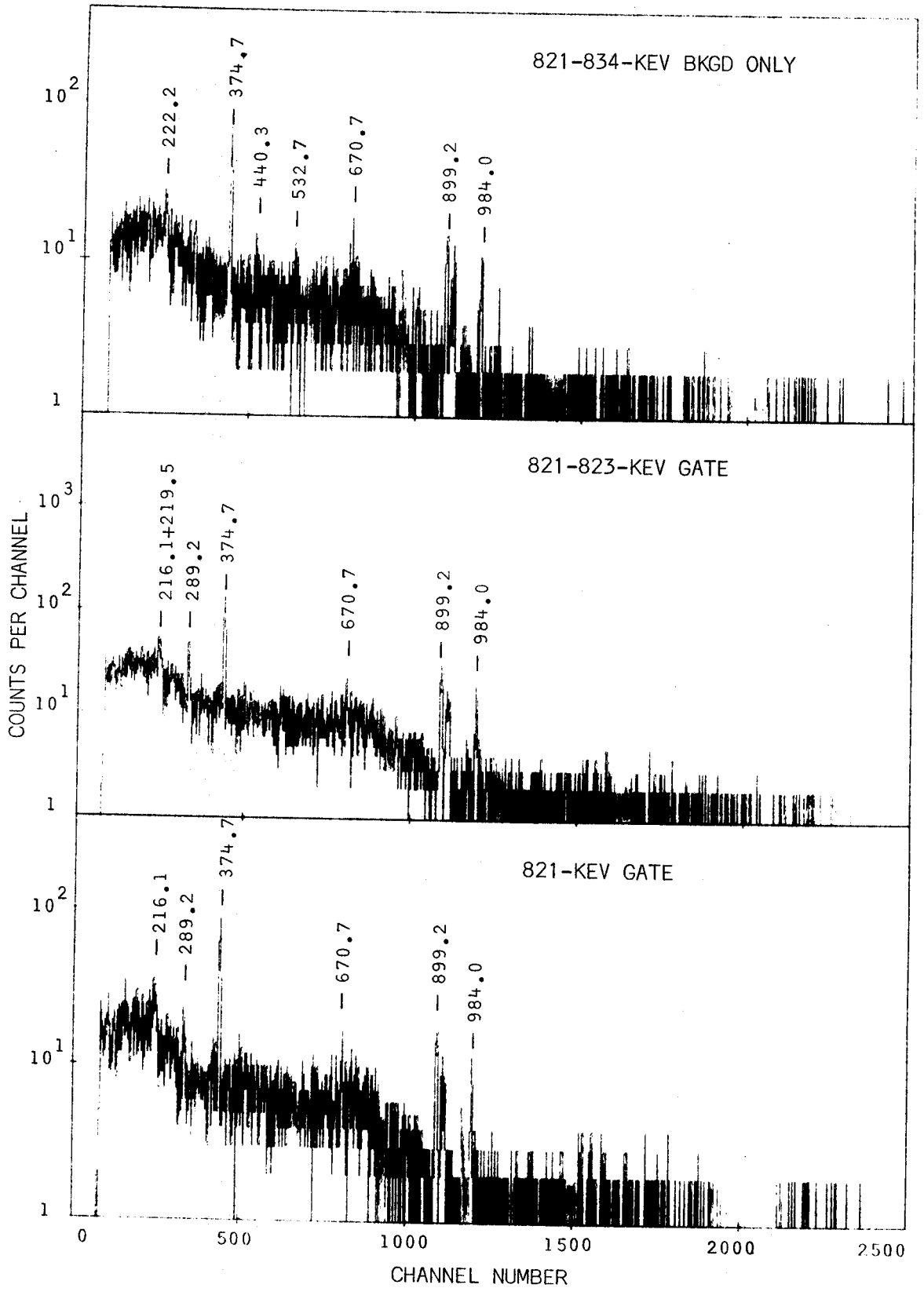

Fig. 24. (continued)

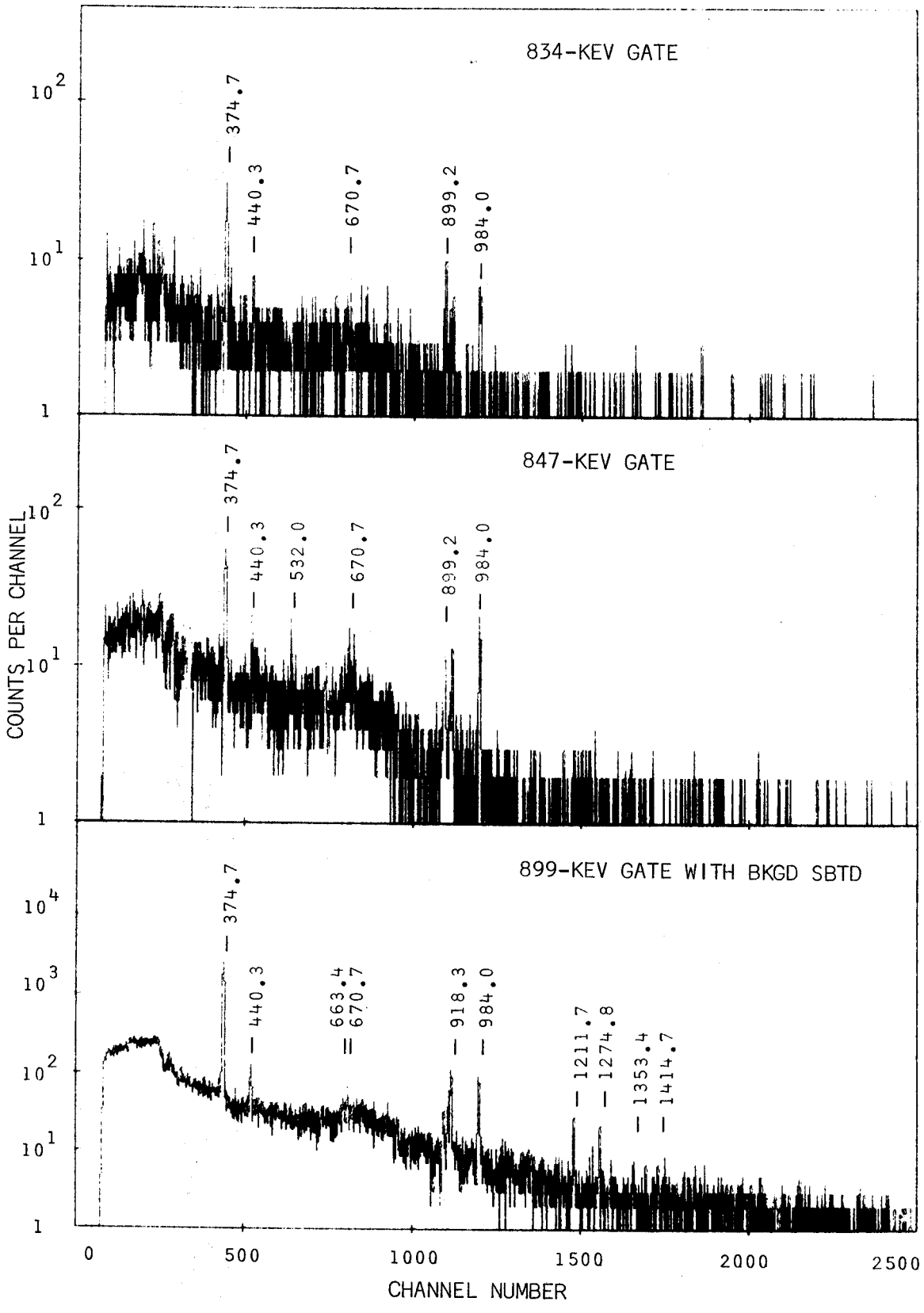

Fig. 24. (continued)

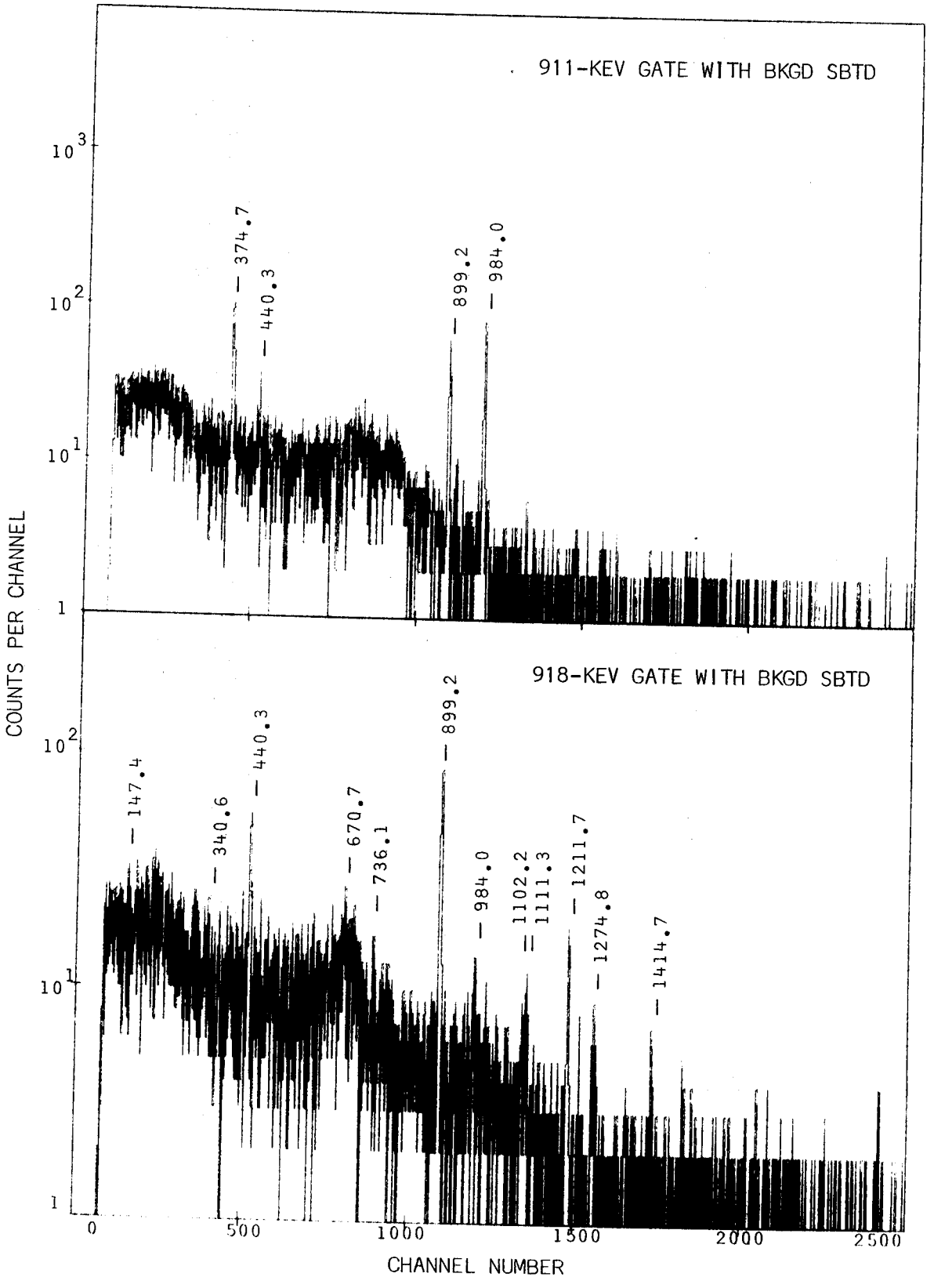

Fig. 24. (continued)

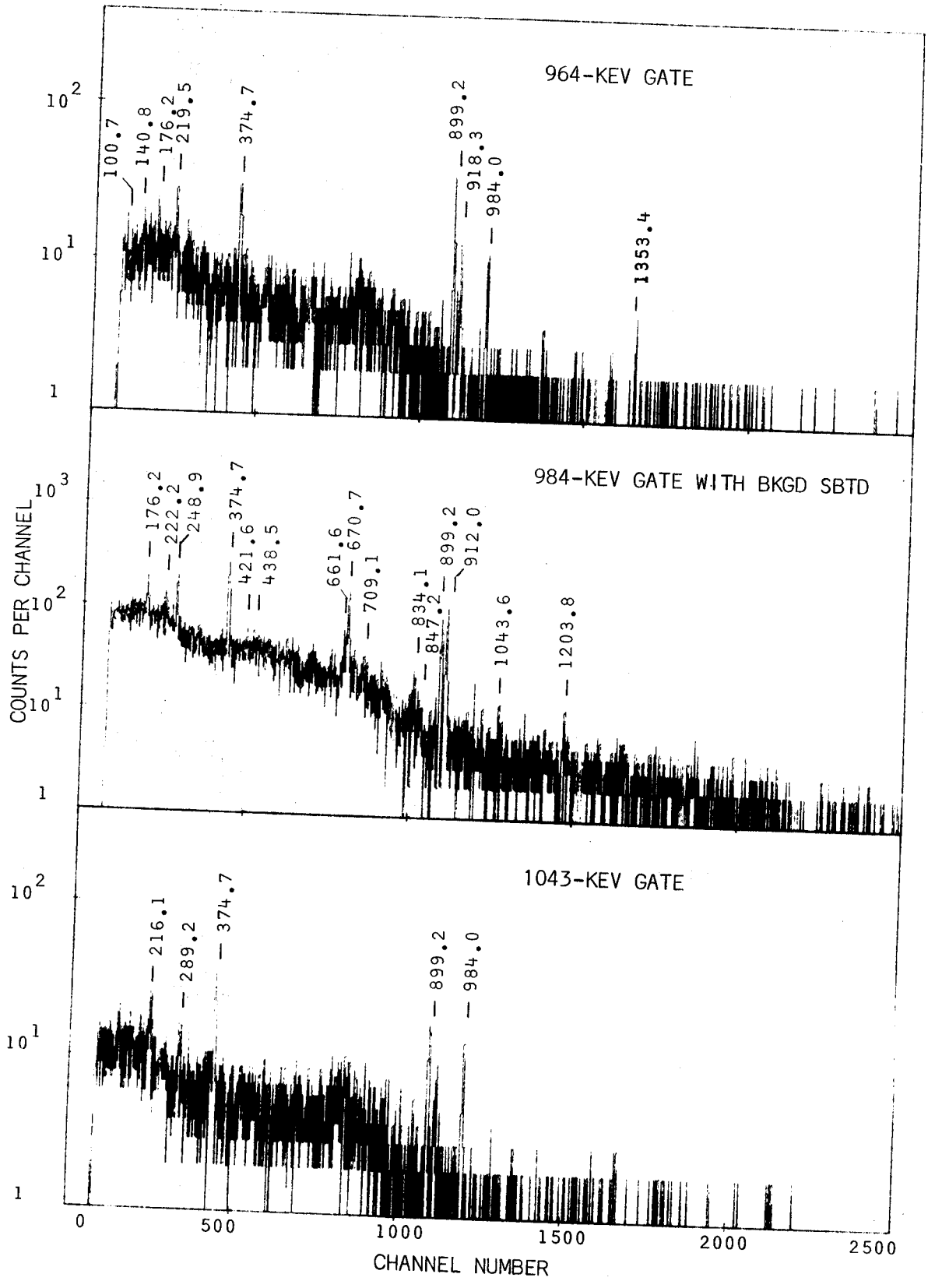

Fig. 24. (continued)

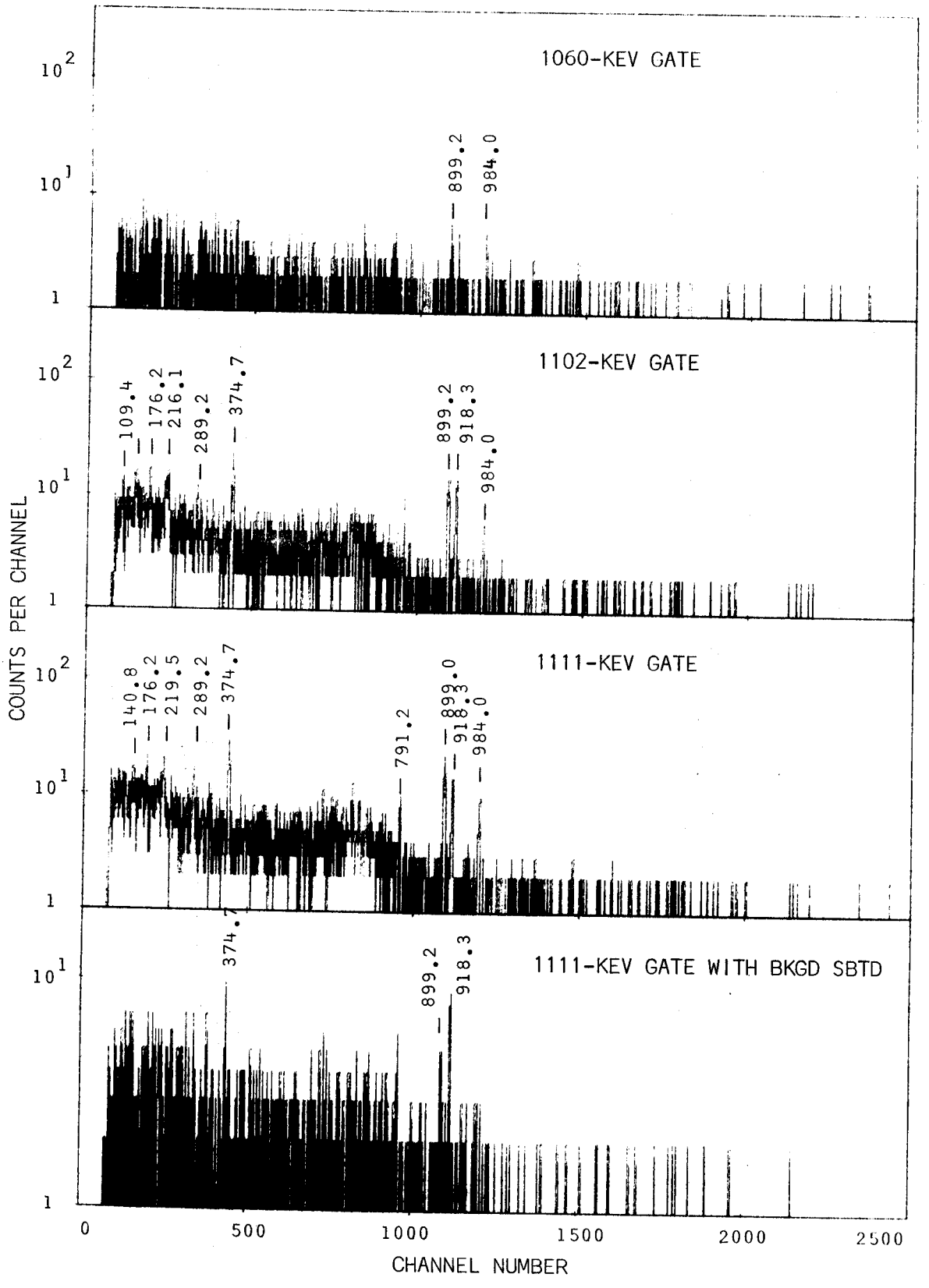

Fig. 24. (continued)

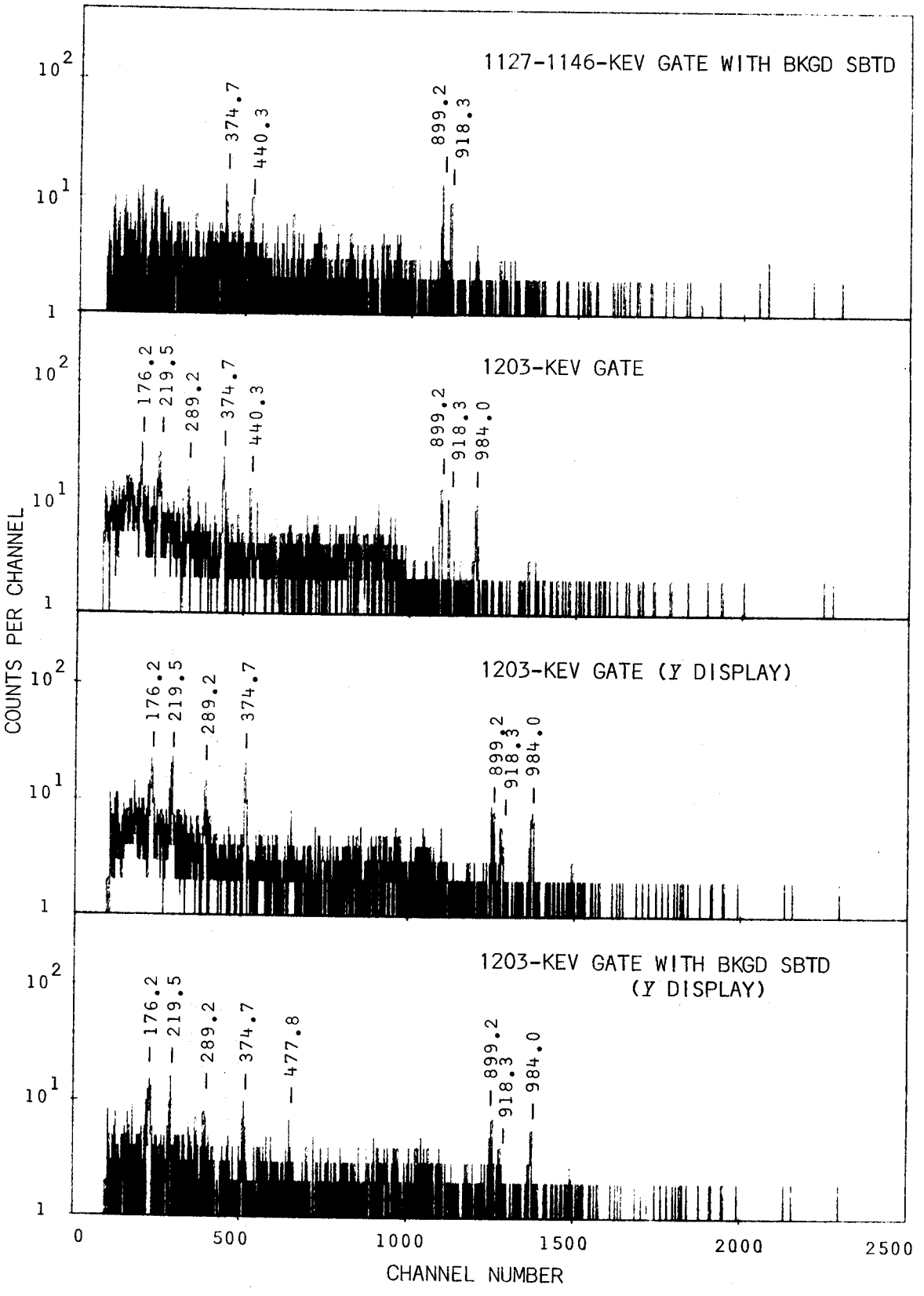

Fig. 24. (continued)

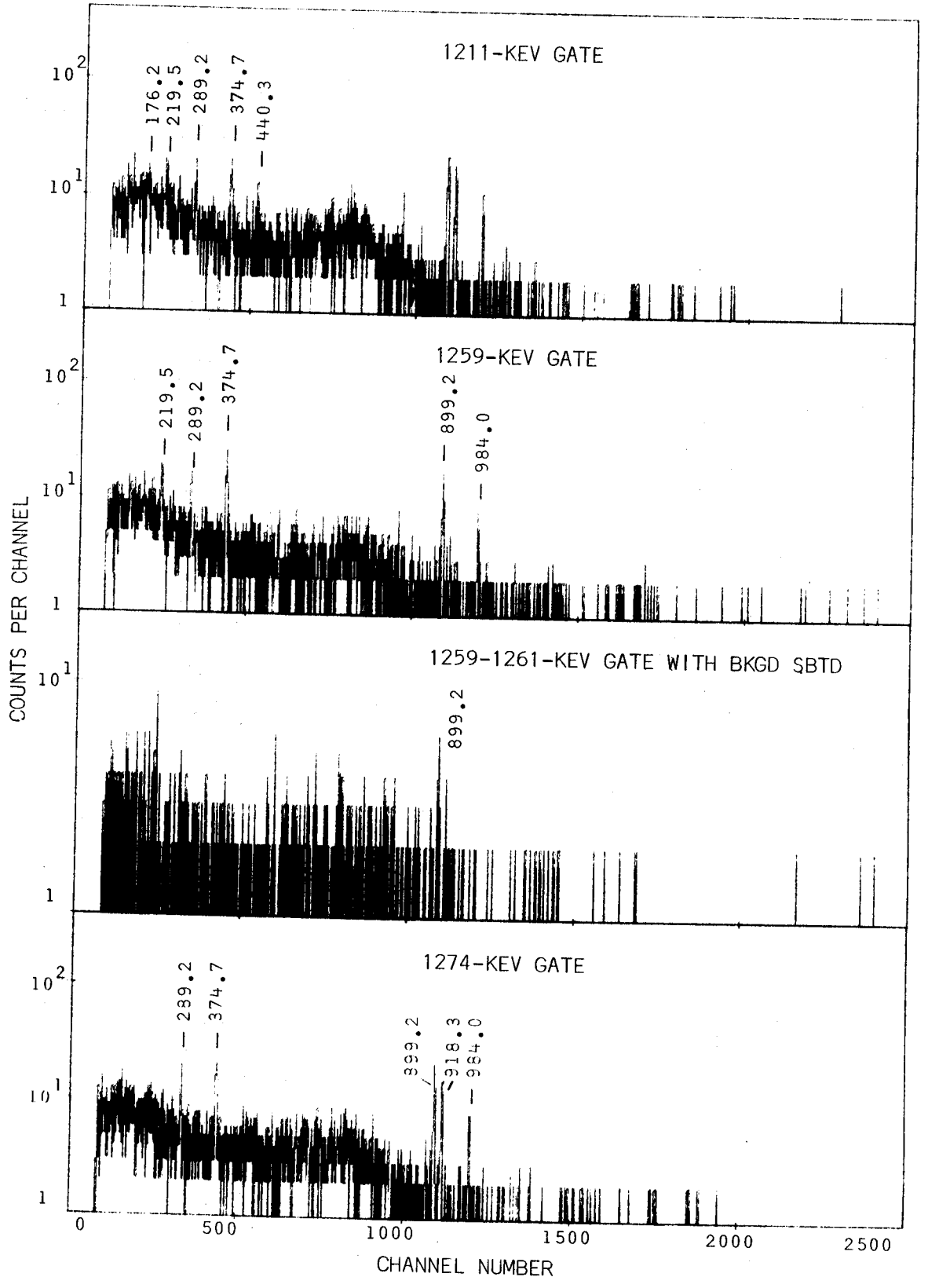

Fig. 24. (continued)

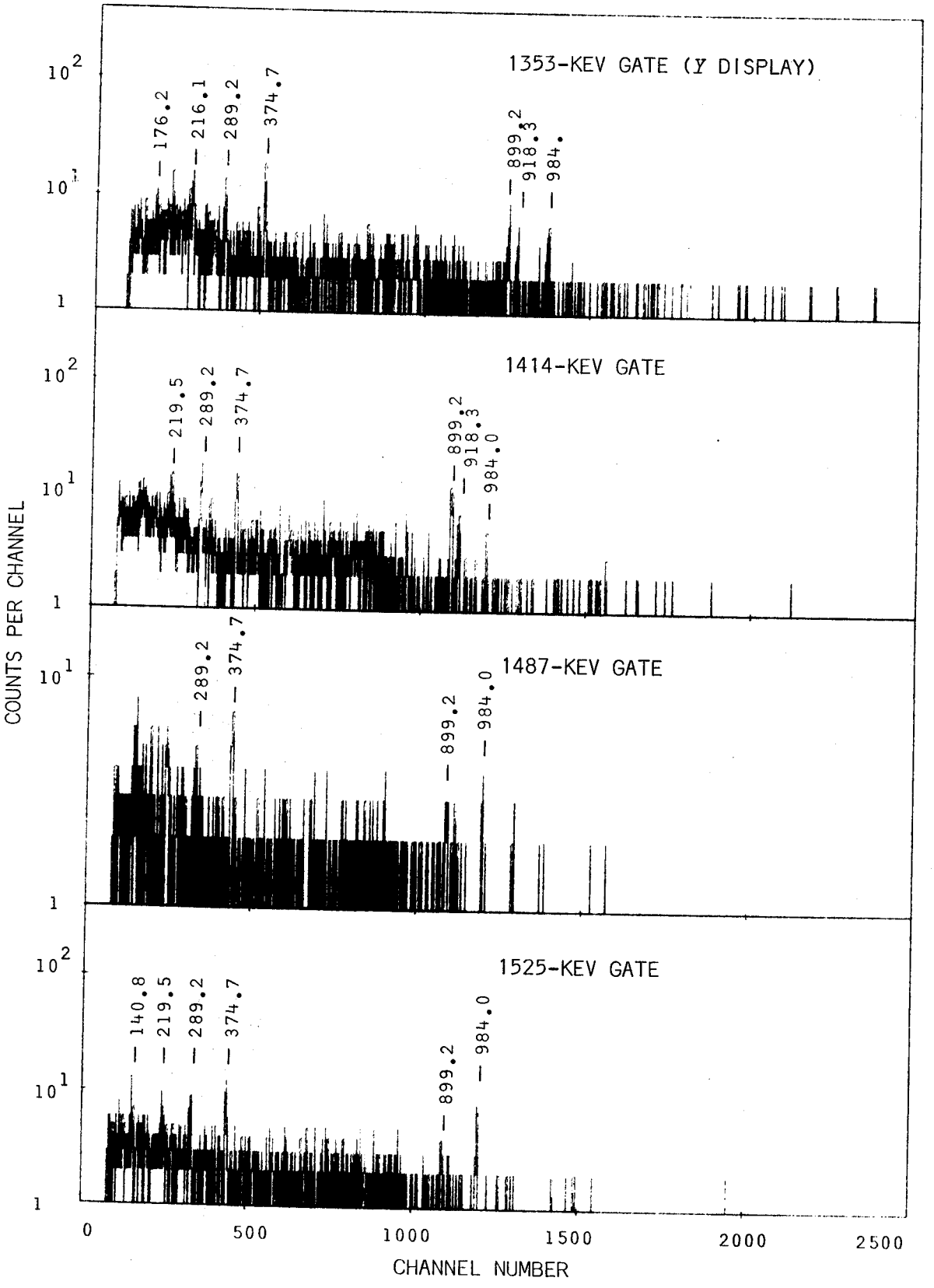

Fig. 24. (continued)

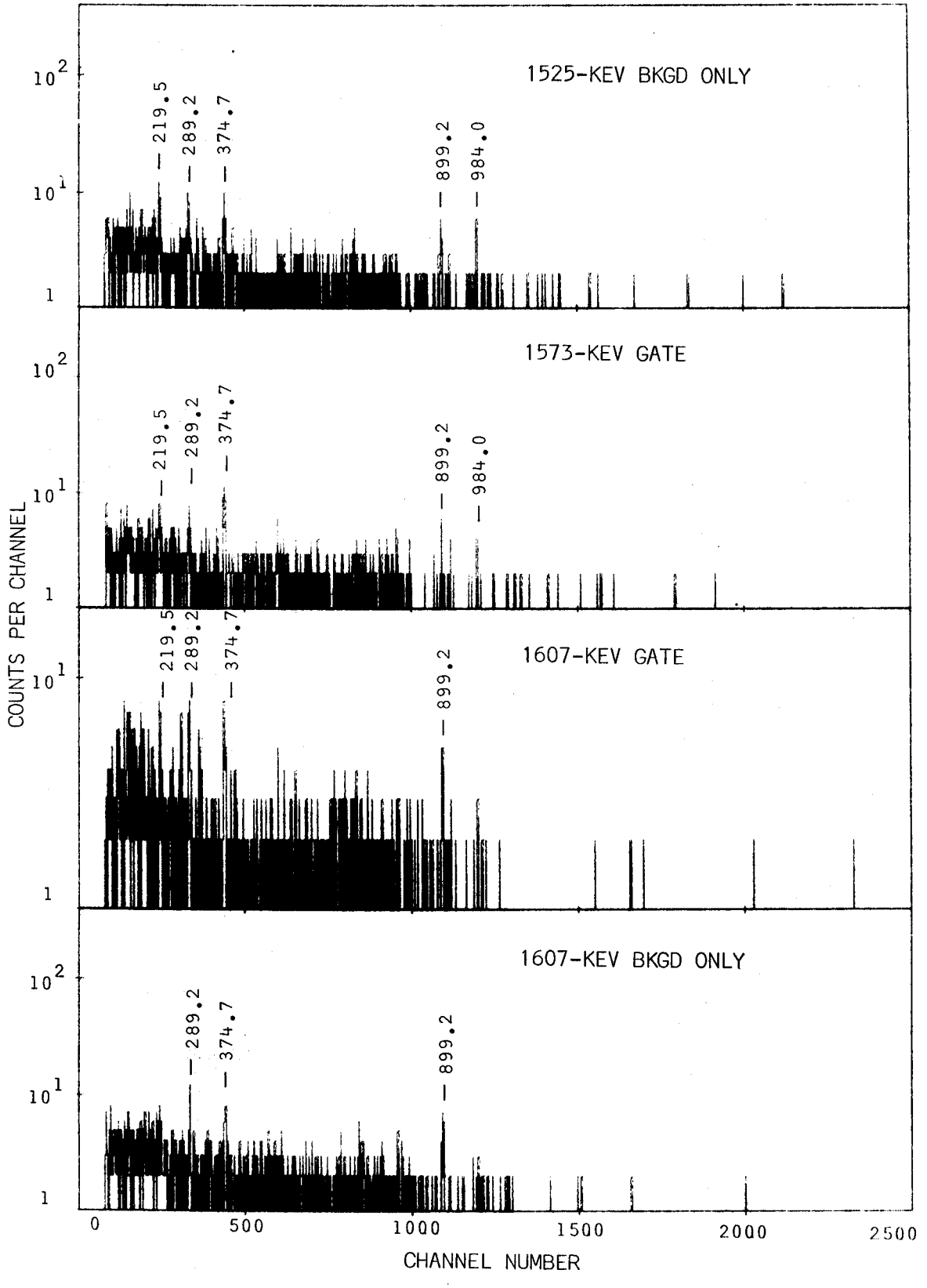

Fig. 24. (continued)

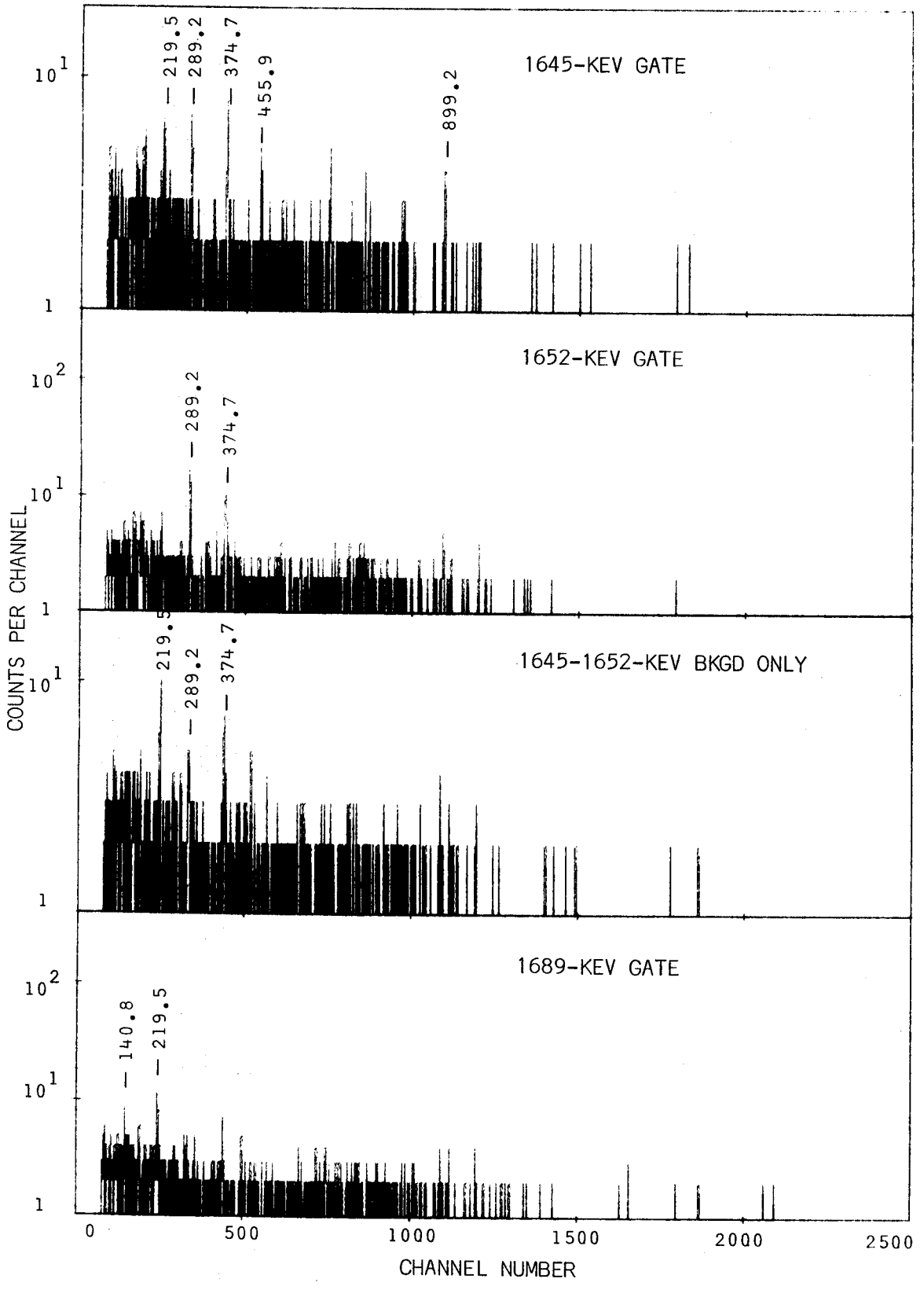

Fig. 24. (continued)

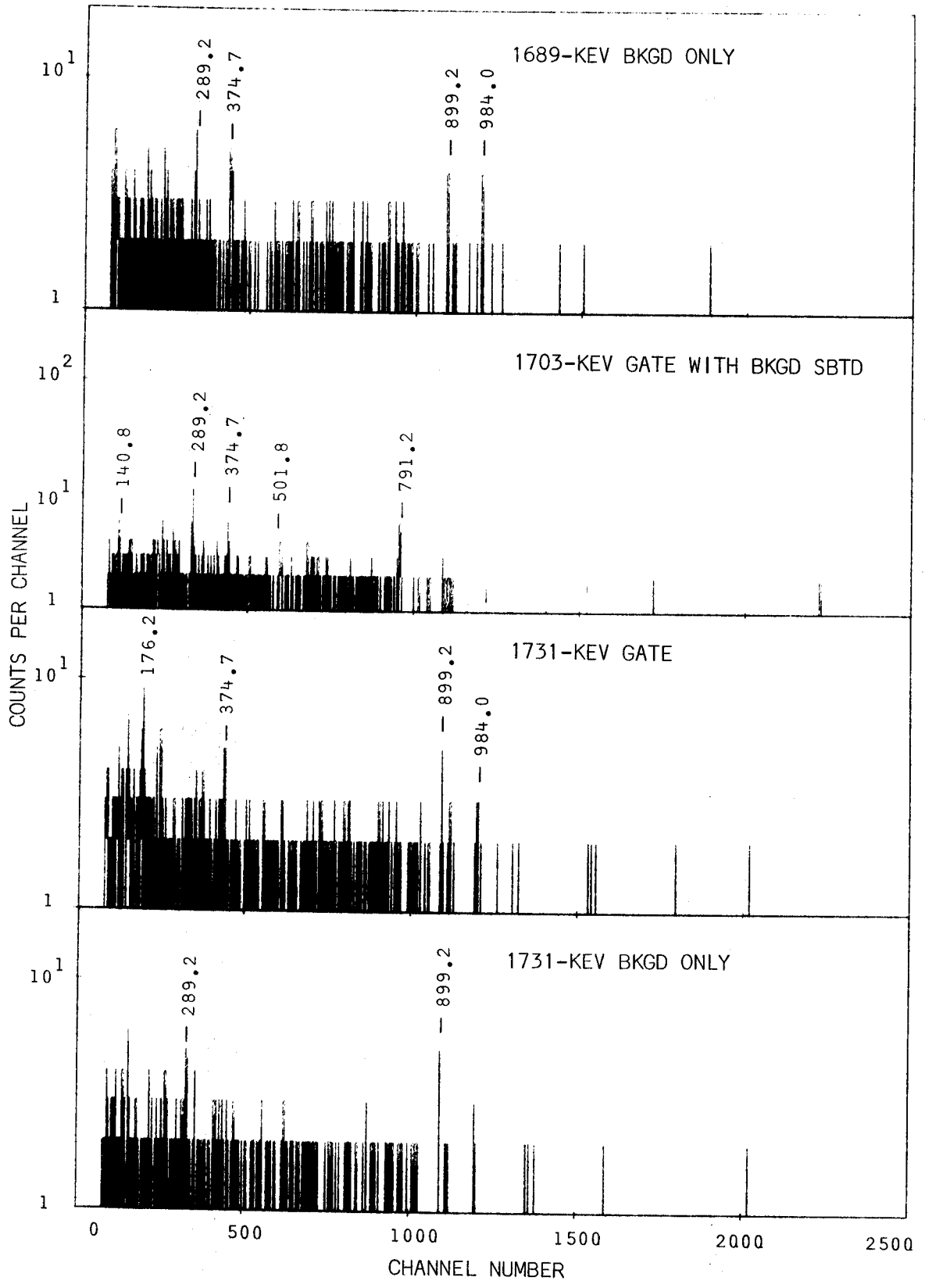

Fig. 24. (continued)

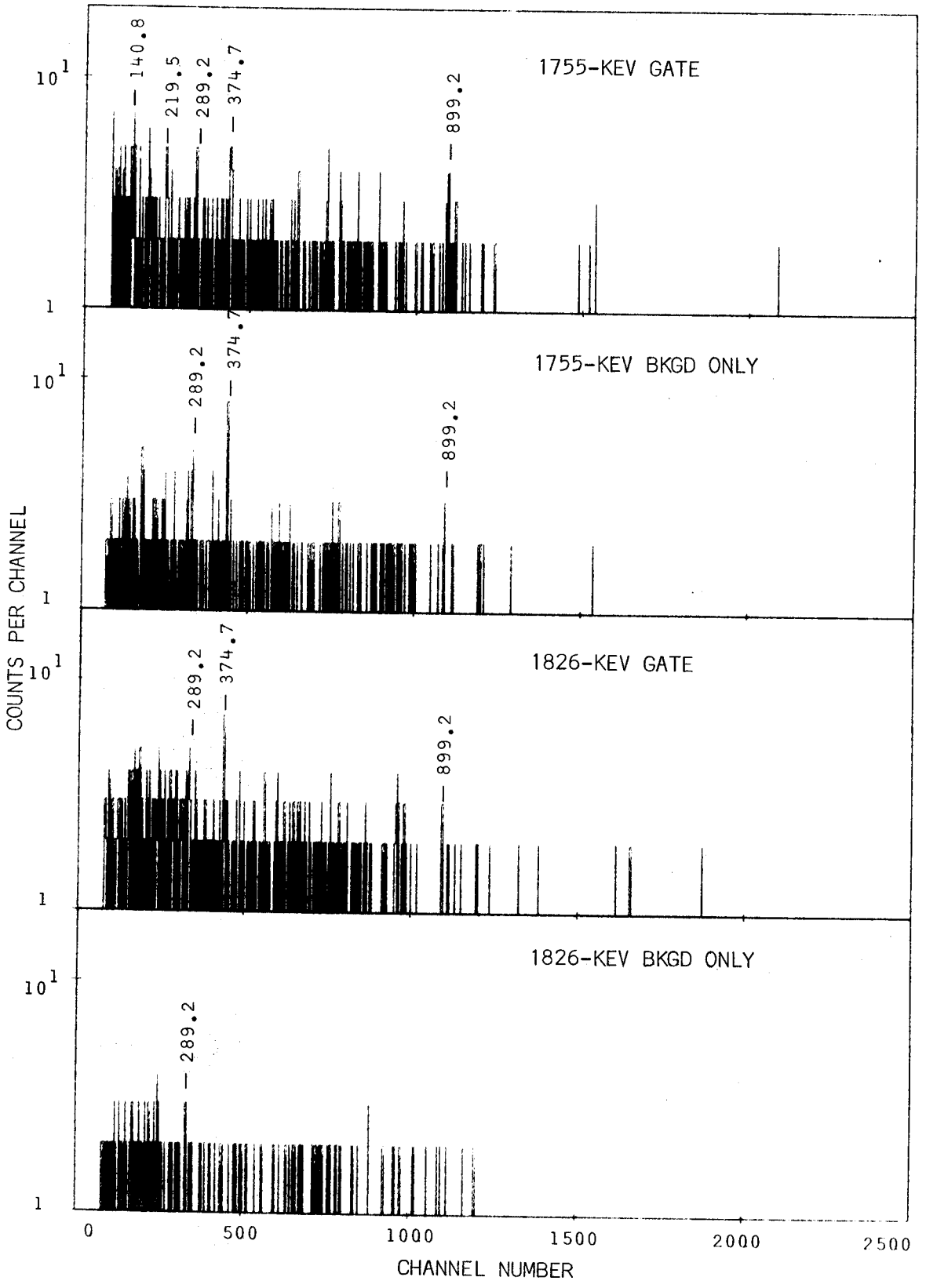

Fig. 24. (continued)

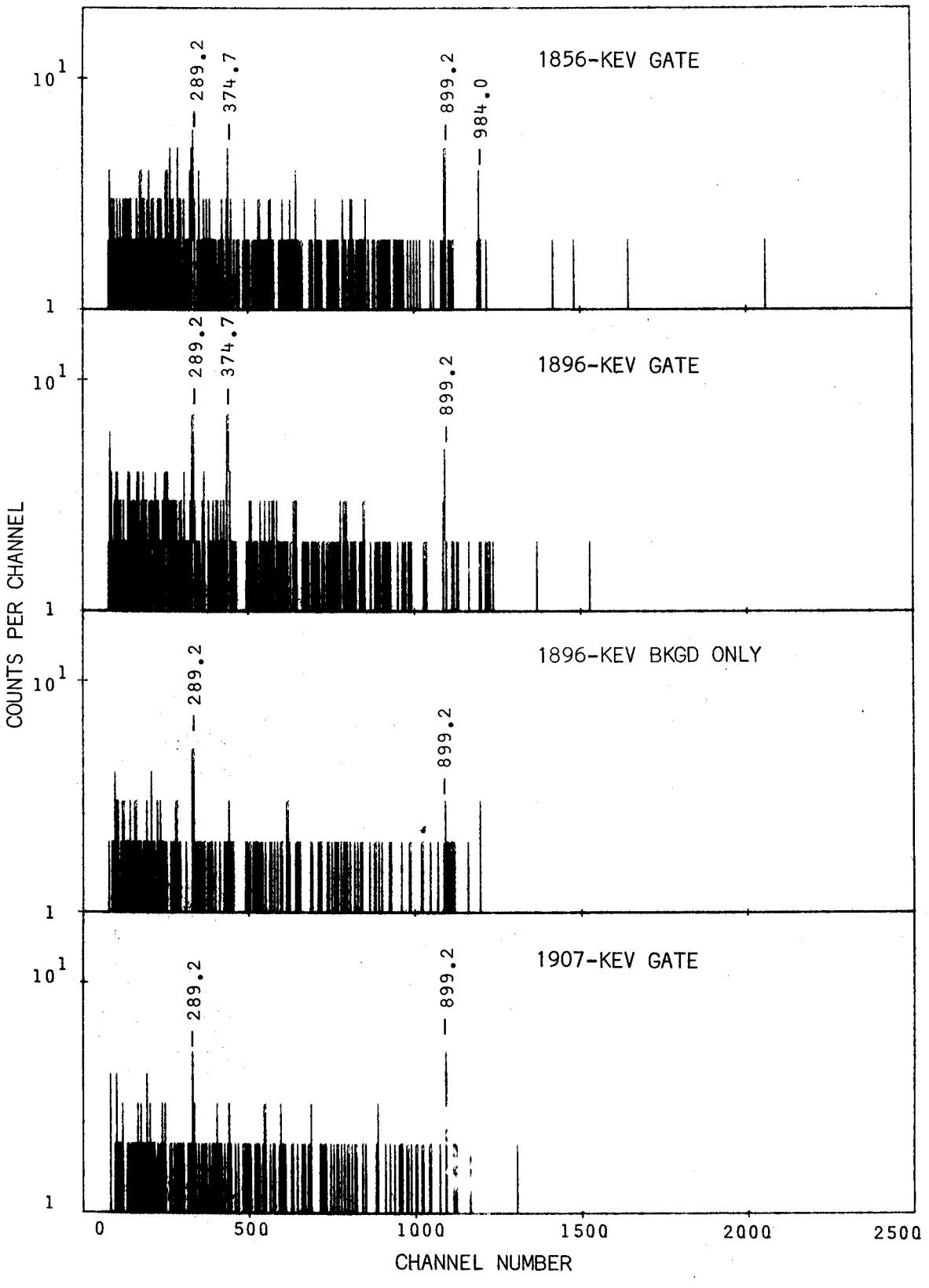

Fig. 24. (continued)

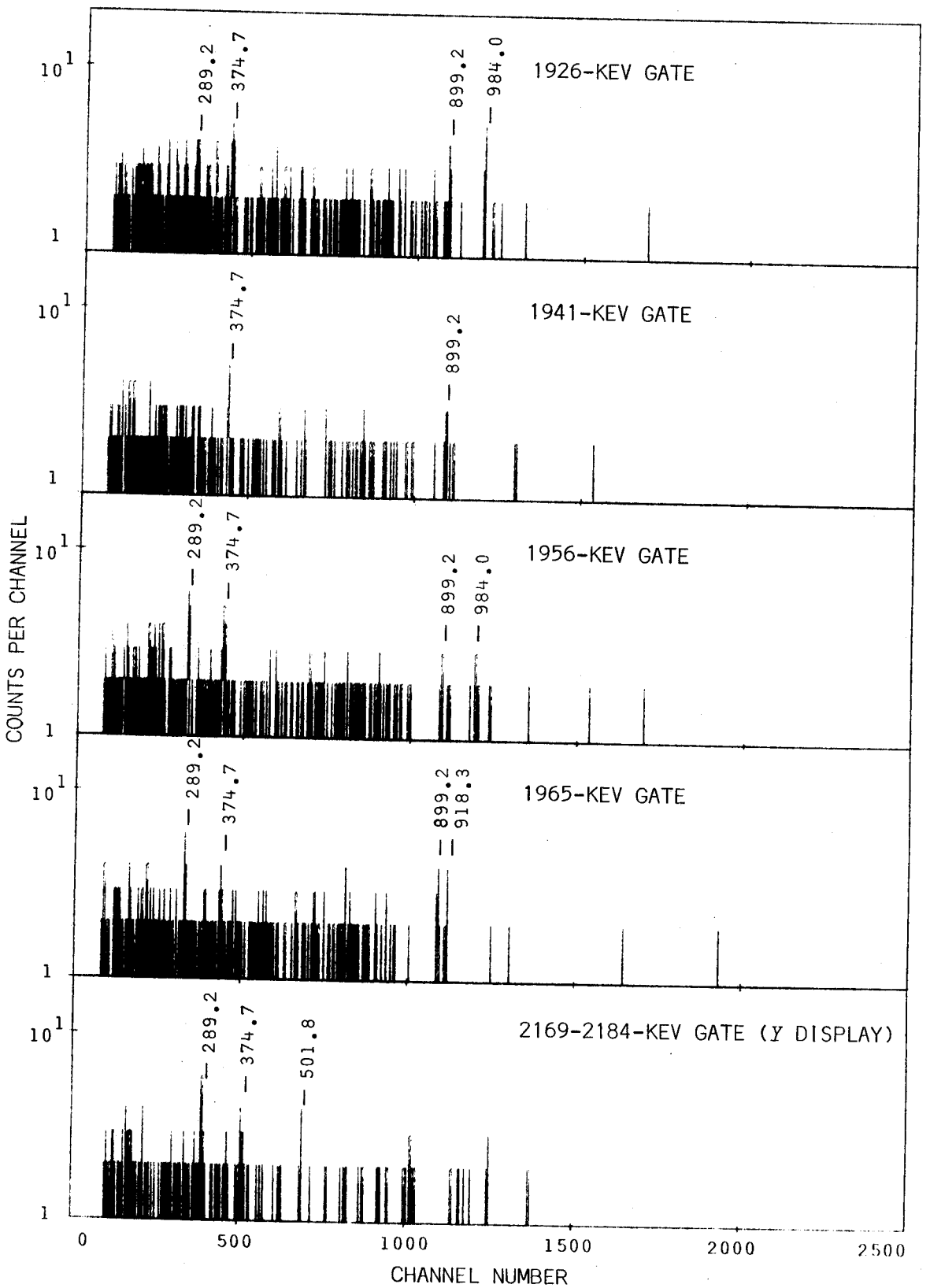

Fig. 24. (continued)

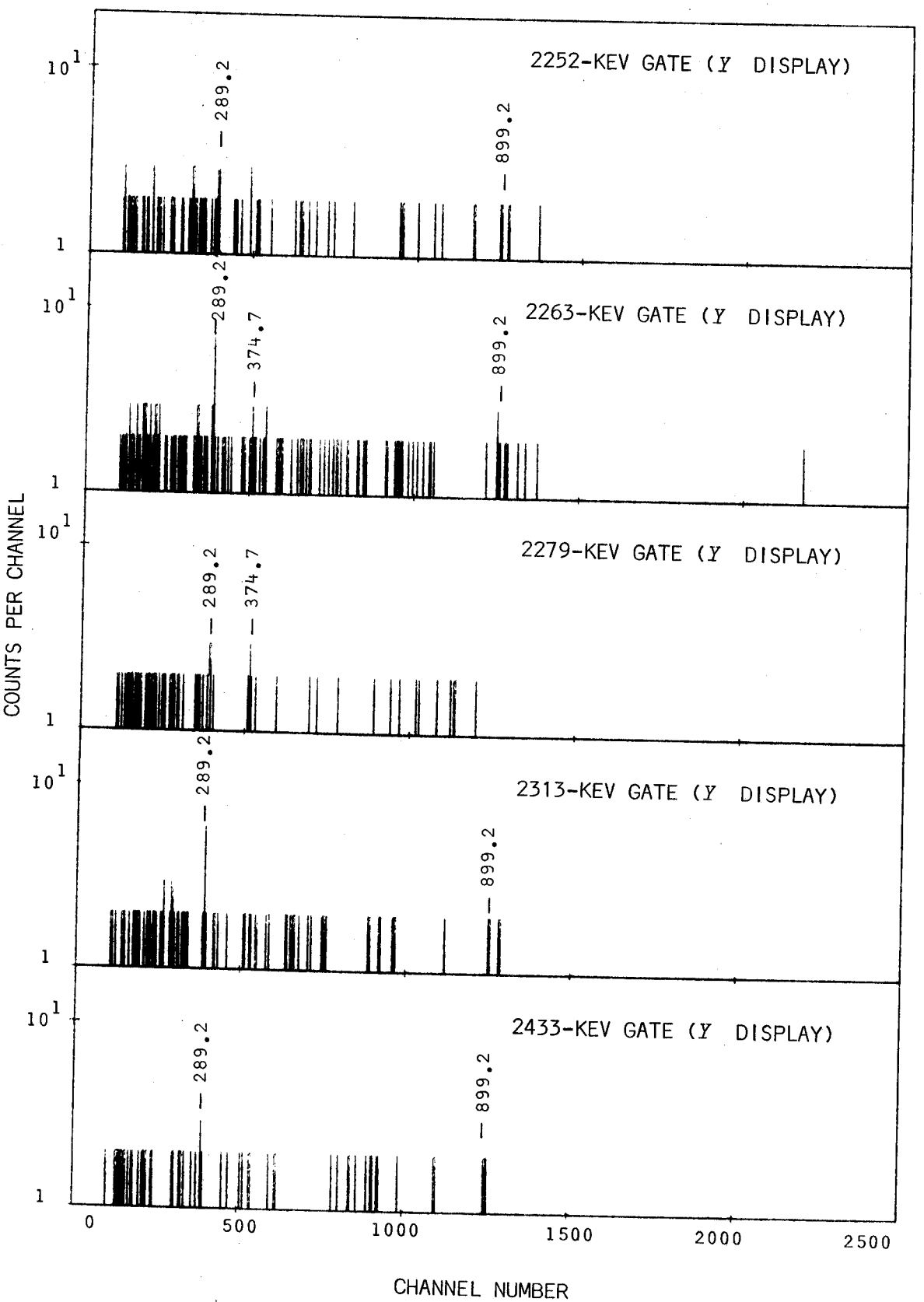

Fig. 24. (continued)

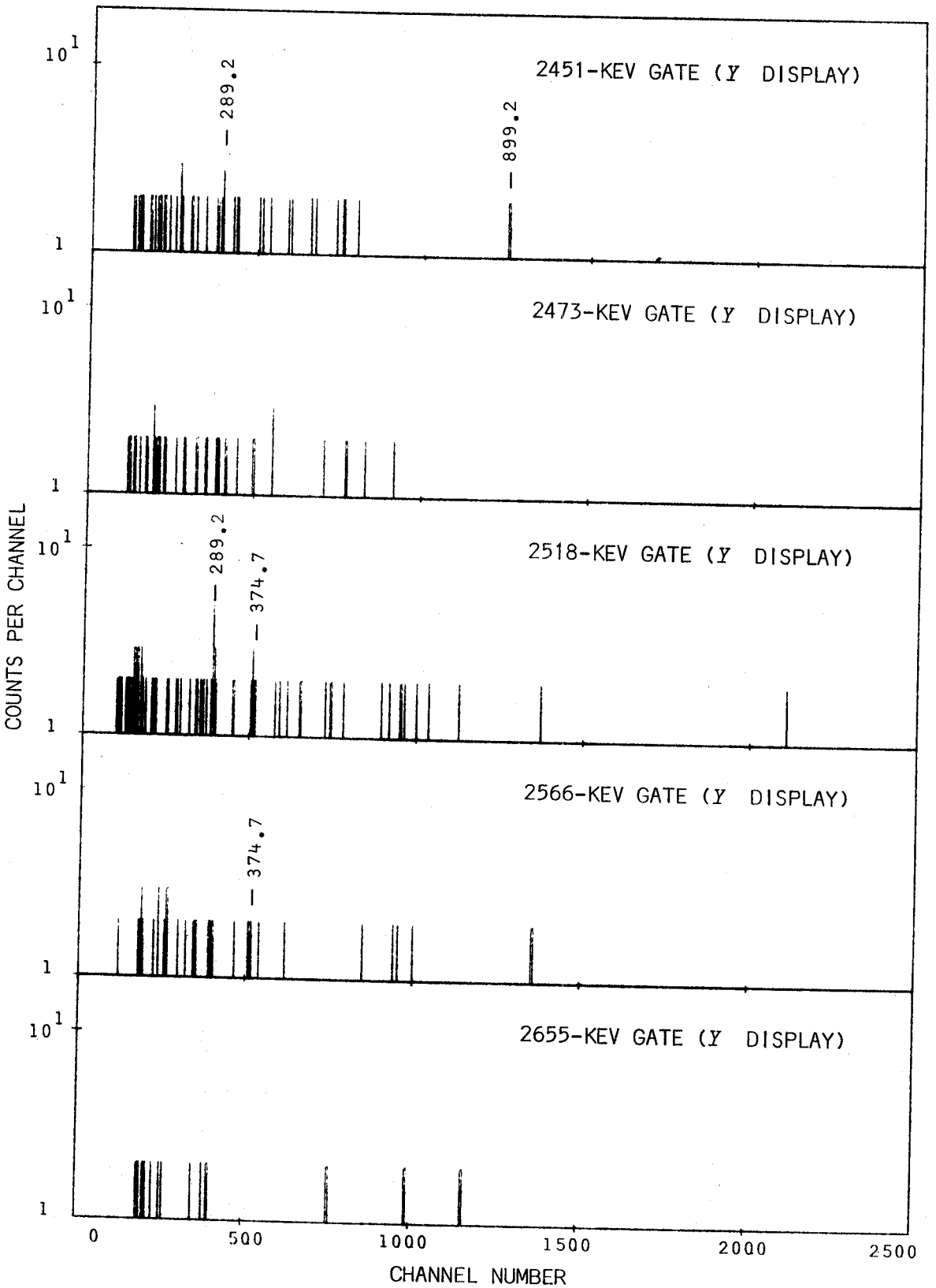

Fig. 24. (continued)

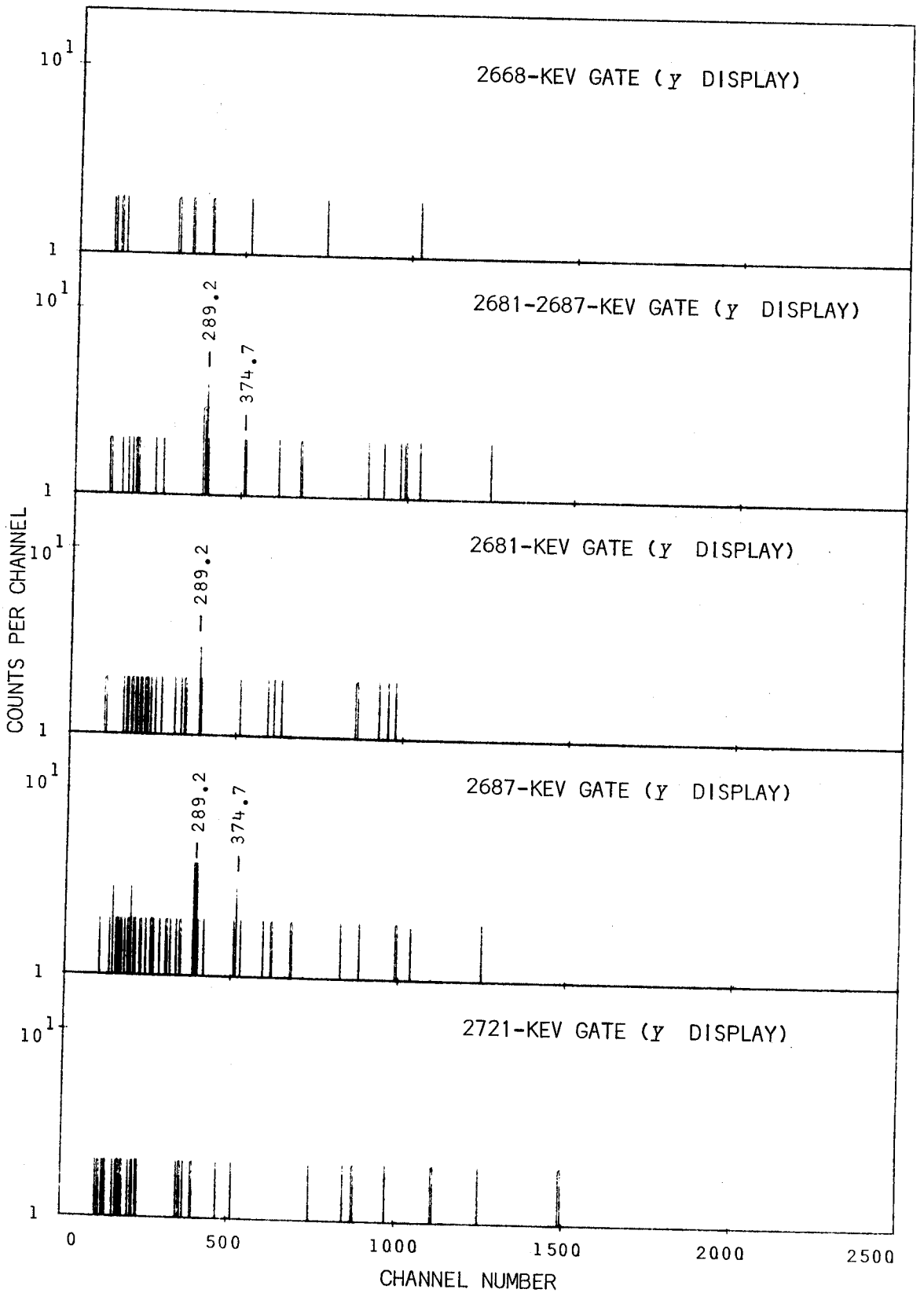

Fig. 24. (continued)

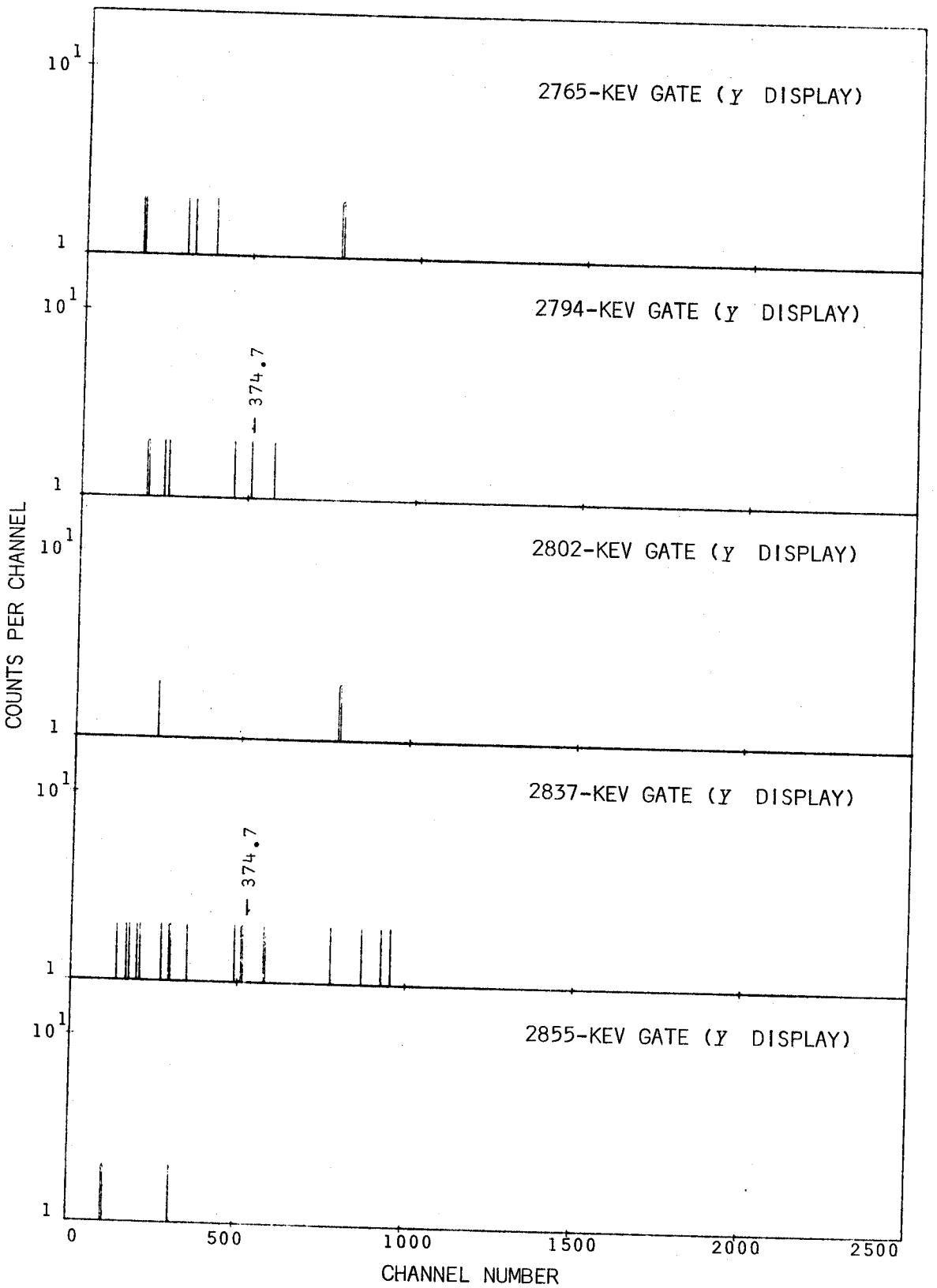

Fig. 24. (continued)

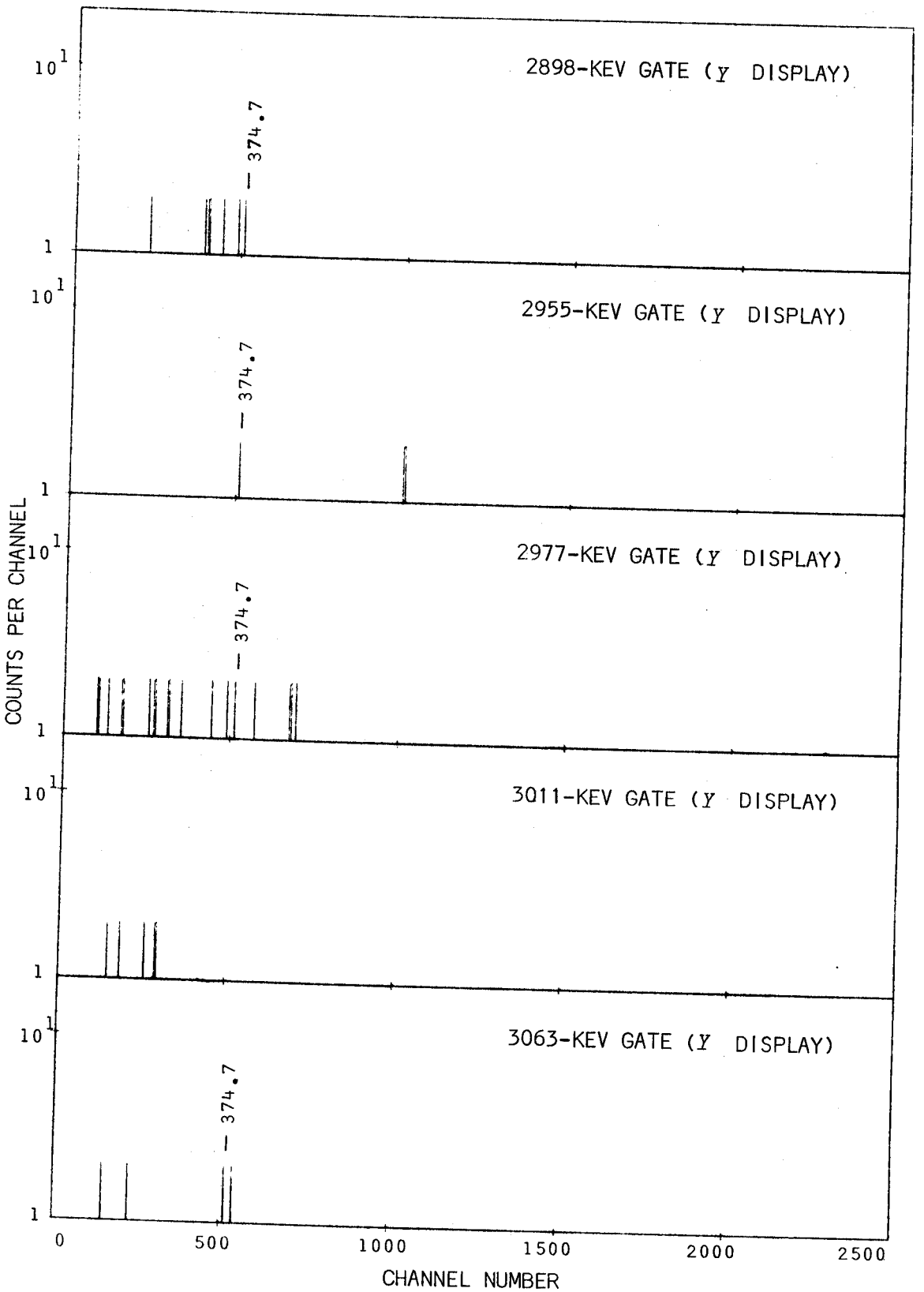

Fig. 24. (continued)

Fig. 25. The level scheme of Pb^{204} showing additional transitions from the Bi^{204} decay which could be placed on the basis of precise energy sums and differences alone. The tolerance allowed for the left side of the figure was ±0.25 keV for γ's having energies <1500 keV and ±0.30 keV for γ's having energies >1500 keV. The tolerance for the right side of the figure was ±0.5 keV. A semicircle at the origin of a transition indicates some coincidence data support for such a placement.

3.1.5. Electron Data and Multipolarities

The γ intensities from the present measurements were compared with the conversion-electron intensity data of Stockendal [St60] and Fritsch et al. [Fr58] in order to gain multipolarity information about some of the transitions seen in the Bi^{204} ε decay. The two sets of data (my γ intensities, their electron data) were normalized for the pure *E*2 899.2-keV transition. The conversion coefficient used was 6.51×10^{-3} [S165] for an 899.2-keV *E*2 transition. The results of these comparisons (with theoretical conversion coefficients [S165]) and the predicted multipolarities are listed in Table 10. Perhaps the most unfortunate facet of this table is that it does not include many of the reasonably strong high energy γ rays, but the electron data are just not available. The theoretical conversion coefficients were also used to construct smooth curves, upon which I have superimposed the experimental points (Figure 26). Only a few error bars are included, since precise error limits were not available for most of the electron data. A few of the transitions have already had multipolarities assigned; these are discussed below.

Internal conversion and scintillation measurements by Stockendal et al. [St58] indicate an experimental *K*-conversion coefficient of 0.37±0.10 for the 289.2-keV transition. Since the theoretical value is 0.38 [S165], an assignment of *M*1 seems entirely reasonable, most of the error being due undoubtedly to the interference of the weak 291.3-keV peak.

The *K*-electron of the 670.7-keV transition was sufficiently weak that only a lower limit could be obtained for the internal

Table 10. Multipolarity of Bi^{204} γ transitions

Transition energy[a] (keV)	K-electron intensity[b]	γ-ray intensity[c]	Experimental α_K[d]	Theoretical α_K[f]				Multipolarity
				M1	M2	E2	E3	
899.2	≡1000 [1000]	≡100.0	≡6.51(-3) [6.51(-3)][e]	-	-	6.51(-3)	-	E2
140.80	- [1230]	0.88	- [9.0(-1)]	2.8(0)	1.4(0)	-	7.4(0)	M1,E3
169.83	440 [370]	0.26	1.1(0) [9.4(-1)]	1.7(0)	8.4(0)	-	-	M1
176.2	2200 [1820]	1.08	1.3(0) [1.1(0)]	1.5(0)	7.0(0)	-	-	M1
212.7	300 [90]	0.34	5.8(-1) [1.8(-1)]	9.2(-1)	4.0(0)	1.5(-1)	-	M1,E2
216.1	1780 [1630]	1.32	8.8(-1) [8.0(-1)]	8.6(-1)	3.5(0)	-	3.7(-1)	M1
219.5	565 [500]	2.19	1.7(-1) [1.5(-1)]	8.3(-1)	3.3(0)	1.4(-1)	3.5(-1)	E2
222.2	1040 [940]	1.00	6.8(-1) [6.1(-1)]	8.1(-1)	3.1(0)	1.3(-1)	3.4(-1)	M1
227.5	80 [80]	0.22	2.4(-1) [2.4(-1)]	7.6(-1)	3.0(0)	1.2(-1)	3.3(-1)	E2,E3
240.4	400 [290]	0.28	9.2(-1) [6.6(-1)]	6.3(-1)	2.5(0)	1.1(-1)	2.8(-1)	M1
248.9	2050 [1820]	2.04	6.5(-1) [5.8(-1)]	5.6(-1)	2.1(0)	1.0(-1)	2.7(-1)	M1
289.2	1650 [1440]	2.75	3.9(-1) [3.4(-1)]	3.7(-1)	1.3(0)	7.1(-2)	1.9(-1)	M1
291.4	220 [570]	0.92	1.6(-1) [3.9(-1)]	3.7(-1)	1.3(0)	7.1(-2)	1.9(-1)	M1,E3
331.1	150 [170]	0.34	2.8(-1) [3.2(-1)]	2.6(-1)	8.9(-1)	5.2(-2)	1.4(-1)	M1
405.8	100 [130]	0.28	2.3(-1) [3.0(-1)]	1.6(-1)	4.9(-1)	3.3(-2)	8.5(-2)	M1
412.2	120 [120]	0.29	2.7(-1) [2.7(-1)]	1.4(-1)	4.4(-1)	3.2(-2)	8.2(-2)	M1
421.6	310 [320]	1.06	1.9(-1) [2.0(-1)]	1.4(-1)	4.2(-1)	-	7.5(-2)	M1
438.5	180 [230]	0.78	1.5(-1) [1.9(-1)]	1.2(-1)	3.8(-1)	-	7.1(-2)	M1
473.5	45 -	0.13	2.3(-1) -	1.0(-1)	3.1(-1)	-	-	M1,M2
501.8	140 [150]	0.88	1.0(-1) [1.1(-1)]	8.8(-2)	2.5(-1)	-	5.2(-2)	M1
522.2	110 [120]	0.62	1.2(-1) [1.3(-1)]	8.0(-2)	2.2(-1)	-	4.8(-2)	M1
532.7	265 [260]	1.30	1.3(-1) [1.3(-1)]	7.6(-2)	2.1(-1)	-	4.6(-2)	M2,M1
543.4	45 [40]	0.29	1.0(-1) [9.1(-2)]	7.2(-2)	2.0(-1)	-	4.3(-2)	M1
661.5	220 [210]	2.66	5.4(-2) [5.2(-2)]	4.5(-2)	1.1(-1)	1.2(-2)	2.8(-2)	M1
663.4	80 [80]	0.82	6.4(-2) [6.4(-2)]	4.4(-2)	1.1(-1)	1.2(-2)	2.8(-2)	M1
670.7	825 [810]	10.7	5.0(-2) [4.9(-2)]	4.1(-2)	1.0(-1)	1.2(-2)	2.7(-2)	M1
709.1	130 [120]	1.44	5.9(-2) [5.4(-2)]	3.8(-2)	9.9(-2)	1.0(-2)	2.4(-2)	M1

Table 10. (continued)

710.5	65 -	1.42	3.0(-2) -	3.6(-2)	9.0(-2)	1.0(-2)	2.4(-2)	*M1,E3*
718.4	90 [50]	0.86	6.8(-2) [3.8(-2)]	3.6(-2)	8.9(-2)	1.0(-2)	2.3(-2)	*M1*
725.2	45 [50]	0.97	3.0(-2) [3.4(-2)]	3.5(-2)	8.9(-2)	9.6(-3)	2.2(-2)	*M1*
791.2	100 [90]	3.39	1.9(-2) [1.7(-2)]	2.6(-2)	6.4(-2)	8.2(-3)	1.9(-2)	*M1,E3*
912.0	525[g] [300][g]	11.4	2.8(-2) [1.6(-2)]	1.9(-2)	4.6(-2)	-	1.4(-2)	*M1*
918.3	125 [110]	10.7	7.4(-3) [6.6(-3)]	1.9(-2)	4.6(-2)	6.4(-3)	1.4(-2)	*E2*
1203.8	26 -	2.09	8.1(-3) -	9.5(-3)	2.2(-2)	3.8(-3)	8.0(-3)	*M1,E3*
				M1	*M2*	*E3*		
100.7	400[h] [270][h]	0.14	1.9(0)[h] [1.3(0)[h]	2.3(0)[h]	3.7(0)[h]	-		*M1*
140.8	350[h] -	0.88	2.6(-1)[h] -	4.5(-1)[h]	4.0(0)[h]	5.0(-1)[h]		*M1*
				M1	*E1*	*E2*		
984.0	30[h] -	58.4	3.3(-4)[h] -	2.6(-3)[h]	3.1(-4)[h]	8.4(-4)[h]		*E1,E2*
80.4	2600[i] -	0.32	5.4(0)[i]	2.6(0)[i]	1.2(-1)[i]	1.3(1)[i]		*M1*

[a] Energies from present study.

[b] Relative *K*-electron intensities without brackets from reference [St58]; relative *K*-electron intensities within brackets from reference [Fr58].

[c] Relative γ-ray intensities from present work.

[d] Values without brackets calculated from [St58] *K*-electron intensities; values within brackets calculated from [Fr58] *K*-electron intensities.

[e] The theoretical value for an *E2* [S165] was used to normalize the electron and γ-ray data.

[f] Theoretical interpolated α_K from graphs prepared from conversion coefficients given in [S165].

[g] The electron intensity for the 912.0-keV peak was found by subtracting the electron intensity of the 911.7-keV peak (a known *E5*) from the electron intensities given in references [St58] and [Fr58] (which are presumed to be the sum of the electron intensities of the 911.7- and 912.0-keV transitions).

[h] These represent relative L_1-electron intensities, experimental α_{L_1}, and theoretical α_{L_1} values for the listed multipolarities, respectively.

[i] These represent relative *L*-electron intensities, experimental α_L, and theoretical α_L values for the listed multipolarities, respectively.

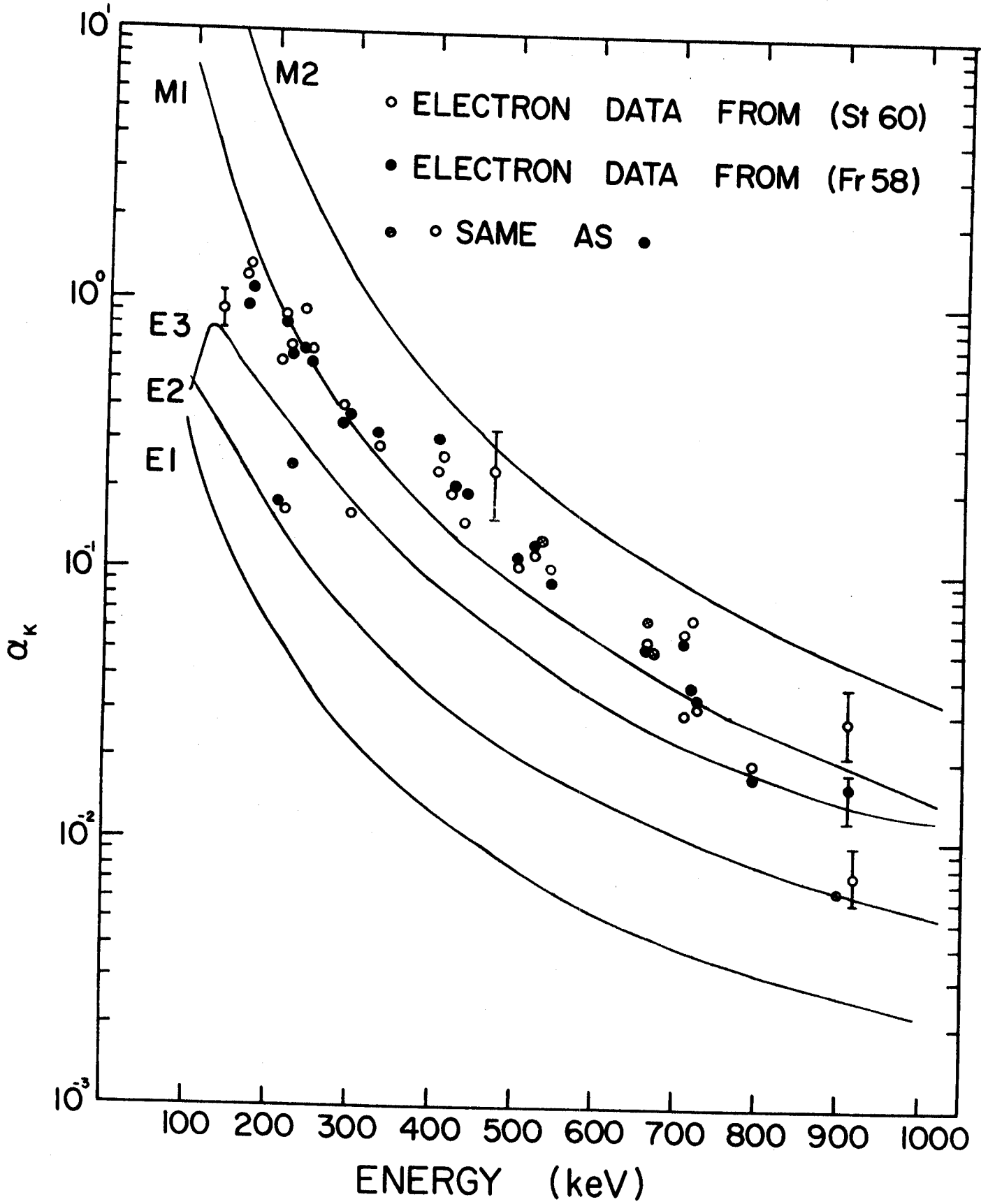

Fig. 26. Experimental conversion coefficients for some Pb^{204} transitions. The smooth curves of the theoretical α_K were prepared from tables in [S165].

K conversion coefficient. However, this limit definitely excludes the $E1$ and $E2$ multipolarities [St58].

For the 899.2-keV transition, the most probable multipolarity assignment is $E2$, as established by [St60,Kr55,He56, and St58].

The 374.7- and 911.7-keV transitions have also been studied in several excellent investigations and their predominantly $E2$ and $E5$ characters, respectively, are well established [St58,St60,Kr55,He56]. Neither of these transitions, though, was predicted to be a pure multipole. Krohn and Raboy [Kr55] found from angular correlation measurements on Bi^{204} that the 374.7-keV γ is $E2$ with a 0.5% admixture of $M3$ and that the 911.7-keV γ is $E5$ with a 1% admixture or $M6$. Herrlander et al. [He56] found a maximum admixture of 0.5% $M6$ for the 911.7-keV γ ray, however, they attempted to separate the Pb^{204m} from Bi^{204} in their work. Perhaps, this explains why they found a lower admixture limit.

With the advent of the realization that the 911.7-keV peak was only part of a closely-spaced doublet, I think I now can explain the hitherto "impurity" in the $E5$ transition. The previous measurements were taken not on the 911.7-keV peak but on the 911.73+911.96-keV doublet. The multipolarity of this additional 911.96-keV γ was calculated from my γ intensities and Stockendal's [St58] electron data by assuming the 911.7-keV γ ray to be a pure $E5$ transition, and using the theoretical conversion coefficient to remove the K electron intensity due to the 911.73-keV transition. When this is done and the K conversion coefficient calculated, it is very clear that the 911.96-keV γ is an $M1$ transition. What the previous experiments have seen then is not an admixture of $E5$ and $M6$ but an admixture of $E5$

(from the 911.7-keV γ) and *M*1 (from the 911.96-keV γ). Using the theoretical conversion coefficient for an *M*1, 911.96-keV γ, I have calculated that 1% *M*6 is equivalent to ≈26% *M*1. Considering the unqualified assumptions on the multipolarities and the difficulties of accurately separating the electron and γ-ray intensities, I think that ≈26% is remarkably close to the 45% that one might have predicted.

3.1.6. Spin and Parity Assignments for Pb^{204}

Curbing the lemming urge to dash headlong into the actual spin and parity assignment discussion, I want to side-step for a moment for a few (hopefully) words of scientific enlightenment. Using the experimental photon intensities for Bi^{204}, the calculated (or experimental) multipolarities of a few of the Bi^{204} γ rays, the estimated decay energy, and the $t_{\frac{1}{2}}$, one can calculate the log *ft*'s and percent feedings to each of the states in Pb^{204}. For those γ rays which do not have calculated multipolarities, I assumed that each was an *M*1 multipole (for the purpose of calculating the log *ft*'s only) as most of the calculated γ rays were *M*1's anyway (see section 3.1.5.). Using the modified DECAY SCHEME program, the feedings and log *ft*'s to each state were calculated; these are found in the left-hand column of Table 11. However, a consideration of the peculiarities of the Bi^{204} decay leads me to question the validity of such a list.

For example, consider the 899.2-keV excited state. This state has both an abnormally high % feeding and subsequently low log *ft*. Because the 899.2-keV state is 2+, this would involve a fourth-forbidden transition from the 6+ Bi^{204} ground state. Consequently, one would expect a considerably larger log *ft* than the 8.1 actually

Table 11. Percent feedings and log ft's for the excited states in Pb^{204}.

Excited state (keV)	Percent[a] feeding	Log ft[a]	Percent[b] feeding	Log ft[b]
899.2	10.14	8.06	0.0	large
1273.9	0.0	large	0.0	large
1562.8	1.16	8.80	1.46	8.72
1817.3	0.0	large	0.0	large
2065.1	1.86	8.44	2.34	8.34
2185.4	10.43	7.64	0.0	large
2257.9	26.75	7.15	33.68	7.10
2385.8	0.61	8.79	0.77	8.69
2434.0	0.28	9.11	0.35	9.01
2480.0	1.00	8.53	1.26	8.43
2506.8	0.0	large	0.0	large
2919.5	2.69	7.86	3.38	7.76
2928.5	9.74	7.30	12.26	7.20
3029.0	2.82	7.77	3.55	7.67
3092.0	3.56	7.62	4.49	7.52
3104.9	0.0	large	0.0	large
3170.0	15.03	6.93	20.06	6.82
3215.0	1.20	6.93	1.51	7.90
3232.0	2.06	7.75	2.60	7.65
3637.8	5.51	7.75	6.94	6.82
3768.4	2.03	7.09	2.56	7.06
3782.0	1.07	7.22	1.34	7.32
3814.4	0.22	7.42	0.28	7.95
3826.2	0.27	7.95	0.33	7.85
3842.2	0.03	8.83	0.04	8.73
3875.7	0.06	8.50	0.08	8.40
3996.1	0.03	8.59	0.03	8.49

Table 11. (continued)

4080.5	0.18	7.47	0.23	7.37
4165.5	0.09	7.35	0.12	7.25
4249.6	0.06	6.03	0.33	6.03

[a]Calculated values from the relative beta intensities as determined from transitions populating and depopulating each state.

[b]Corrected values after the relative beta intensities to the 899.2- and 2185.4-keV states were arbitrarily set to zero.

found. Two possible reasons for the discrepancy are available: first, many weak γ rays may be feeding the 899.2-keV state directly from higher-lying states (but unobservable in the coincidence data), and second, there may be a low-lying low-spin isomeric state (e.g., 2+) in Bi^{204} which directly populates the 2+ 899.2-keV excited state in Pb^{204}. Such a feeding (from a 2+ Bi^{204} isomeric state) would account for some of the unexpectly large percent feeding to the 899.2-keV level. A preliminary test for such a possibility is presently in the planning stages. By observing the intensity fluctuations (if any) in the 899.2-keV peak as a function of time after bombardment, one should get some idea of whether such an argument is feasible or not. Another argument might be made concerning the precision of the intensity calibrations. Since the calibration error ranges from 5 to 15% for peaks of reasonable size (i.e., >3% of the 899.2-keV peak), much of the 10.1% feeding to the 899.2-keV state could be due to calibration errors in the intensities of the γ's populating and depopulating the 899.2-keV state. It also appears that only the high-spin states are populated by the ε decay of the 6+ Bi^{204} ground state. It is almost a certainty that there are other low-spin states which are only weakly populated and are, therefore, difficult to place using the present techniques (because the transitions are weak). Presumably, these states would feed other low-spin states, e.g., the 2+ 899.2-keV state. This, in turn, would decrease the large percent feeding and increase the subsequently low log *ft*. One or more of the forementioned possibilities makes it understandable why such a large percent feeding

was found for the 2+ 899.2-keV state.

Also, consider the 2185.4-keV isomeric level. It would have to be a third-forbidden β transition from the 6+ Bi^{204} ground state to the 9- Pb^{204m} isomeric state and as such should have a large log *ft*. The spin and parity of the 2185.4-keV level has been previously established as 9- [Fr58,St58,Kr55]. It is on the basis of such an assignment that the following argument can be made. As I have been unable to identify any of the γ's directly feeding the 2185.4-keV state, the log *ft* "appears" to be 7.6. However, this β transition (to the 9- isomeric state) is third-forbidden and nearly all the populating intensity should come from γ feeding from higher-lying high-spin states. These would have the tendency to decrease the feeding and increase the log *ft*.

A much more accurate set of percent feedings and log *ft*'s might result if arbitrarily I were to set the input and output transition intensities equal for these two states, i.e., assume no β feeding to either of these states. The right column of Table 11 shows the result of doing this. One could argue that what I have done is to arbitrarily force the data into values I want to believe. Rather, this set of feedings and log *ft*'s represent what should be more realistic values for these parameters in light of all the present and previously reported data. Note that the log *ft*'s are increased by only about 0.1.

3.1.6.A. Ground, 899.2-, 1273.9-, and 2185.4-keV States

The ground state is assigned 0+, as would be expected for an even-even nucleus ($_{82}Pb^{204}_{122}$). The remaining three levels comprise a portion of the Pb^{204m} decay scheme and as such have been thoroughly

investigated (section 1.2.5.). These investigations revealed a 911.7-keV $E5$ transition, an 899.2-keV $E2$ transition, and a 375.0-keV $E2$ transition. These suggest a 0+, 2+, 4+, 9- spin (and parity) sequence for the states in Pb^{204m}. This sequence was also confirmed by the detailed angular correlation experiments of Krohn and Raboy [Kr54,Kr55], although it was necessary to assume some small multipole mixing to account precisely for the results. The (p,t) data of Holland et al. [Ho69] and the associated Distorted Wave-Born Approximation (DWBA) calculations also suggest the 0+, 2+, 4+, 9- spin sequence. Thus, I also assign the ground, 899.2-, 1273.9-, and 2185.4-keV states spin and parities of 0+, 2+, 4+, and 9-, respectively, as these assignments are also internally consistent with the present data.

3.1.6.B. 1562.8-keV State

The 1562.8-keV state was first revealed by Fritsch et al. (section 1.2.5.A.) in their study of the Pb^{204m} decay. They found a 622.2-keV $E5$ γ depopulating the 2185.4-keV isomeric state and a 289.2-keV $M1$ γ depopulating the 1562.8-keV state. This latter multipolarity was also confirmed by the present data (Table 10). The $M1$ character of the 289.2-keV transition suggests a 3+, 4+, or 5+ assignment. The 622.2-keV $E5$ γ depopulating the well-known 9- isomeric level suggests 4+ or 14+. The rather large log ft (for the Bi^{204} decay) of 8.7 would appear to indicate an allowed or first-forbidden transition. However, not all the γ's feeding the 1562.8-keV state have been placed with a high-degree of confidence. This means that the log ft most likely should be larger than 8.7. Because of this, I

suggest that the possibility that it is really a second-forbidden transition from the 6+ Bi^{204},is not ruled out. While the log ft value is inconclusive the remaining data appear to suggest a 4+ assignment for the 1562.8-keV state.

3.1.6.C. 1817.3-keV State

The very strong 918.3-keV $E2$ γ to the 899.2-keV 2+ level immediately limits the possible assignment to 0+ through 4+. The log ft, being arbitrarily large, tells one absolutely nothing. DWBA calculations by Holland et al. [Ho69] suggest a 4+ assignment, although 3+ cannot be excluded because of the intrinsic spins of the proton and triton. Some minor information can be obtained from the non-existence of specific transitions (if one is careful). One might assume that the spin is ≤ 5 as Pb^{204m} does not appear to populate this state. Also, nothing (i.e., no transition) appears to populate both the 899.2-keV 2+ state and this level, which might lead one to say that the spin is ≥ 4. This last argument is weak, but it does add a small measure of evidence to a 4+ assignment, although 3+ cannot be ruled out entirely.

3.1.6.D. 2065.1-keV State

The 791.2-keV $M1$ γ transition (to the 4+ 1273.9-keV state) suggests a possible assignment of 3+, 4+, or 5+; similarly, the 501.8-keV $M1$ γ transition (to the 4+ 1562.8-keV state) also suggests 3+, 4+, or 5+ assignments. The log ft of 8.3 probably implies an allowed transition (negative parity states ruled out on basis of the $M1$ transitions) which would allow spins (and parity) of 5+, 6+, and 7+. Combining the log ft and multipolarity data limits the assignment to 4+ or 5+. Little more can be deduced from the higher-lying levels, so the state at 2065.1 keV is assigned 4+ or 5+. The intensity balance on this

level appears to be quite good and can probably be trusted. This limits the assignment of the 2065.1-keV state to 5+.

3.1.6.E. 2257.9-keV State

The state at 2257.9 keV is assigned 5+ or 6+ on the basis of the 984.0-keV *E*2 γ (which allows 2+ to 6+) and the log *ft* of 7.1 which is almost certainly an allowed transition (suggesting a 5+, 6+, or 7+ assignment). No preference between 5+ and 6+ is available at this point, so they are assigned with equal weight. Actually, this is unfortunate since many of the high-lying states will have to be based upon this level, but (tragically) the data do not warrant any other assignment.

3.1.6.F. 2385.8-keV State

The only concrete evidence for the assignment of this level is the log *ft* value, inasmuch as the multipolarities for both depopulating γ's are unknown. The high log *ft* of 8.7 suggests an allowed or first-forbidden transition ,i.e., an assignment of 5±, 6±, or 7±. Assuming the γ's to be *M*1, *E*2, or *E*1, I find possible assignments of 2+ through 7+ and 3- through 7-. From the log *ft* alone, then, I suggest an assignment for the 2385.8-keV state of 5±, 6±, and 7±.

3.1.6.G. 2434.0-keV State

The 176.2-keV *M*1 transition from this state (to the 5+ or 6+ 2257.9-keV level) implies an assignment of 4+, 5+, 6+, or 7+. The log *ft* of 9.0 is one of the largest of any of the Pb^{204} levels. This probably suggests an allowed transition (first-forbidden ruled out by the *M*1). This suggests 5+, 6+, and 7+ assignments. Eliminating the non-common elements, I propose that the 2434.0-keV state is 5+, 6+, or 7+.

3.1.6.H. 2480.0-keV State

The 222.2-keV *M*1 γ to the 2257.9-keV state allows a 4+, 5+, 6+, or 7+ assignment. The log *ft* of 8.4 would appear to suggest a first-forbidden or an allowed transition. The first-forbidden transition can be ruled out since the *M*1 transition extablishes the parity as positive. This leaves, therefore, 5+, 6+, or 7+ for the 2480.0-keV state.

3.1.6.I. 2506.8-keV State

The 248.9-keV *M*1 γ to the 2257.9-keV (5+,6+) state limits the state to 4+, 5+, 6+, or 7+ and also eliminates the possibility of - parity states. The log *ft* tells nothing about this state. It is terribly frustrating that the assignment for this level cannot be reduced further, as there are 5 higher-lying states (some of which must be populated by allowed transitions) which feed this state (3 by known *M*1's), implying a 4+ to 8+ assignment. The data appear to justify only a 4+, 5+, 6+, or 7+ assignment for the 2506.8-keV state.

3.1.6.J. 2919.5-keV State

The level at 2919.5-keV is assigned 5+ or 6+. On the basis of the low log *ft* of 7.8 one would expect an allowed or first-forbidden transition. The possibility of negative parity states is eliminated by a 661.6-keV *M*1 γ to the 5+ or 6+ 2257.9-keV state (allowing a 4+, 5+, 6+, or 7+ assignment) and by a 412.2-keV *M*1 γ to the poorly known (4+ to 7+) 2506.8-keV state. Note also, that a 1645.6-keV γ populates the 4+ 1273.9-keV state, but none is found to populate the 2+ 899.2-keV state. This weakly suggests a ≥5+ assignment, which is

consistent with the present assignment. The 1102.2-keV γ populates the 4+(3+) 1817.3-keV state; on this basis one might tentatively rule out 7+ as a possible assignment.

3.1.6.K. 2928.5-keV State

The assignment for this state follows exactly the same reasoning as for the previous state, having analogous transitions to the same states. A 421.6-keV *M*1 γ to the 2506.8-keV state would suggest external quantum numbers of 3+ to 8+. However, a strong 670.7-keV *M*1 γ to the 2257.9-keV level rules out the 3+ and 8+ possibilities. The 4+ assignment can be discarded on the basis of a quite low log *ft* of 7.2, an allowed normal or *l*-forbidden transition. As a result, the 2928.5-keV state is finally narrowed to 5+ or 6+, the 7+ being weakly ruled out by the strong 1111.3-keV γ to the 4+ (3+) 1817.3-keV state (cf. analogous transition in section 3.1.6.J.).

3.1.6.L. 3029.0-keV State

The 522.2-keV *M*1 γ transition to the 2506.8-keV state would suggest that the 3029.0-keV state is 3+ to 8+, not very selective, to be sure. This can be limited to 4+ to 8+ as a result of the weak 100.7-keV *M*1 γ to the 2928.5-keV level. The log *ft* of 7.7 is somewhat high for an allowed transition, but considering the undoubtedly complex structure of 4-neutron-hole states (possibly core-coupled), one would expect the β transition to be hindered. Assuming, then, an allowed transition rules out 4+ and 8+, this leaves the 3029.0-keV state with possible assignments of 5+, 6+, or 7+. The 1755.3- and 1211.7-keV γ's to the 4+ 1273.9- and 4+ (3+) 1817.3-keV states, respectively, also shakily rule out the 7+ assignment. This means the state

at 3029.0 keV has an assignment of 5+ or 6+.

3.1.6.M. 3092.0-keV State

Solely on the basis of the log ft of 7.5, I propose an assignment of 5±, 6±, or 7± for the 3092.0-keV level. Rather unfortunately, no electron data are available for the strong 1274.8-keV γ to the 1817.3-keV state. Assuming that the 1274.8-keV γ is an $M1$, $E1$, $M2$, or $E2$, one might be tempted to rule out 7± as a possibility. As a consequence I somewhat riskily, suggest that the 3092.0-keV state is 5± or 6±. This assignment is weakly supported by a 1958.1-keV γ which goes to the 4+ 1273.9-keV state.

3.1.6.N. 3104.9-keV State

The state at 3104.9 keV is assigned 4+ to 8+ on the basis of the transitions to the 5+ or 6+ 2257.9- and 4+ to 7+ 2506.8-keV states and an arbitrarily large log ft. The negative parity states can be ruled out by an $M1$ 532.7-keV γ from the 3637.8-keV state which will be shown shortly to be 5+, 6+, or 7+.

3.1.6.O. 3170.0-keV State

The log ft of 6.8 for this level is the second lowest in the present Bi^{204} decay scheme and this obviously would suggest an allowed transition (or possibly a first-forbidden but this will be ruled out by an $M1$ from positive parity states, as discussed below). This implies an assignment of 5+, 6+, or 7+. Confirmation of this comes from a 912.0-keV $M1$ γ to the well-known 2257.9-keV state (5+ or 6+). I can thus suggest a 4+ to 7+ assignment. Also, a 140.8-keV $M1$ γ to the 3029.0-keV level suggests the range of 4+ to 7+. Coupling these possibilities rules out the 4+ and reduces the 3170.0-keV state to either

5+, 6+, or 7+. The existence of a transition to the 4+ 1273.9-keV state would appear to remove the 7+ possibility, so the final assignment is now 5+ or 6+.

3.1.6.P. 3215.0-keV State

Little can be said about this state, inasmuch as only the log *ft* is known. The 7.9 log *ft* value would appear to suggest either an allowed or first-forbidden transition, thereby implying 5±, 6±, or 7±. It is tempting to call the 1652.0-keV an *M*1 or *E*2 transition but I can find no overt rationale for doing so. But, as it populates a 4+ state, I am only somewhat poorly justified in ruling out the 7±. This reduces the assignment to 5± or 6± for the 3215.0-keV state.

3.1.6.Q. 3232.0-keV State

The log *ft* of 7.6 for this state seems somewhat high, but, once again, allowing for the complex internal structure surely to be associated with some of the Pb^{204} levels, this seems to suggest an allowed transition and a 5+, 6+, or 7+ assignment. The - parity states (from a first-forbidden transition) were ruled out because of a 725.2-keV *M*1 transition to the 2506.8-keV state, though this does not limit the spin assignment at all. The strong 1414.7-keV γ to the 4+ (3+) 1817.3-keV state might mean that one could be pardoned the sin of ruling out 7+. The same can be said of the 1958.1-keV γ.
I postulate a 5+ or 6+ 3232.0-keV state.

3.1.6.R. 3637.8-keV State

Two *M*1's, a 709.1-keV γ to the 5+ or 6+ 2919.5-keV state, and a 718.4-keV γ to the 5+ or 6+ 2928.5-keV state both appear to suggest spin and parities of 4+ to 7+ for the 3637.8-keV state. The

very low (for Pb^{204}) log *ft* of 6.8 surely implies an allowed β transition and a 5+, 6+, or 7+ assignment. The level at 2627.8 keV is subsequently assigned 5+, 6+, or 7+. The 1203.8-keV γ to the 2434.0-keV state certainly does not conflict with such an assignment.

3.1.6.S. 3768.4-keV State

The state at 3768.4 keV can only be assigned 5±, 6±, or 7± on the basis of its quite low log *ft* of 7.1 (suggesting an allowed or first-forbidden β transition). The very strong 1703.3-keV γ to the 2065.1-keV level very likely is an *M*1 or *E*2 although no electron data are available (tragically); this precludes any further legitimate reduction in the assignment. However, as it appears more likely that allowed transitions are hindered than first-forbidden transitions accelerated, I postulate only the + parity states, or 5+, 6+, or 7+.

3.1.6.T. 3782.0-keV State

The log *ft* of 7.3 indicates an allowed or first-forbidden transition. This suggests 5±, 6±, or 7±. The three depopulating transitions to the 5±, 6±, or 7± 2434.0-keV state, the 4+(3+) 1817.3-keV state, and the 5+ or 6+ 2257.9-keV state would appear to suggest that the 7± assignment can be tentatively ruled out. On this basis I propose that the spin and parity assignment for the 3782.0-keV state is 5± or 6±.

3.1.6.U. 3814.4-, 3826.2-, 3842.2-, 3875.7-, 3996.1-, 4080.5-, 4165.5-, 4249.6-keV States

Each of these has been assigned a spin entirely on the basis of the admittedly shakey log *ft* values. In inverse order, the transition to the state at 4249.6 keV is almost certainly an allowed

transition, its 6.0 log ft being the lowest (by 0.8) of any of the Pb^{204} log ft's. This suggests 5+, 6+, or 7+ for the 4249.6-keV state. The log ft's of 7.2 and 7.4 for the states at 4165.5 and 4080.5 keV, respectively, appear to be be indicative of an allowed or first-forbidden transition, thereby implying 5±, 6±, or 7± for these states. The next three lower levels, at 3996.1, 3875.7, and 3842.2 keV, are also assigned 5±, 6±, or 7± on the basis of their higher log ft's (8.5, 8.4, and 8.7, respectively). The final two levels, at 3826.2 and 3814.4 keV, fall in an unfortunately ambiguous region, having log ft's of 7.8 and 8.0, respectively. I finally decided once again to classify these as allowed or first-forbidden β transitions, thus suggesting 5±, 6±, or 7± as possible spin (and parity) assignments. It is frightfully tempting to call these last two allowed transitions, as one would expect the log ft's to be large, owing to the almost certain complex particle-hole rearrangements which must occur in the β transitions. Conservatism got the upper hand in these assignments, however, and the negative parity states are thereby included. Each of these states (except for the 4165.5-keV state) has one depopulating transition to the 1562.8-keV state. This weakly suggests that the 7± assignment might be ruled out, but tells one nothing about the parity of the states. The 4165.5-keV state must remain as 5±, 6±, or 7± as its depopulating γ is to the 5+, 6+, or 7+ 2434.0-keV state, which adds no information at all concerning the spin or parity of the 4165.5-keV state.

3.1.6.V. Comments

This last section on spin and parity assignments necessarily

concludes the Bi^{204} experimental sections. The theoretical or semi-theoretical discussion of the meaning (or "so what") of the Pb^{204} level scheme is left to a later chapter (Chapter IV). Before leaving, however, I must express a note of personal pessimism. Throughout the process of constructing the Bi^{204} decay scheme and making the associated external quantum number assignments, I have attempted to remain extremely pessimistic and conservative. In such a complicated decay scheme to do otherwise would possibly be to do irreparable harm to later investigations of the same isotope. Rather than mislead others by constructing an impressively large and complicated decay scheme of only "half-baked" data, I have chosen to propose a scheme which is smaller but much more firmly founded.

3.2. Electron Capture Decay Scheme of Bi^{203}

3.2.1. Introduction

Just as it was imperative to produce clean Bi^{204} sources, thus enabling one to identify the many Bi^{204} γ rays, so it is with the Bi^{203} sources. Bi^{203} has the added difficulty of being inseparable (by half-life or chemistry) from Bi^{204}, these having nearly identical $t_{\frac{1}{2}}$'s and, of course, identical chemical properties. As a consequence the previous investigations of Bi^{203} [Fr56,No58,St60] had to contend with a multitude of Bi^{204} peaks, many only poorly identified; the resulting work was anything but complete. Novakov et al. [No58] reported some 20 transitions from conversion-electron studies, and Fritsch [Fr56] reported essentially the same list, while Stockendal [St60] measured the internal conversion coefficients of several transitions by comparing the conversion lines to the photolines excited in an external uranium converter. Both Novakov et al. and Fritsch used permanent-magnet spectrometers in their investigations, but Novakov et al. have also used double-focusing β and scintillation spectrometers, e-γ and γ-γ coincidence measurements in their work. The highest γ-ray energy reported to date has been a 1896-keV transition, while the decay energy has been reported to be 3.2 MeV [Vi66]. Thus, once again, a number of high-lying levels, as yet unplaced, might be expected. Novakov et al. have ventured to propose a tentative dedecay scheme based upon their e-γ and γ-γ coincidence work (Figure 27).

While the decay scheme of Bi^{203} seems to be more concretely rooted by Novakov's coincidence data than Bi^{204} was by the work of Fritsch et al. [Fr58] and Stockendal et al. [St58], with recent

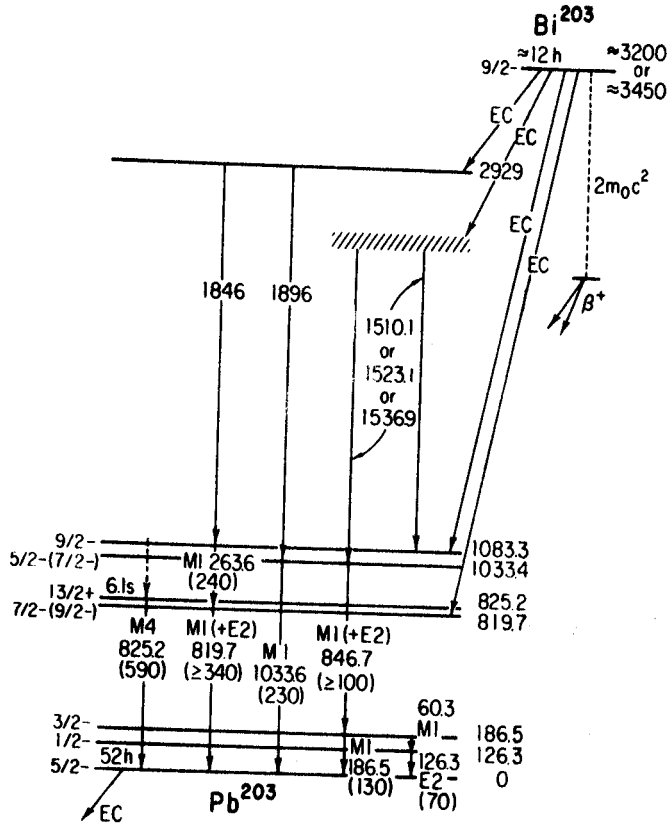

Fig. 27. Previously reported Bi^{203} decay scheme [No58].

advances in Ge(Li) spectroscopy technology and the fact that Bi^{204} is now reasonably well-known, it was felt that a re-investigation of the Bi^{203} decay could yield a great deal of new information. In truth, some 147 γ rays were identified, this being some 122 more than previously reported. Many changes and additions were made in the previously proposed decay scheme for Bi^{203}. These changes are discussed in the subsequent sections.

3.2.2. Source Preparation

The Bi^{203} sources were prepared by bombarding 97.22% Pb^{206} separated isotope (as $Pb(NO_3)_2$, obtained from ORNL Isotope Division) with 40-45 MeV protons from the MSU cyclotron for 1-2 h at 1-2 μA. The details of this production (including excitation function studies) were discussed in section 2.1. The short-lived contaminants were identified (most notably Bi^{202}, $t_{\frac{1}{2}}$=1.6 h, and Pb^{202m}, $t_{\frac{1}{2}}$=3.6 h) by taking spectra of the samples at various times after the bombardment and noting the large intensity variations of the peaks as they die out. The long-lived contaminants ($Bi^{205,206}$) were revealed by counting samples after they have been allowed to decay for 3-7 days and analyzing the remaining peaks. Once again no chemical separations were necessary, making this an easy radioactive source preparation technique.

3.2.3. Bi^{203} γ-Ray Spectra

3.2.3.A. Singles Spectra

The same two detectors described in section 3.1.3.A. were

used to determine the energies and intensities of the Bi^{203} γ rays. However, whereas the 2.5% Ge(Li) detector was used primarily for the Bi^{204} spectra, the 3.6% Ge(Li) detector was the primary detector used during this study because of its better resolution (typically 2.1 keV FWHM at 1.33 MeV).

The γ rays were determined by comparison with a number of well-known calibration sources listed previously in Table 5. A quick and efficient method of checking these energies was performed by also calibrating the major peaks of Bi^{203}, using the Bi^{204} peaks as internal calibration standards. The Bi^{204} peaks so used are compiled in Table 6. Just as with the Bi^{204} decay, the centroid of each standard peak was determined by MOIRAE and/or SAMPO (section 2.3.1.B.); the centroids of these peaks are fit to a least-square n^{th} (n = 2 commonly) degree curve, which then serves as the calibration curve. The calibration curve then returns the energies of the large unknown Bi^{203} γ rays from their own centroids. The weak Bi^{203} γ rays were calculated by repeating the process, using the now well-determined large Bi^{203} peaks as internal standards. A γ-ray singles spectrum of Bi^{203} (and Bi^{204} concurrently) utilizing the 3.6% detector is shown in Figure 28. A list of the energies and relative intensities of the γ rays from the ε decay of Bi^{203} is given in Table 12. The energies are the arithmetic mean values for several runs (2-3) taken at different times, different proton beam energies, and different Ge(Li) detectors. The corresponding uncertainties in the energies are slightly larger than the Bi^{204}, owing to fewer spectra that were averaged and because of Bi^{204} contamination, these uncertainties were: the major

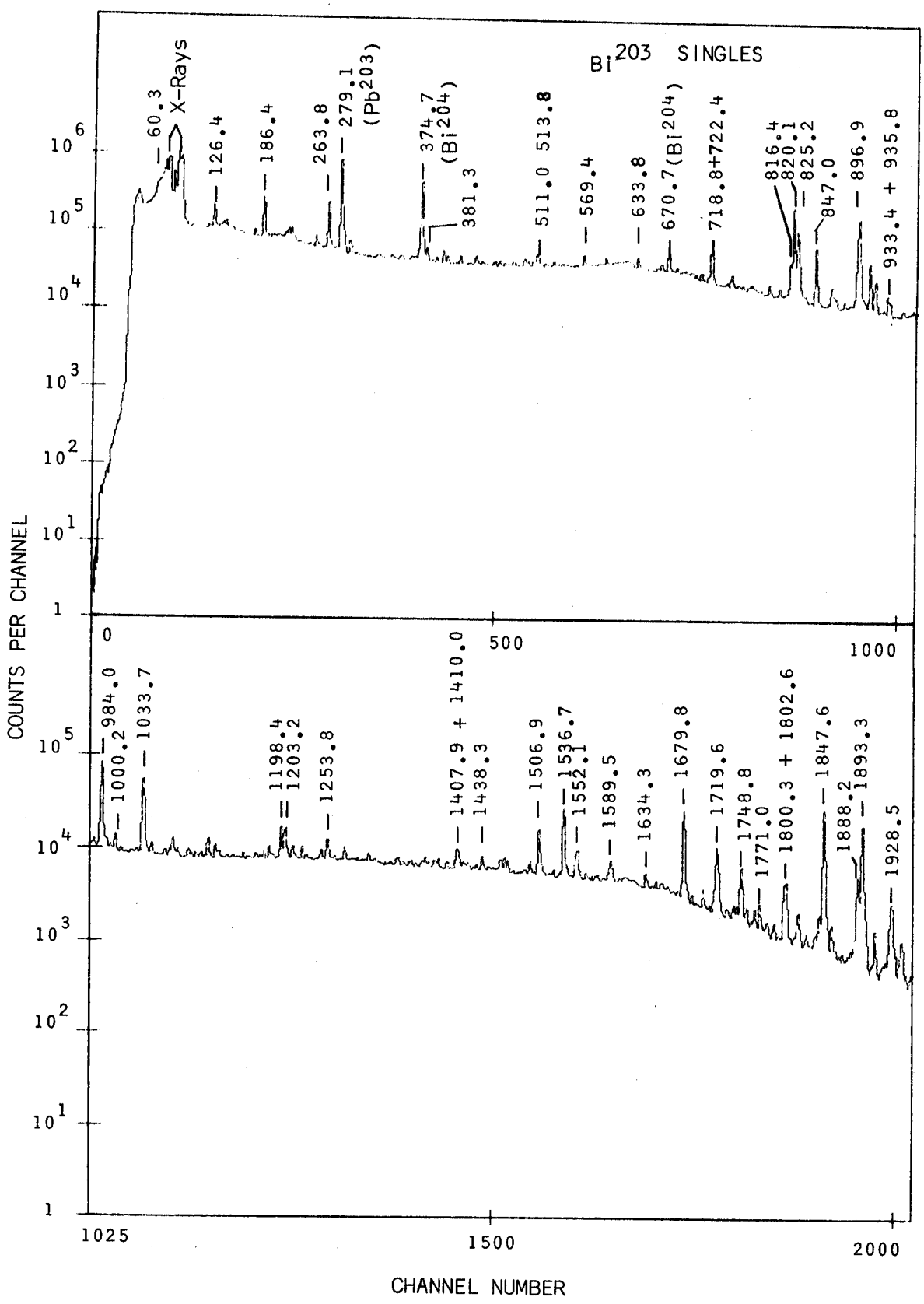

Fig. 28. Bi^{203} singles γ-ray spectrum taken with a 3.6% detector having a resolution of 2.1 keV FWHM (at 1.33 MeV) in this run.

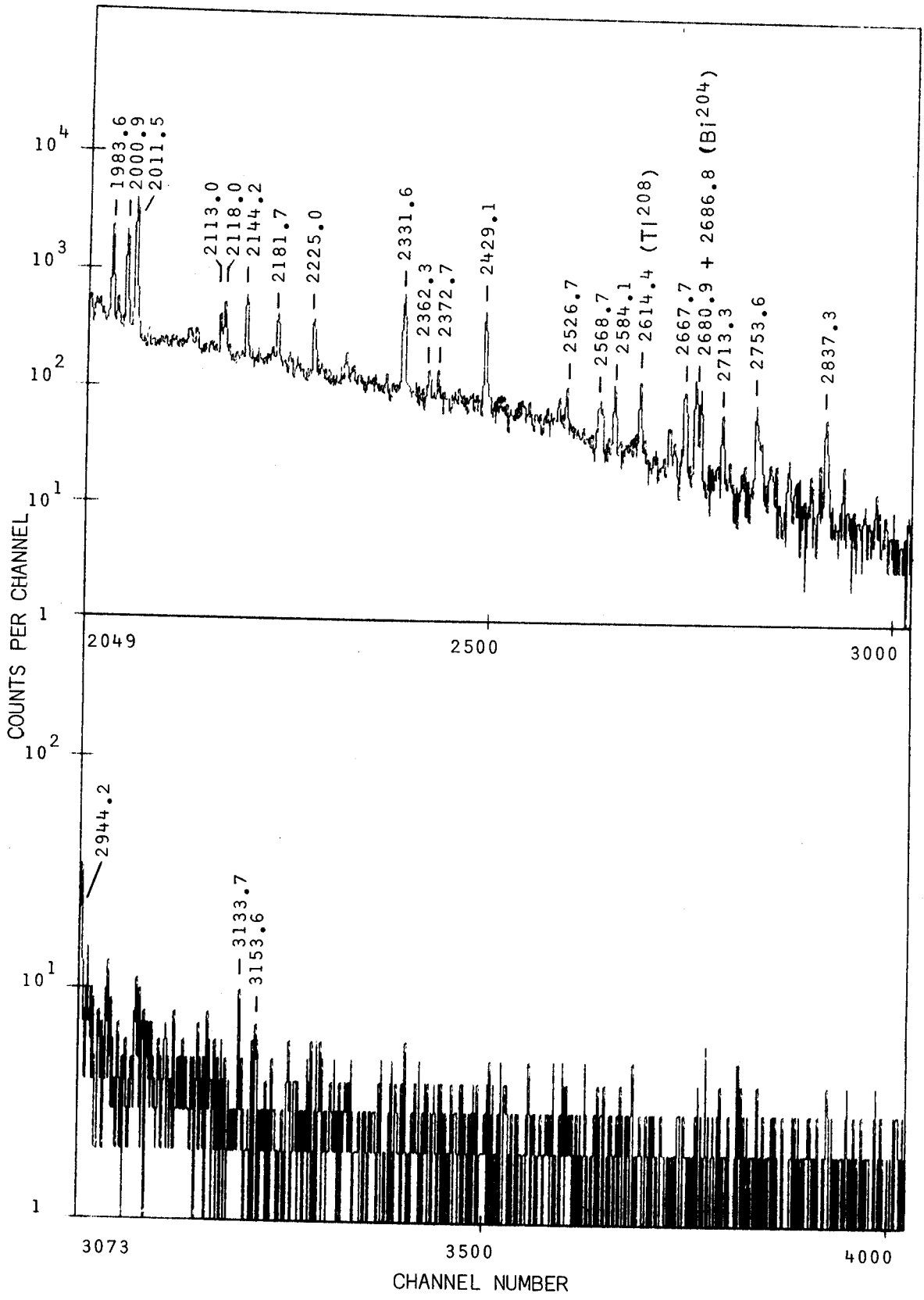

Fig. 28. (continued)

Table 12. Energies and relative intensities of γ rays present in the ε decay of Bi^{203}.

Measured γ-ray energy (keV)	Relative Intensity	Measured γ-ray energy (keV)	Relative Intensity
5.0[a]	6.62[b]	542.90	0.95
59.97	0.48[c]	569.36	4.82
100.44	2.16	595.47	2.34
119.90	0.82	619.99	1.52
126.44	14.00	626.82	1.15
136.76	2.12	633.76	4.63
186.35	20.25	646.72	0.94
195.98	0.50	696.66	0.78
201.19	0.70	718.78	2.85
212.42	1.88	722.35	16.91
252.22	0.91	739.92	1.08
263.85	20.56	746.20	4.28
270.92	2.03	754.54	0.91
295.25	0.42	758.20	0.98
298.62	0.31	768.88	2.31
323.59	0.42	772.05	1.41
338.29	1.62	779.48	0.74
381.34	3.65	816.45	12.50
392.11	0.99	820.20	≡100.0
406.09	1.70	825.20	54.50
416.25	0.39	847.03	23.01
432.65	0.60	866.63	5.43
461.59	0.60	869.97	2.82
477.15	0.39	896.90	45.60
483.95	0.98	905.9	3.68
498.08	3.05	927.82	0.78
507.72	1.40	933.45	4.82
513.80	<6.1	935.83	2.09

Table 12. (continued)

940.80	1.05	1409.98	1.55
951.89	1.07	1421.39	0.63
1000.20	2.99	1431.79	0.26
1007.12	0.38	1438.30	1.82
1033.69	27.01	1465.05	2.13
1069.27	4.56	1469.23	1.71
1074.59	1.58	1496.35	1.74
1087.80	1.15	1506.94	10.52
1091.18	0.91	1510.37	1.12
1111.71	3.33	1536.68	24.20
1120.20	2.83	1552.12	6.40
1123.89	1.09	1502.78	0.44
1153.00	0.76	1582.06	0.45
1166.87	0.71	1589.48	1.02
1184.46	1.75	1634.34	1.56
1188.06	0.61	1646.31	0.64
1198.43	6.68	1667.32	0.32
1203.23	4.46	1672.09	0.51
1215.10	≈0.37	1679.80	26.26
1223.80	2.02	1709.13	0.28
1228.69	0.53	1716.02	1.37
1245.92	2.02	1719.64	11.94
1253.80	3.91	1739.52	0.76
1303.30	1.43	1743.55	0.88
1310.20	0.43	1748.82	5.92
1343.58	0.32	1771.00	1.50
1370.55	0.59	1787.89	0.40
1373.15	1.11	1800.30	3.35
1381.77	1.57	1802.55	3.82
1385.40	1.28	1816.90	1.65
1395.87	0.80	1842.01	2.25
1407.88	2.50	1847.58	36.22

Table 12. (continued)

1856.70	0.85	2181.67	0.49
1888.21	8.15	2225.02	0.41
1893.28	27.15	2331.52	1.08
1908.32	1.14	2362.31	0.17
1923.04	0.38	2372.67	0.15
1928.50	4.05	2526.69	0.16
1968.00	0.56	2568.69	0.16
1983.26	2.79	2584.06	0.20
1991.21	0.31	2667.73	0.48
2000.94	2.76	2713.33	0.38
2011.51	5.50	2753.61	0.14
2078.00	0.18	2792.85	0.03
2084.77	0.39	2944.18	0.10
2113.04	0.39	3133.66[d]	≈0.02
2117.98	0.52	3153.61[d]	≈0.01
2144.22	0.71		

[a]Energy calculated from the difference in the 820.2- and 825.2-keV states in the Pb^{203} level scheme (Figure 31).

[b]Intensity of the 5.0-keV transition calculated from the γ-ray intensity of the 825.2-keV transition as proposed in [Do68].

[c]The 59.97-keV transition lies under a portion of the Pb x-rays, making an accurate determination of its intensity difficult. The listed intensity was calculated from the *K* conversion coefficient [S165] and the published *K*-electron intensity [St60].

[d]These transitions are somewhat questionable. They were found in only one of the Bi^{203} spectra and no overt cause (i.e. misplaced standards or background) could be determined for their presence. As a result, they are only tentatively included.

calibration peaks, ±0.2 keV; the remaining peaks in the 0-1000-keV region, ±0.30 keV; in the 1000-3000-keV region, ±0.5 keV.

The relative intensities are also the averages from these individual runs, the uncertainities, of course, being larger than in the energy determination. The large Bi^{203} peaks (>3% of the 820.2-keV γ ray) have statistical uncertainities ranging from ±5-15%; the remaining peaks have intensity uncertainities up to ±25%. The relative photopeak efficiency curves (at various distances) for the 2.5% and 3.6% Ge(Li) detectors were calculated from measurements of standard γ-ray intensity calibration sources. The results were, for convenience primarily, incorporated into the MOIRAE $E(I)$ program, allowing one to by-pass the relative peak area step completely.

3.2.3.B. Anti-coincidence Spectra

What was previously said (section 3.1.3.B.) about the characteristics and validity of anti-coincidence data certainly still holds true. To summarize those comments: enhanced peaks in an "anti" may be non-cascade ground-state transitions or non-cascade transitions feeding a long-lived isomeric state, while little can be said about those peaks which are not enhanced.

An anti-coincidence spectrum (Figure 18 shows a block diagram for the experimental set up) was collected on a Bi^{203} source in attempt to reveal those direct non-cascade ground-state transitions or γ's feeding the 825.2-keV isomeric state. Figure 29 illustrates the Bi^{203} anti-coincidence spectrum taken using the 2.5% Ge(Li) detector, the split NaI(Tl) annulus, and an auxiliary 3"×3" NaI(Tl) detector. The

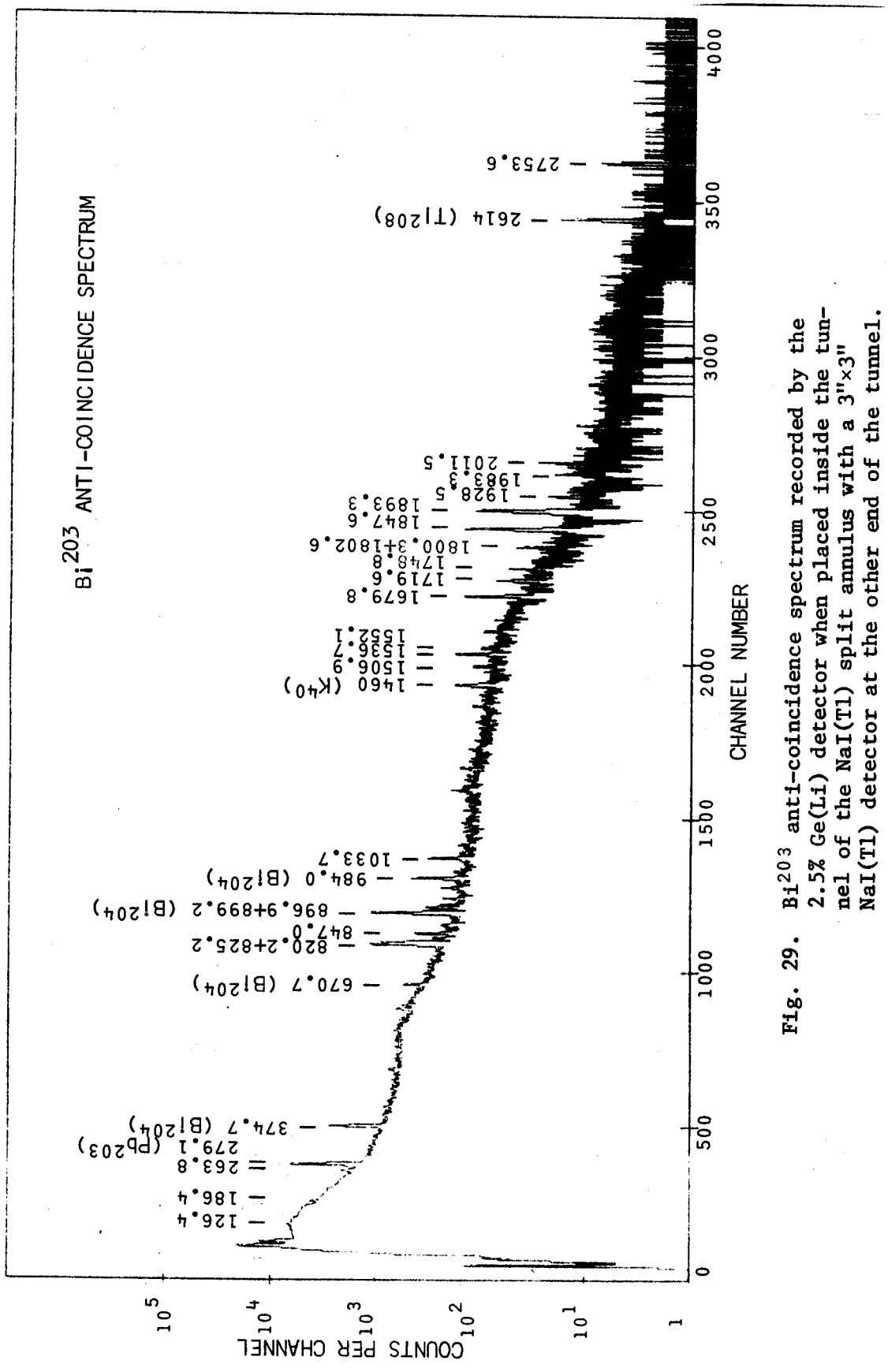

Fig. 29. Bi^{203} anti-coincidence spectrum recorded by the 2.5% Ge(Li) detector when placed inside the tunnel of the NaI(Tl) split annulus with a 3"×3" NaI(Tl) detector at the other end of the tunnel.

3"×3" NaI(Tl) detector was inserted into the end of the annulus opposite the 2.5% Ge(Li) detector in order to obtain nearly 4π geometry. Rather unfortunately, only a few peaks appear to be even moderately enhanced. Table 13 lists a few of the Bi^{203} γ's with their relative intensities in the singles and "anti". These data, in conjunction with the prompt-coincidence data, will be indispensible in construction of the Bi^{203} decay scheme.

3.2.3.C. Double Escape Coincidence Spectra

No double escape coincidence experiment was performed during the Bi^{203} investigation. The reasoning for this was two-fold; first, the very efficient 3.6% Ge(Li) detector (which was used to obtain the Bi^{203} singles spectra) depresses DE peaks in singles spectra of even the most intense peaks in the high energy region to a point where they are indiscernable; and second, inasmuch as the major DE peaks of Bi^{204} are well-known, a DE calibration curve for the detector is easily constructed, any Bi^{203} DE peaks then being interpolated from such a calibration curve. As a result all Bi^{203} DE peaks were simply identified and removed from consideration as full-energy peaks.

A rather worthwhile experiment, though not indispensable, would be a precise 511-511-γ coincidence experiment to determine the very small β^+ feedings (about 0.014 positrons for each 825.2-keV γ [Kr54].) This experiment has not yet been performed on Bi^{203}, as it does not substantially affect the present results, but it should be done before the decay of Bi^{203} can be classified as "complete" (if indeed any decay as complex as Bi^{203} will ever be "complete").

Table 13. Results of the Bi^{203} anti-coincidence experiment.

γ-ray energy (keV)[a]	Singles intensity[b]	Anti-coincidence intensity[b]
126.4	25.6	10.8
186.4	37.2	4.08
263.8	37.7	9.80
569.4	8.83	2.21
722.4	31.0	20.2
746.2	7.85	3.55
820.2	183.0	139.2
825.2	≡100.0	≡100.0
847.0	42.3	32.7
933.4	8.84	7.25
1000.2	5.50	4.36
1033.7	49.5	34.9
1069.3	8.36	52.8
1120.2	5.19	4.35
1198.4	12.2	11.0
1407.9	4.58	3.61
1506.9	19.3	17.4
1536.7	44.4	36.2
1552.1	12.7	9.69
1679.8	48.2	40.4
1719.6	21.9	18.0
1748.8	10.8	7.0
1800.3	6.14	4.42
1802.6	7.00	4.62
1847.6	66.5	54.5
1888.2	14.9	10.0
1893.3	49.8	47.5
1928.5	7.43	7.14
1983.3	5.12	4.83

Table 13. (continued)

2000.9	5.12	3.19
2011.5	10.0	9.05
2753.6	0.25	3.67

[a] γ-ray energies from present study.

[b] Singles and anti-coincidence normalized for the 825.2-keV γ.

3.2.3.D. Prompt-coincidence Spectra

The prompt-coincidence spectra for Bi^{203} were collected utilizing the Multiparameter Ge(Li)-Ge(Li) Spectrometer described in section 2.2.2.B. Some 8 million coincidence events were recorded on magnetic tape during a 76-h run. The *X* and *Y* integral spectra from each tape were analyzed and some 3.5 million events discarded because of gain shifts on one or the other axes. The resolution, when all events were recovered, was about 3.0 keV FWHM (at 1.33 MeV) on each axis. Figure 30 shows the *X* and *Y* integral coincidence spectra. During data recovery, gates are set on each peak or region (with or without background subtraction) on one integral spectra, say *X*, and displayed from the opposite side, *Y* (section 2.2.2.B.) Periodically, gates are set on a peak on the opposite side (*Y*) and the other side displayed (*X*) in order to verify the validity of the coincidence data storage system.

Once again, with few exceptions, no intensities were calculated for each Bi^{203} peak appearing in a Bi^{203} coincidence spectra. As in Bi^{204}, only a masochist or a madman would attempt to analyze <u>all</u> the Bi^{203} peaks appearing in these coincidence spectra. The principle difficulty in the Bi^{203} coincidence spectra was the poor statistics in the middle energy region (1000-2500 keV). In addition, the ever-occurring problem of very small peaks, many of which could not be distinquished in the integral coincidence spectra, nearly caused me to throw up my hands in disgust and decide to honeymoon (I was married during the writing of this thesis) till the 1980's (presumably nuclear spectroscopy technology will continue to advance). Unable to do so,

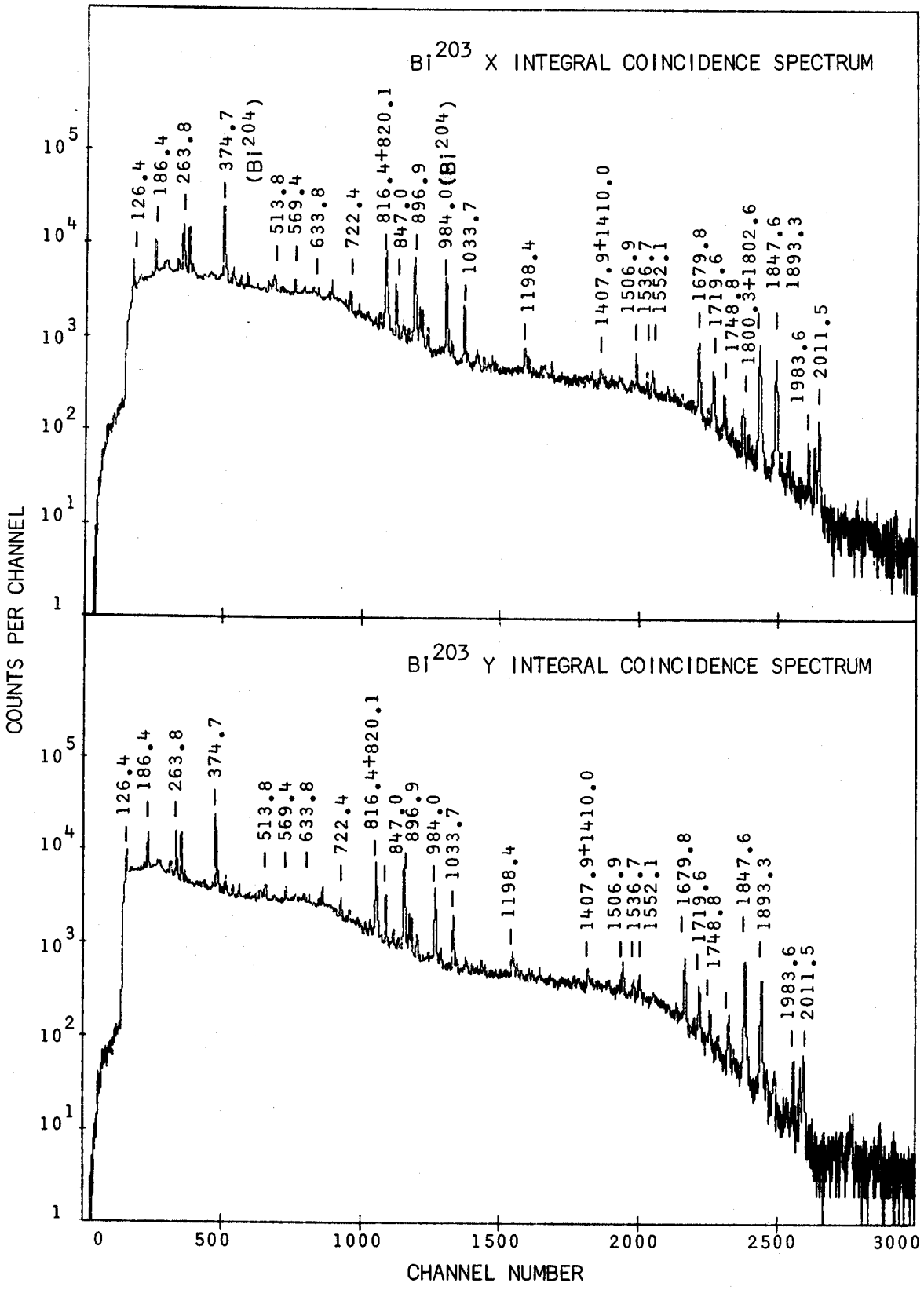

Fig. 30. Bi^{203} integral coincidence spectra taken using the multiparameter Ge(Li)-Ge(Li) spectrometer (section 2.2.2.B.). The *X* and *Y* spectra were taken with the 3.6% and 2.5% Ge(Li) detectors, respectively.

I was faced with a mass of "useless" coincidence data on small peaks. In most cases, they neither confirm nor deny and hence are as nearly "useless" as is possible.

Actually, I should not leave the reader with a false conception in this section. Most of the Bi^{203} (and Bi^{204}) coincidence data are excellent, only the extremely weak γ rays yield little in the way of coincidence data. In light of the "state of the art" several years ago, these data can be classified as nothing short of fantastic.

The advantages (and disadvantages) of background subtraction were discussed in section 3.1.3.D. The Bi^{203} spectra listed in the following pages are amply marked, and most have had the backgrounnd subtracted, though in some cases it was advantageous not to do so inasmuch as the regions adjacent to the peak of interest were filled with many peaks or multiplets of peaks.

3.2.3.E. Delayed-coincidence Experiments

In addition to the 6.1-s, 825.2-keV Pb^{203m}, only one state has been previously reported to have a measureable half-life, a 75-ns 126.3-keV Pb^{203} state [Be61]. Once again, the 6.1-s 825.2-keV state has a lifetime just too long to be effectively studied by a delayed-coincidence spectrum. The best handle to a transition feeding the 825.2-keV state should be the anti-coincidence, but the "anti" experiment failed to reveal any conclusive results about such a feeding. More will be said of this in section 3.2.4., which deals with the actual construction of the Bi^{203} decay scheme.

Conversely, the 75-ns 126.3-keV state is short enough to be studied effectively by a delayed-coincidence experiment. Fortunately (or unfortunately as one may see it) the resolving time on the prompt-coincidence experiment was usually ≈100 ns. This means that >50% of the events in the 126.3-keV peak are real (the remaining being chance events), which is sufficient to get an excellent "delayed"-coincidence spectrum from the prompt-coincidence data.

For these reasons, plus time and expense considerations, no separate delayed-coincidence spectrum was taken.

3.2.4. Construction of the Pb^{203} Level Scheme

Figure 31 shows schematically the ε decay of Bi^{203} to levels in Pb^{203} as evaluated from my data. These 25 excited states and 51 γ rays were placed using primarily singles and coincidence data (taken under the EVENT RECORDER program), aided, of course, by intensity balances and energy sums. Much of what was said in section 3.1.4. about the logic and sequential construction of decay schemes holds equally true here and will not be repeated. Unlike Bi^{204}, though, Bi^{203} is a much more "typical" decay scheme. The ground state of Bi^{203} is 9/2-, while Pb^{203} has a 5/2- ground state, thus allowing for little possibility of direct feeding to the ground state as it would have to be a second-forbidden transition. The Bi^{203} scheme also has several transitions (not just one as in Bi^{204}) going to the ground state Pb^{203}. The major advantage of the Bi^{203} decay (over the Bi^{204} decay), though, lies in its much more intense transitions, even in the high energy regions.

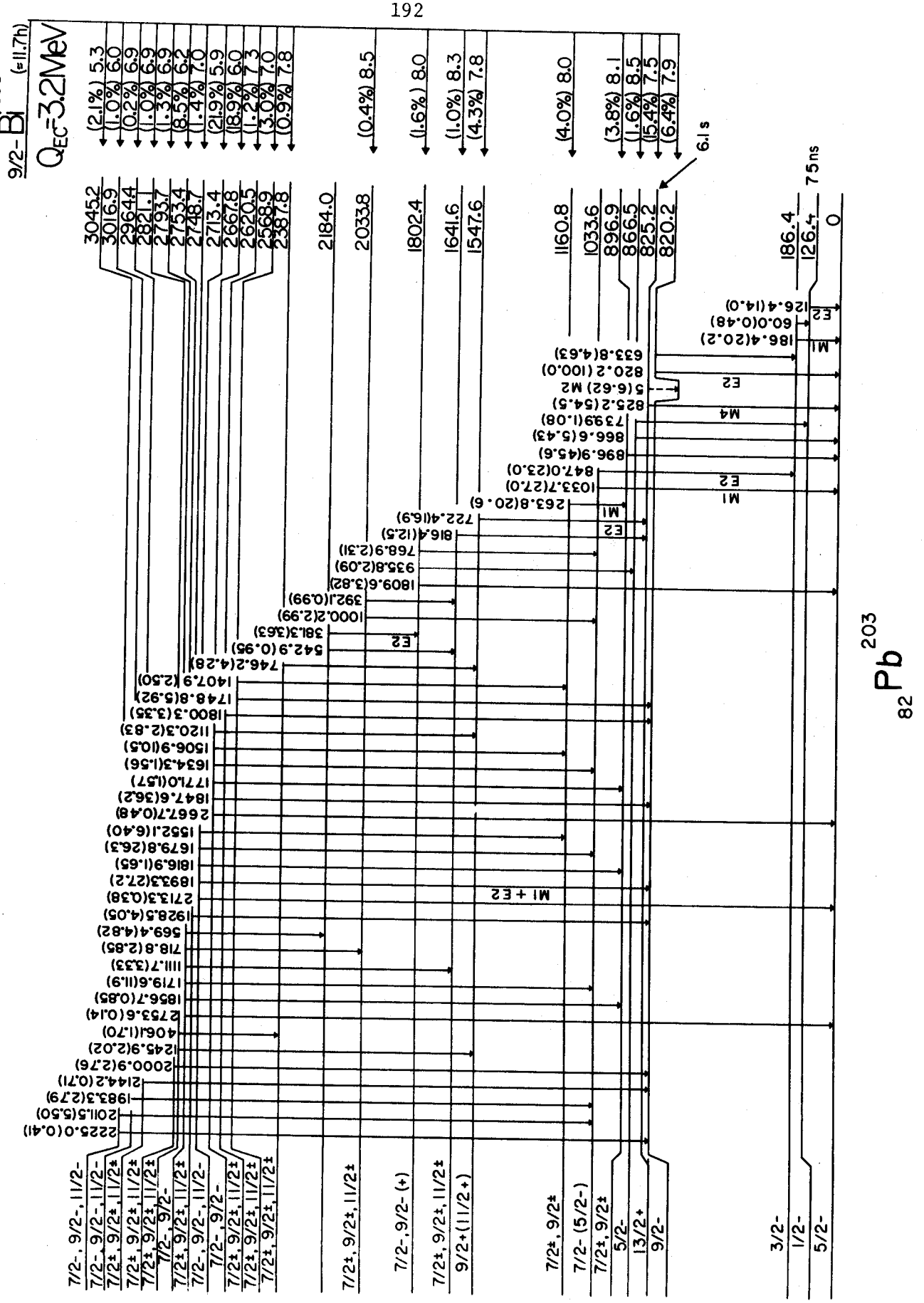

Fig. 31. The ε decay scheme of Bi^{203} proposed by the present study. All transitions were placed using coincidence data alone, without the use of energy sums.

A rather amusing, though not initially catastrophic, characteristic does present itself however. Because the Bi^{203} γ rays in the singles are "obscured" by the Bi^{204} "background" the energies and intensities of the γ rays of the Bi^{203} are somewhat less precise than they were for Bi^{204}, but, oddly enough, the decay scheme was easier to construct and the levels and transitions much more surely placed than those in the Bi^{204} scheme. Without further verbage I would now like to tackle the "logic" behind the construction of the Bi^{203} decay scheme presented in Figure 31.

3.2.4.A. 825.2-keV Level

The 825.2-keV 6.1-s isomeric state was not actually "placed" by the present investigation, but nevertheless has been well established by many previous investigations on Pb^{203m} (section 1.2.6.B.). Additional evidence supporting this placement was found in the Bi^{203} anti-coincidence spectrum, in which the 825.2-keV γ is enhanced, and in the integral prompt-coincidence spectra, in which the 825.2-keV γ is depressed. Inasmuch as this level has been well characterized (and there is no overt reason for suspecting its placement), I also "place" a level at 825.2 keV, which corresponds to the 825.2-keV Pb^{203m} state.

3.2.4.B. 126.4- and 186.4-keV Levels

These states were previously placed by Novakov et al. in their tentative decay scheme [No58] (Figure 27) which was constructed from data obtained by conversion-electron spectro-

metry and e-γ and γ-γ coincidence techniques. However, this work was performed before the advent of high-resolution Ge(Li) spectroscopy, and, while NaI(Tl) detectors are highly efficient, they do not provide the necessary high-resolution required for such a complicated decay scheme as that of Bi^{203}. As good as their data were, one must be rather wary of blindly accepting the work as comprehensive. The 126- and 186-keV coincidence spectra (found in Figure 33 at the end of section 3.2.4.) reveal strongly enhanced 633.8- and 847.0-keV γ's. (Even though the 126.4-keV state has a $t_{\frac{1}{2}}$ of 75 ns, the coincidence apparatus had a 100-ns resolving time, so not all of the coincidence data are killed completely.) The 633.8/847.0 intensity ratio in each spectrum is the same. Three possibilities are thereby suggested:

1) the 126.4- and 186.4-keV γ's are populating the same state,
2) the 126.4- and 186.4-keV γ's are depopulating the same state,
3) the 126.4- and 186.4-keV transitions are adjoined by a 60-keV transition such that the 186.4-keV γ is the cross-over transition.

When one considers that the 126.4-keV γ is an *E*2 (cf. section 3.2.5.) and the 186.4-keV γ is an *M*1, it becomes evident that these transitions are among the most intense in the singles spectrum. Additionally, the delayed γ-γ coincidence data of Bergström et al. [Be61] indicate that the *L* conversion

electrons of the 60-keV transition are in delayed coincidence with the L conversion-electrons of the 126.4-keV transition. All these data seem to lead me to confidently postulate states at 126.4 and 186.4 keV. In order to account precisely for the coincidence data (i.e., the very strong enhancement of the 847.0-keV γ in both the 126- and 186-keV coincidence spectra), I must assume that there is indeed a 60-keV transition connecting these states. A 59.97-keV γ was definitely found in the present study, and, coupled with Bergström's coincidence data, there seems to be little doubt about these placements.

3.2.4.C. 820.2-keV Level

The 820.2-keV γ is the most intense γ in the Bi^{203} γ-ray spectrum. If this were not a ground-state transition, then one would expect to see other transitions of comparable intensity that would de-excite the level fed by the strong 820.2-keV transition. There are two γ rays having relative intensities >50%, but neither of these is revealed in the 820.2-keV coincidence spectrum. As a result, I am led to place another level at 820.2 keV in the Pb^{203} level scheme. Further evidence for such a placement comes from the Pb^{203m} studies of Doebler et al. [Do68] in which they showed that an unobserved 5-keV transition competes with the 825.2-keV γ from the isomeric state. (They really showed that an 820.2-keV γ was present in the Pb^{203m} decay in addition to the 825.2-keV γ, but this, in turn, implies the presence of the unobserved 5-keV transition.) A consideration of the intensities of the 825.2- and 820.2-keV

γ's in the Bi^{203} singles immediately suggests a state at 820.2-keV (rather than at 5 keV). With such a wealth of data, the assignment of a state at 820.2 keV seems quite unimpeachable.

During the present investigation I attempted a cursory search aimed at confirming this unobserved 5-keV transition. This search was undertaken with a Si(Li) x-ray detector having a 150 Å gold surface barrier contact. The detector is coupled to an ORTEC model 117 preamplifier with cooled FET first stage. The useful efficiency range is ≈5 to 100 keV. One spectrum obtained with this detector in a singles mode is seen in Figure 32.

Two problems worked against me finding the 5-keV transition. First, the detector has somewhat poor efficiency for γ rays in the 5-10-keV range. Second, as an $M2$ the 5-keV transition will be highly converted and consequently be extremely difficult to detect with the Si(Li) detector. In spite of all this,it appears that I may be observing the 5-keV transition in the x-ray spectrum. A word of caution! The 5-keV "bump" in Figure 32 is significantly broader than the other x-rays in the same region; consequently, this should not be taken as "proof" of the 5-keV transition. In addition, because care was not exercised in preparing the x-ray sample, absorption by the sample and sample holder probably eliminated the relatively abundant conversion electrons. The experiment is presently being re-investigated.

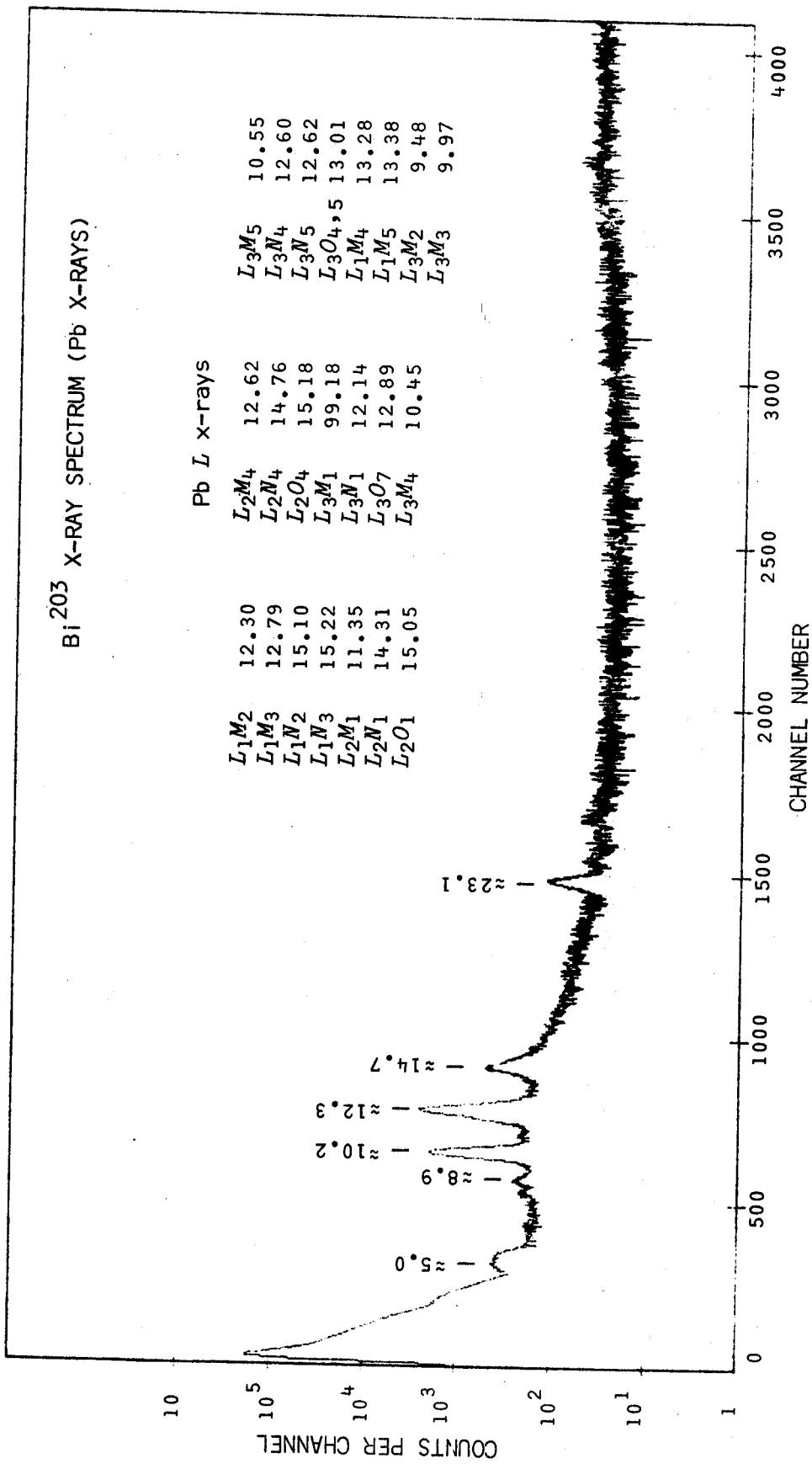

Fig. 32. Low energy spectrum of Bi^{203}, taken with a Si(Li) x-ray detector. A partial list of Pb *L* x-rays is included.

3.2.4.D. 866.4- and 1802.4-keV Levels

These states are established by the mutual enhancements of several γ's in opposing coincidence spectra. That is, the 866.5-keV γ is strongly enhanced in the 935-keV coincidence spectrum and the 935.8-keV γ is enhanced in the 866-keV spectrum. The 866.5-keV γ was placed as the lowest member of the cascade on basis of its much greater intensity (over 2-1/2 times that of the 935.8-keV γ). I, therefore, place levels at 866.5 and 1802.4 keV. Final support for this placement was revealed when a 739.9-keV γ was found to be feeding the 126.4-keV state (cf. 126-keV coincidence spectrum).

3.2.4.E. 896.9- and 1160.8-keV Levels

One of the most rewarding and notable characteristics of Bi^{203} coincidence data is the appearance of reasonably strong peaks in some of the coincidence spectra. Throughout the Bi^{204} decay I constantly fought a "peak vs. background" battle in the coincidence spectra because of the many very weak γ's in Bi^{204}. Fortunately, Bi^{203} has many more intense γ's, thereby making many of the cascades revealed in the coincidence spectra easier to identify. Such is the case with the γ's between these states. The 897-keV gated spectrum shows strongly enhanced peaks at 263.8, 1407.9, 1506.9, and 1552.1 keV (plus Bi^{204} peaks in coincidence with the 899.2-keV γ). The 264-keV coincidence spectrum reveals enhanced peaks at 896.9, 1407.9, 1506.9, and 1552.1 keV. The 1408-, 1507-, and 1552-keV spectra in turn show only the 263.8- and 896.9-keV γ's, and in the same ratio as in the singles. The conclusion is quite evident -

a state exists at 1160.8 keV (the sum of the 896.9- and 263.8-keV γ's in cascade). The question remaining, however was whether the 896.9-keV γ was feeding a 263.8-keV state or whether the 263.8-keV γ was feeding an 896.9-keV state. A state was placed at 896.9 keV on the basis of the large intensity of the 896.9-keV transition. It is 50% greater than the intensity of the 263.8-keV transition, even considering the *M*1 character of the 263.8-keV γ. As a result, I place states at 896.9 and 1160.8 keV with a high degree of certainty.

Sometime after placement of these and other states, I found yet other data confirming such assignments. In the 897-keV spectrum one finds small enhancements of the 1771.0-, 1816.9-, and 1856.7-keV γ's. These transitions depopulate other well-known levels (placed in later sections) and feed the 896.9-keV state. Having three such transitions virtually eliminates all doubt concerning placements of these levels.

3.2.4.F. 1033.6-keV Level

The level placed at 1033.6 keV is one of the least ambiguous of the Pb^{203} level scheme. In the 186-keV coincidence spectrum the largest enhancement is of the 847.0-keV transition, suggesting that the 847.0-keV γ feeds the 186.4-keV state (and depopulates the 1033.6-keV level). In the 847- and 1034-keV coincidence spectra I also find a number of peaks definitely enhanced- e.g., the 1000.2-, 1679.8-, 1719.6-, 1983.3-, and 2011.5-keV γ's. Conversely, in the 1000-, 1680-, 1720-, 1983-, and 2011-keV coincidence spectra I see only the 847.0- and 1033.7-keV transitions enhanced (in the proper intensity ratio also). Such coincidence data clearly indicate a level

at 1033.6 keV. As one may note by looking at Figure 33, the coincidence data on these peaks are excellent, far superior to almost anything found in the Bi^{204} section. With such an overwhelming array of evidence, a level at 1033.6 keV appears to be absolutely certain.

3.2.4.G. 1547.6- and 1641.6-keV Levels

These levels have a common character in that they both feed the 825.2-keV isomeric state. This makes the assignments difficult and tentative. The placements are based, at least partially, upon the assumption that such a level will be "locked" in to several of the well-known higher-lying levels.

The 722-keV coincidence spectrum reveals an enhanced γ at 1120.2 keV, and, perhaps, one at 1245.9 keV (although this last γ is questionable). The 1120- and 1246-keV coincidence spectra reveal a single strongly enhanced Bi^{203} γ at 722.4-keV. Finally, the 722.4-keV γ appears to be very slightly enhanced in the anti-coincidence spectrum (which suggests that it may be feeding either the ground or isomeric state). This leads me to place a state at 1547.6 keV, such that the 1120.2- and 1245.9-keV γ's "lock" in (with precise energy sums) with the 2667.8- and 2793.7-keV states (to be discussed later).

The 816-keV coincidence spectrum reveals enhanced γ's at 392.1, 406.1, 542.9, 746.2, and 1111.7 keV. Conversely, the 543-, 392-, 746-, and 1112-keV coincidence spectra reveal the 816.4-keV peak enhanced. Consider the 816.4-keV γ feeding the isomeric state. If the 542.9-, 392.1-, and 1111.7-keV γ's each feed the resulting 1641.6-keV state, then each transition also "locks" in with a well-known level (cf. Figure 31). Additional coincidence evidence on the 392.1-keV tran-

sition (section 3.2.4.P.) suggests that this transition is correctly placed. A level at 1641.6 keV seems quite certain in light of this data.

3.2.4.H. 2033.8-keV Level

The initial placement of this level rested entirely upon the enhancement of the 1000.2-keV γ in the 847- and 1034-keV coincidence spectra and the reciprocal relationship (i.e., the 1000-keV spectrum revealed enhanced γ's of 847.0 and 1033.7 keV). No other peaks of comparable intensity were enhanced in the 1000-keV spectrum. Later in section 3.2.4., a 392.1-keV transition depopulating this state has been discussed (section 3.2.4.G.) and a transition feeding the state (from a well-known level) will soon be confidently placed from coincidence data, thus firmly establishing the 2033.8-keV state.

3.2.4.I. 2184.0-keV Level

In the 1802- and 935-keV coincidence spectra the 381.3- and 569.4-keV γ's are moderately enhanced. In the 381-keV spectrum, not only are the 1802.6- and 935.8-keV γ's enhanced, but also a 768.9-keV transition. The 768.9-keV transition was also enhanced in the 847- and 1034-keV spectra, which seems to suggest that the 768.9-keV γ populates the 1033.6-keV level and depopulates the 1802.4-keV state. The 569-keV spectrum does not reveal the 768.9-keV transition. These coincidence relationships appear to suggest that the 381.3-keV γ feeds the 1802.4-keV state, which, in turn, places a level at 2184.0 keV. The 569.4-keV γ must then feed the 2184.0-keV level (suggesting a level around 2753 keV).

3.2.4.J. 2387.8-keV Level

The level at 2387.8 keV is certainly not one of the better characterized levels, but no one ever said nature was completely cooperative. The placement was based upon the strongly enhanced 746.7-keV γ in the 816-keV coincidence spectrum and upon the inverse relationship as well. No other γ-ray spectrum of a γ in coincidence with the 816.4-keV γ revealed an enhanced 746.2-keV transition, the implication being that the 746.2-keV transition directly feeds the 1641.6-keV state. Such a feeding, in turn, implies a level at 2387.8 keV. The placement rests upon the assumption that the 1641.6-keV state is correct, but such an assumption is somewhat flimsy, as the 816.4-keV γ feeding the 825.2-keV isomeric state has not been confirmed with absolute certitude. If the 1641.6-keV state is in reality a good level, then the 2387.8-keV state can be quite confidently placed.

3.2.4.K. 2568.9-keV Level

Both the 264- and 897-keV coincidence spectra (Figure 33) have an enhanced transition at 1407.9 keV. The 1408-keV gated coincidence spectrum has only two enhanced γ's, at 263.8 and 896.9 keV, in the same intensity ratio as in the Bi^{203} singles. This purports a state at 2568.9 keV, based upon the 1407.9-keV γ feeding the 1160.8-keV state. A second, more intense transition confirms such a placement. The 820- and 1749-keV coincidence spectra also show reciprocally enhanced γ's (i.e., the 820.2-keV transition is enhanced in the 1749-keV spectrum and the 1748.8-keV γ is strongly enhanced in the 816-820-keV coincidence spectrum). No other γ is seen in the 1749-keV

spectrum, by virtue of which one can conclude that this is a direct feeding with no intermediate γ's. The 1748.8-keV transition to the 820.2-keV state also impels me to accept a state at 2568.9 keV. While no other γ's have been firmly placed with regard to this level, the excellent coincidence data leaves no room for doubt about its existence. If all the levels were placed with such clarity, decay scheme preparation time and effort would be reduced significantly.

3.2.4.L. 2620.5-keV Level

Similar to the 2387.8-keV level, the 2620.5-keV state is based upon a single transition - a 1800.3-keV γ to the 820.2-keV state. This is quite clearly seen by noting the 1800-keV coincidence spectrum, in which the 820.0-keV γ is definitely enhanced. To be certain, one must also compare the 1802.2-keV spectrum, as the 1800.3- and 1802.6-keV γ's form a doublet in the singles spectrum. The 1802-keV spectrum, however, reveals, in addition to the 820.2-keV γ, γ's of 381.3 and 569.4 keV. The 820.2-keV enhanced transition is almost certainly a result of overlap of the 1802.6-keV γ (in the gating procedures) with the 1800.3-keV γ. Based upon the already discussed placement of the 1802.6-keV transition and this coincidence data, I quite confidently suggest a state at 2620.5 keV. This is just another example of how superbly useful the multiparameter coincidence system is. In conventional coincidence spectroscopy one would never have been able to separate the 1802 and 1800-keV coincidence spectra clearly, yet here is an outstanding case where this has been successfully done with relative ease.

3.2.4.M. 2667.8-keV Level

In such a complicated decay scheme as Bi^{203} (in which most of the transitions are quite weak), to find a level which is depopulated by 6 transitions to well-known lower-lying states and to find coincidence data to support such assignments is, without a question, quite convincing. So begins the fate of the 2667.8-keV level. The The 820- and 264-keV spectra reveal enhanced γ's of 1847.6 and 1506.9 keV, respectively. Conversely, the 1507- and 1848-keV spectra reveal the 263.8- and 820.2-keV γ's, respectively. Intermediate states ruled out, these simultaneously suggest a state at 2667.8 keV. These in themselves would be sufficient to place the state definitely, but, to add wood to the fire, additional transitions go even further in clarifying the level. Weak γ's of 1771.0 and 1634.3 keV are seen in the 879- and 1033-keV coincidence spectra, respectively. The inverse relationships also are found to hold true (cf. Figure 33). If there is a level at 1547.6 keV as I have postulated, then the 1120.2-keV γ in coincidence with the 722.4-keV transition also depopulates this state. I would rather use this as evidence of the existence of the 1547.6-keV state though, as the 1547.6-keV state is less certain than the 2667.8-keV level.

The last of the 6 depopulating transitions to be placed was the 2667.7-keV γ. The 2667.7-keV was not seen in the integral coincidence spectra, nor was it enhanced in any of the spectra of peaks gated upon in the integral spectra. This led me to suggest that it is a ground-state transition. The only other states that it could feed (without exceeding the decay energy of Bi^{203}) are the

126.4- and 186.4-keV states, but it was not seen in either the 126- or 186-keV coincidence spectra. As a result, I propose that the 2667.7-keV γ does depopulate the 2667.8-keV state. (A sum peak was ruled out on the basis of intensity vs. source-to-detector measurements.) With such an avalanche of data, I believe that I can be quite audacious and say that there is absolutely a state at 2667.8 keV in Pb^{203}.

3.2.4.N. 2713.4-keV Level

The 2713.4-keV state happily falls into the same situation as the previous state, that is, it has 5 depopulating γ transitions, three of which have large relative intensities. The state was first revealed by enhanced γ's of 1552.1 keV (in the 264- and 897-keV spectra), 1679.8 keV (in the 847- and 1034-keV spectra), and 1893.3 keV (in the 820-keV spectrum). In the 1552-keV spectrum the 263.8- and 896.9-keV γ's are enhanced, as are the 847.0- and 1033.7-keV γ's in the 1680-keV spectrum. Also, in the 1893-keV spectrum the 820.2-keV γ is definitely enhanced. Each of the γ's, placed so as to feed the appropriate lower-lying energy state, suggests a level at ≈2713 keV. Additional support came from an 1816.9-keV transition which was found to be weakly enhanced in the 897-keV coincidence spectrum (and the 896.9-keV γ was enhanced in the 1817-keV spectrum). The last transition, a 2713.3-keV γ, was placed as a ground-state transition on the basis of essentially the same argument as that for the 2667.7-keV γ. That is, it is not seen in the 126- or 186-keV coincidence spectra and cannot populate any higher states (inasmuch as it would exceed the decay energy for Bi^{203}). Such a wealth of coincidence data can hardly fail to convince one of a level at 2713.4 keV.

3.2.4.O. 2748.7-keV Level

Only one γ transition depopulating (and none populating) this state has been placed with any degree of confidence. In the 820-keV coincidence spectrum one can find the 1928.5-keV γ quite clearly enhanced, and in the 1928-keV spectrum, the 820.2-keV γ is likewise enhanced. If the coincidence relationships were not so explicit, I might be tempted not to place this transition. Such not being the case, I propose a level in Pb^{203} at 2748.7 keV solely upon the excellent coincidence data.

3.2.4.P. 2753.4-keV Level

The state at 2753.4 keV was first suggested by the 820-keV coincidence spectrum in which the 1719.6-keV γ is strongly enhanced, and conversely, by the 1720-keV spectrum in which the 820.2-keV γ is the only enhanced transition. Confirmation was amply available - the 381- and 1802-keV coincidence spectra reveal a strong 596-keV γ; the 897-keV spectrum reveals a weakly enhanced transition of 1856.7 keV; and the 1857-keV spectra also reveal a relatively intense 896.9-keV γ. Further proof comes from the 392-, 1000-, and 719-keV coincidence spectra, in which all the evidence leads one to believe that the 718.8-keV γ feeds the 2033.8-keV state (cf. Figure 33). This also suggests the state at 2753.4 and at the same time seems to lend even further evidence for the state at 1641.6 keV (which in turn feeds the 825.2-keV isomeric state). Even more proof for these two states (at 2753.4 and 1641.6 keV) is elucidated by the 816-keV coincidence spectrum. There is a strong 1111.7-keV transition which (when coupled with the 1111-keV spectrum's data) suggests a 1111.7 keV γ as populating the

1641.6-keV state (thus placing the depopulated state at 2753.3 keV). As if all these transitions were not sufficient, the anti-coincidence experiment showed an enhanced 2753.6-keV γ. The only logical explanation is that the 2753.6-keV γ directly populates the ground state. If one is still unconvinced then surely no further evidence will succeed in changing his opinion; therefore without further ado I make that classic announcement - a Pb^{203} excited state exists at 2753.4 keV.

3.2.4.Q. 2793.7-keV Level

The 816- and 746-keV gated coincidence spectra reveal an enhanced transition of 406.1 keV. The 1246-keV spectrum shows that the 722.4-keV γ is in coincidence with a 1245.9-keV γ. These relationships are certainly not among the most clearly defined during the Bi^{203} study - yet, they seem more than sufficient to allow me to postulate a state at 2793.7 keV.

3.2.4.R. 2821.1-, 2964.4-, and 3016.9-keV Levels

The states at 2821.1, 2964.4, and 3016.9 keV are placed on the basis of rather meager evidence. In each case only one associated transition has been clearly revealed, but these transitions are well defined by ample coincidence data and can be quite confidently assigned.

A state at 2821.1 keV is suggested by the 820-keV coincidence spectrum in which the 2000.9-keV γ is undoubtedly enhanced. This, alone, is not necessarily conclusive. However, the 2001-keV spectrum reveals only the 820.2-keV γ in definite coincidence. The state at 3016.9 keV is similarly suggested by the 847- and 1034-keV coincidence spectra in which the 1983.3-keV γ is significantly en-

hanced. Checking the reverse relationships, I find the 847.0- and 1033.7-keV transitions also enhanced in the 1983-keV spectra (no other clearly enhanced γ's are observed). These excellent data surely suggest a state at 3016.9 keV. The last of these states, at 2964.4 keV, is also placed as a result of the enhancement of a single γ, at 2144.2 keV. In the 2144-keV coincidence spectra (Figure 33) the 820.2-keV peak is only moderately enhanced, but, inasmuch as the reciprocal relationship is also well defined in Figure 33, I suggest that there is a high probability of a state at 2964.4 keV.

3.2.4.S. 3045.2-keV Level

The final level placed during the present γ-ray studies of Bi^{203} is one at 3045.2 keV. This was done on the basis of a 2225.0-keV γ being in coincidence with the 820.2-keV transition, on the basis of a 2011.5-keV transition being in direct coincidence with the 820.2-keV transition, and on the basis of a 2011.5-keV transition being in coincidence with the 847.0- and 1033.7-keV γ's (i.e., the 2011.5-keV γ populates the 1033.6-keV state previously assigned). These coincidence relationships are easily confirmed by noting the 847-, 1034-, 2225-, and 2011-keV coincidence spectra in Figure 33.

3.2.4.T. Comments

Once again a few closing words appear to be in order. The construction of the Bi^{203} decay scheme shown in Figure 31 was tedious, though not nearly so difficult as that of the Bi^{204} decay scheme. While the majority of the Bi^{203} peaks are of low intensity (<4% of the 820.2-keV peak), a number are of sufficient intensity to make the coincidence data completely unambiguous. The decay scheme

for Bi^{203} which I have presented in Figure 31 is the most consistent of which I was able to construct. Note the changes that have been made in the previously suggested decay scheme (Figure 27). The 263.8- and 1847.6-keV γ's have been assigned new placements on the basis of excellent coincidence data. The state at 1083.3 keV is consequently removed. Also, many more transitions (39) and levels (17) have been placed with good confidence.

The 51 γ's placed in the present study represent >80% of the photon intensity. These 51 γ's were placed primarily upon coincidence data, energy sums being somewhat risky. During the course of this study many other transitions and levels were suggested by the coincidence data and energy sums, but sufficient evidence was lacking to place these with a high degree of confidence. Figure 34 shows a level scheme of Pb^{203} showing additional transitions from the Bi^{203} decay which could be placed on the basis of precise energy sums alone. The dashed lines indicate new states suggested by admittedly poor coincidence data plus energy sums while the semicircles indicate that some coincidence data supports such a placement for that transition.

3.2.5. Electron Data and Multipolarities

The γ-ray intensities from the present measurements were compared with the conversion-electron intensity data of Novakov et al. [No58], Fritsch [Fr56], and Stockendal [St60] in order to learn something about the multipolarities of some of the transitions seen in the Bi^{203} ε decay. The two sets of data (the present γ-ray intensities and the previously published electron data) were normalized for the pure *M*4 825.2-keV transition of Pb^{203m}. The conversion coef-

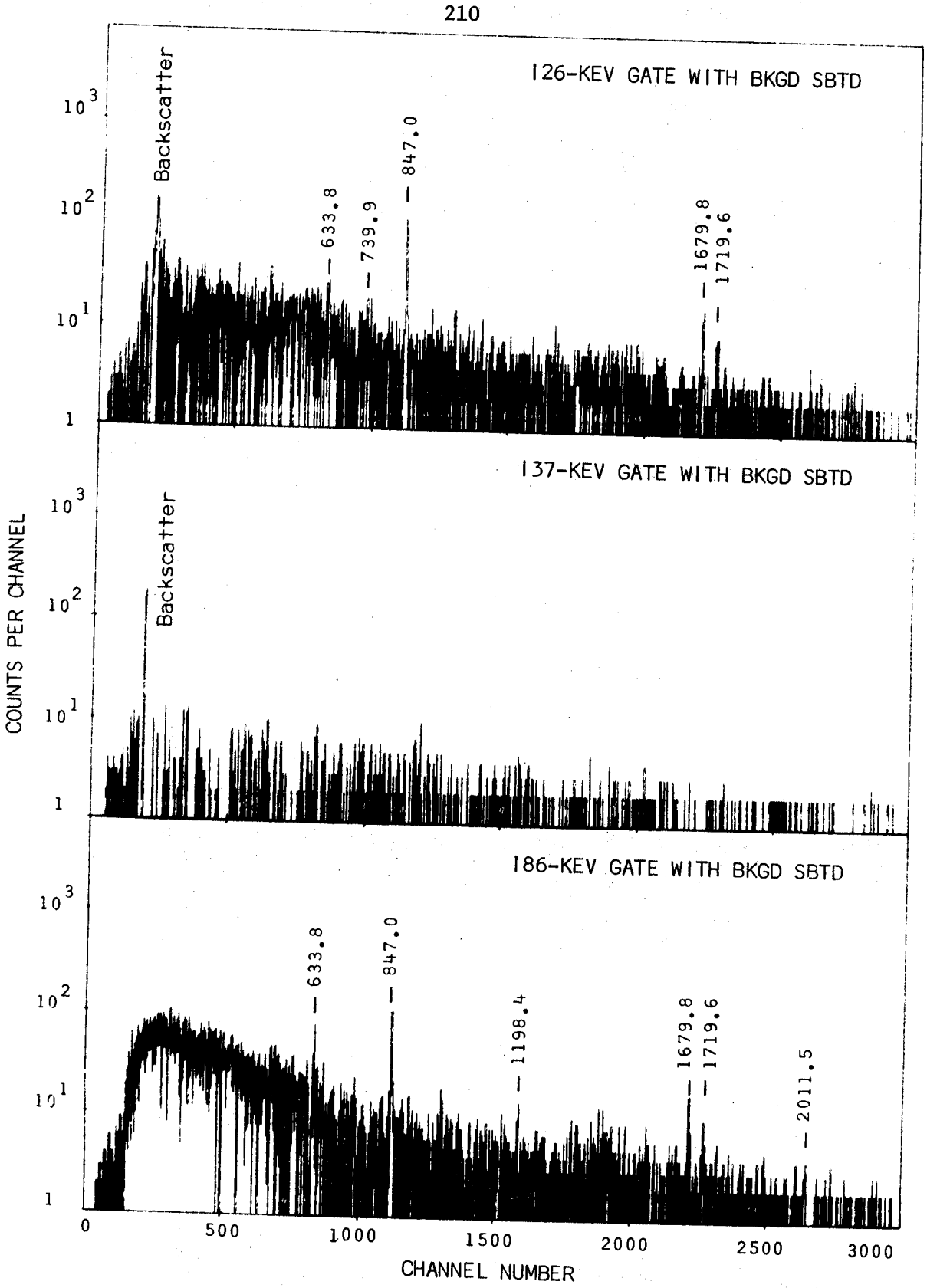

Fig. 33. The γ-γ coincidence spectra from the Bi^{203} decay. The spectra were recovered from the coincidence data stored on magnetic tapes using EVENT data-taking routine. The titles of the coincidence spectra have the same meanings as those in Figure 24.

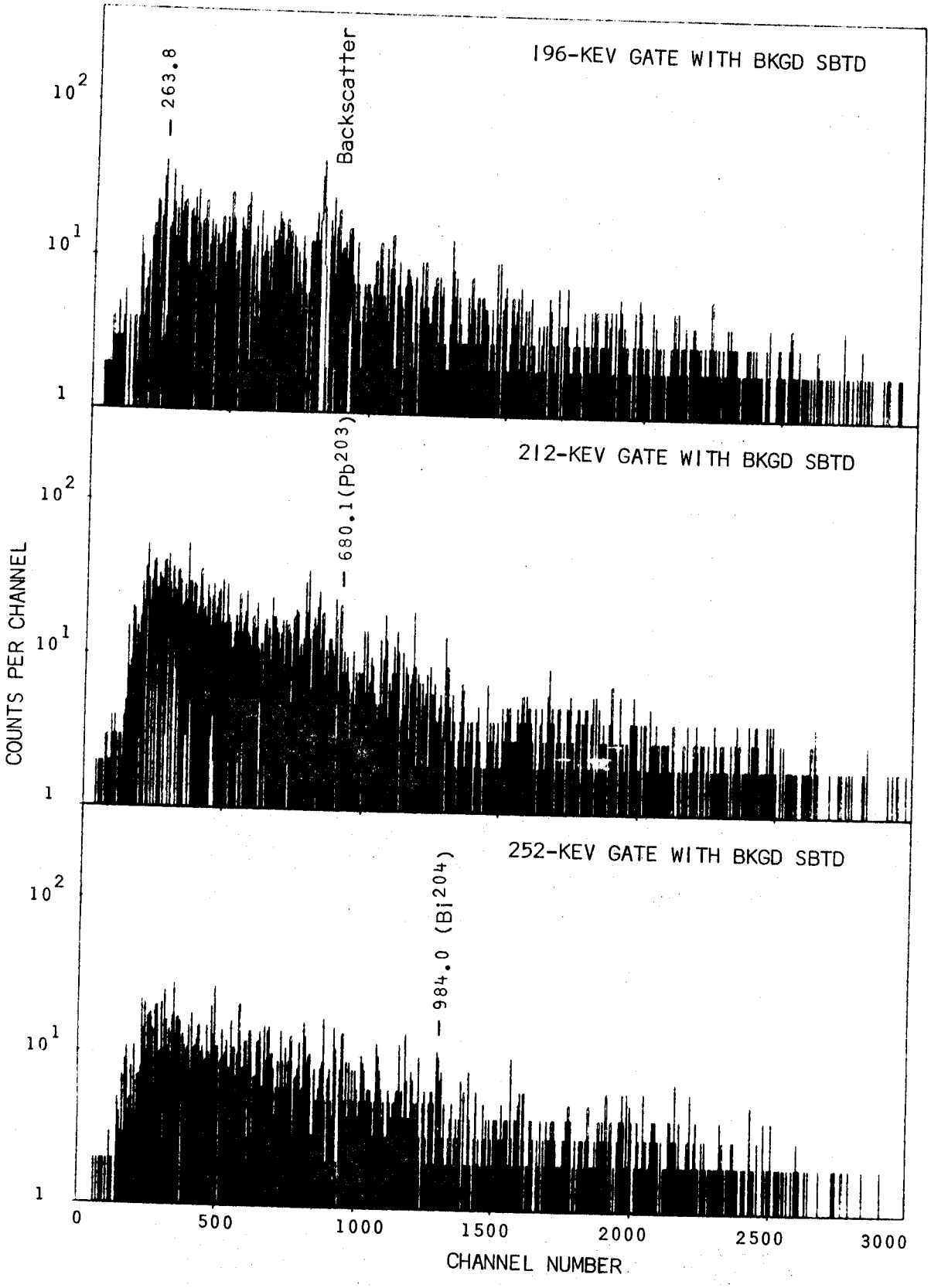

Fig. 33. (continued)

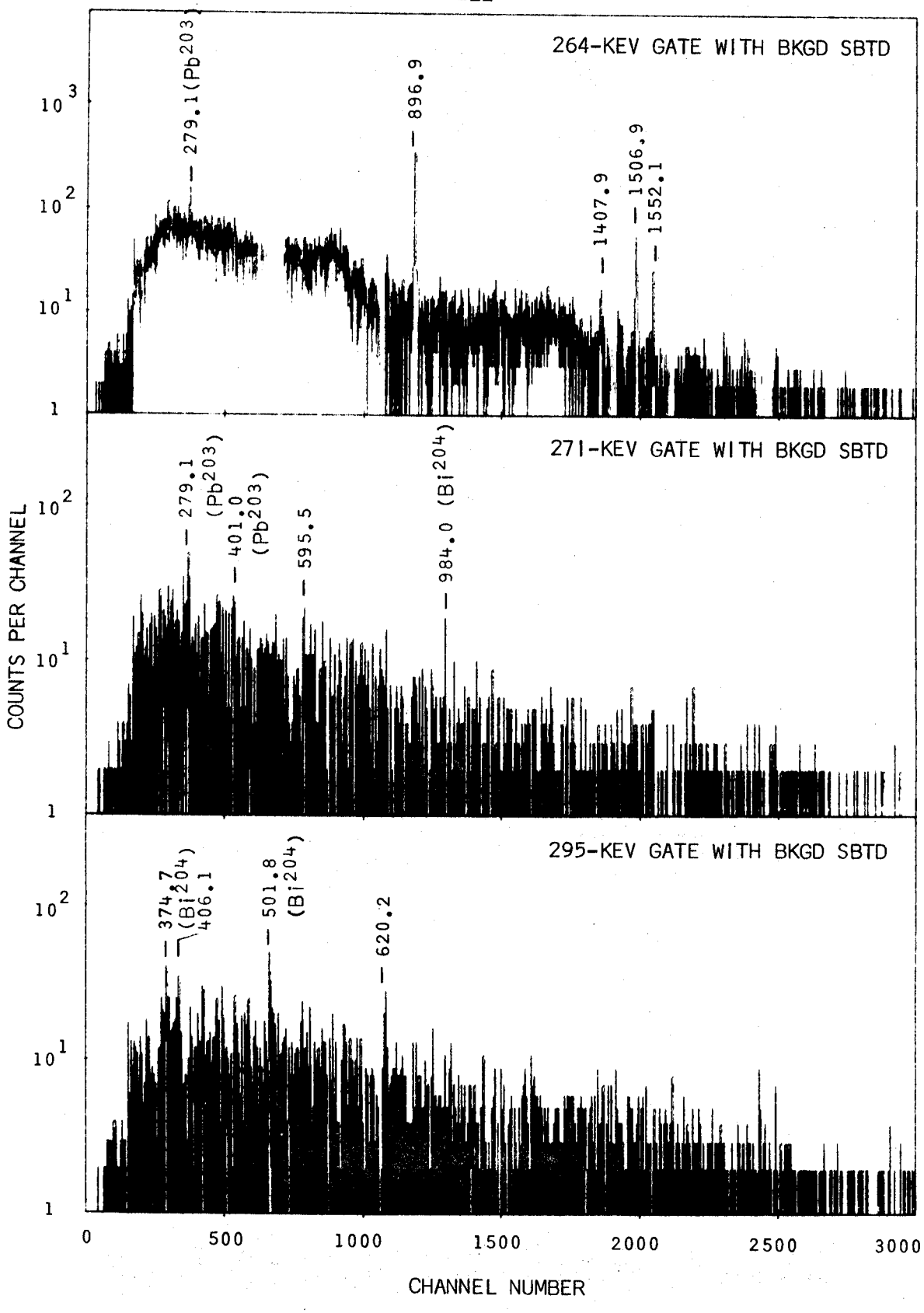

Fig. 33. (continued)

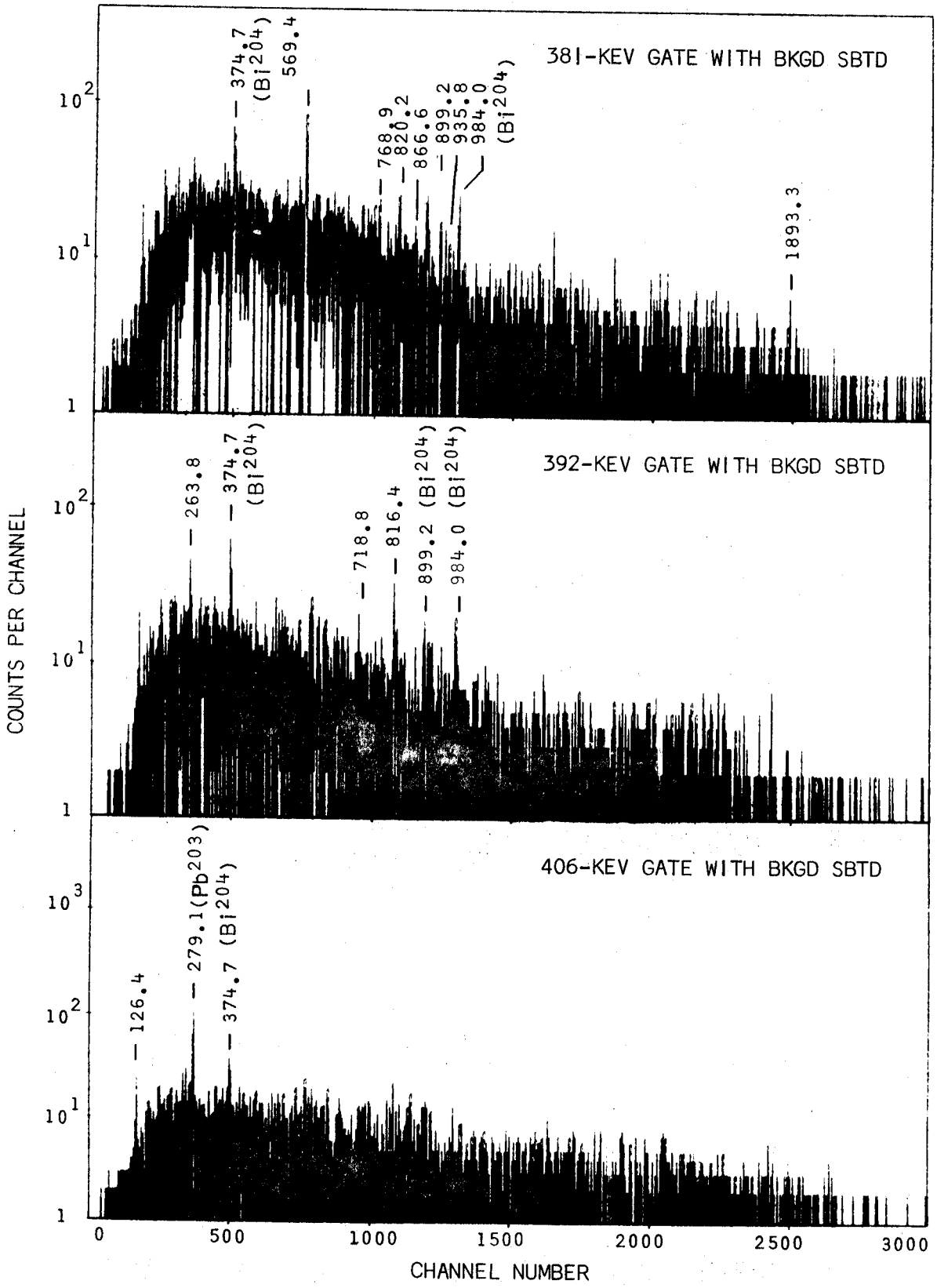

Fig. 33. (continued)

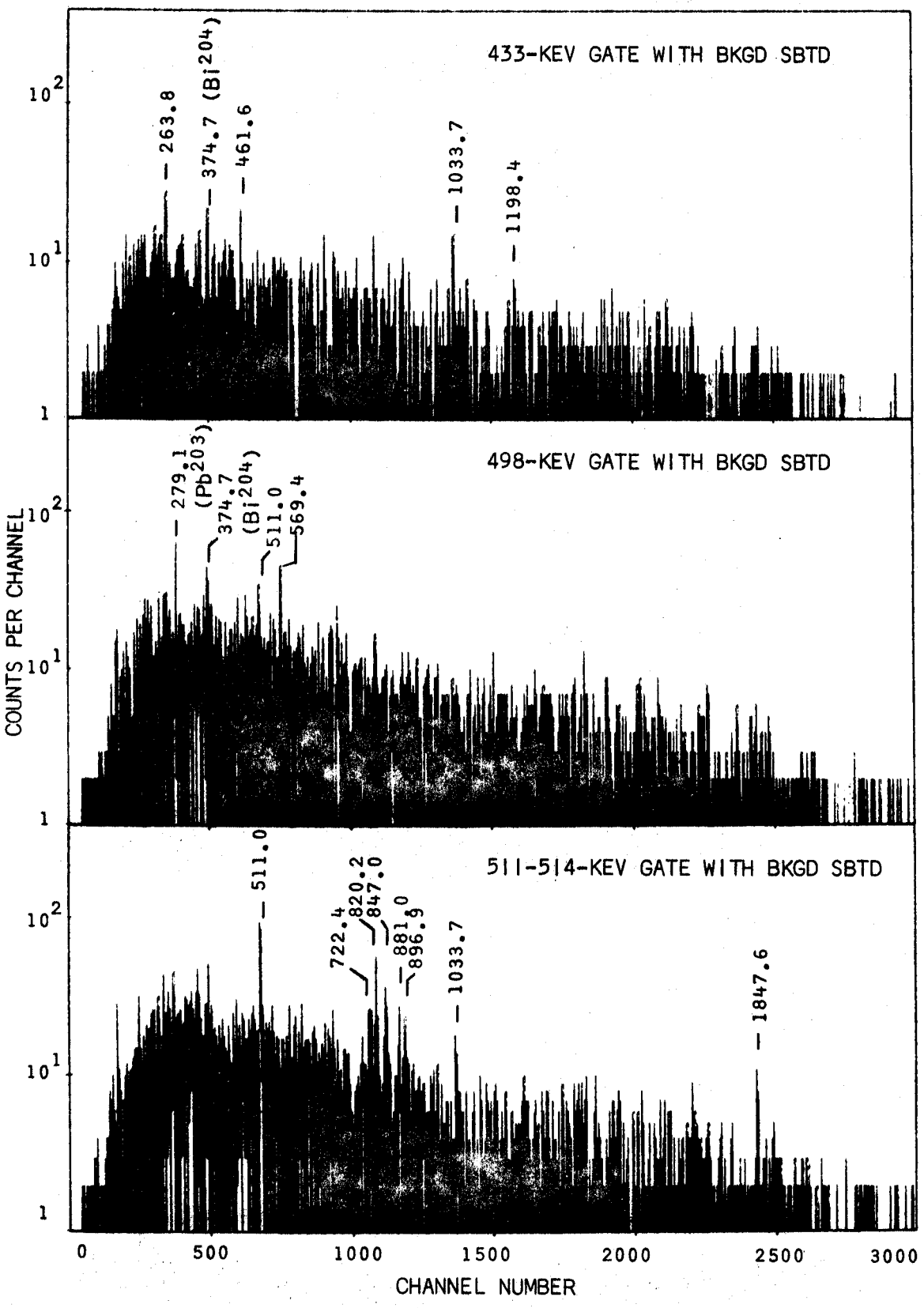

Fig. 33. (continued)

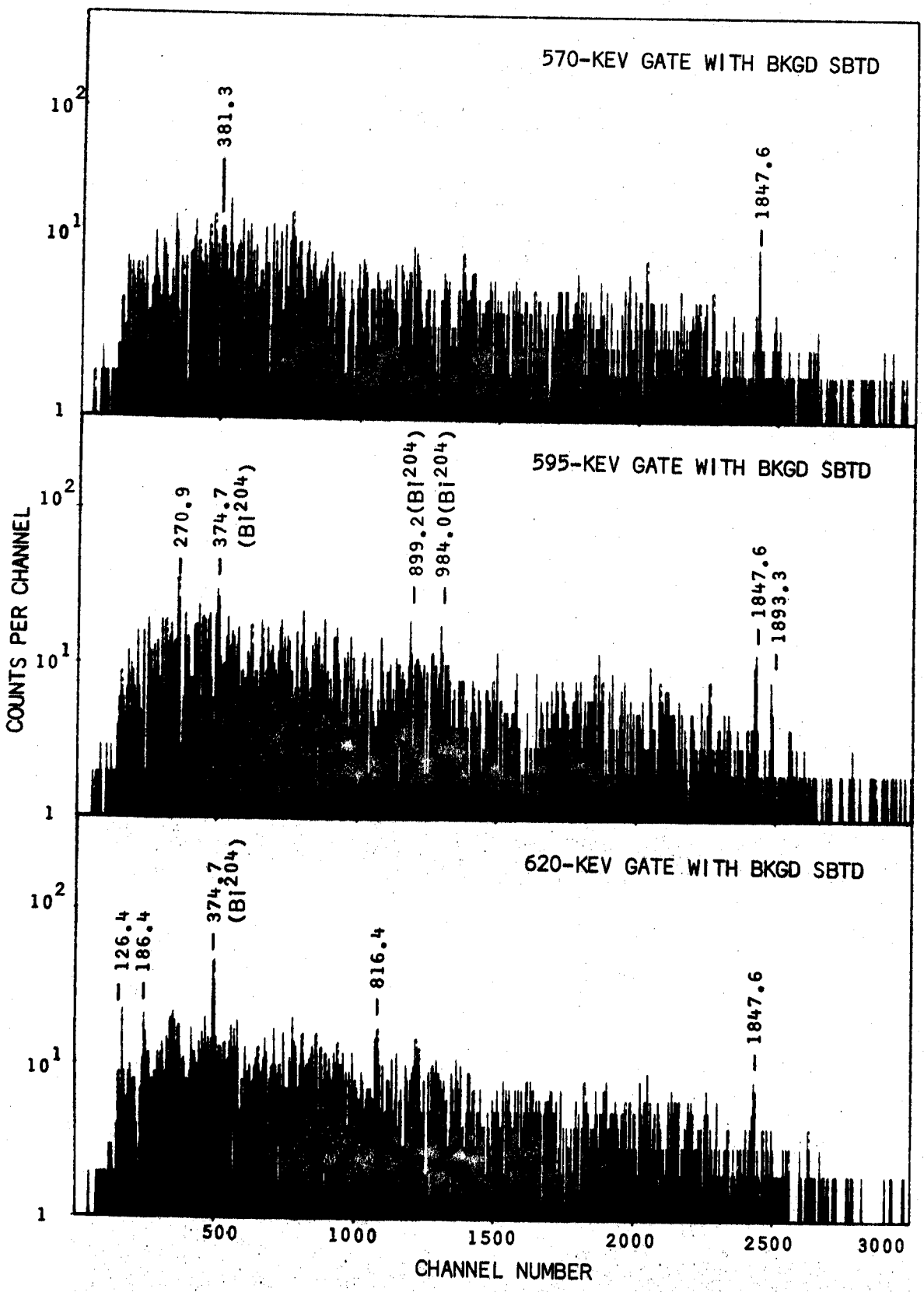

Fig. 33. (continued)

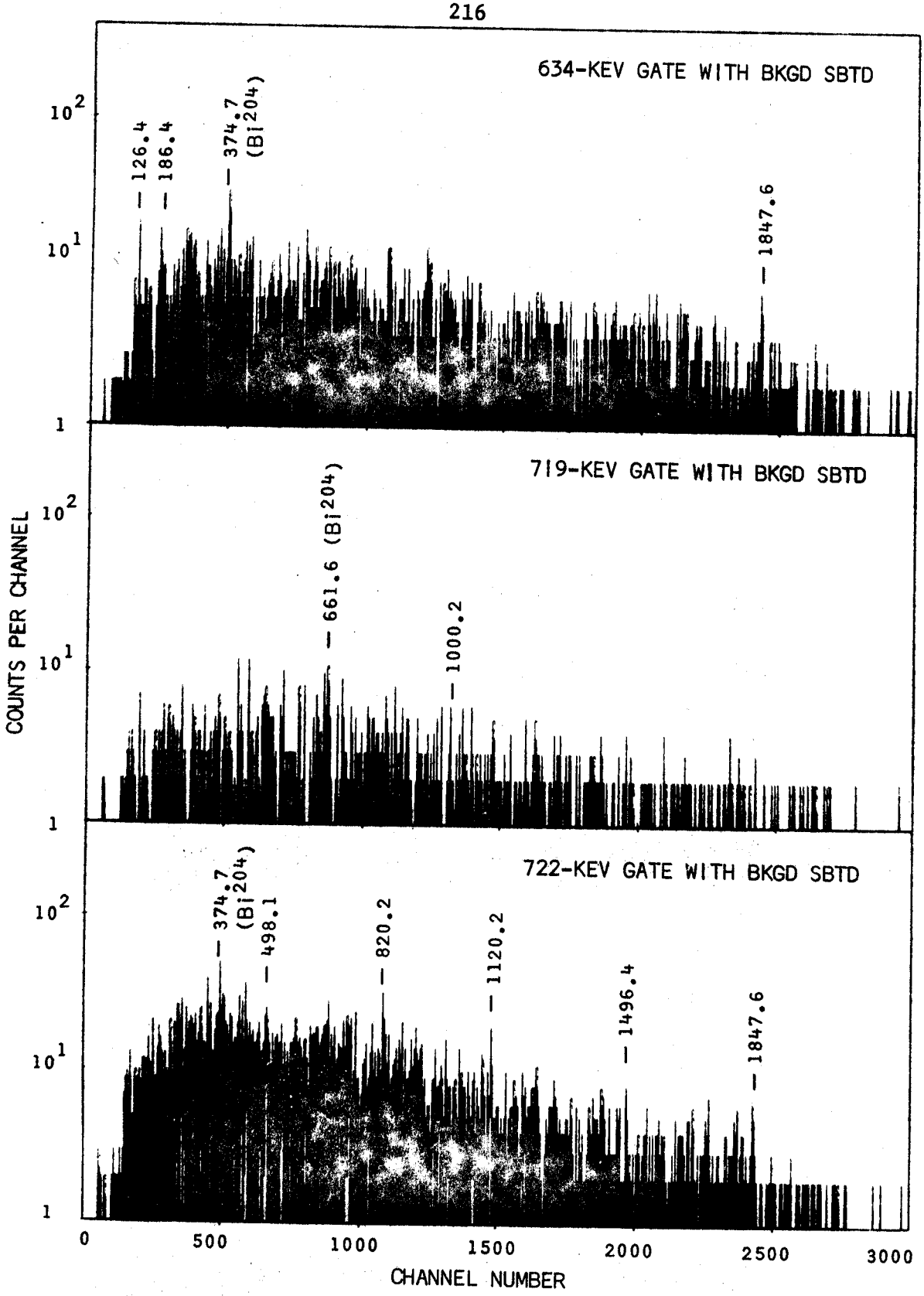

Fig. 33. (continued)

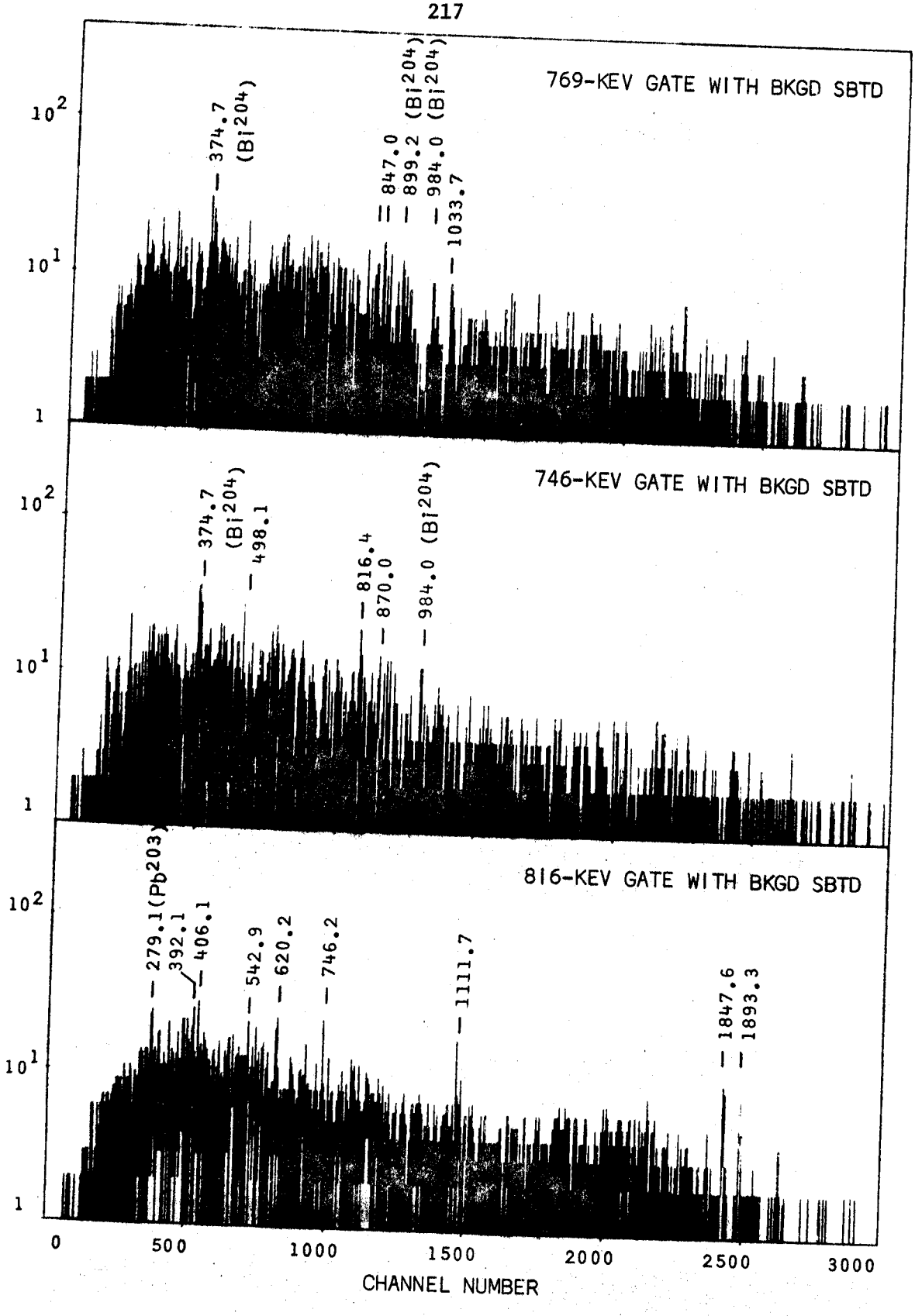

Fig. 33. (continued)

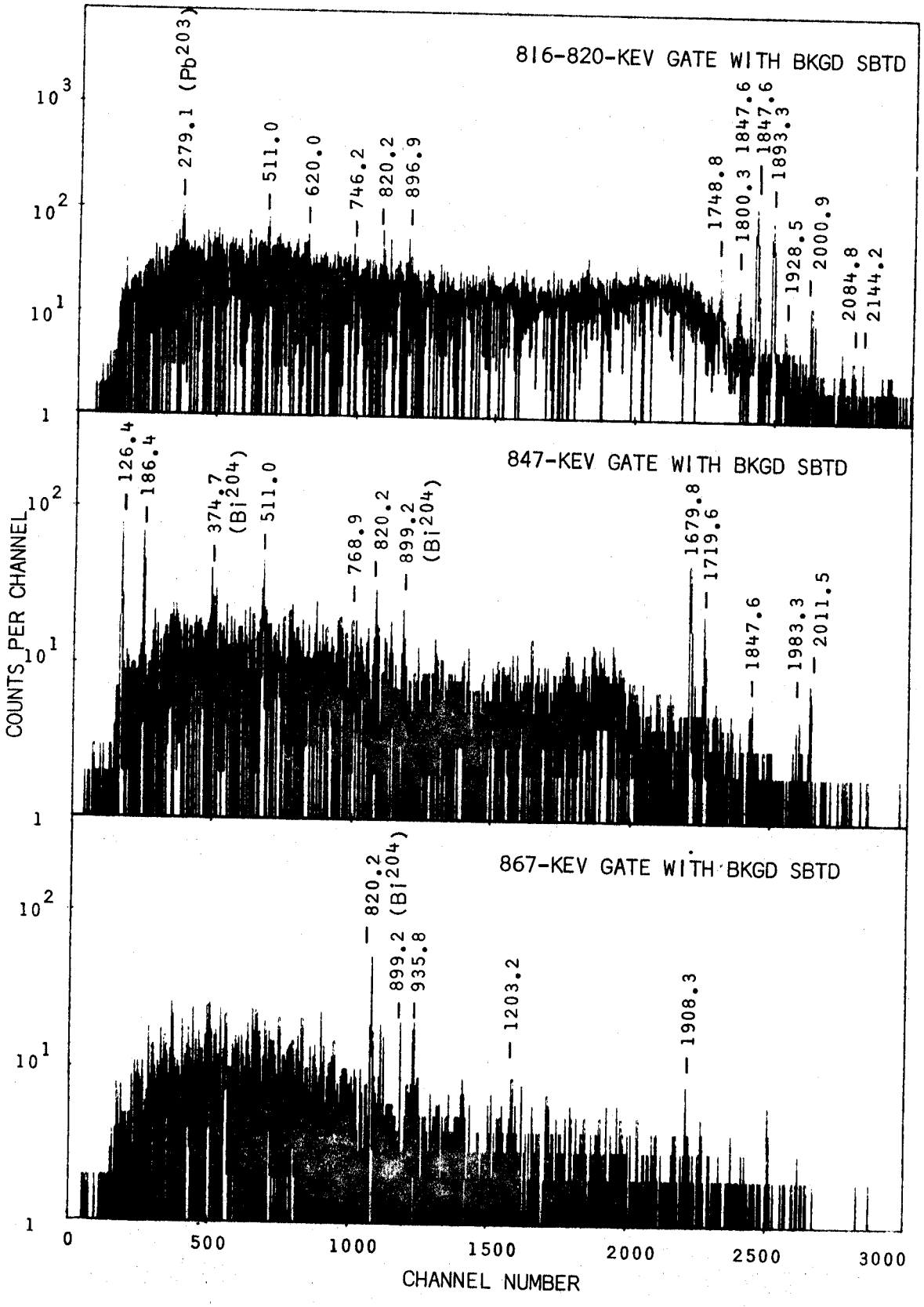

Fig. 33. (continued)

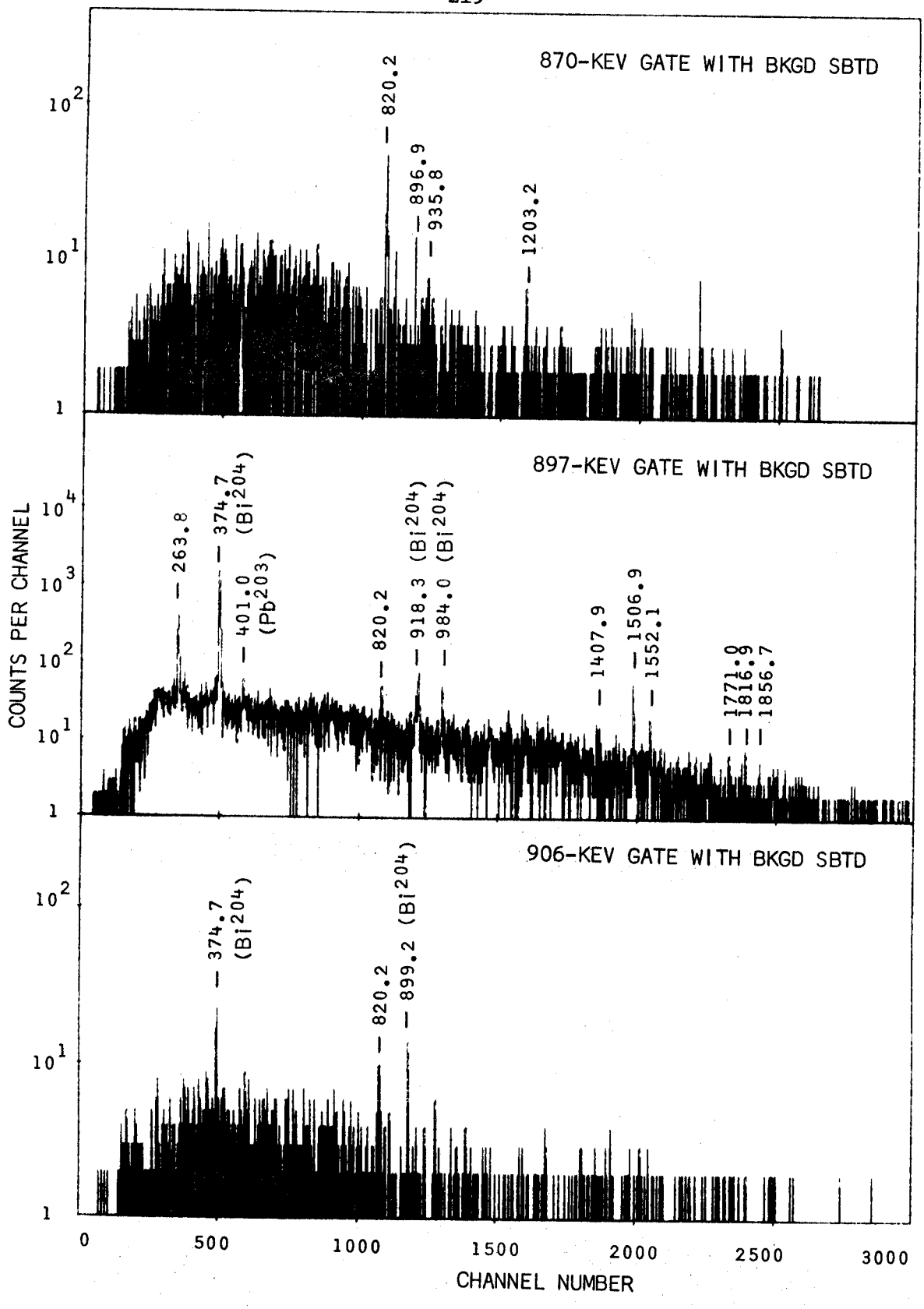

Fig. 33. (continued)

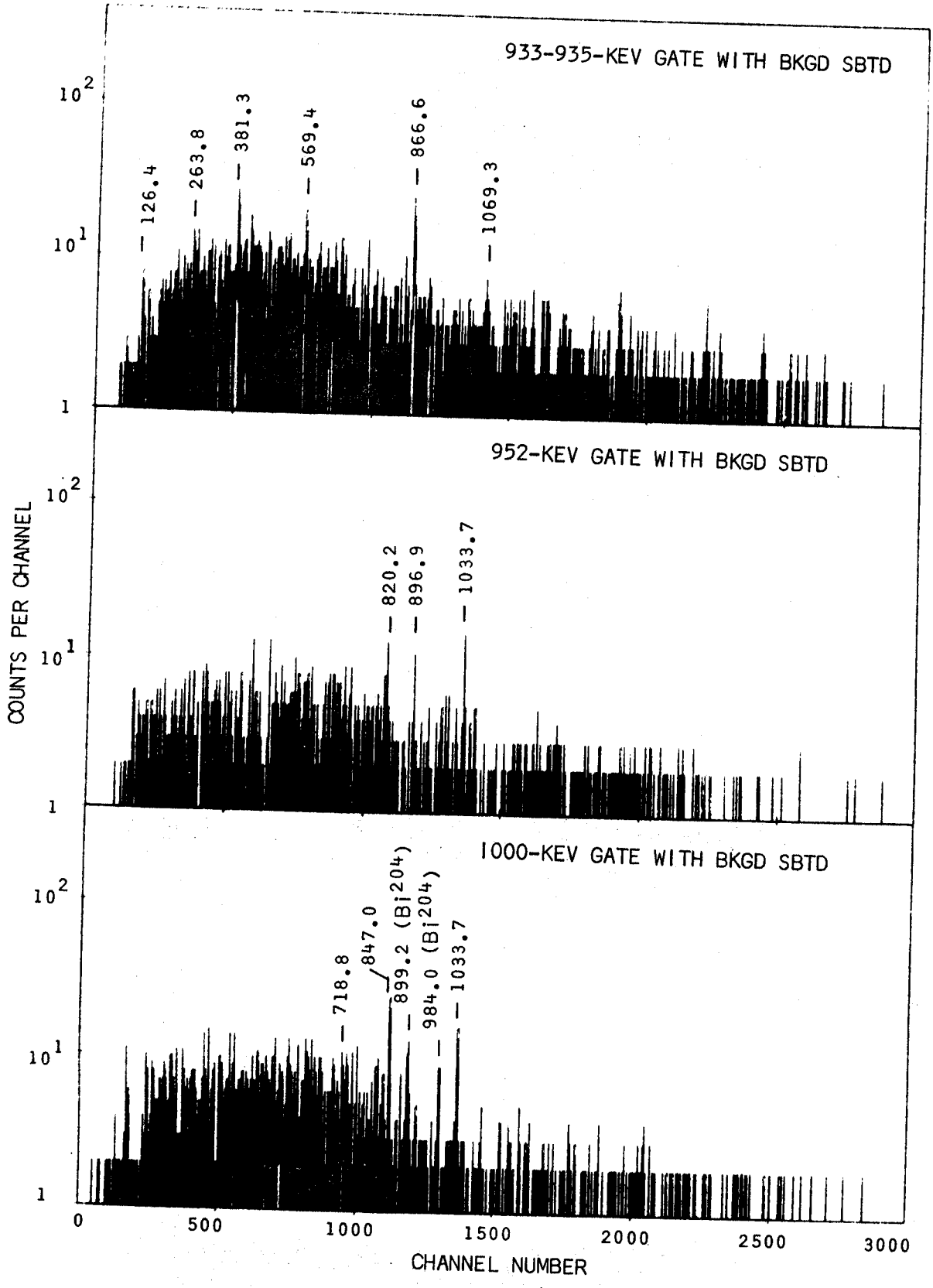

Fig. 33. (continued)

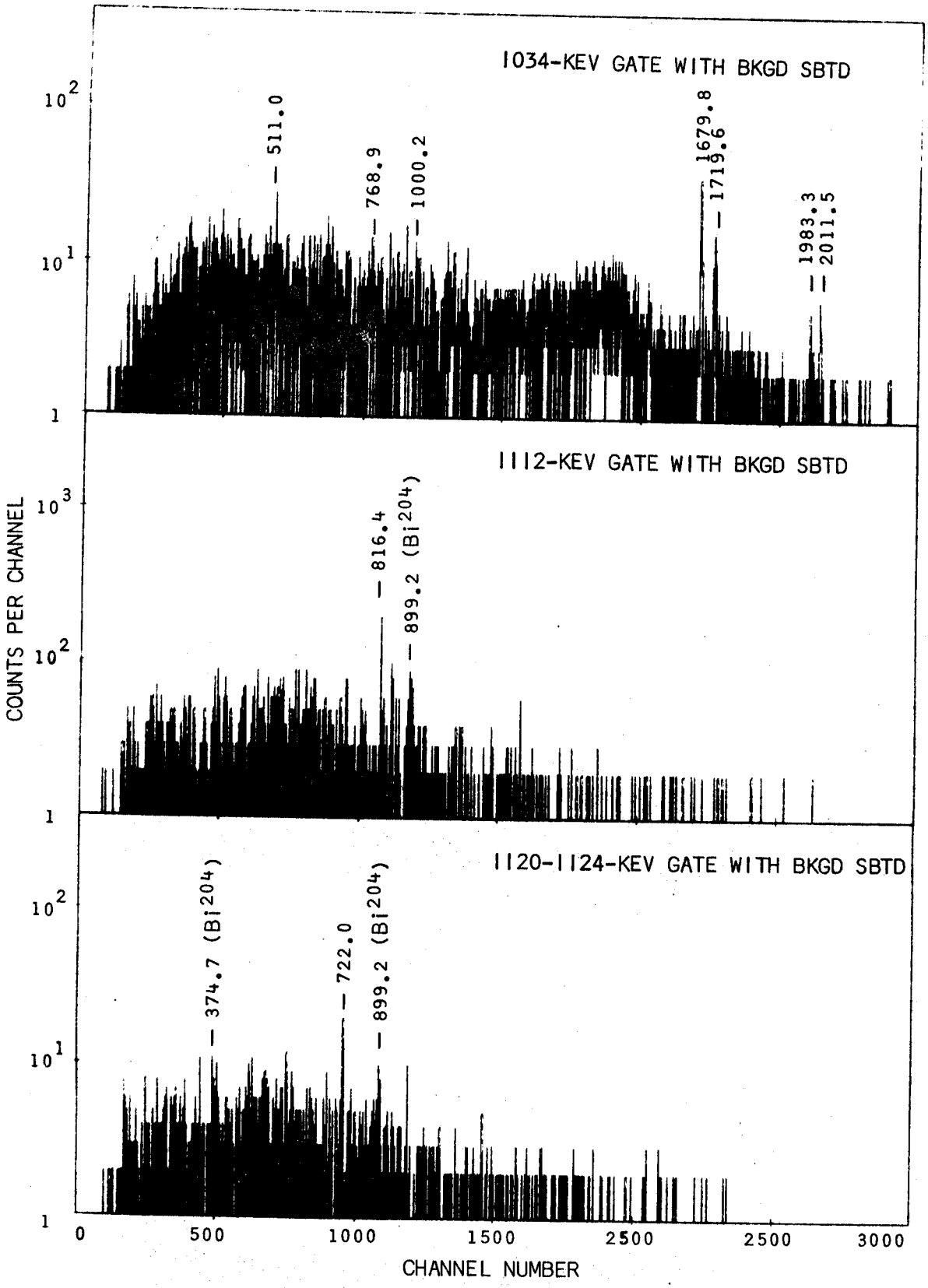

Fig. 33. (continued)

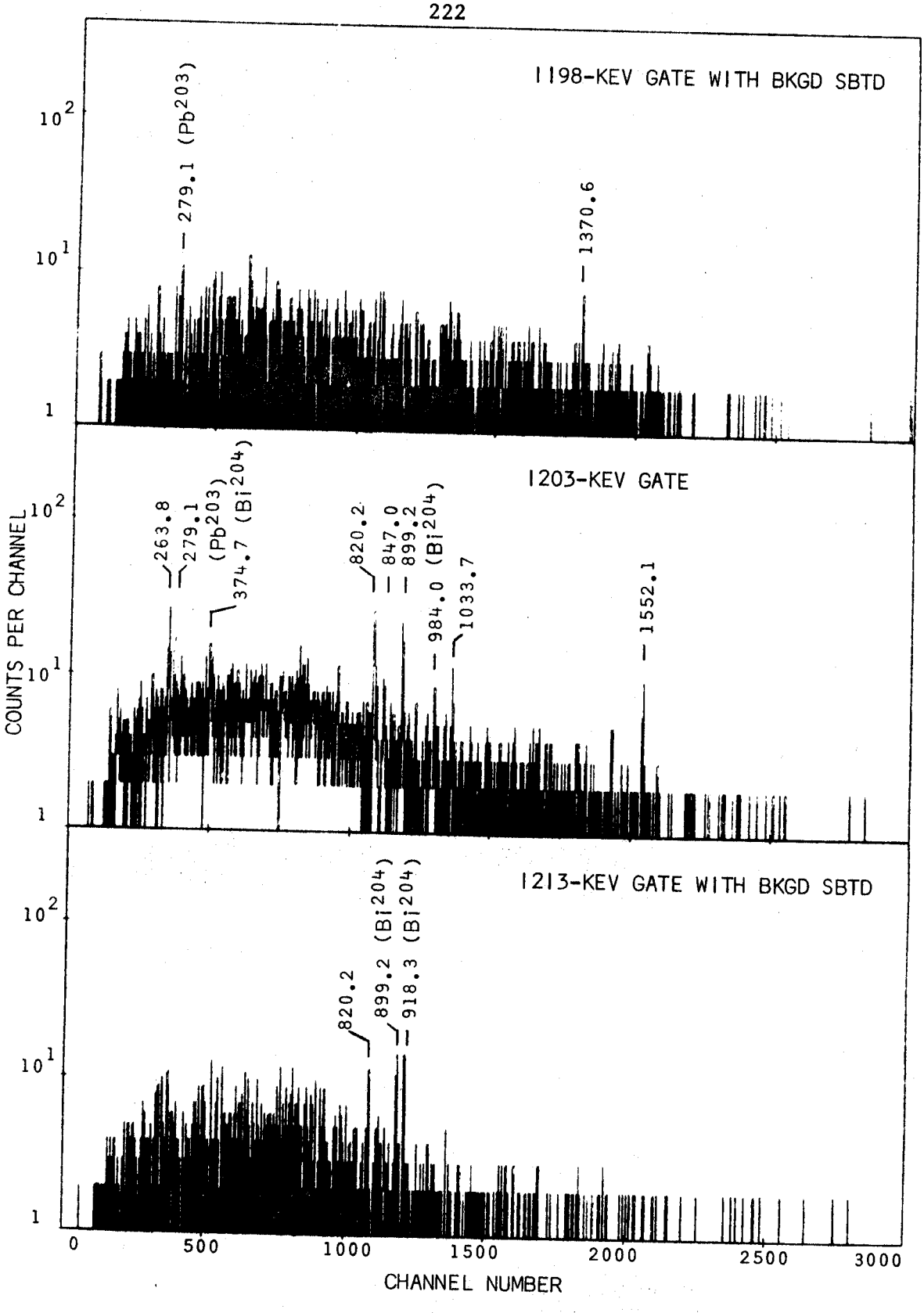

Fig. 33. (continued)

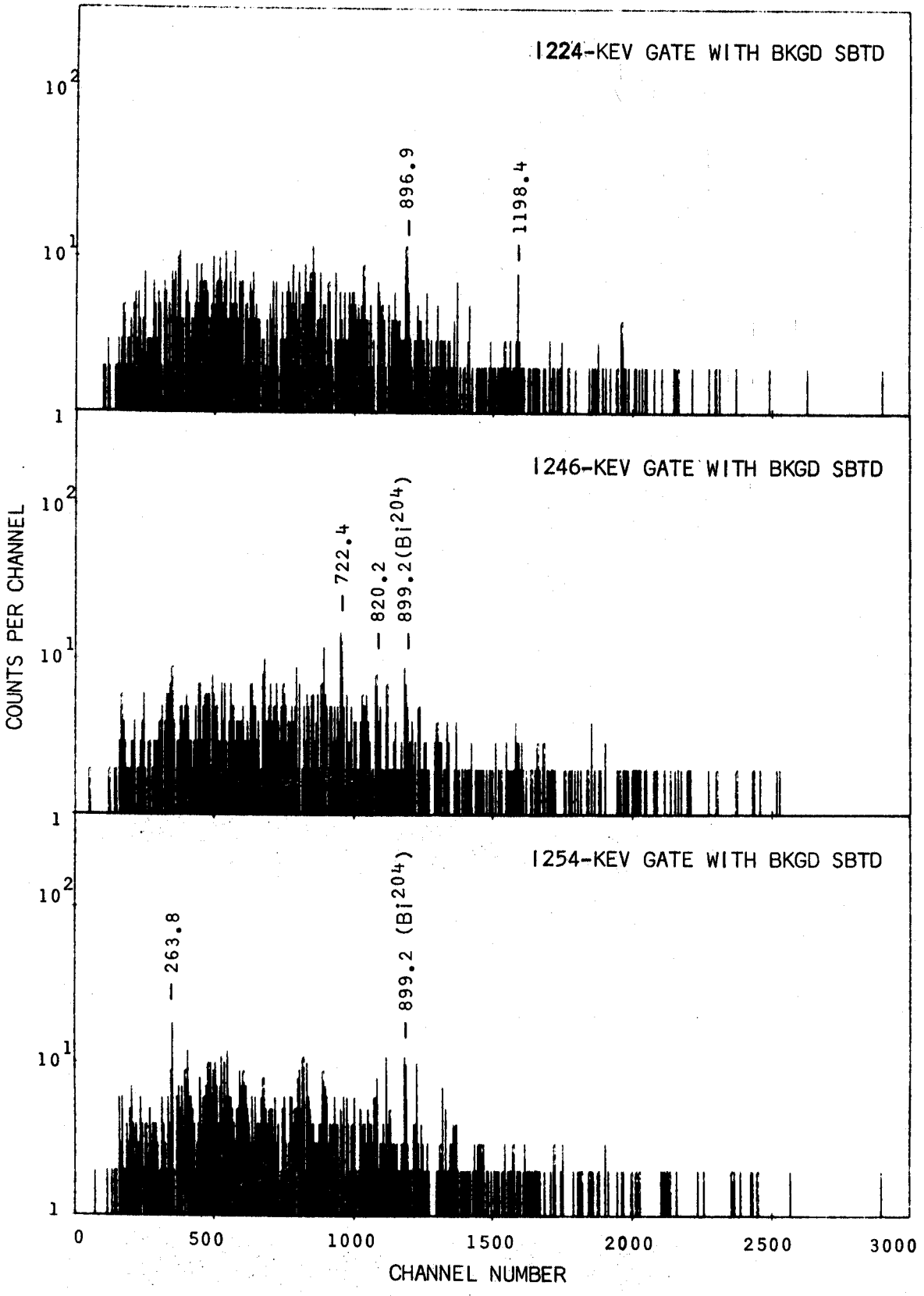

Fig. 33. (continued)

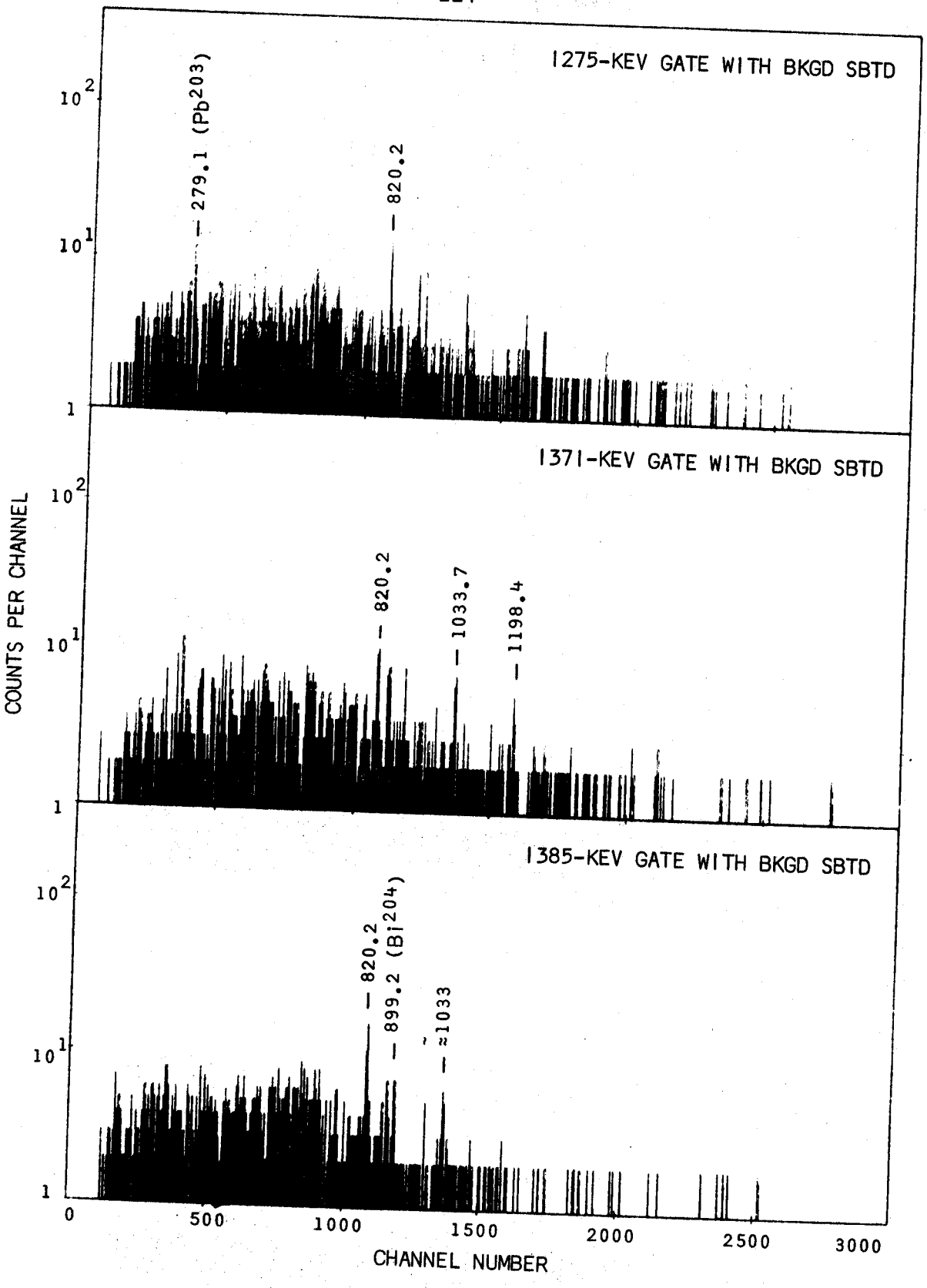

Fig. 33. (continued)

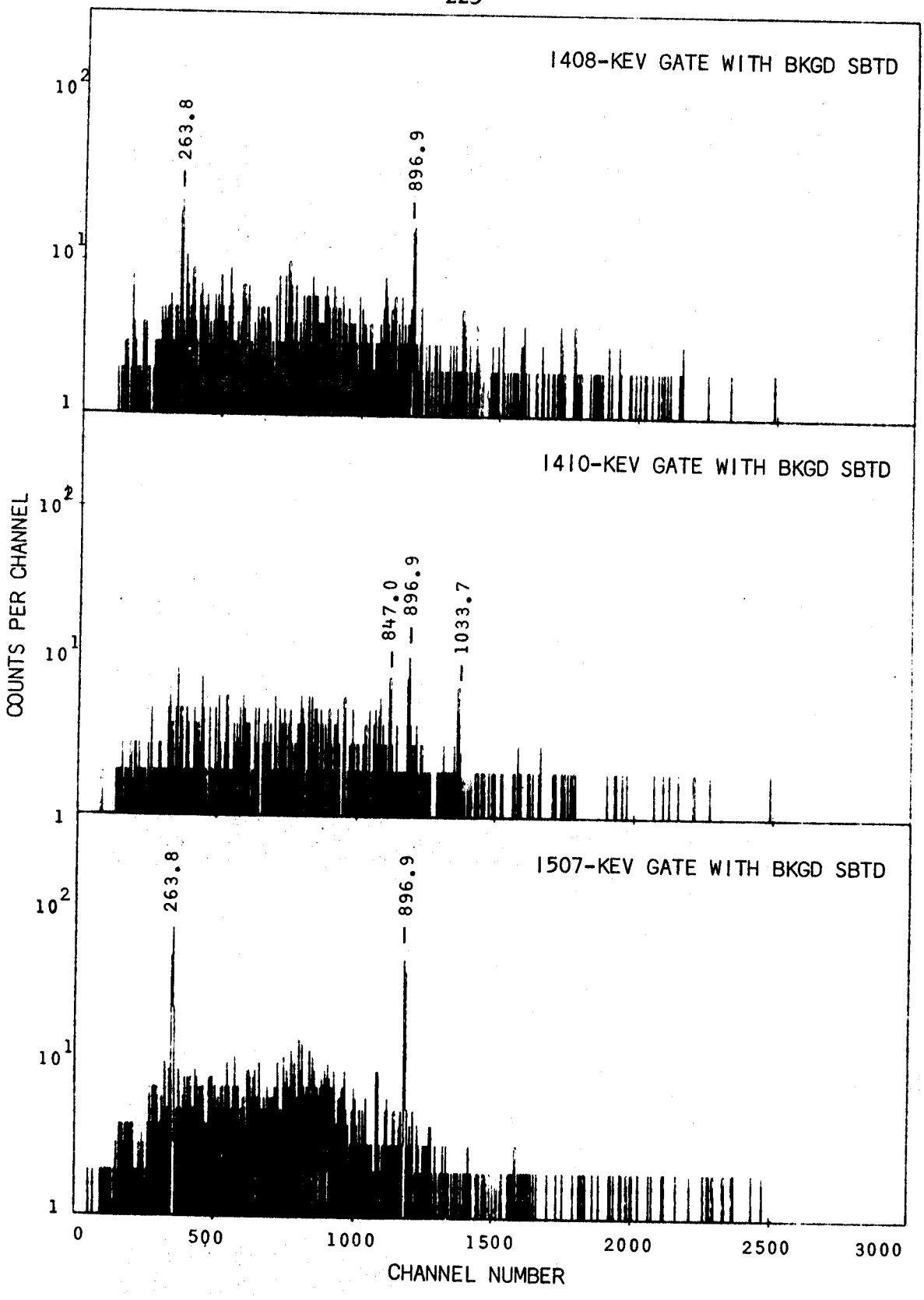

Fig. 33. (continued)

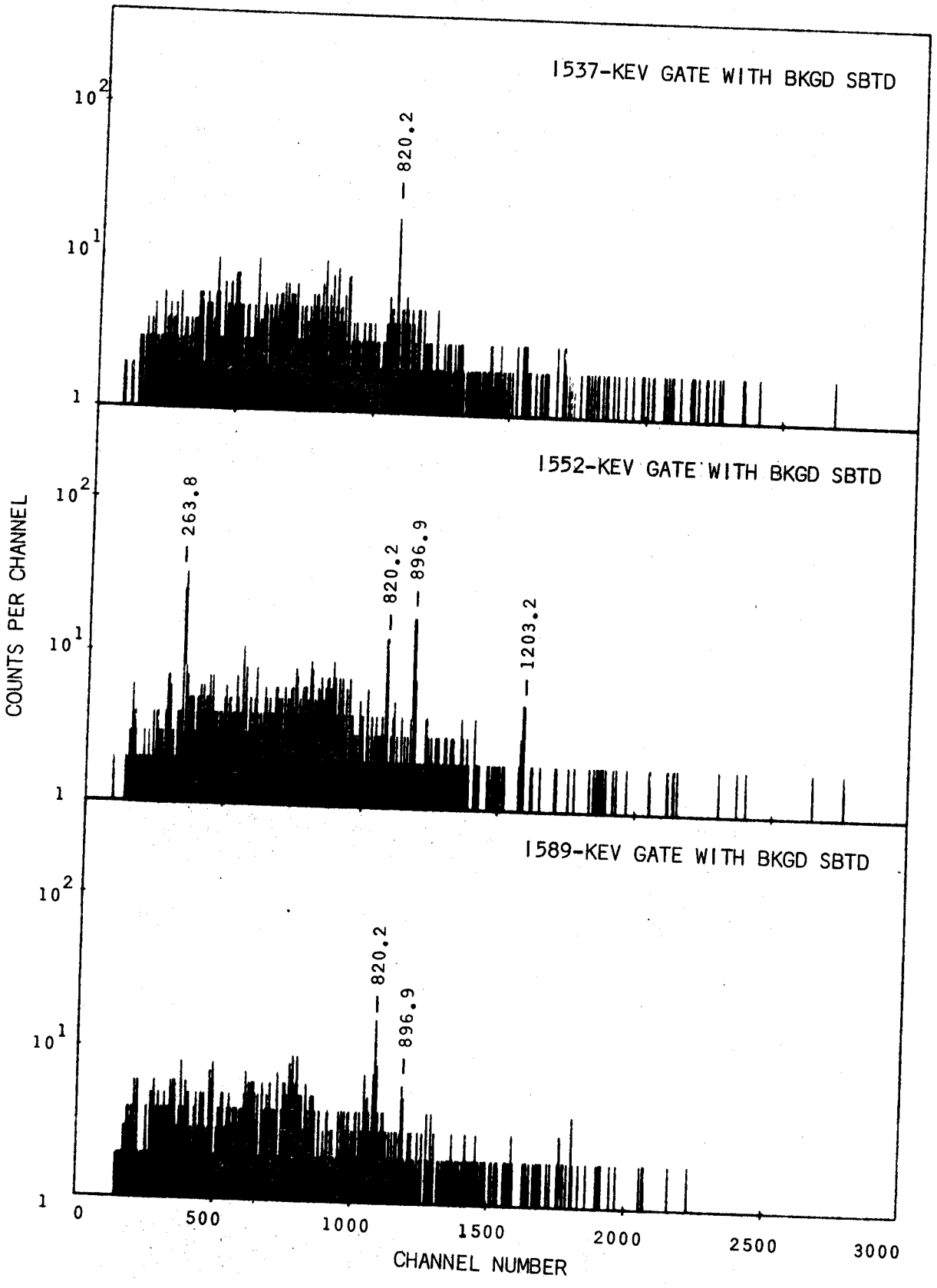

Fig. 33. (continued)

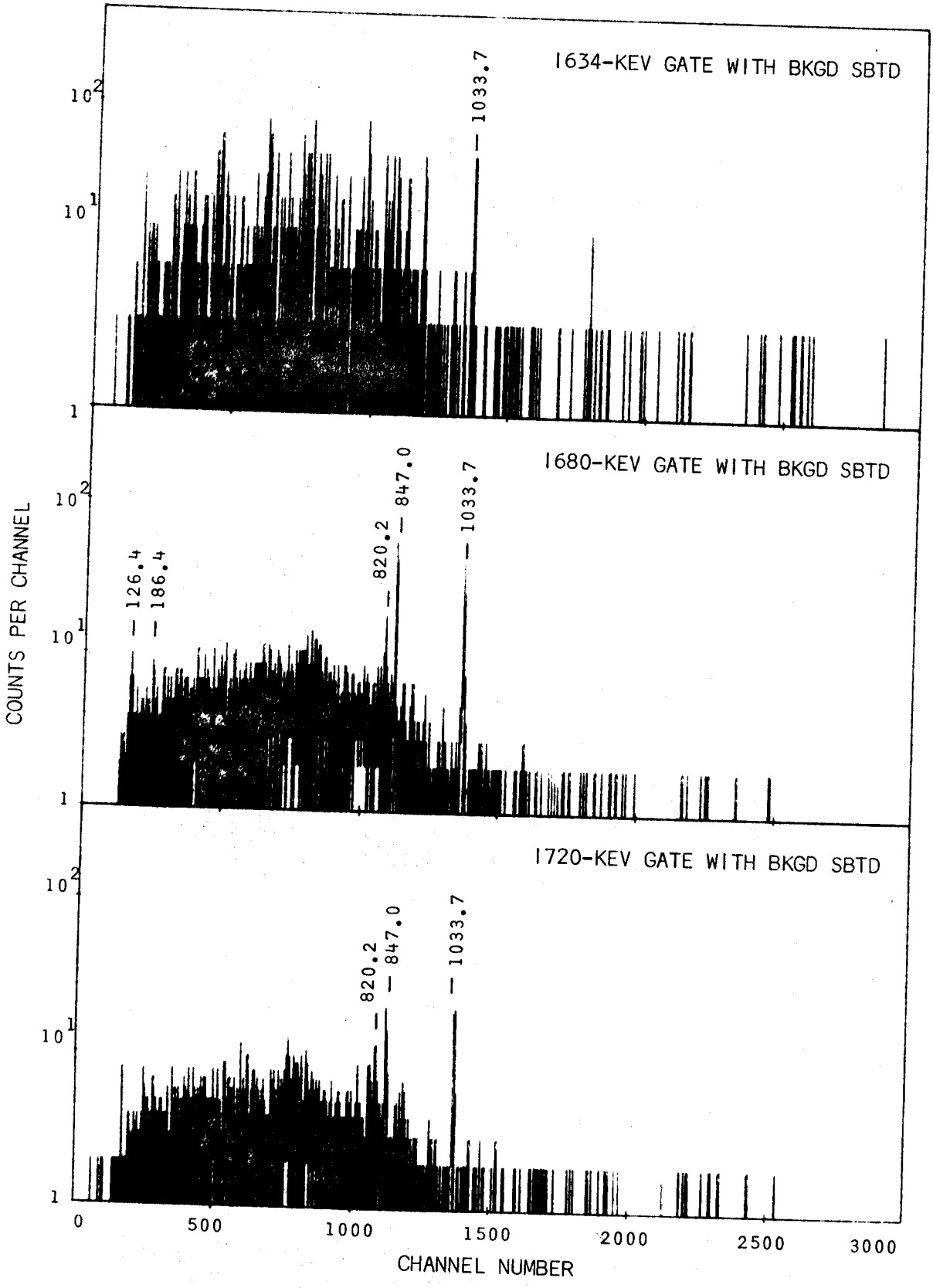

Fig. 33. (continued)

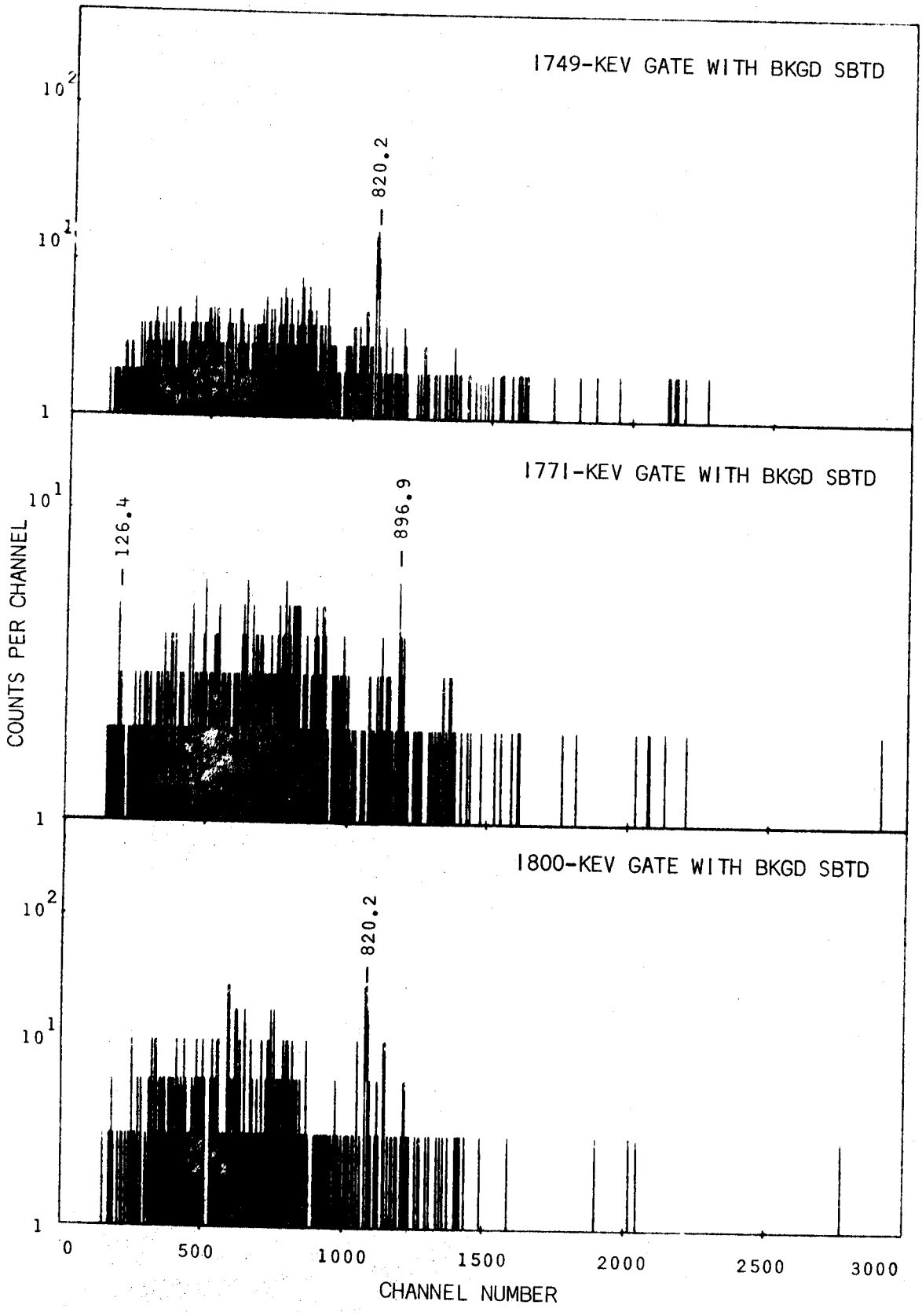

Fig. 33. (continued)

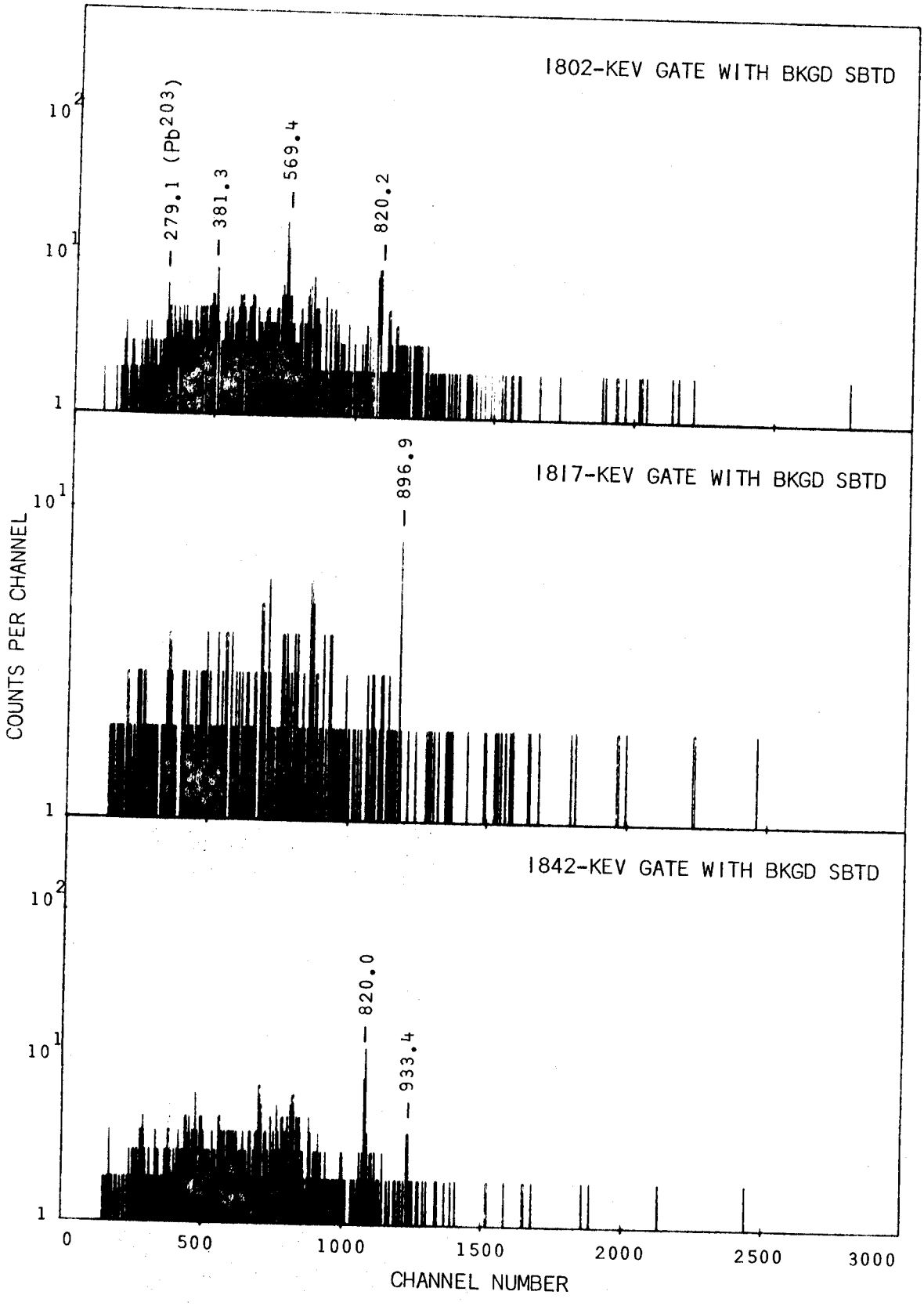

Fig. 33. (continued)

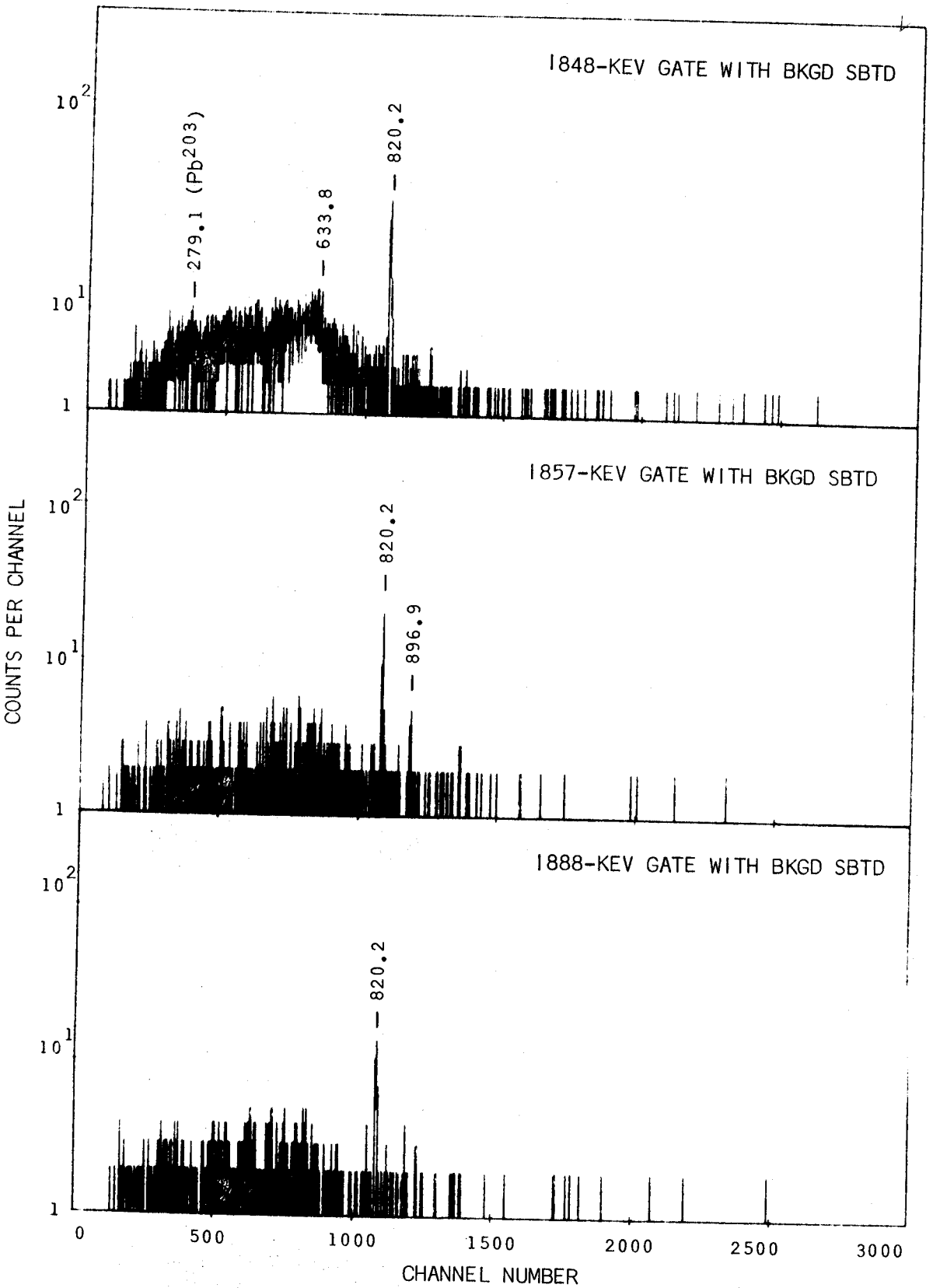

Fig. 33. (continued)

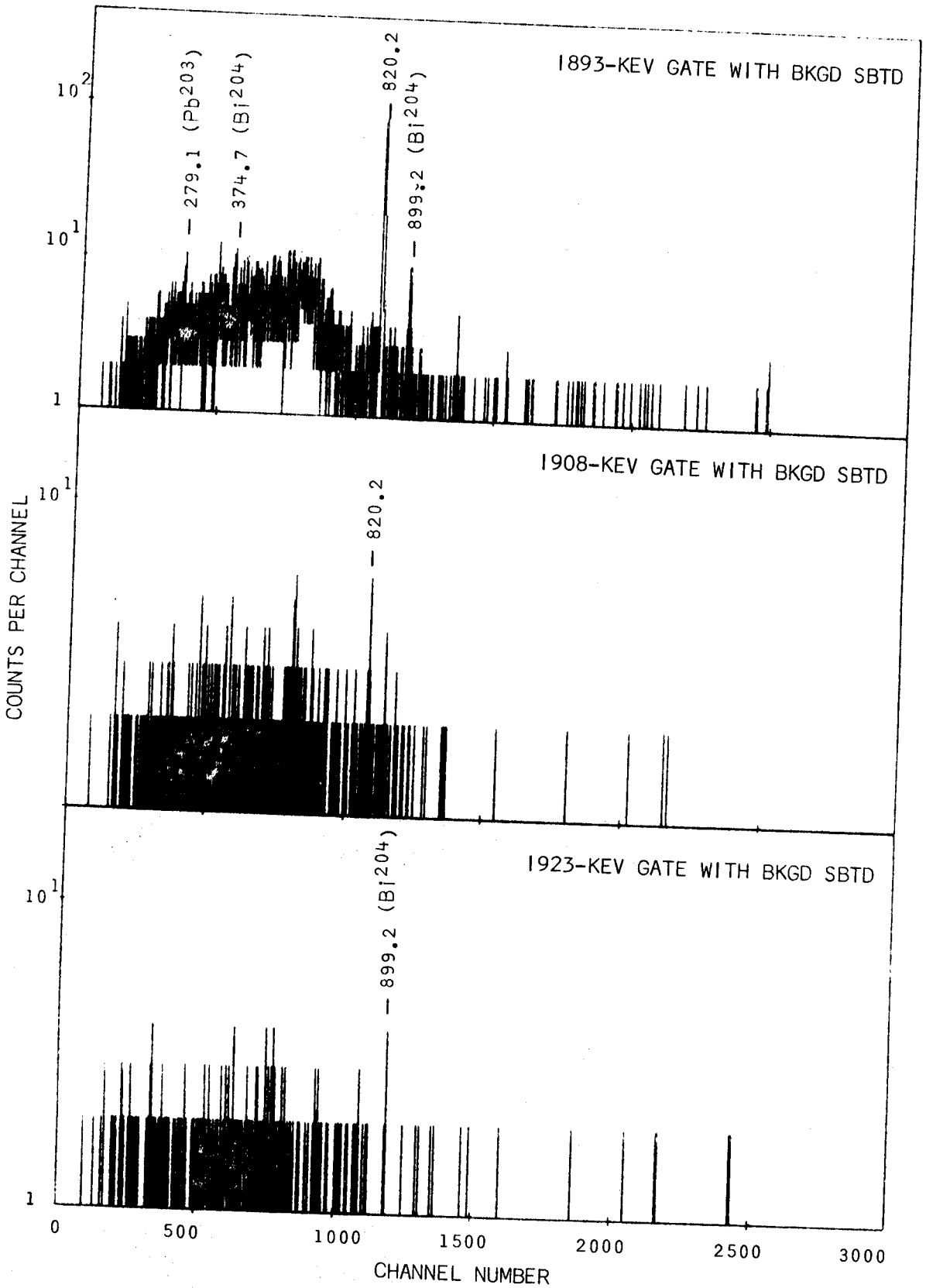

Fig. 33. (continued)

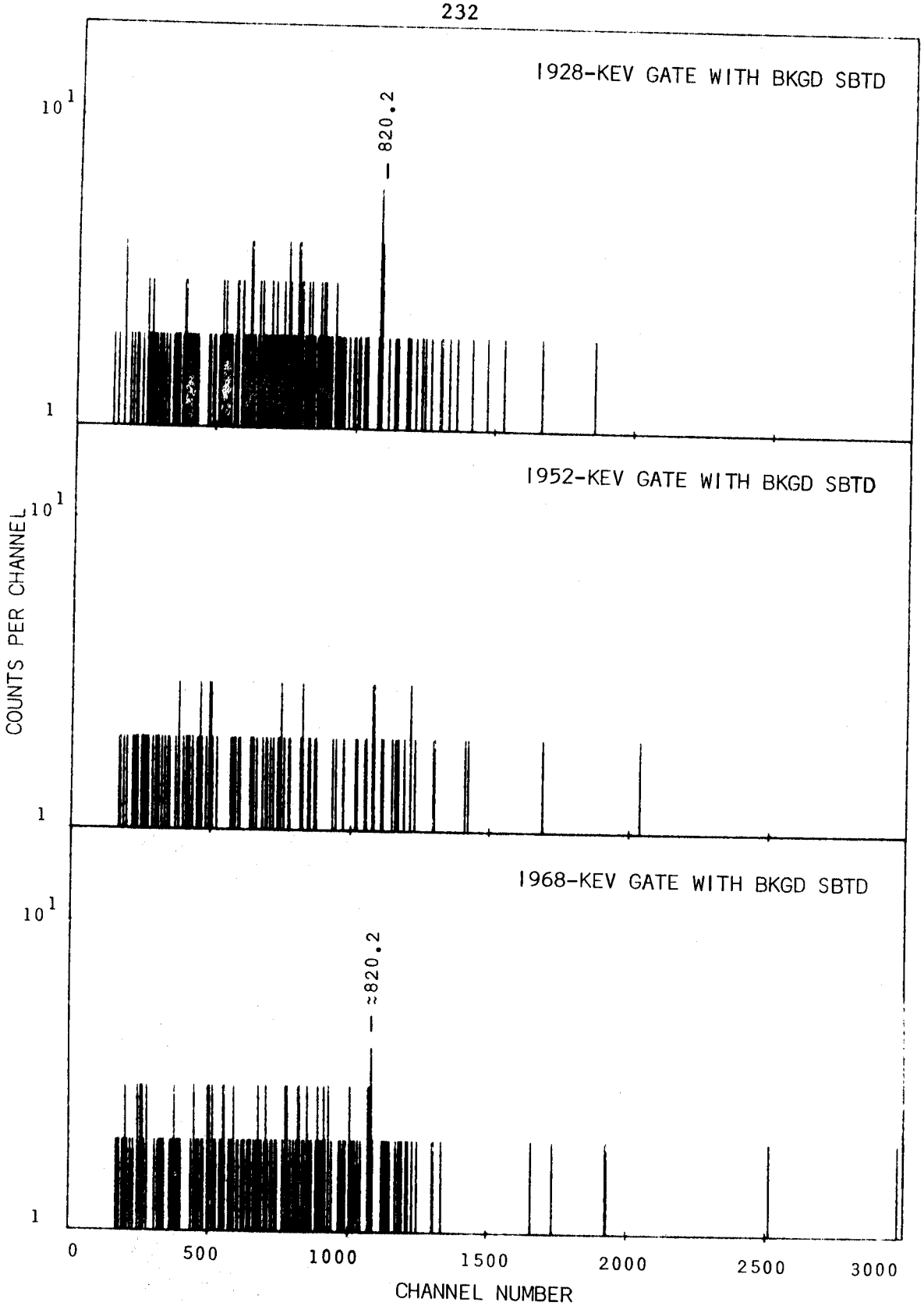

Fig. 33. (continued)

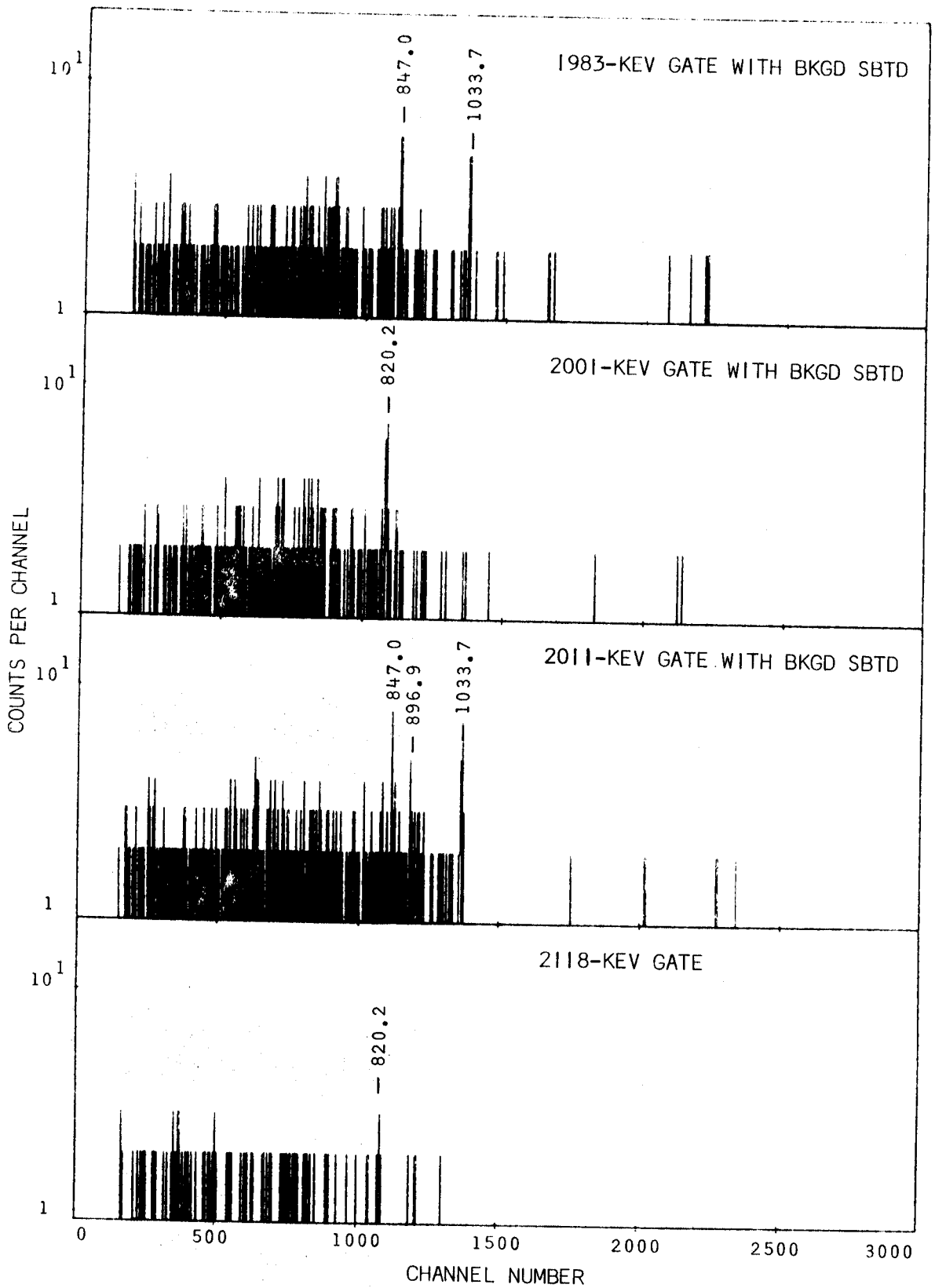

Fig. 33. (continued)

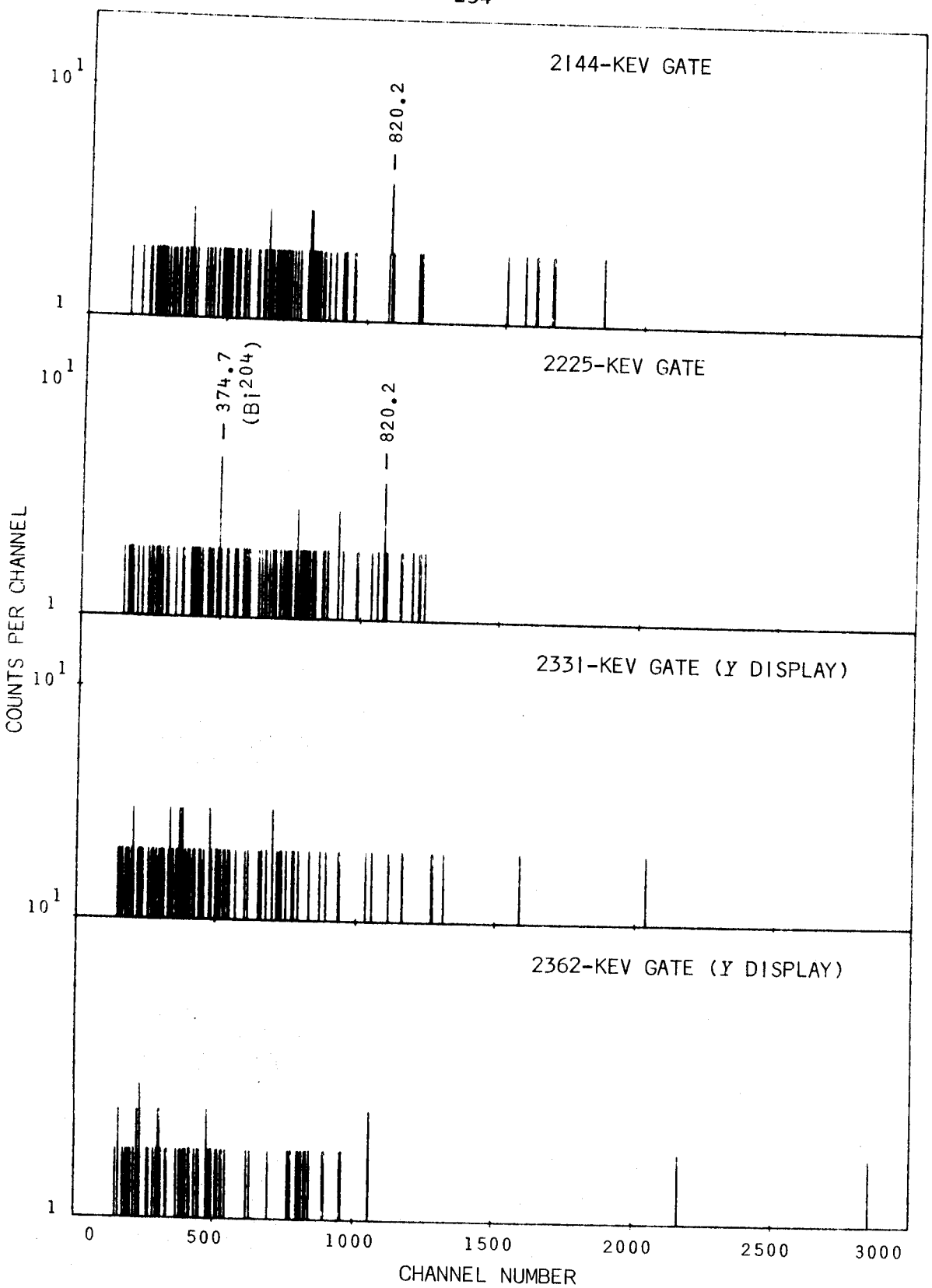

Fig. 33. (continued)

Fig. 34. The level scheme of Pb^{203} showing additional transitions from the Bi^{203} decay which could be placed on the basis of precise energy sums and differences alone. The tolerance allowed was ±0.25 keV for γ's having energies <1500 keV and ±0.30 keV for γ's having energies >1500 keV. A semicircle at the origin of a transition indicates some coincidence data support for such a placement.

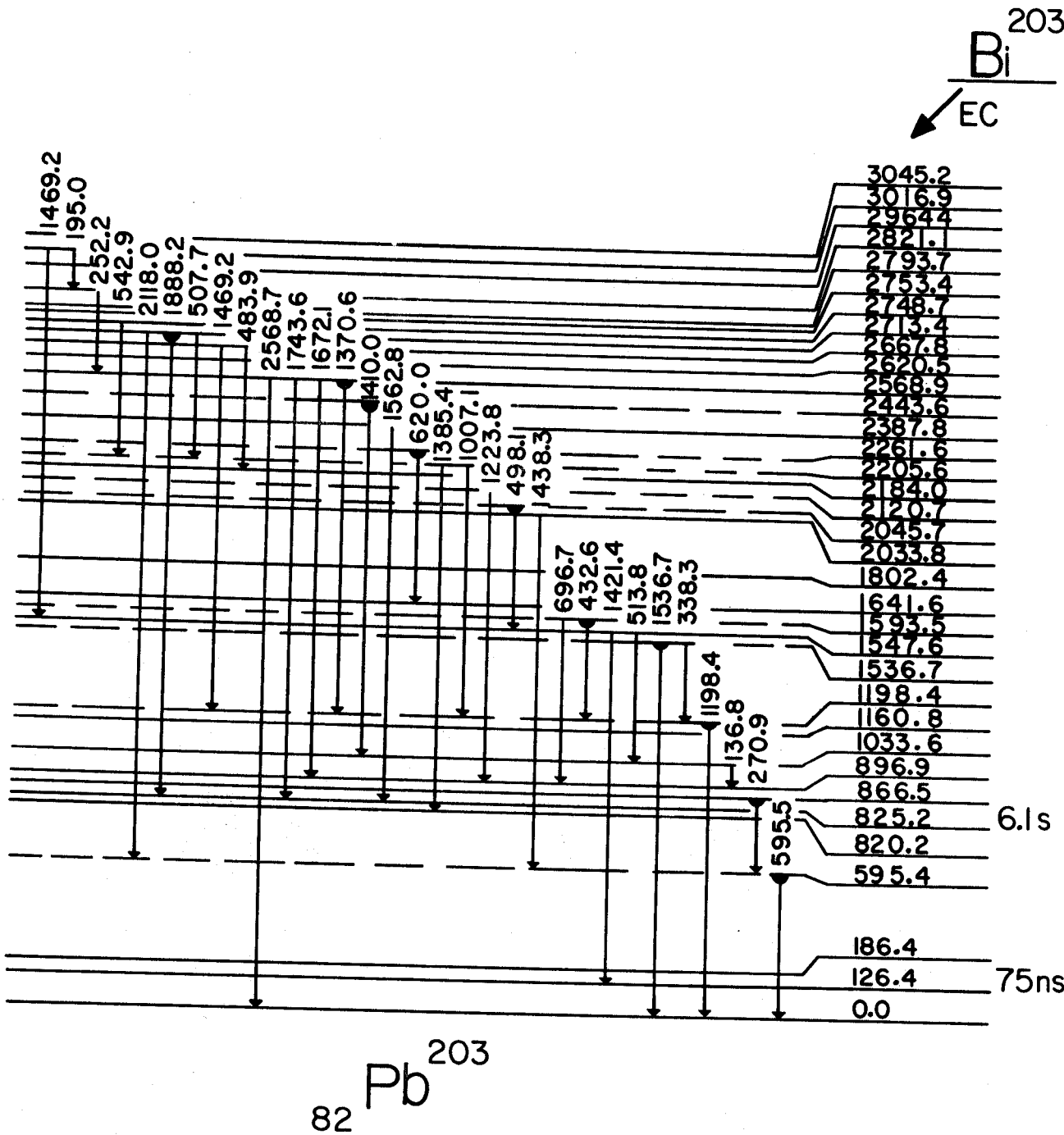

Fig. 34. (continued)

ficient used for this normalization was 0.217 [S165]. The results of these calculations (including selected theoretical conversion coefficients [S165])and the predicted multipolarities are listed in Table 14. The theoretical conversion coefficients were also used to construct smooth curves of *M*1, *M*2, *M*3, *M*4, *E*1, *E*2, and *E*3 multipolarities over a 100-2000-keV range, upon which I have superimposed the experimental points (Figure 34). The error bars were calculated using the published errors for the electron data (Novakov et al. [No58], ±15%, and Stockendal et al. [St60], ±15%) and the errors listed in section 3.2.3.A. for the γ-ray data. Such a graphical presentation of the complicated Bi^{203} (and Bi^{204}) multipolarity data is by far a much more efficient and more easily assimilated method of presentation than that of the table. While many more of the Bi^{203} intense transitions are listed in Table 14 than in the corresponding Bi^{204} table (Table 10), it still is unfortunate that more electron data is unavailable, as this would make precise characterization of the spin and parities for the Pb^{203} scheme much more accessible. Several of the transitions listed in Table 14 (cf. Figure 35) have previously been assigned multipolarities on the basis of conversion-electron ratios and absolute conversion-coefficient measurements. These assignments and their relation to the assignments in this table are discussed below.

The 825.2-keV transition is the transition associated with the 6.1-s $i_{13/2}$ Pb^{203m} state. The *K* conversion coefficient of the 825.2-keV transition has been measured by Stockendal et

Table 14. Multipolarity of Bi^{203} γ transitions.

Transition energy[a] (keV)	K-electron intensity[b]	γ-ray intensity[a]	Experimental α_K[d]	Theoretical α_K[f]				Multi-polarity
825.2	≡1000 [1000]	54.5	≡2.17(-1) [2.17(-1)][e]	*M4* 2.17(-1)	-	-	-	*M4*
126.4	545 [330]	14.0	4.6(-1) [2.9(-1)]	*E1* 1.9(-1)	*E2* 3.8(-1)	*E3* 6.4(-1)	*M1* 3.8(0)	*E2*
186.4	1410 [670]	20.2	8.2(-1) [3.9(-1)]	*E1* 6.8(-2)	*E2* 1.9(-1)	*E3* 5.1(-1)	*M1* 1.2(0)	*M1,E3*
263.8	753 [750]	20.6	4.3(-1) [4.3(-1)]	*E3* 2.1(-1)	*M1* 4.6(-1)	*M2* 1.6(0)	-	*M1*
626.8	- [9]	1.15	- [9.2(-2)]	*E3* 3.0(-2)	*M1* 4.8(-2)	*M2* 1.3(-1)	*M3* 2.6(-1)	*M2,M1*
722.4	30[c] [12]	16.9	2.1(-2)[c] [8.4(-3)]	*E1* 4.0(-3)	*E2* 9.4(-3)	*E3* 2.4(-2)	-	*E2,(E3)*
758.2	- [≈10]	0.98	- [1.2(-1)]	*M2* 7.4(-2)	*M3* 1.4(-1)	*M4* 2.6(-1)	-	*M3*
820.1	83 [83]	≡100.0	9.8(-3) [9.8(-3)]	*E2* 7.2(-3)	*E3* 1.7(-2)	*M1* 2.5(-2)	-	*E2*
847.0	19 [22]	23.0	9.8(-3) [1.1(-2)]	*E2* 6.8(-3)	*E3* 1.6(-2)	*M1* 2.3(-2)	-	*E2,E3*
933.4	- [8]	4.82	- [2.0(-2)]	*E3* 1.3(-2)	*M1* 1.8(-2)	*M2* 4.2(-2)	-	*M1*
1033.7	34 [31]	27.0	1.5(-2) [1.4(-2)]	*E3* 1.0(-2)	*M1* 1.3(-2)	*M2* 3.0(-2)	-	*M1*
1184.5	- [2.4]	1.75	- [1.6(-2)]	*E3* 7.8(-3)	*M1* 9.5(-3)	*M2* 2.2(-2)	-	*M2,M1*
1253.8	- [2.4]	10.6	- [2.7(-3)]	*E1* 1.4(-3)	*E2* 3.3(-3)	*E3* 7.0(-3)	*M1* 8.3(-3)	*E2*
1510.1	- [1.7]	1.12	- [1.8(-2)]	*M2* 1.2(-2)	*M3* 2.0(-2)	*M4* 3.2(-2)	-	*M3,M2*
1536.7	60[c] [12]	24.2	2.9(-2)[c] [5.8(-3)]	*E2* 2.3(-3)	*E3* 4.8(-3)	*M1* 4.9(-3)	*M2* 1.1(-2)	*M1,E3*
1847.6	- [2.5]	36.2	- [8.1(-4)]	*E1* 7.2(-4)	*E2* 1.8(-3)	*M1* 3.1(-3)	-	*E2,E1*
1893.3	- [3.6]	27.2	- [1.6(-3)]	*E1* 7.0(-4)	*E2* 1.7(-3)	*M1* 2.8(-3)	*E3* 3.2(-3)	*E2*

[a] Energies and relative γ-ray intensities from present study.

[b] Relative *K*-electron intensities without brackets from reference [No58]; relative *K*-electron intensities within brackets from reference [St60].

[c] Relative *K*-electron intensities from reference [Fr58].

[d] Values without brackets calculated from [No58] *K*-electron intensities; values within brackets calculated from [St60] *K*-electron intensities.

[e] The theoretical value for an *M4* [S165] was used to normalize the electron and γ-ray data.

[f] Theoretical interpolated α_K from graphs prepared from conversion coefficients given in [S165].

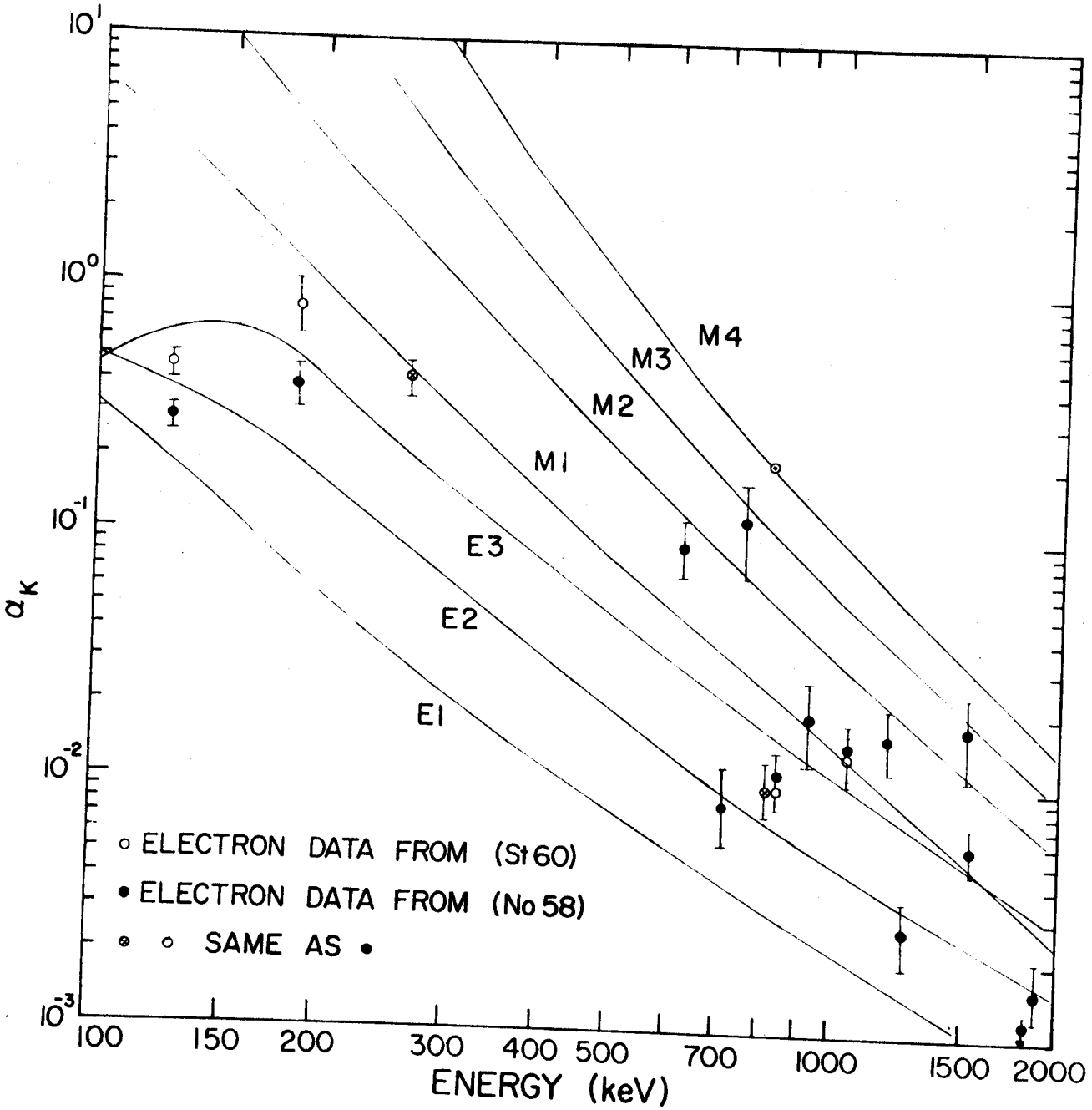

Fig. 35. Experimental conversion coefficients for some Pb^{203} transitions. The smooth curves of the theoretical α_K were prepared from tables in [S165].

al. [St60] by the method of external conversion to be 0.24±0.05. This should be compared with the theoretical value of 0.217 given by Sliv and Band [S165] for an $M4$ transition of this energy. This was the transition (and multipolarity) that was used to normalize to the electron and γ-ray data.

The 126.4-keV γ has been assigned an $E2$ by Novakov et al. [No58] on the basis of the measured $(L_1 + L_2)/L_3$ ratio. The L-subshell ratios given in [St60] also verify such an assignment. Finally, the 126.2-keV state has a $t_{\frac{1}{2}}$ of 75 ns [Be61] which is in good agreement with the single-particle transition half-life [Le67] for an $E2$ of this energy. The present data also confirm such an assignment.

Little need be said about the 186.4-keV transition. Both Novakov et al. [No58] and Stockendal [St60] reported an $M1$ multipolarity for the 186.4-keV transition based upon independent studies of conversion-electron ratios. However, Table 14 indicates an assignment of $M1$ or $E3$ on the basis of an α_K of 0.82 (from [No58] electron data) or 0.39 (from [St60] electron data). The theoretical values are 0.51 and 1.2 for an $E3$ and $M1$, respectively [S165]. Novakov's electron data appear to predict the $M1$ while Stockendal's data seem to suggest an $E3$ assignment. If the previous investigations [No58,St60] are correct in the $M1$ assignment, then it appears as if Novakov's electron data is more precise.

The 263.8-keV transition has previously been assigned $M1$

[No58] and $M1$ or $M2$ [Fr58] multipolarities. A third investigation [St60] calculated the α_K as 0.53±0.10 or 0.67±0.10 depending upon whether the interfering 169.8-keV Pb^{204} L line is of $M1$ or $E1$ character. The Pb^{204} 169.8-keV transition was shown to be $M1$ by the present study, thereby eliminating the 0.67±0.10 value. The remaining 0.53±0.10 value agrees very well with the theoretical value of 0.46 for an $M1$ of that energy. All these data corroborate an $M1$ assignment for the 263.8-keV transition.

The 381.3-keV transition had no electron data available, but the K-experimental conversion coefficient unambiguously suggests a multipolarity of $E2$ for this transition [St60].

The 820.2- and 847.0-keV transitions have been previously assigned $E2$ multipolarities on the basis of the measured K conversion coefficient and internal conversion ratios [St60]. The 820.2-keV transition assignment is clearly substantiated by the present study (cf. Table 14). In the 847.0-keV transition, however, a disparity between the [No58] and [St60] electron data results. The [No58] data suggest an $E2$ assignment, while the [St60] data appears to imply $E3$. Considering the previous results plus the present investigation, the $E2$ assignment appears much more reasonable. Once again the Novakov et al. data seem to be slightly better than the equivalent electron data of Stockendal [St60].

Finally, the 1033.8-keV transition K/L conversion ratio was remeasured by Stockendal [St60] and found to be consistent with the $M1$ assignment previously suggested by Novakov et al. [No58]. The present data also substantiate such an assignment (cf. Table 14).

3.2.6. Spin and Parity Assignments for Pb^{203}

As in section 3.1.6., I have used the experimental photon intensities for Bi^{203}, the calculated (or experimental) conversion coefficients of some Bi^{203} γ rays, the Bi^{203} decay energy, and the Bi^{203} $t_{\frac{1}{2}}$ to calculate the percent feedings and log ft's to each of the states in Pb^{203}. For those γ rays without reported multipolarities, I assumed each was an $M1$ multipole (for the purpose of calculating log ft's only). Using the modified DECAY SCHEME program, the feedings and log ft's to each state were calculated; these are found in the left-hand column of Table 15. The validity of such a list is seriously questioned by the well-defined spins of the 126.4- and 186.4-keV levels. The 1/2- and 3/2- assignments would suggest highly-forbidden β transitions with their resulting large log ft's.

A much more readily believed set of percent feedings and log ft's would result if the feedings to the 126.4- and 186.4-keV states were arbitrarily set to zero. This, not being unreasonable, (cf. section 3.1.6.) was done and the new set of values are found in the right-hand column of Table 15. This last set of values was used in establishing the external quantum numbers (i.e., spin and parity) of the levels in Pb^{203}.

3.2.6.A. Ground, 820.2-, and 825.2-keV States

The ground state has been assigned 5/2- by several former investigations [St60,No58,Do68]. This is also consistent with an odd nucleon (hole) in the $f_{5/2}$ shell-model orbit.

The 13/2+ assignment of the 825.2-keV state follows

Table 15. Percent feedings and log ft's for the excited states in Pb^{203}.

Excited state	Percent feeding[a]	Log ft[a]	Percent feeding[b]	Log ft[b]
126	1.87	8.68	0.0	large
186	2.28	8.58	0.0	large
820	6.13	7.94	6.39	7.92
825	14.8	7.56	15.4	7.54
866	1.50	8.53	1.57	8.51
896	3.63	8.14	3.79	8.12
1033	0.0	large	0.0	large
1160	3.88	8.00	4.05	7.98
1547	4.10	7.78	4.28	7.76
1641	1.00	8.34	1.05	8.32
1802	1.51	8.06	1.58	8.04
2033	0.38	8.49	0.40	8.47
2184	0.0	large	0.0	large
2387	0.88	7.78	0.91	7.76
2568	2.86	7.02	2.99	7.00
2620	1.14	7.33	1.19	7.31
2667	18.1	6.04	18.9	6.02
2713	21.0	5.88	21.9	5.86
2748	1.38	6.99	1.44	6.97
2753	8.13	6.20	8.48	6.18
2793	1.26	6.91	1.32	6.89
2821	0.94	6.96	0.98	6.94
2964	0.24	6.95	0.25	6.93
3016	0.95	5.97	0.99	5.95
3045	2.01	5.32	2.10	5.31

[a]Calculated values from relative beta intensities as determined from transitions populating and depopulating each state in Figure 31.

[b]Corrected values after the relative beta intensities to the 126.4- and 186.4-keV states were arbitrarily set to zero.

directly from the $M4$ character of the 825.2-keV γ. This assignment is consistent with the assignments in references [St60 and No58]. Indeed, this was the transition and multipolarity used to normalize the electron and γ-ray data in section 3.2.5. The log ft of 7.5 is hardly large enough for a first-forbidden unique transition. Considering the difficulty of finding the γ's populating the isomeric state, this is not horribly surprising.

The 9/2- assignment of the 820.2-keV level was firmly fixed by the study of Pb^{203m} by Doebler et al. [Do68]. The $E2$ character of the 820.2-keV transition quite clearly suggests 9/2- through 1/2- assignments. The discovery of a 5.0-keV transition in Pb^{203m} [Do68] suggests that the 1/2- through 7/2- can be eliminated. The 633.8-keV transition between the 820.2-keV and 186.4-keV levels (cf. Figure 31) must then be an $M3$, which, being highly converted, makes it surprising that the previous conversion-electron studies did not report such a transition.

3.2.6.B. 126.4- and 186.4-keV States

The 60.0-, 126.4-, and 186.4-keV γ's have $M1$, $E2$, and $M1$ multipolarities, respectively. The $E2$ 126.4-keV transition suggests 1/2- to 7/2- for the 126.4-keV state. The $M1$ 186.4-keV transition suggests 3/2- to 7/2- for the 186.4-keV state. The large log ft's for these states probably rules out the 7/2- assignment. The $M1$ 60.0-keV transition from the 5/2-, 3/2- 186.4-keV state would suggest 1/2- to 5/2- for the 126.4-keV state. Comparing the low-lying Pb^{203} excited states to those in Pb^{205} and to the shell-model level scheme in this region (cf. Chapter IV), it becomes apparent that the assignment for the 126.4- and 186.4-keV states

should be 1/2- and 3/2-, respectively. These are the same assignments proposed by Novakov et al. [No58]. In addition, if the assignment were other than I have suggested, then one might expect to see more transitions to these states from the high-spin high-lying states in Pb^{203}.

3.2.6.C. 866.5-keV State

No multipolarity data on any transitions to or from the 866.5-keV state are known. The state, however, does populate both the 1/2- 126.4-keV level and the 5/2- ground state. Assuming the transitions to be predominantly *M*1, *E*1, or *E*2, this would appear to suggest an assignment of $1/2^{\pm}$, $3/2^{\pm}$, $5/2^{\pm}$, or $7/2^{\pm}$. The large log *ft* of 8.5 possibly suggests an allowed or first-forbidden transition and the resulting $7/2^{\pm}$, $9/2^{\pm}$, or $11/2^{\pm}$ assignment. However, the intensity balance does not appear to be very good. This might mean that the log *ft* should actually be larger than it appears to be. These data lead me to possible assignments of $5/2^{\pm}$ or $7/2^{\pm}$. If the 866.5-keV state were 7/2-, then the depopulating transitions would be *M*1 and *M*3 (for the 866.6- and 739.9-keV γ's, respectively); for 7/2+ they would be *E*1 and *E*3; and for 5/2+ they would have to be *E*1 and *M*2, respectively. Branching ratios for these possibilities do not correspond to what is found experimentally. The only reasonable assignment is 5/2-. This would require multipolarities of *M*1 and *E*2 for the 866.6- and 739.9-keV transitions, respectively. The branching ratio is consistent if one allows for collective enhancement of the *E*2. As a result, I assign the state at 866.5-keV a spin and parity of 5/2-.

3.2.6.D. 1033.6-keV State

The state at 1033.6-keV has been previously assigned as

7/2- or 5/2- [No58]. Table 14 indicates that the 1033.7-keV γ is an *M*1 transition, thereby suggesting states of 3/2-, 5/2-, or 7/2-. The 847.0-keV γ is an *E*2 multipole and subsequently suggests an assignment of 1/2- through 7/2-. The log *ft* is arbitrarily large and suggests a highly forbidden transition. As only ≈80% of the Bi^{203} γ-ray intensity has been placed, the log *ft* value could easily be suspected. From the multipolarity data alone I suggest the 1033.6-keV state is 7/2-, with 5/2- still a possibility.

3.2.6.E. 896.9- and 1160.8-keV States

Only the strong 896.9-keV transition was found to depopulate the 896.9-keV state. Sadly, no multipolarity data are available for this transition, i.e., no electron data have been reported. The 8.1 log *ft* suggests an allowed or first-forbidden transition. These support an assignment of 7/2±, 9/2±, or 11/2±. 11/2± can almost certainly be ruled out if the 896.9-keV γ can be assumed to be *M*2, *M*1, *M*2, or *M*1. While I am tempted to reduce this to only the + parity assignments, to do so is uncertain and even dishonest. Because no population of the 1/2- 126.4- or 3/2- 186.4-keV states is found, I think that I can safely assign 7/2± or 9/2± to the 896.9-keV state. If 9/2+ were a valid assignment, one might expect to see a transition to the 13/2+ state (which one does not). However, allowing for complex internal rearrangements, one cannot fully disregard such an assignment.

The 1160.8-keV state assignments are based upon an *M*1 263.8-keV γ to the relatively poorly assigned 7/2±, 9/2± 896.9-keV state. This obviously allows 5/2±, 7/2±, 9/2±, and 11/2±. However,

it is populated by strong transitions from higher-lying states which have - parity based upon their log ft's. While not an absolute test, this appears to suggest that the 1160.8-keV state is of negative parity although one cannot be absolutely certain. The log ft of 8.0 suggests, then, an allowed or first-forbidden transition or 7/2±, 9/2±, or 11/2±. The final assignment for these states is 7/2± or 9/2±.

3.2.6.F. 1547.6- and 1641.6-keV States

These levels are included under a single heading because their only depopulating transitions are to the 825.2-keV isomeric state. The 1547.6-keV state has a single depopulating transition of 722.4 keV which has been determined (section 3.2.5.) to be either $E2$ or $E3$, depending upon which set of electron data one is willing to believe. These assignments would suggest 7/2-, 9/2±, 11/2±, 13/2±, 15/2±, 17/2±, or 19/2-. The log ft of 7.8 would appear to suggest an allowed or first-forbidden transition and values of 7/2±, 9/2±, or 11/2±. Coupling these choices one is left with 7/2-, 9/2±, or 11/2±. Having decidedly more confidence in the Stockendal [St60] electron data (on the basis of previous results) than in Fritsch's electron data [Fr56], I further reduce this assignment to 9/2+ or 11/2+. 7/2- can also be tentatively eliminated as no transition to the ground state is seen. If the 722.4-keV transition is a true $E2$ multipole and not just an $M1$ with a large admixture of collectively enhanced $E2$, then the assignment would be necessarily 9/2+. Uncertain of this, I leave the assignment as 9/2+ (11/2+).

The 816.4-keV γ depopulating the 1641.6-keV state has no assigned multipolarity. The log ft of 8.3 might suggest an assign-

ment of 7/2±, 9/2±, or 11/2±. This state does not populate any of the well-defined lower excited states, but this would simply suggest that $I\pi$ is ≥11/2±. Owing to the undoubtly complex internal structure of many of these high-lying states, this is not really a good test for spin and parity assignments. Therefore, I shall leave well enough alone and retain an assignment of 7/2±, 9/2±, or 11/2± for the 1641.6-keV state.

3.2.6.G. 1802.4- and 2033.8-keV States

The 1802.4-keV state has three depopulating γ transitions, to the 7/2- (5/2-) 1033.6-keV state, to the 7/2- 866.5-keV state, and to the 5/2- ground state. These would (weakly) suggest an assignment of 1/2- to 9/2-. No multipolarity data exist for any of these transitions. The 8.0 log ft is apparently allowed or first-forbidden. This allows an assignment of 7/2±, 9/2±, or 11/2±. The - parity states cannot be absolutely excluded so I suggest the 1802.4-keV state is (in order of preference) 7/2-, 9/2-(7/2+, 9/2+).

The 2033.8-keV state has transitions to the 7/2- (5/2-) 1033.6-keV state and to the nebulous 1641.6-keV state. The log ft of 8.5 appears to imply an allowed or first-forbidden β transition, once again this suggests 7/2±, 9/2±, or 11/2±. The γ transitions from this state tell me next to nothing, and any conjecture as to the nature of their multipolarities is certainly to be extremely tentative. Pessimistically, then, the assignment of the 2033.8-keV state is left as 7/2±, 9/2±, or 11/2±.

3.2.6.H. 2184.0- and 2387.8-keV States

The 381.3-keV γ, which depopulates the 2184.0-keV state, has been calculated to be *E*2. This implies an assignment of 3/2± through 13/2+. The arbitrarily large log *ft* reveals nothing. The only remaining depopulating transition is the 542.9-keV γ to the poorly defined 1641.6-keV level. The 569.4-keV γ feeds the 2184.0-keV state from the 7/2-, 9/2- 2753.4-keV state (cf. section 3.2.6.M.). These data do not appear to be very conclusive, so the 2184.0-keV state is left as 3/2+ to 13/2±.

The 2387.8-keV state is assigned 7/2±, 9/2±, or 11/2± primarily on the basis of the log *ft* of 7.8 (allowed or first-forbidden transitions). The single depopulating transition goes to the 9/2+ (11/2+) 1547.6-keV state, but this does not tell a great deal.

3.2.6.I. 2568.9-keV State

The log *ft* of 7.0 could suggest an allowed or first-forbidden transition. This would mean a spin and parity of 7/2±, 9/2±, or 11/2±. However, the two depopulating transitions are to positive parity states, and this would lead me to suggest that the transitions are *M*1, *E*1, *E*2, when coupled with the reasonably low log *ft*. The 7/2±, 9/2±, or 11/2± assignment is entirely consistent with such transitions. Nothing more can be said with much confidence about this state.

3.2.6.J. 2620.5- and 2748.7-keV States

The 1800.3-keV transition to the 9/2- 820.2-keV state is the only γ associated with the 2620.5-keV level. The log *ft* of 7.3

suggests an allowed β transition (or possibly first-forbidden). Unfortunately, this tells very little about the character of the 2620.5-keV state. The assignment must be left deliberately ambiguous, as 7/2±, 9/2±, or 11/2±.

The same arguments hold true of the 2748.7-keV state with the substitution of "1928.5-keV" for the "1800.3-keV".

3.2.6.K. 2667.8-keV State

Of the six depopulating transitions of this state, only the 1847.6-keV γ has been assigned a multipolarity (*E*2 or *E*1). The *E*1 appears to be correct although *E*2 cannot be absolutely excluded. This suggests (the transition is feeding the 9/2- 820.2-keV level) an assignment of 7/2+, 9/2+, or 11/2+ (or possibly 5/2-, 7/2-, 9/2-, 11/2-, or 13/2-). The log *ft* of 6.02, however, clearly suggests an allowed transition. (But note that Alburger and Pryce [A154] have suggested that in such a heavy nucleus allowed and first-forbidden transitions whould compete favorably.) On this basis and the realization that log *ft*'s are not as sensitive a test as one might like to suppose, I propose an assignment of 7/2-, 9/2-, or 11/2-. The reasonably strong 2667.8-keV γ to the ground state (5/2-) also might suggest the 7/2- and 9/2- as the most likely assignments. The remainder of the depopulating transitions go to states which have assignments that are consistent with this assignment. Consequently, I assign 7/2-, 9/2- to the 2667.8-keV state.

3.2.6.L. 2713.4-keV State

While five depopulating transitions are known for this

state, only one (the 1893.3-keV γ) has an experimental multipolarity assignment. If the 1893.3-keV γ is a pure $E2$ as Table 14 appears to indicate, then, the spin and parity of the 2713.4-keV state is limited to 5/2- through 13/2-. The log ft of 5.9 almost conclusively labels it as an allowed transition, suggesting 7/2-, 9/2-, or 11/2- assignments. Unfortunately, no other data are available so the assignment must remain as 7/2-, 9/2-, or 11/2.

3.2.6.M. 2753.4-keV State

The 6.2 log ft suggests 7/2-, 9/2-, or 11/2- for an allowed transition. Six depopulating transitions would normally establish the assignment of a level quite securely - if only the multipolarities were known. The strongest depopulating transitions populate the 7/2- (5/2-) 1033.6-keV state and the 5/2- ground state, respectively. This would appear to limit the spin and parity to ≤9/2- The remaining depopulating transitions go to levels that are too poorly defined to be of much value to the present assignment. Consequently, the 2753.4-keV state is assigned 7/2- or 9/2-.

3.2.6.N. 2793.7-keV State

The 406.1-keV transition to the 2387.8-keV state (7/2±, 9/2±, 11/2±), and the 1245.9-keV γ to the 1547.6-keV state (9/2+, 11/2+), certainly tell little about this state. The 6.9 log ft suggests an allowed transition, although first-forbidden cannot be strictly ruled out. At best, the assignment can be reduced to 7/2±, 9/2±, or 11/2±.

3.2.6.0. 2821.1-, 2964.4-, and 3016.9-keV States

Each of these states was placed on the basis of a single transition, well established through coincidence data. The states at 2821.1- and 2964.4-keV are depopulated by 2000.9- and 2144.2-keV γ's, respectively, to the 9/2- 820.2-keV state. The log ft's are 6.9 for each state. This would suggest either an allowed or first-forbidden transition, thereby suggesting an assignment of 7/2±, 9/2±, 11/2± for both states. The transition to the 9/2- 820.2-keV state adds no further information, as these transitions could easily be $E1$ or $M1$. However, it would be tempting to assume $M1$ multipolarities, which would limit the assignments to 7/2-, 9/2-, 11/2-. One might also be tempted to rule out 7/2- and 9/2- on the argument that no transitions from these states feed the 7/2- (5/2-) 1033.6-keV state. In lieu of the undoubtedly complex structure of these states, it might be reasoned that complex internal rearrangements hinder such possible transitions. To be entirely honest, I do not feel justified in reducing the assignment in this manner, so I conservatively leave the assignment of the 2821.1- and 2964.4-keV states at 7/2±, 9/2±, or 11/2±.

The state at 3016.9 keV has a single transition; it feeds the 1033.6-keV 7/2- (5/2-) state. This suggests 3/2±, 5/2±, 7/2±, 9/2±, and 11/2±, not very helpful to be sure. The log ft of 6.0 would most probably limit the assignment to allowed transitions, or a state having 7/2-, 9/2-, or 11/2-. No additional information is available, so I cannot reduce the assignment further.

3.2.6.P. 3045.2-keV State

The 3045.2-keV state has two depopulating transitions, one to a 820.2-keV state and a second to the 1033.6-keV state. The intensity ratio is 0.41/5.5. This would seem to suggest that the 3045.2-keV state should have an assignment of 5/2±, 7/2±, 9/2±, or 11/2±. The low log ft of 5.3 almost certainly rules out the positive parity states. The low log ft also would rule out the 5/2- state. The consistent assignment would therefore appear to be 7/2-, 9/2- or 11/2-.

3.2.6.Q. Comments

This last section on spin and parity assignments necessarily concludes the Bi^{203} experimental sections. The theoretical or semi-theoretical discussion of the meaning (or "so what") of the Pb^{203} level scheme is left to a later chapter (Chapter IV). The remaining comments on the Pb^{203} investigation are identical to those found in the last section on the Pb^{204} experimental results; and rather than repeat them here one should refer to section 3.1.6.V. for the appropriate details.

CHAPTER IV

DISCUSSION OF RESULTS

As I implied in the introduction to Chapter I, one of the fundamental functions of experimental nuclear and particle science is to provide a detailed test of the current nuclear models. Perhaps, I might even be naive enough to hope that the present study would significantly contribute to the formulation of a new, more sophisticated, more comprehensive nuclear model. The experimental chapter (Chapter III) has already described the "wealth" of information uncovered by the present investigation. It is frightfully tempting, then, simply to close this thesis with an impressive comparison of the present data with the previously reported results - and, with a flourish, quit. If anyone has had the stamina and fortitude to "wade" through Chapter III, he certainly does not deserve such a fate. Such a closing would also leave the inquisitive reader with the anticipated reply of "so what". The content of this chapter is designed to tie the loose ends together, and to attempt some, albeit simple, explanation of the Bi^{203} and Bi^{204} decays in terms of the current nuclear models. In section 4.1. a deliberately cursory comparison with the previously reported results is presented. The shell-model discussions are found in section 4.2. Section 4.2.1. discusses the nuclear shell-model level spacings near Z=82 and N=126 in the Pb isotopes. Sections 4.2.2. and 4.2.3. also deal with the Pb^{203} and Pb^{204} level schemes,

respectively, in terms of the current models and previously performed calculations. Section 4.3. is what might be called the Grand Finale, i.e., a final summary of the topics covered in this thesis, and a few proposals for future investigations.

4.1. Comparison With Other Investigations

4.1.1. Pb^{204} Experimental Data

The two previous major investigations [St58,Fr58] of the Bi^{204} ε decay utilized high-resolution permanent-magnet conversion-electron spectrometers. Excellent transition energies in the low energy region (<1.0 MeV) were obtained and are in good agreement with the present values. Rather than list all 67 previously reported transitions, I would refer the reader to reference [Nu65] which includes a compilation of the results from both of these investigations. The electron data (i.e., K and L relative electron intensities) for these transitions can also be found in Table 10. Only the 78.6-, 90.9-, 92.2-, and 368.0-keV transitions previously reported were not found in the present study, though many more were added (some 143). Also, inasmuch as the tentative decay scheme proposed by Stockendal et al. [St58] was based almost entirely upon energy sums, little can be gained by a detailed comparison with the decay scheme proposed in the study. The changes (and primarily the additions) made in this decay scheme by the present study have already been discussed (section 3.1.4.) and will not be rehashed here. Rather tragically though (fortunately for me however), this will be the first reported investigation of the Bi^{204} γ rays specifically, and no data exist for this comparison.

It is rather interesting, however, to compare the results of recently reported scattering data with the present results. Holland et al. [Ho69] have investigated the $Pb^{206}(p,t)Pb^{204}$ reaction

and reported 15 excited states. These are tabulated in Table 16 (cf. Figure 23). Also, tabulated in Table 16 are the states revealed in the Bi^{204} ε decay which apparently are equivalent in energy to the (p,t) data. Quite remarkable agreement is evident. One other investigation [Re67] has reported data on the same reaction. The resolution was significantly poorer and very few states were reported - none of additional significance. A third group [Bj67] has reported performing a $Pb^{204}(d,d')Pb^{204}$ reaction. The results of their investigation are also included in Table 16. It is rather intriguing to note that they report a new state at 1.353 MeV. In neither (p,t) study nor the present ε decay study has this state been seen. A reinvestigation of the (d,d') reaction might well be in order - hopefully, to confirm such a state. At present DWBA calculations are being performed [Ho69] to determine the spins (and parities) of some of these states accurately. It should be quite rewarding and exciting to learn of their results, as a more detailed comparison with the states revealed by the decay of Bi^{204} should then be possible.

4.1.2. Pb^{203} Experimental Results

The several investigations of Bi^{203} already discussed [No58,Fr58,St60] have revealed a wealth of information about the Pb^{203} excited states, their associated transitions, the spins and parities of these excited states, and some about the multipolarities of a few of the Pb^{203} transitions. For an excellent summary of the previous Bi^{203} data one should consult reference [Nu65]. The previously proposed decay scheme and the multipolarity data have already been compared earlier and will not be repeated (cf. section 3.2.5.). Rather

Table 16. Comparison of Pb^{204} excited states revealed by scattering reactions with those of present study.

E_{scatt} (MeV)[a]	E_{scatt} (MeV)[b]	E_{scatt} (MeV)[c]	E_{ε} (MeV)[d]
0.0	0.0	0.0	0.0
0.899	0.90	0.90	0.899
1.274	1.27	1.27	1.274
-	-	1.353	-
1.569	1.56	1.5	1.563
1.663	-	-	1.720[e] + 1.727[e]
1.824	-	-	1.817
1.932	-	-	1.936
2.173	-	-	2.185
2.267	2.2	2.268	2.258
2.482	-	-	2.480 + 2.506
2.642	-	2.630	-
2.831	2.8	-	-
2.898	-	-	2.912[e] + 2.920 + 2.928
3.139	-	-	3.170
3.246	-	-	3.232
3.461	-	-	3.461[e]

[a]Energies from $Pb^{206}(p,t)Pb^{204}$ reaction [Ho69]. The reported energy error was ±25 keV.

Table 16. (continued)

[b]Energies from $Pb^{206}(p,t)Pb^{204}$ reaction [Re67].

[c]Energies from $Pb^{204}(d,d')Pb^{204}$ reaction [Bj67].

[d]Energies of Pb^{204} excited states revealed by ε decay of Bi^{204} (present study).

[e]Excited states suggested, but not confirmed, in the secondary Pb^{204} level scheme (Figure 25).

sadly, only one scattering reaction producing Pb^{203} has been reported. Bjerregaard et al. [Bj67] have investigated the $Pb^{204}(p,d)Pb^{203}$ reaction. Their results are tabulated in Table 17. Also tabulated are the states revealed by the present study which most likely correspond to their reported states. While not extensive, quite close agreement is evident. DWBA calculations were attempted, but inconclusive results were reported with no new spin assignments being made.

The comments made in sections 4.1.1. and 4.1.2. seem to be rather perfunctory but enlightening - and so they are. I would like to think that this is not necessarily the fault of the author. Instead, it points up the fact that comparatively little was actually known about the $Pb^{203,204}$ excited states and related γ-ray transitions, and precisely for this reason was the present investigation undertaken.

Table 17. Comparison of $Pb^{204}(d,t)Pb^{203}$ scattering data to the present study.

E_{scatt} (MeV)[a]	E_{ε} (MeV)[b]
0.0	0.0
0.12	0.126
0.19	0.186
0.82	0.820 + 0.825
1.03	1.034
1.56	1.547
2.25	-
2.77	2.748 + 2.753

[a] Taken from reference [Bj67]. Energies have reported error limits of ±0.02 MeV.

[b] Energies from ε decay scheme proposed in the present study.

4.2. Shell-Model Characteristics of the Pb^{204} and Pb^{203} Level Schemes

While neither extensive nor intensive, a cursory treatment of the shell-model calculations on the $Pb^{207,206,205}$ isotopes has already been presented in the Introduction (Chapter I). In short, these calculations have used the experimental single-hole energies of Pb^{207} plus various residual interaction potentials (i.e., nucleon-nucleon interactions) and configuration mixing to calculate the theoretical energy levels in several Pb nuclei near Pb^{208}. For Pb^{206} quite excellent agreement was obtained, but for Pb^{205} the calculations have already become considerably more sensitive in the theoretical evaluation and the results are comparatively lousy. Perhaps, the present re-investigations of Pb^{205} [Ko70], Pb^{204}, and Pb^{203} at MSU will rekindle serious theoretical interest in these Pb isotopes and lead to their re-examination in light of the current nuclear models.

Having nearly completed the experimental investigations of Pb^{204} and Pb^{203}, I soon began to consider the characteristics of the $Pb^{204,203}$ level schemes in terms of the several nuclear models of interest (the shell model, the collective vibrational model, and the quasi-particle model). With trepidation and yet a certain boldness, an attempt was made to "analyze" the results of Chapter III. After several unsuccessful bouts with the shell and collective models, it gradually became apparent that these decays are quite unwilling to yield their information so easily. This meant that the present discussion is considerably less detailed than originally hoped. However, it is hopeful that the present experimental investigation and brief theo-

retical presentation will lay a new foundation and, perhaps, suggest a few guidelines for a reconsideration of the fundamental structure of these isotopes.

As Pb^{204} was the first to be experimentally investigated, "equal time" requires that the Pb^{203} level scheme be discussed first. Actually, the reason for taking Pb^{203} first is not nearly so naive. While more work of a theoretical nature has been done on Pb^{204}, Pb^{203} appears to be far simpler and, therefore, more easily described. Once Pb^{203} is completed, the more difficult Pb^{204} level scheme will be undertaken.

4.2.1. Nuclear Level Spacings in the Pb Region near $Pb^{203,204}$

Previous theoretical studies have shown that it is possible to explain some of the experimental information in the Pb isotopes by using either pure shell-model calculations or by modifying them by the inclusion of collective-motion terms. It is fairly evident, though, that because of the hole-hole residual interactions and the configuration mixing as well as other difficulties, shell-model calculations advanced by Kisslinger and Sorensen [Ki60] appears to avoid some of these difficulties (details will be discussed in section 4.2.3.), and are more easily handled from a strictly qualitative viewpoint. For the most part, the present discussion will be confined to a discussion of the decay characteristics in terms of the shell and collective models.

In attempting to assign the shell-model configurations in these nuclei, one first must know the nuclear level spacings of the shell orbits. The spacing of the ground and first two excited states

in the adjacent odd-mass Tl isotopes gives one some idea of the single-proton configurations near the Z=82 closed shell. Figure 36 shows the ground and first two excited states in the odd-mass Tl isotopes. The spins of 1/2+, 3/2+, and 5/2+, respectively, are consistent with the shell-model assignments, $s_{1/2}$, $d_{3/2}$, and $d_{5/2}$. The two states immediately above the Z=82 closed shell are the $h_{9/2}$ and $f_{7/2}$ orbitals; this can be determined from the ground and first excited states in Bi^{209}, which has a single unpaired proton outside the Z=82 closed shell.

For neutron numbers just below the N=126 closed shell, the odd neutron (in Pb^{203}) can populate the $f_{5/2}$, $p_{1/2}$, $p_{3/2}$, $i_{13/2}$, $f_{7/2}$, or $h_{9/2}$ orbits in the ground or low-lying states. The large pairing energy of the $i_{13/2}$ orbit forces neutrons to fill it in pairs and not by odd particles (perhaps the reason why no $i_{13/2}$ ground states have yet been observed). Examining the systematics of the better-known odd-mass isotopes having a closed Z=82 shell and an unpaired neutron, one can get some idea of the ordering of the shell-model orbits in this region. These systmatics (Figure 37) indicate that most probably the neutron states (i.e., holes) are, in order of increasing energy, $f_{5/2}$, $p_{3/2}$, and $p_{1/2}$. Figure 38 shows a compilation of the experimental and theoretical data for the $f_{5/2}$, $p_{3/2}$, and $p_{1/2}$ neutron level spacings in the lead region [Be61]. The quasi-particle calculations of Kisslinger and Sorensen for Pb^{203} appear (Figure 38) to predict an order of $f_{5/2}$, $p_{3/2}$, and $p_{1/2}$. However, it is apparent from Figures 37 and 38 that the spacing between the $p_{1/2}$ and $p_{3/2}$ is probably small in Pb^{203}, as the qualitative quasi-particle calculations indicate an inversion of these orbitals quite near Pb^{203}. As experimental systematics are,

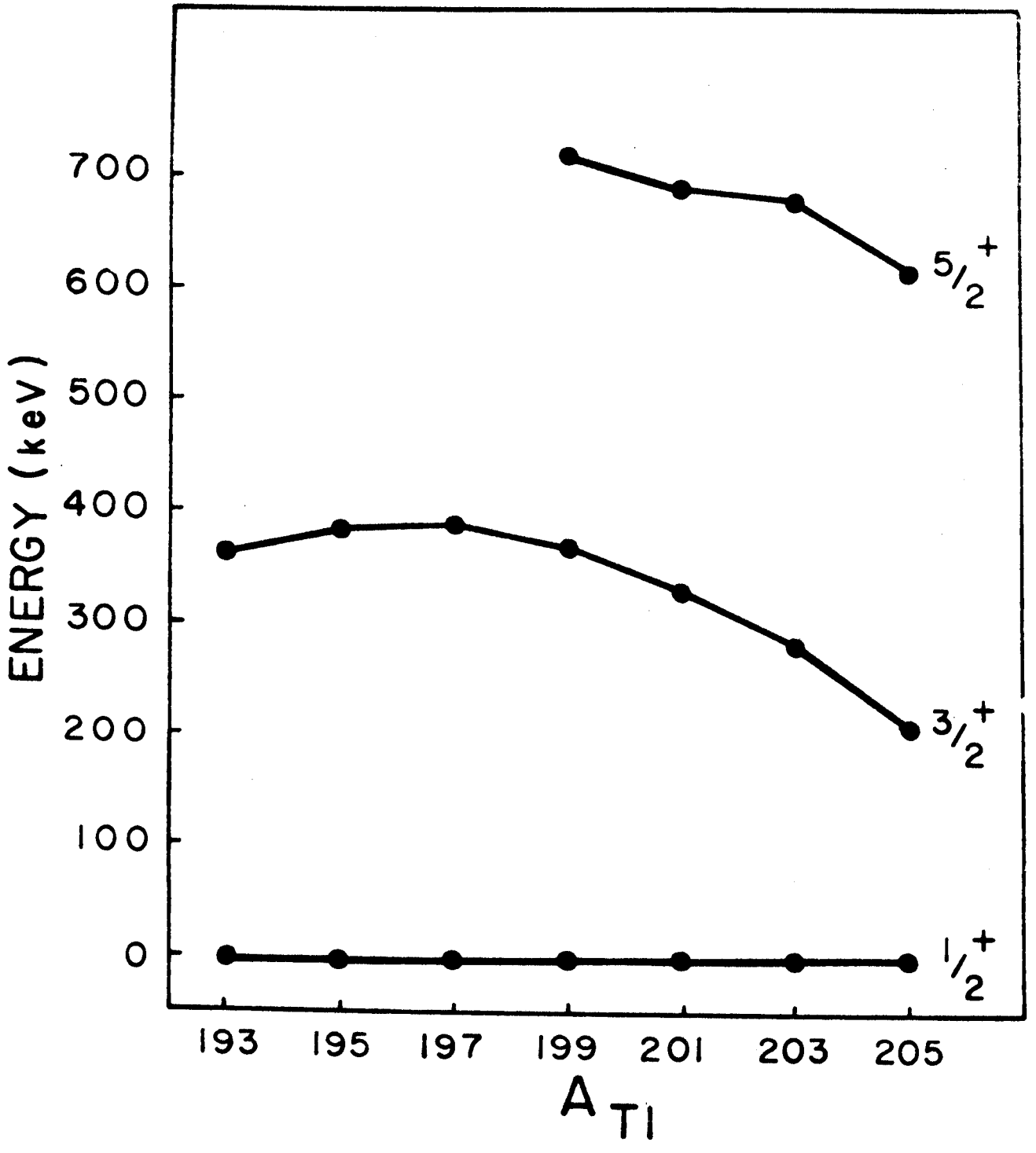

Fig. 36. Systematics of the low-lying 1/2+, 3/2+, and 5/2+ states in odd-mass Tl isotopes. These should be relatively pure $s_{1/2}$, $d_{3/2}$, and $d_{5/2}$ shell-model states [Do70a].

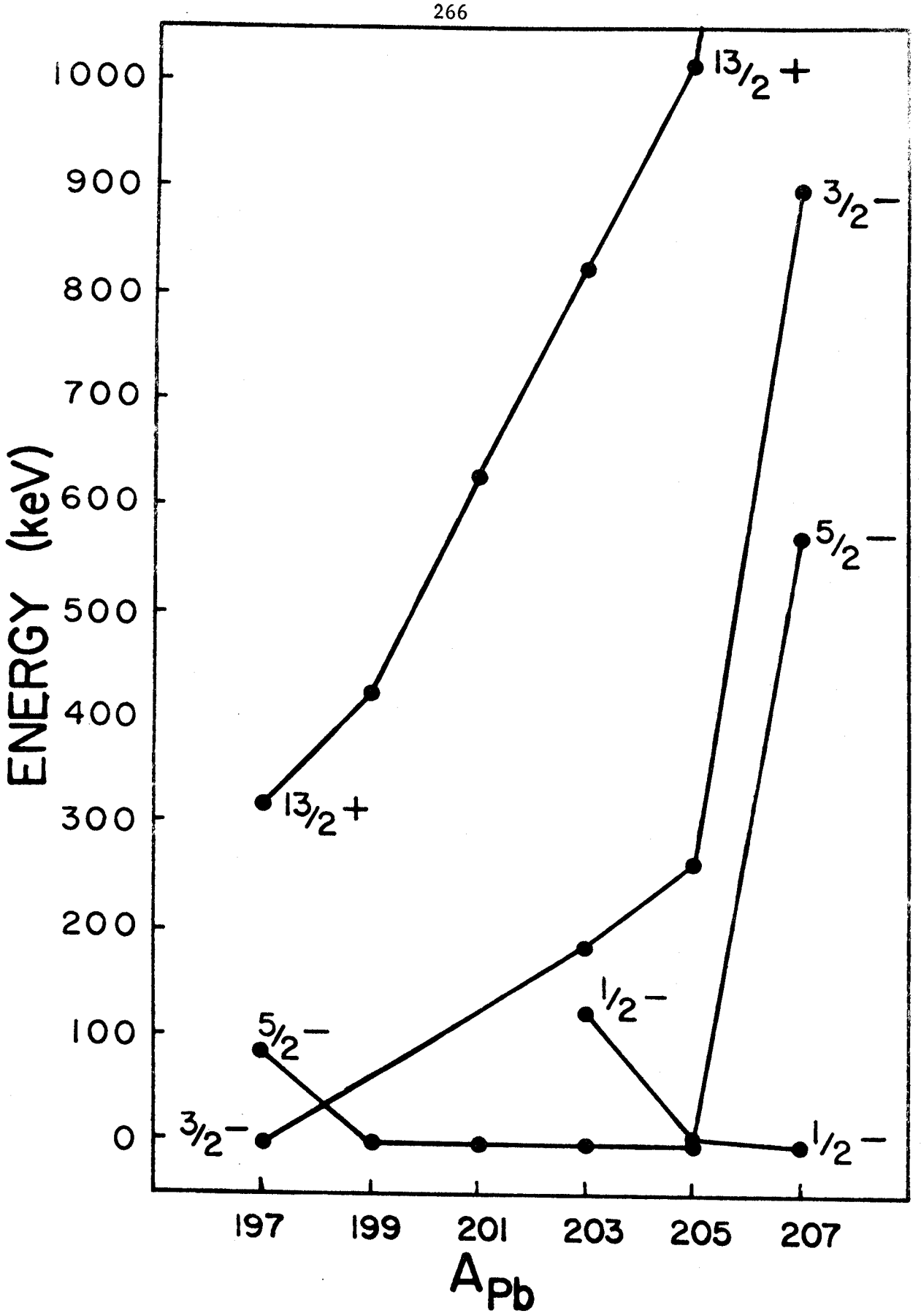

Fig. 37. Systematics of the $f_{5/2}$, $p_{1/2}$, $p_{3/2}$, and $i_{13/2}$ states in the odd-mass neutron-deficient Pb isotopes [Do70a].

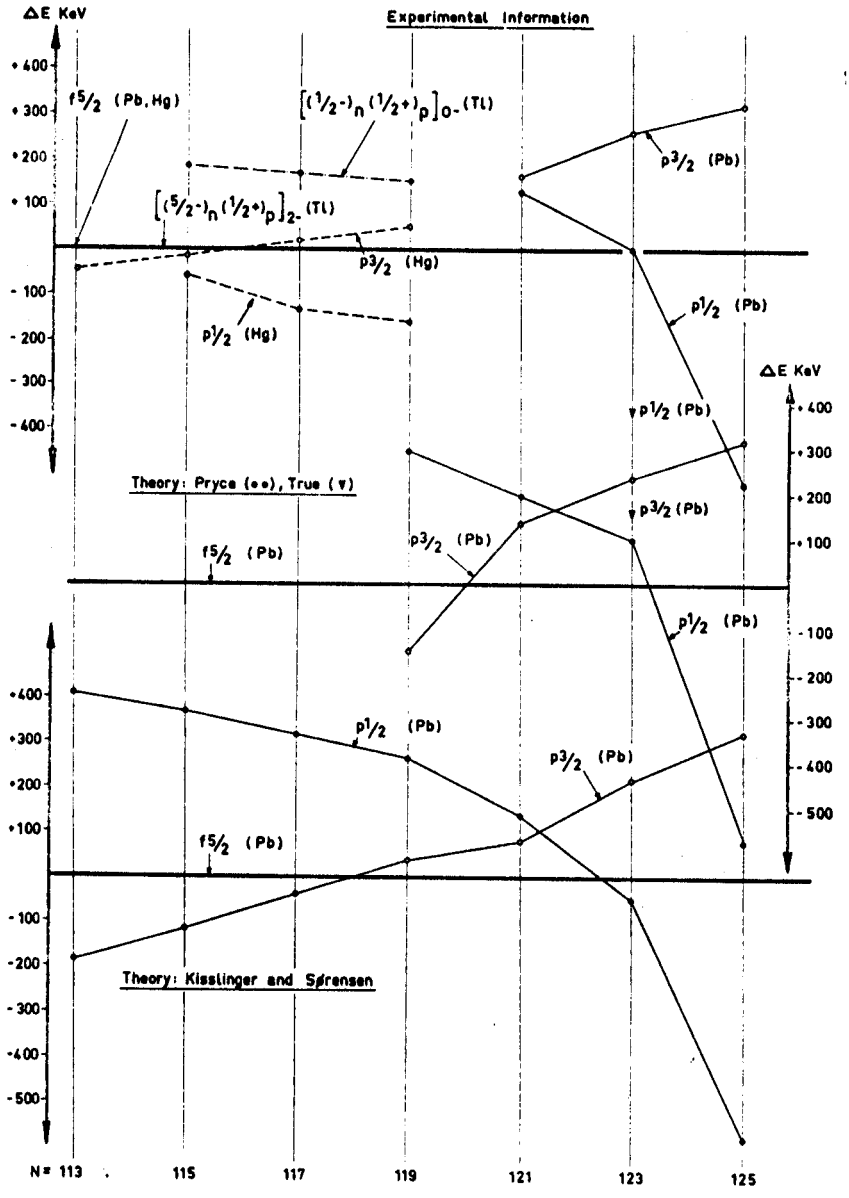

Fig. 38. Compilation of experimental and theoretical data for the $f_{5/2}$, $p_{3/2}$, and $p_{1/2}$ neutron level spacings in the lead region [Be61].

no doubt, more reliable in this case than the semi-qualitative theoretical calculations, the ordering is taken as $f_{5/2}$, $p_{1/2}$, $p_{3/2}$ for neutrons immediately below the N=126 closed shell.

The neutron orbits above the N=126 closed shell can be found by considering the low-lying states in Pb^{209}. These indicate that the level ordering should be, in order of increasing energy, $g_{9/2}$, $i_{11/2}$, and $j_{15/2}$. The energy spacings are also large enough that these levels should not have crossed upon reaching Pb^{203}. Figure 39 illustrates the nuclear shell-model orbits near the Z=82 and N=126 which will be used in the subsequent discussions. The $i_{13/2}$, $f_{7/2}$, and $h_{9/2}$ orbits are included in the same order as in Pb^{207}.

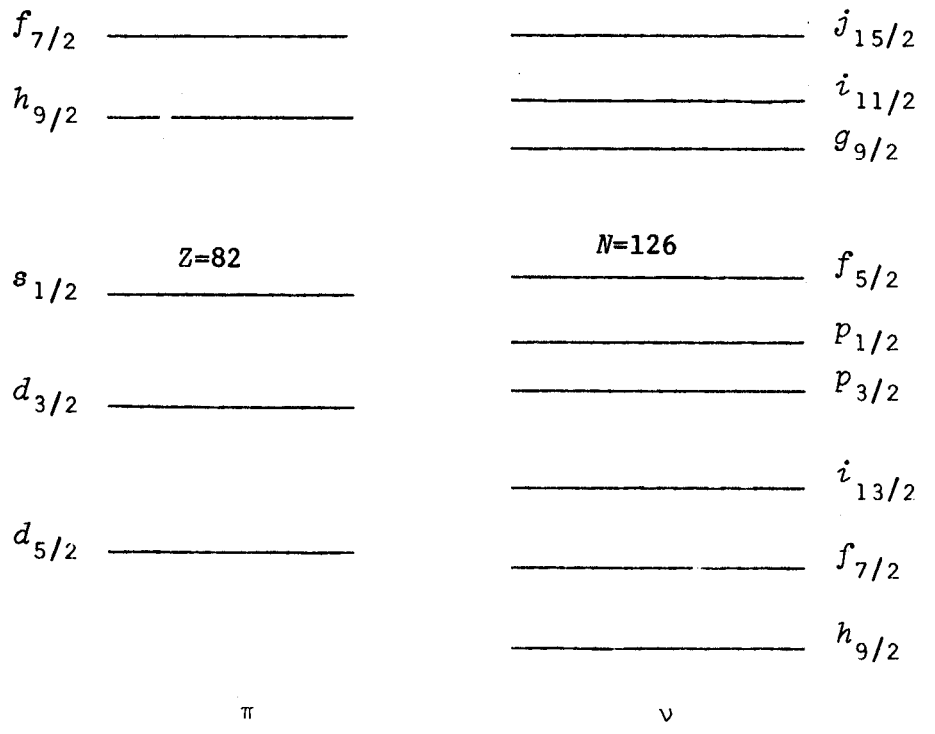

Fig. 39. Shell-model orbitals near N=121 and Z=82.

4.2.2. Discussion of Pb^{203} Results

Having at least qualitatively determined the level spacings in Pb^{203}, I can finally return to the original purpose of this chapter - an evaluation of the shell-model characteristics of the Bi^{203} ε decay. This section has two subdivisions, but they are not necessarily to be considered mutually exclusive. The second section concerns the characteristics of the β transitions to the Pb^{203} excited states, while the first deals with some possible configurations of a few low-lying Pb^{203} excited states. Because the two descriptions are not exclusively independent some cross-referencing may be necessary, but this should not prove too confusing.

4.2.2.A. Pb^{203} Excited States - Shell-Model States

The order of the neutron orbits has already been established (section 4.2.1.). Before charging into a description of the shell-model states, consider the question which invariably arises concerning the collective and/or core-coupled states. The position of the first 2+ quadrupole vibration state in the adjacent (to Pb^{203}) nuclei are experimentally known: Pb^{202}, at 961.4 keV [Mc57], and Pb^{204}, at 899.2 keV [Fr58,St60,Cr70a]. The energy range of states in Pb^{203} certainly does not preclude such vibrational characteristics, but it has been suggested [Hy64] that these isotopes should be considered as predominantly multi-particle states, with only minor overtones of collective vibrational states. This appears to be confirmed by the lack of $E2$ admixtures in the $M1$ transitions, as is borne out by Figures 26 (Bi^{204}) and 35 (Bi^{203}). For this reason I will not consider collective effects extensively but only briefly touch on them.

In all of the following remarks it must be recalled that only a few of the states of the nucleus are being discussed, and to be entirely correct the collective modes and configuration interactions with all possible states should be included. As a result, these comments should be considered as only tentative - but (optimistically) thought provoking.

In attempting to assign shell-model configurations in this even-odd nucleus, one can assume that the low-lying states should result primarily from multiple neutron hole-particle configurations. The proton core-excited states would be expected to lie high enough not to cause significant configurational mixing in the low-lying states, and it is precisely for these states (i.e., low-lying states) that one is most likely to be able to assign a configuration. Unless otherwise specified, all shell-model orbitals are assumed to apply to neutrons, and as such, the standard notation for neutrons (ν) will be omitted.

The ground state of Pb^{203} has already been suggested to have a configuration of $f_{5/2}$. This is simply the 121st neutron occupying the lowest available neutron shell-model orbital. The next two states have well-defined spins and parities and appear to be good single-particle states. The 1/2- 126.4-keV state almost certainly has $(f_{5/2})^2(p_{1/2})^{-1}$ (formed by promoting a $p_{1/2}$ neutron to the $f_{5/2}$ orbit) as the predominant configuration in its wave function. The half-life of this state, though, is some 6× slower than the analogous state in Pb^{207}. The quasi-particle effect according to the Kisslinger and Sorensen treatment [Ki60] suggests a slowdown

factor of 25×; as a consequence, Bergström et al. [Be61] suggest that this might indicate the influence of strong collective effects. However, they also forgot that Pb^{203} is composed of 5 hole-states, not 1 hole-states, which, per se, makes for less pure configurations. According to the Moszkowski single-particle estimate [Mo55], however, the 126.4-keV $E2$ should have a half-life of ≈115 ns as compared to the observed 75 ns. The agreement is not terribly poor. The discrepancy raised by Bergström (above) does have a possible explanation; Kisslinger and Sorensen [Ki60] used the Pb^{207} single-hole energies in the Pb^{203} calculations, and to be strictly correct, new single-hole energies should be employed for each isotope of interest (in this case Pb^{203}). In this way the large theoretical slowdown (25×) would possibly be decreased. Such a theoretical re-evaluation would be most welcome. As a consequence, I suggest that the 126.4-keV state has the dominant configuration of $(f_{5/2})^2(p_{1/2})^{-1}$. The single-particle estimates apparently justify such an assignment; also, 0.126 MeV would be quite low for collective effects to appear when compared to the collective states in the adjacent Pb nuclei.

The second excited state, a 3/2- 186.4-keV level, has all indications of having an analogous configuration. The most obvious configuration for such a low-lying 3/2- energy level is $(f_{5/2})^2 (p_{3/2})^{-1}$, easily formed by promoting a $p_{3/2}$ neutron into the $f_{5/2}$ orbital. If true, then the 60-keV $M1$ transition corresponds to a $p_{1/2} \xrightarrow{M1} p_{3/2}$ single-neutron transition.

The excited state at 820.2-keV has been quite unambiguously assigned 9/2-. Ostensibly, this could be a 2+ single phonon vi-

brational state coupled to (or based upon) the $f_{5/2}$ ground state. Such a configuration, $(2+)_{vib}(f_{5/2})$ spans spin values from 1/2 to 9/2. Considering that the spins of the high-lying states are predominantly 7/2, 9/2, and 11/2, one would not normally expect to see the lower spin states of the vibrational states, e.g., say ≤5/2. The 9/2- spin of the 820.0-keV state certainly makes it look like a likely candidate. The branching ratio of the *E*2 820.2-keV γ and the *M*3 633.8-keV γ, however, severly questions such an assignment. Single-particle estimates [Mo55] suggest a ratio of 8.1×10^6, while experimentally a ratio of ≈22 is observed. It is rather curious why the *M*3 should be so terrifically enhanced. The 820.2-keV state almost certainly is not a pure single-particle state, and if it is collective in nature, then the 633.9-keV transition might be expected to be even more hindered than in the single-particle case (a weak argument, however). On this basis, a collective state at 820.2 keV is tentatively ruled out. One other possible configuration that might be predominant for this state is a multipole-hole state of $(f_{5/2})^{-3}(p_{1/2})^{-1}(p_{3/2})^{-1}$. This would suggest a $f_{5/2} \rightarrow p_{1/2}$ single-neutron transition, for the 633.8-keV transition.

The fourth excited state (at 825.2 keV) is the well-known 825.2-keV, 6.1-s isomeric state. The adjacent odd-neutron lead isotopes have systematically decreasing 13/2+ states, from a 13/2+ 1634-keV Pb^{207} state to a 13/2+ 424-keV state in Pb^{199}, so a 13/2+ 825.2-keV isomeric state in Pb^{203} is not unreasonable. The assignment here is practically unambiguous, as the 13/2+ assignment requires

that the $i_{13/2}$ state be involved somehow in the configuration. The 825.2-keV state can quite confidently be assigned an $(i_{13/2})^{-1}\ (f_{5/2})^2$ configuration, and the transition to the ground state then may be represented as $(i_{13/2})^{-1}\ (f_{5/2})^2 \xrightarrow{M4} (f_{5/2})^1$.

The next logical configuration to look for would be one which involved predominantly a configuration with a hole in the $f_{7/2}$ shell-model orbit. Such a configuration might be $(f_{7/2})^{-1}(f_{5/2})^2$. It is also possible that such a state could be significantly fragmented. The states at 896.9 (7/2±,9/2±) and 1033.6 (7/2- [5/2-]) keV all satisfy the spin and parity requirements, and are so closely spaced that systematics are unlikely to tell one much. In a previous paragraph it was noted that the collective 2+ states fell at 961- and 899-keV in Pb^{202} and Pb^{204}, respectively. Interpolating, one might suspect the center of gravity of the compound collective multiplet in Pb^{203} should lie somewhere in the vicinity of 930 keV which, just possibly, could be a 2+ vibrational state coupled to the $f_{5/2}$ odd neutron. This suggests, tentatively, the 896.9-keV state as a strong candidate. Not only does it decay directly to the ground state, but it also does not populate any intermediate states. These data are certainly not conclusive evidence, but the $[(2+)_{vib}\ (f_{5/2})]_{7/2-,9/2-}$ configuration can tentatively be assigned to the 896.9-keV state. The subsequent discussion should also help to lend credence to such an assignment.

If the 896.9-keV state is indeed one of the collective states, then one possibility remains for the $(f_{5/2})^2(f_{7/2})^{-1}$ configuration, the well-defined 1033.6-keV state. The analogous state in

Pb^{207} lies at 2.3 MeV. The single-hole state similar to the 825.2-keV state in Pb^{203} lies at 1634 keV in Pb^{207}. If the $f_{7/2}$ and $i_{13/2}$ are depressed approximately alike in the transition from Pb^{207} to Pb^{203} (not necessarily a good assumption, though) [Kr68] then one might simplistically expect the $(f_{5/2})^2(f_{7/2})^{-1}$ state to lie somewhere near 1.15 MeV. This suggests that the 1033.6-keV level is, perhaps, most likely to have such a configuration. This is also the state (compared to that at 866.5 keV) that has very fast transitions to the ground and second excited states. I suggest, then, that one component of the 1033.6-keV state is $(f_{5/2})^2(f_{7/2})^{-1}$.

The 866.5-keV state is the last state for which I attempt to assign a specific configuration in this section. It might just be possible that 866.5-keV state is of the same collective vibrational nature as the 896.6-keV level but possessing one of the remaining spin values. The small splitting between the levels (≈30 keV) might easily be accounted for by neutron-neutron and/or neutron-core interaction perturbations as well as by configuration mixing of near-lying, similar spin states. Quite cautiously, one can then assign the core-coupled $[(2+)_{vib}(f_{5/2})]_{5/2-}$ configuration to the 866.5-keV state and the remaining $[(2+)_{vib}(f_{5/2})]_{7/2-,9/2-}$ state to the 896.9-keV state. This also makes Bergström claim [Be61] that the 126.4-keV state has some collective behavior more palatable, as I find a definite transition between the 866.5- and 126.4-keV states (nominally, an $E2$ transition). From single-particle estimates this $E2$ is too fast, which may mean that the transition goes partially by collective de-excitation.

The higher-lying states are much too difficult to evaluate in simple shell-model terminology (partially because the spins are more poorly defined). To be entirely proper, one would have to consider not only the multiple neutron-hole particle configurations, but also the residual interparticle interactions, the collective vibrational modes, the various core-coupled states, and also the core-excited proton states. In addition, with a high level density almost a certainty, configuration mixing between all these modes of excitation cannot be neglected. It is perhaps naive to have even hoped to have assigned configurations to the low-lying Pb^{203} excited states, but one should be forgiven a streak of optimism at times. Before continuing to a discussion of the β transitions involved in the Pb^{203} decay, a final comment is in order. Until more multipolarity data are available so that the spins (and parities) of the states are better defined, or until more scattering data are available, the configurations discussed above should be considered strictly tentative. Table 18 summarizes the results of this section, and includes the probable dominant configurations of several low-lying states in Pb^{203}.

4.2.2.B. Bi^{203} β Transitions

The first step is to consider the ground state of Bi^{203}. The spin has been measured by atomic beam techniques [Li59] to be 9/2-. Presumably, this is an $h_{9/2}$ proton (one proton outside the Z=82 closed shell). The normal selection rules for electron capture favor transitions in which the change in spin (ΔI)=0 or ±1. For an electron capture β transition a proton must change into a neutron. If the Bi^{203} ground state is $\pi h_{9/2}$ and the Pb^{203} ground state is

Table 18. Possible neutron configurations for some low-lying excited states in Pb^{203}.

Excited state (keV)	Spin and parity	Possible configuration
0.0	5/2-	$(f_{5/2})$
126.4	1/2-	$(f_{5/2})^2(p_{1/2})^{-1}$
186.4	3/2-	$(f_{5/2})^2(p_{3/2})^{-1}$
820.2	9/2-	$(f_{5/2})^3(p_{1/2})^{-1}(p_{3/2})^{-1}$
825.2	13/2+	$(f_{5/2})^2(i_{13/2})^{-1}$
866.5	5/2-	$[(2+)_{vib}(f_{5/2})]_{5/2-}$
896.9	7/2±,9/2±	$[(2+)_{vib}(f_{5/2})]_{7/2-,9/2-}$
1033.6	7/2-[5/2-]	$(f_{5/2})^2(f_{7/2})^{-1}$

$\nu f_{5/2}$, then the transition to the ground state would go by $\pi h_{9/2} \rightarrow \nu f_{5/2}$. This would involve an unfavorable, second-forbidden transition and is not to be expected. Now, electron capture into states with I=7/2, 9/2, or 11/2 would satisfy the selection rules. A consideration of the spins plus the selection rules leads one not to expect transitions to the first two excited states (126.4 and 186.4 keV), which are 1/2- and 3/2-, respectively. Such transitions would be fourth- and second-forbidden transitions, respectively, and as such are not likely to be seen in competition with other more likely transitions.

The relatively high log ft's of the 820.2-, 825.2-, 866.5-, 896.9-, and 1033.6-keV states are also easily accounted for. Consulting Table 18, one can see that to change a $h_{9/2}$ proton (in Bi^{203}) configuration into any of the neutron configurations of these low-lying states would involve considerable internal rearrangements, and are, therefore, less likely; the higher log ft's are an immediate consequence. For those states which appear to be vibrational in nature (866.5- and 896.9-keV states) the higher log ft's are not terribly surprising. Transitions to these states not only involve a particle change but also a change in the collective nature of the nucleus.

The intermediate states (>1 MeV and <2.6 MeV) are nearly untouchable by the present discussion. Nothing distinguishing marks any of these states, and until more data are obtained to narrow down their spins and parities, nothing of considerable value will be forthcoming.

The transitions to the high-lying states (which have poorly defined spins and parities) do have low log ft's, In fact, all states

>2.65 MeV have log ft's <7.0, and three states have values <6.0 (cf. Figure 31). The highest state placed by this study, 3045.2 keV, has the very low log ft of 5.3. This certainly implies an allowed transition. In the succeeding paragraph several possible β transitions to these excited states are suggested, but final assignment of a specific transition to a specific level must await more experimental and theoretical data.

One possibility was that the $h_{9/2}$ proton was being converted into one of the neutron orbitals above the N=126 closed shell, that is, the $g_{9/2}$, $i_{11/2}$, or $j_{15/2}$. The $g_{9/2}$ orbital in Pb^{207} lies 2.77 MeV above the $p_{1/2}$ orbital (which closes out the N=126 shell). With 3.2 MeV of decay energy such a transition appears to be a possibility. However, a $\pi h_{9/2} \rightarrow \nu g_{9/2}$ transition would be first-forbidden and should not have such a low log ft as 5.3 or 5.9 (for the 3045.2- and 2713.4-keV states, respectively). Alburger and Pryce [A154] have suggested (without proof) that in such a heavy nucleus allowed and first-forbidden transitions should compete favorably. This might mean that one of the low log ft transitions may go by such a transition, but almost assuredly not any transitions having log ft's <6. Similar reasoning might be used for a $\pi h_{9/2} \rightarrow \nu i_{11/2}$ transition, while the $\pi h_{9/2} \rightarrow \nu j_{15/2}$ transition should not be seen at all (a second-forbidden unique transition). These transitions may account, then, for a couple of the middle-log ft range states. Sadly, no systematics of adjacent nuclei are available to allow one to place accurate energy limits on these various transitions.

A third possibility is best explained in terms of the

Kisslinger and Sorensen quasi-particle model. According to their model there is a finite probability that the orbitals below the Fermi surface may be unoccupied. This means that some probability exists for finding holes in the $h_{9/2}$ and $f_{7/2}$ orbitals below the N=126 closed shell. Conversely, there is some noninteger probability that neutrons exist in the orbitals above the Fermi surfaces. In addition, even the simple shell-model predicts $h_{9/2}$ and $f_{7/2}$ holes at high energies. Consider the $h_{9/2}$ proton of Bi^{203}. The most favored transition one could hope for would be a $\pi h_{9/2} \rightarrow \nu h_{9/2}$. This would be possible if the $\pi h_{9/2}$ is converted into the $\nu h_{9/2}$ quasi-particle. One of the low log ft states very likely has a large portion of such a configuration in its wavefunction. Along the same line of reasoning, the transition could be the allowed (l-forbidden) transition - $\pi h_{9/2} \rightarrow \nu f_{7/2}$. Very likely one of the high-lying excited states has such a dominant configuration.

One last case might be suggested. If enough energy is available it is possible to convert an internal $d_{3/2}$ proton of Bi^{203} to a $f_{5/2}$ neutron in Pb^{203}. A first forbidden transition to be sure, but it should complete favorably with the slower allowed transitions in the heavy elements [A154]. Such a transition might be represented $(\pi h_{9/2})^1(\pi d_{3/2})^4 \rightarrow (\nu f_{5/2})^1(\pi h_{9/2})^1 (\pi d_{3/2})^{-1}$.

4.2.2.C. Conclusion

The foregoing discussion has been admittedly qualitative and cursory. However, until more data of both a theoretical and experimental nature are available little can be said with much cer-

tainty concerning the characteristics of the β transitions and/or Pb^{203} excited states. I fully realize that such an evaluation is hardly sufficient - but - perhaps, a foundation and stimulus has been laid for future re-evaluation of this isotope.

4.2.3. Discussion of Pb^{204} Results

Having made some qualitative predictions concerning the Bi^{203} decay, it is now time to return to the more difficult Bi^{204}. As it will turn out, little can be said with much confidence concern ing the shell-model configurations of Pb^{204} excited states. In lieu of such assignments this discussion also includes (section 4.2.3.A.) a survey of the previous theoretical calculations on Pb^{204}, followed by a few qualitative predictions.

4.2.3.A. Shell-Model Calculations on Pb^{204}

The earliest shell-model calculations by True [Tr56] utilized the theory of Alburger and Pryce [Pr52,A154] to predict the expected energy levels in Pb^{204}. Pryce [Pr52] suggested that in the case of the two-hole Pb^{206} the energies of the single-hole states can be taken to be the energies of the low-lying single-hole states in Pb^{207}. The single-particle states then combine (in Pb^{206}), in the first approximation, to give a set of degenerate states with an energy equal to the sum of the Pb^{207} single-hole states. Because of nucleon-nucleon interactions, the degeneracy is removed and the states are split, some being raised in energy and some lowered in energy. Pryce did not calculate this interaction explicitly but, using a zero-range nuclear force of pure singlet exchange character,

he "estimated" the interaction parameters by a rough empirical method. Explicit configuration mixing effects were also estimated by additional empirical adjustment. True used this same method to calculate the levels in Pb^{204} by assuming that the states are based upon configurations of four neutron holes, where each hole in Pb^{204} will have the same energy as the analogous single-neutron hole in Pb^{207}. The energy shifts in each set of degenerate states were estimated using the semi-empirical two-particle interaction parameters previously reported by Alburger and Pryce [A154]. Configuration interaction was not included in his preliminary calculation. Figure 40 shows some 49 distinct levels calculated by True below 2.5 MeV of excitation (arranged by spins). The principal success was the prediction of the 9- state at 2.05 MeV. This compares well with experimental 9- state at 2185 keV. An unpublished recalculation (cited in [St58]) of True's energy values (but using new interaction parameters) has been performed by Blomquist, but at this time it remains a mystery as to which set yields better results.

Using a nuclear model patterned after the BCS superconductivity theory, Kisslinger and Sorensen (KS) [Ki60] have also calculated the levels of Pb^{204}. Their quasi-particle model idealizes the residual interactions between nucleons as a pairing force (the short-range force) plus a long-range quadrupole force. Using the Pb^{207} neutron single-hole energies to establish their parameter choices, they were able to predict many excited states in Pb^{204}. These are graphically depicted in Figure 41.

Several additional investigations [Ri64,Ri63, and Kr68] have been patterned after the Kisslinger and Sorensen quasi-particle

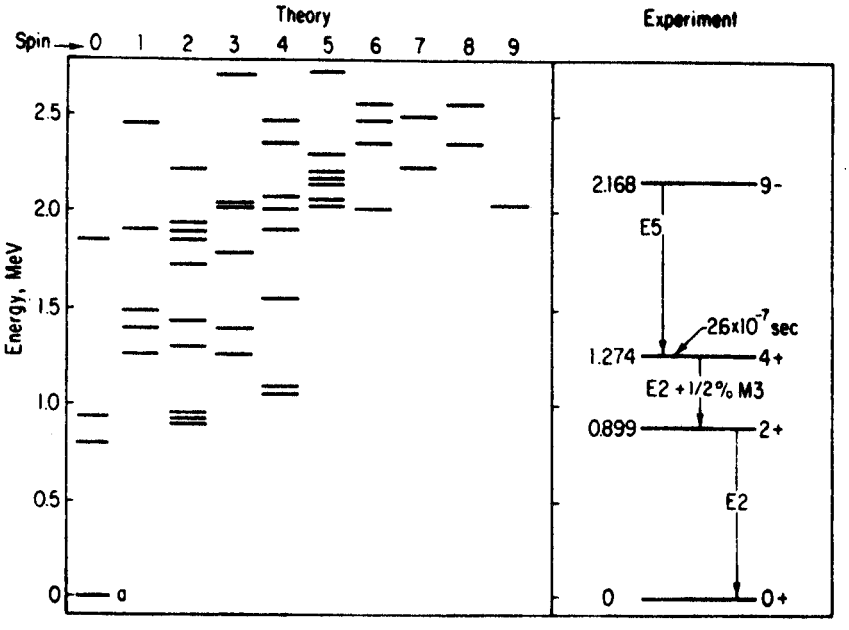

Fig. 40. The energy levels of Pb^{204} calculated by True [Tr56] according to the model formulated by Pryce [Pr52].

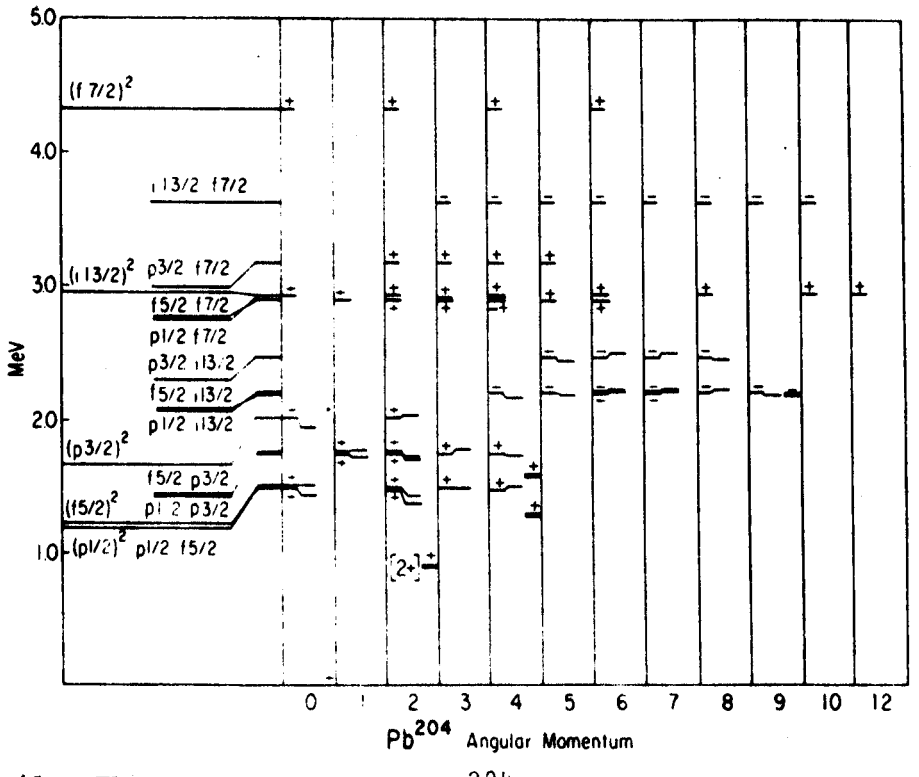

Fig. 41. The energy levels of Pb^{204} as calculated by Kisslinger and Sorensen [Ki60]. On the left are the labeled unperturbed states. For each spin the horizontal line to the left gives the energy of the state; the second horizontal line shows the effect of the inclusion of the P_2 force. The lines to the right are a few experimental levels. The level marked [2+] is the collective 899.2-keV level.

model and/or pairing model. Richardson and Sherman [Ri64] have calculated exact eigenstates of the pairing force Hamiltonian for the $Pb^{206,204,202}$ isotopes. They also used an interaction strength which was larger than that used by Kisslinger and Sorensen, who used the approximate BCS theory of superconductivity to study the pairing model. The larger interaction strength used by Richardson and Sherman plus the exact solutions appear to lead to an error only 1/3 as large (for the states involved in the Pb^{204m} decay) as in the calculations in which the weaker pairing interaction was used (Kisslinger and Sorensen). The second investigation, by Kriechbaum and Urban (KU)[Kr68] used a model closely resembling that of KS. They also used the pairing force as the short-range component but instead of a quadrupole P_2 force they used a quadrupole plus octupole force as the long-range component. The results are not substantially different from that of KS, except that the states appear to be slightly perturbed toward lower energies. It is interesting to note the $f_{5/2}$, $p_{1/2}$, and $p_{3/2}$ level spacings predicted by such a calculation (Figure 42). Whereas the KS quasi-particle model predicts a 5/2-, 3/2-, and 1/2- spin for the low-lying states in Pb^{203}, the KU model correctly predicts 5/2-, 1/2-, and 3/2- spin sequence experimentally observed.

One last theoretical paper needs to be mentioned. Hadermann and Simonius [Ha67] have calculated the energy levels of Pb^{206} and Pb^{204} using a delta force to approximate the residual interactions. The long-range force is assumed to be included in the mean potential and was not explicitly calculated. The energies and transition rates are calculated using the quasi-boson approximation [Ha67], which is strictly

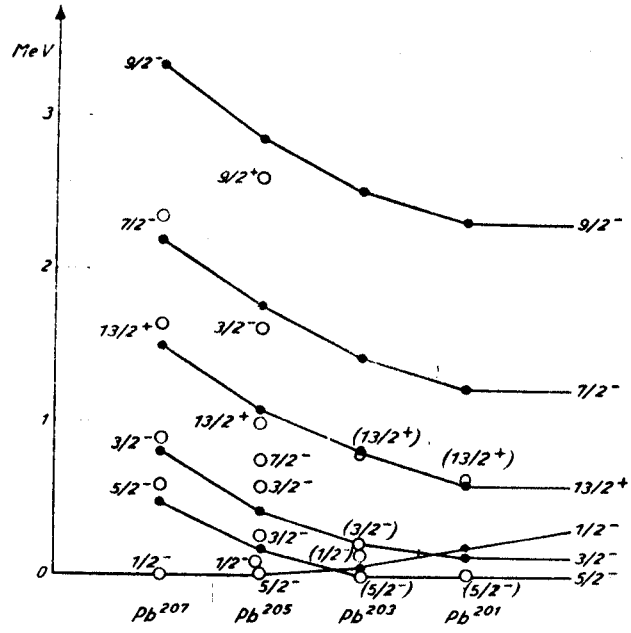

Fig. 42. Theoretical neutron level spacings in the lead region, as calculated by Kriechbaum and Urban [Kr68]. Residual interactions were approximated by a short-range pairing force and a long-range quadrupole plus octupole force. The small black dots are the theoretical values. The large open circles are experimental values.

exact for only 1 pair outside the closed shell. The Pb^{204} calculation was only briefly touched, and the correlation between the calculated and experimental energy levels was not terribly good.

For a more complete understanding and appreciation of the theoretical calculations mentioned, one should really return to the original papers. It was not the intention to present a detailed description of each of these methods, but rather to summarize the general content of the theoretical attempts on the Pb^{204} level scheme. What it does point up, however, is how relatively little has been done on light-lead isotopes. Once again, the original plan of action was to include a correlation between the experimental data and the energy levels predicted by the various methods and models. Two problems precluded this correlation. First, the spins and parities of the Pb^{204} excited states are far too ambiguous to say anything concerning these levels with much confidence. Second, the present investigation, as well as those preceeding, seem to indicate that one of the basic assumptions in these calculations is "all wet". Each of the forementioned has assumed that the single-hole energies of the Pb^{207} single-neutron hole states are good representations of the single-neutron holes in the $Pb^{206-202}$ isotopes. Considering the theoretical evaluations of the level spacings ([Ki60,Kr68]) and the Pb odd-mass isotope systematics (Figure 37), this does not appear to be a valid assumption. Rather, one should use the single-hole energies of the isotope of interest, or, at worst, the adjacent isotopes. Table 19 compares the single-hole energies in Pb^{207} to the hole-particle energies (for analogous states) in Pb^{203}.

Table 19. Single-hole energies in Pb^{207} and Pb^{203}.

Hole configuration[a]	Pb^{207} energy (keV)	Pb^{203} energy (keV)
$(p_{1/2})^{-1}$	0	126
$(f_{5/2})^{-1}$	570	0
$(p_{3/2})^{-1}$	900	186
$(i_{13/2})^{-1}$	1634	825
$(f_{7/2})^{-1}$	2350	1034

[a]All paired nucleons (neutrons) are ignored in the configuration.

A re-evaluation of these calculations in terms of this new set of values would be most welcome here. Actually, it is not quite this simple. The states in Pb^{203} are really five-hole states. Although four of these presumably do tend to remained paired, they still could affect the "single-hole" energy. In other words, a "single-hole" state in Pb^{203} is not perfectly a single-hole state, but will be perturbed a little from the true "Pb^{203} single-hole" position. This is what complicates the calculations so - the Pb^{207} single-hole energies are not good for this region, the "single-hole" energies for Pb^{203} from above are better, but what is really needed are the true single-hole energies for Pb^{203}. Perhaps, a re-evaluation of these calculations with the "single-hole" energies in Table 19 would still be fruitful.

When the time comes that the spin and parity assignments are better-defined and the theoretical calculations have been re-considered, then a correlation such as proposed earlier would be of great interest.

4.2.3.B. Pb^{204} Excited States and Bi^{204} β Transitions

One first needs to estimate the configuration of the Bi^{204} ground-state spin. Using atomic beam experiments the ground state has previously been shown to be 6+. Bi^{204} is a nucleus with one proton outside the Z=82 closed shell and five neutron holes in the N=126 closed shell. From section 4.2.1. the order of shell orbits just below the N=126 closed shell was found to be $f_{5/2}$, $p_{1/2}$, $p_{3/2}$, $i_{13/2}$, $f_{7/2}$, and $h_{9/2}$. I assume that the extra proton is in the $\pi h_{9/2}$ level (in analogy with stable Bi^{209}) and that the unpaired neutron is in the $f_{5/2}$ shell. By a theorem due to Kurath [A154], the lowest state of a configuration with one proton in a level j and one neutron hole in a level j' is the one with $I=j+j'-1$, which in the present case is 9/2 + 5/2 -1 =6. The parity is even, leaving a configuration of $[(\pi h_{9/2})(\nu f_{5/2})]_{6+}$ for the ground state of Bi^{204}; this is in agreement with experiment.

The ε decay should, therefore, go preferentially to states having spins of 5+, 6+, or 7+, in Pb^{204} (if these are energetically possible). Only one transition to an excited state in Pb^{204} appears to be reasonably fast in the ε decay, a transition to the state at 4250 keV, with a log ft of 6.0. Consider now that the 83rd proton in Bi^{204} is in the $\pi h_{9/2}$ shell. Also, consider the shells (orbits) above the N=126 level. From Figure 39 these are $g_{9/2}$, $i_{11/2}$, and $j_{15/2}$.

A very plausible ε decay transition could take place by converting an $h_{9/2}$ proton into a neutron in one of these levels. The $\pi h_{9/2} \rightarrow \nu j_{15/2}$ or $\nu d_{5/2}$ transition would necessarily involve second-forbidden (unique) and first-forbidden (unique) transitions. Thus, these are almost certainly out of question when one considers a log ft of 6.0. The remaining transitions, $\pi\ h_{9/2} \rightarrow \nu g_{9/2}$ and $\pi h_{9/2} \rightarrow \nu i_{11/2}$, are both first-forbidden transitions and also should not be so fast.

The two possible β transitions which <u>do</u> appear feasible were discussed in section 4.2.2.B. when the Bi^{203} decay was discussed. These will only be fleetingly re-mentioned here. One possible transition was converting the $\pi h_{9/2}$ proton into a neutron to fill the $(\nu h_{9/2})^{-1}$ hole. The second suggested transition involved converting an internal $\pi d_{3/2}$ proton into a $\nu f_{5/2}$ neutron. Such a transition would result in a proton broken pair state and would be expected to lie high, but just how high only more calculations will reveal. In Pb^{206} Alburger and Pryce [A154] suggest that an analogous transition occurs to states around ≈3.3 MeV. Perhaps the 3170.0-keV state is populated by such a transition. This is all that will be said concerning the β transitions, as anything further is purely conjecture and cannot be substantiated by evidence at this time.

The Pb^{204} excited states are also only poorly understood. The 0+ ground state has the configuration $(\nu f_{5/2})^2$ as would be anticipated (from the shell-model) for this even-even nucleus. The first excited state at 899.2 keV has a spin and parity of 2+. Kisslinger and Sorensen have shown that this state is collective in

nature and as such should correspond to a one-phonon vibrational state. This was not totally unexpected inasmuch as several investigations [Kr68,Ri64,Ki60] had shown that there existed an anomaly in the 899.2-keV state. (In spite of the criticisms I aimed at the prior theoretical investigations, they did find that all the Pb^{204m} states including the second 4+ state, were predicted reasonably well except for the "peculiar" 899.2-keV state.)

Only the three remaining states in Pb^{204m} (at 2185.4, 1562.8, and 1273.9 keV) are sufficiently well-defined to make any predictions. Following the arguments of Kisslinger and Sorensen some possibilities can be advanced. From simple shell-model theory the 9- state necessarily involves the $i_{13/2}$ state, as this is the only nearby orbit which can yield a negative parity for this state. The most obvious configuration would be a $[(f_{5/2})^3(i_{13/2})^{-1}]_{9-}$; or in or in other words, an $i_{13/2}$ and an $f_{5/2}$ quasi-particle coupled to their maximum value. The 9- 2185.4-keV state decays into two 4+ states by a 0.912 and a 0.622 MeV $E5$ transition. The quasi-particle calculations of Kisslinger and Sorensen suggest that the 1273.9-keV state is composed mainly of two $f_{5/2}$ quasi-particles, while the 1562.8-keV state is mainly one $f_{5/2}$ and one $p_{3/2}$ quasi-particle. As these lie so closely in energy one might well expect an admixture of these configurations due to mixing. On the other hand, True [Tr56] claims that the 1273.9-keV 4+ state is composed of 72% $(p_{1/2})^2(p_{3/2})(f_{5/2})$ and 28% $(p_{1/2})^2(f_{5/2})^2$. However, until further theoretical data

become available these assignments must certainly remain tentative.

The remaining 25 excited states will not be assigned specific configurations, not for any lack of possible assignments, but because one could assign any hypothetical configuration to many different possible states. Before abandoning the Pb^{204} excited states, some mention should be made of the previously published scattering data, particularly the (p,t) reaction. In such a reaction one would expect to see excited states in Pb^{204} which could be produced by simply "plucking" pairs of neutrons from various orbitals. A number of the states revealed in the (p,t) reaction [Ho69] are also revealed by the Bi^{204} ε decay. Some of these possible configurations might be $(f_{5/2})^{-2}(X)^{-2}$ where $X = p_{1/2}$, $p_{3/2}$, $i_{13/2}$, $f_{7/2}$, or $h_{9/2}$. Other excited states of Pb^{206} from which a neutron pair could be "plucked" out are also possible, but listing all these tentative configurations does not lead one very far. Suffice it to say, that the excited states of Pb^{204} are sufficiently complex that no single configuration is likely to be assigned at this time with much confidence.

4.3. General Summary

During the present investigation high-resolution γ-ray spectroscopy has been employed to study the very complex ε decay schemes of Bi^{203} and Bi^{204}.

A fairly detailed Introduction deals with the characteristics and structure of each of the Pb isotopes as one moves from Pb^{208} (a doubly-closed shell nucleus) to Pb^{203}. Somewhat lengthy for a traditional introduction, it thoroughly "sets the stage" for a discussion and subsequent investigation of the characteristics of $Pb^{203,204}$. Theoretical, as well as experimental, data are taken under consideration.

A rapid survey of the apparatus and methods utilized for data acquisition and reduction is given. Several routine computer programs (TAKE CARE, VALTAVA, and COINPLOT) are introduced. Hardly sophisticated, they are nevertheless, samples of (and solutions for) the inordinate difficulties encountered in the construction of very complex decay schemes (such as those of Bi^{203} and Bi^{204}).

The versatility of γ-ray spectroscopy in studies of the behavior of nuclear states is evidenced by the $Bi^{203,204}$ decay schemes formulated in this investigation. Some 210 and 147 γ rays were identified in the $Bi^{204,203}$ decays, respectively. In addition, 60 γ-rays were placed between 30 excited states in Pb^{204} comprising almost 90% of the photon intensity. In the Bi^{203} decay scheme 51 γ-rays were placed between 25 Pb^{203} excited states, including >80% of the photon intensity. Supplementary decay schemes show additional transitions which can be placed on the basis of precise energy sums alone.

Comparisons with previous conversion-electron and reaction studies on each isotope are made. Shell-model level spacings in the vicinity of $Pb^{203,204}$ and the various theoretical calculations on these isotopes are discussed. Some perfunctory comments and suggestions were made concerning possible shell-, collective, and quasi-particle configurations of a few selected excited states.

It seems rather unbelievable that this thesis is nearly completed, but before concluding I feel compelled to make a few suggestions concerning the direction of future investigations of these isotopes. The recent advances in nuclear spectroscopy technology are almost certain to continue, and with such advances a re-investigation of these isotopes in a few years will, no doubt, become worthwhile, particularly in the realm of coincidence information. Presently, however, the most fruitful direction would be in the field of theoretical re-calculations. A quote from [Hy64] expresses this conviction quite amply - "...quantitative assignment of experimental and theoretical levels and transitions cannot be made without more refined treatment of the theory and more extensive experimental work on the decay scheme." The "more extensive experimental work" is now available - the next step should be toward a theoretical re-evaluation.

BIBLIOGRAPHY

BIBLIOGRAPHY

A

[A153] D. E. Alburger and M. H. L. Pryce, Phys. Rev. 92, 514 (1953).

[A154] D. E. Alburger and M. H. L. Pryce, Phys. Rev. 95, 1482 (1954).

[A155] D. E. Alburger and A. W. Sunyar, Phys. Rev. 99, 695 (1955).

[Ås57] B. Åström, Arkiv Fysik 12, 237 (1957).

[Au67] R. L. Auble, D. B. Berry, G. Berzins, L. M. Beyer, R. C. Etherton, W. H. Kelly, and Wm. C. McHarris, Nucl. Inst. Methods 51, 61 (1967).

[Au67a] R. L. Auble, Wm. C. McHarris, and W. H. Kelly, Nucl. Phys. A91, 225 (1967).

B

[Ba57] J. Bardeen, L. N. Cooper, and J. R. Schrieffer, Phys. Rev. 108, 1175 (1957).

[Ba67] Machine language program for on-line data-taking written for the MSU cyclotron computer by D. Bayer, (1967).

[Be56] R. E. Bell and H. M. Skarsgard, Can. J. Phys. 34, 745 (1956).

[Be57] I. Bergström and G. Anderson, Arkiv Fysik 19, 415 (1957).

[Be61] I. Bergström, C. J. Herrlander, P. Thieberger, and J. Uhler, Arkiv Fysik 20, 93 (1961).

[Be69] D. Beery, Gamma Ray Spectroscopy Studies of the Excited States of Odd Proton (Odd Mass) Nuclei in the Z=50-62, N=64-82 Region, thesis, MSU (1969).

C

[Cr70] J. B. Cross, The name TAKE CARE was chosen to remind the user of the unreliability of precise energy sums in the construction of complex decay schemes, MSU (1970).

[Cr70a] J. B. Cross, Ph.D. Thesis, Michigan State University, 1970.

D

[Do68] R. E. Doebler, Wm. C. McHarris, and C. R. Gruhn, Nucl. Phys. A120, 489 (1968).

[Do70a] R. E. Doebler, Wm. C. McHarris, and W. H. Kelly, to be published.

[Du52] D. C. Dunlavey and G. T. Seaborg, Phys. Rev. 85, 757 (1952).

E

[El54] L. G. Elliott, R. L. Graham, J. Walker, and J. L. Wolfson, Phys. Rev. 93, 356 (1954).

[El57] J. P. Elliott and A. M. Lane, "The Nuclear Shell Model" to Handbuch der Physik 39, 301 (1957).

F

[Fi55] V. K. Fischer, Phys. Rev. 99, 764 (1955).

[Fr56] A. R. Fritsch, Univ. Calif. Rad. Lab. Report UCRL-3452, June, 1956.

[Fr58] A. R. Fritsch, J. M. Hollander, J. Inorg. Nuclear Chem. 6, 165 (1958).

G

[Ge65] J. S. Geiger, R. T. Graham, I. Bergström, and F. Brown, Nucl. Phys. 68, 352 (1965).

[Gi70] G. C. Giesler, Wm. C. McHarris, R. A. Warner, and W. H. Kelly, Ge(Li)-Ge(Li) Compton Scattering Problems, (to be published).

[Gr65] Average of: U. Gruber, R. Koch, B. P. Maier, and O. W. B. Schutt, Z. Naturforsch. 20A, 929 (1965), and E. J. Seppi, H. Henrikson, F. Boehm, and J. W. M. Dumond, Nucl. Instr. Methods 16, 17 (1962).

[Gr66] C. R. Gruhn and Wm. C. McHarris, "On the Decay of Bismuth-204", paper submitted to Session III of the International Conference on Nuclear Physics, Gatlinburg, Tennessee, 12-17 Sept. 1966.

[Go51] M. Goldhaber and A. W. Sunyar, Phys. Rev. 83, 906 (1951).

[Gu68] R. Gunnick, R. A. Meyer, J. B. Niday, and R. P. Anderson, Nucl. Instr. Methods 65, 26 (1968).

H

[Ha67] J. Hadermann and M. Simonius, Helv. Phys. Acta. 40, 531 (1967).

[He56] C. J. Herrlander, R. Stockendal, J. A. McDonell, and I. Bergström, Nucl. Phys. 1, 643 (1956).

[He61] C. J. Herrlander, Arkiv Fysik 20, 71 (1961).

[He68] R. L. Heath and R. J. Gehrke, IN-1218 (Dec. 1968).

[Ho52] N. J. Hopkins, Phys. Rev. 88,,680 (1952).

[Ho53] J. M. Hollander, I. Perlman, and G. T. Seaborg, Revs. Mod. Phys. 25, 469 (1953).

[Ho67] G. E. Holland, Nelson Stein, C. A. Whitten Jr., and D. A. Bromley, Proc. of the Intl. Conf. on Nucl. Structure, Tokyo (1967).

[Ho69] G. E. Holland, private communication (1969).

[Hy64] E. K. Hyde, I. Perlman, and G. T. Seaborg, "The Nuclear Properties of the Heavy Elements", Englewood Cliffs, N. J., Prentice-Hall, Chapter 10 (1964).

J

[Jo58] C. M. Johansson and I. P. K. Lindgren, Nucl. Phys. 9, 44 (1958).

K

[Ke57] M. J. Kearsley, Nucl. Phys. 4, 157 (1957).

[Ki60] L. S. Kisslinger and R. A. Sorensen, Dan. Mat.-fys. Medd. 32, No. 9 (1960).

[Kn57] B. B. Kinsey, Handbuch der Physik 40, Berlin: Springer-Verlag (1957).

[Ko70] K. Kosanke, Wm. C. McHarris, and W. H. Kelly, to be published.

[Kr68] M. Kriechbaum and P. Urban, Physica Austriaca 28, 109 (1968).

[Kr54] V. E. Krohn and S. Raboy, Phys. Rev. 95, 1354 (1954).

[Kr55] V. E. Krohn and S. Raboy, Phys. Rev. 97, 1017 (1955).

L

[La60] A. N. Lane and E. D. Pendlebury, Nucl. Phys. 15, 39 (1960).

[Le67] C. M. Lederer, J. M. Hollander, and I. Perlman, Table of Isotopes, 6th Ed., Wiley, 1966.

[Li59] I. P. K. Lindgren and C. M. Johansson, Arkiv Fysik 15, 445 (1959).

M

[Ma57] J. B. Marion, Gamma-Ray Calibration Standards, Univ. of Maryland Technical Report 653 (1957).

[Ma68] J. B. Marion, Nucl. Data A4, 301 (1968).

[Mc53] F. K. McGowan and E. C. Cambell, Phys. Rev. 99, 695 (1955) and F. K. McGowan, Phys. Rev. 92, 524 (1953).

[Mc57] A. McDonell, R. Stockendal, C. J. Herrlander, and I. Bergström, Nucl. Phys. 3, 513 (1957).

[Mc70] Wm. C. McHarris, R. G. Au, D. L. Bayer, W. Benenson, R. A. DeForest, W. H. Kelly, and W. E. Merritt, an invited paper given for the International Conference on Radioactivity in in Nuclear Spectroscopy, 11-15 August 1969.

[Mi68] Michigan State University, Nuclear Chemistry Annual Report, COO-1779-4, 1968.

[Mi69] Michigan State University, Nuclear Chemistry Annual Report, COO-1779-13, 1969.

[Mo55] S. A. Moszkowski, in Beta- and Gamma-Ray Spectroscopy, edited by K. Siegbahn, Interscience Publishers, N. Y., 1955.

[My65] W. D. Myers and W. J. Swiatecki, "Nuclear Masses and Deformations" UCRL AEC Contract No. W-7405-eng-48, UCRL-11980, TID-4500, May, 1965.

N

[Ne50] H. M. Neumann and I. Perlman, Phys. Rev. 78, 191 (1950).

[No58] T. Novakov, R. Stockendal, M. Schmorak, and B. Johansson, Arkiv Fysik 14, 85 (1958).

[Nu65] Nuclear Data Sheets (The National Academy of Sciences -- National Research Council); reissued by Academic Press, 1965.

P

[Pb53] Early reference to Pb^{203} given in Revs. Mod. Phys. 25, 589 (1953).

[Pe60] L. Persson and Z. Sujkowski, Arkiv Fysik 19, 309 (1960).

[Pe61] L. Persson and R. Stockendal, Arkiv Fysik 19, 303 (1961).

[Pr52] M. H. L. Pryce, Proc. Phys. Soc. A65, 723 (1952).

[Pr54] J. R. Prescott, Proc. Phys. Soc. 67A, 254 (1954).

[Pr56] M. H. L. Pryce, Nucl. Phys. 2, 226 (1956).

R

[Ra67] Average of: A. V. Ramayya, J. H. Hamilton, S. M. Brakmavar, and J. J. Pinajian, Phys. Lett. 24B, 49 (1967) and J. J. Reidy and M. L. Wiedenbeck, Nucl. Phys. 70, 518 (1965).

[Re67] G. M. Reynolds, J. R. Maxwell, and Norton M. Hintz, Phys. Rev. 153, 1283 (1967).

[Ri63] R. W. Richardson, Phys. Lett. 5, 82 (1963).

[Ri64] R. W. Richardson and N. Sherman, Nucl. Phys. 52, 253 (1964).

[Ri58] W. Riezler and G. Kauw, Z. Naturforsch. 13A, 904 (1958).

S

[Sc56] M. Schmorak, R. Stockendal, J. A. McDonell, I. Bergström, and T. R. Gerholm, Nucl. Phys. 2, 193 (1956).

[Sl65] L. A. Sliv and I. M. Band, in Alpha-, Beta-, and Gamma-Ray Spectroscopy, edited by K. Siegbahn, North Holland Publ. Co., Amsterdam (1965).

[St55] R. Stockendal, J. A. McDonell, M. Schmorak, and I. Bergström, Arkiv Fysik 11, 165 (1956).

[St58] R. Stockendal, T. Novakov, B. Johansson, and M. Schmorak, Arkiv Fysik 14, 65 (1958).

[St60a] R. Stockendal, Phys. Rev. 118, 1074 (1960).

[St60] R. Stockendal, Arkiv Fysik 17, 579 (1960).

[Su50] A. W. Sunyar, D. Alburger, G. Friedlander, M. Goldhaber, and G. Scharff-Goldhaber, Phys. Rev. 83, 906 (1951).

[Su61] Z. Sujkowski, Arkiv Fysik 20, 243 (1961).

T

[Te47] Templeton, Howland, and I. Perlman, Phys. Rev. 72, 755 (1947).

[Th54] S. Thulin, Physica 20, 521 (1954).

[Tr56] W. W. True, Phys. Rev. 101, 1342 (1956).

[Tr58] W. W. True and K. W. Ford, Phys. Rev. 109, 1675 (1958).

[Tr61] W. W. True, Nucl. Phys. 25, 155 (1961).

V

[Va54] J. Varma, Phys. Rev. 94, 1688, 7954 (1954).

[Ve63] S. H. Vegors, R. L. Heath, and D. G. Proctor, Nucl. Phys. 48, 230 (1963).

[Vi66] V. E. Viola, Jr., and G. T. Seaborg, J. Inorg. Nucl. Chem. 28, 697 (1966).

W

[Wa54] A. H. Wapstra, D. Maeder, G. J. Nijgh, and L. Th. M. Ornstein, Physica 20, 169 (1954).

[Wa58] G. J. Nijgh, A. H. Wapstra, L. Th. M. Ornstein, N. Salomons-Grobben, J. R. Huizenga, and O. Almen, Nucl. Phys. 9, 528 (1958).

[We51] V. F. Weisskopf, Phys. Rev. 83, 1073 (1951).

[We56] G. K. Wertheim and R. V. Pound, Phys. Rev. 102, 185 (1956).

[Wh67] D. H. White and D. J. Groves, Nucl. Phys. A91, 453 (1967).

APPENDICES

TAKE CARE FORTRAN Listing

```
FORTRAN
      1    C
      2    C      PROGRAM TAKE CARE
      3    C
      4    C      THIS PROGRAM WILL OPERATE IN TWO DIFFERENT MODES, TAKE, AND/OR CARE
      5    C      TAKE WILL CALCULATE THE DIFFERENCE BETWEEN ALL THE INPUT LEVELS
      6    C      AND COMPARE THE DIFFERENCES TO THE KNOWN LIST OF GAMMAS (WITHIN
      7    C      A SPECIFIED TOLERANCE) AND OUTPUT ANY GAMMAS SATISFYING THE CONDITION
      8    C      CARE WILL SCAN UP THE KNOWN SET OF ENERGY LEVELS AT 1 KEV INTERVALS
      9    C      AND OUTPUT ANY GAMMAS WHICH SATISFY THE DIFFERENCE BETWEEN THE
     10    C      HYPOTHETICAL LEVEL AND THE KNOWN LEVELS
     11    C      THE INPUT PARAMETERS ARE FOUND ON THE FOLLOWING CARDS
     12    C      ITS,IQ,KAREN,DEL,BI,IA,IB,IRS,IC,ID
     13    C      FORMAT IS (I3,2I2,2F3.2,5I2)
     14    C      ITS - THE NUMBER OF KNOWN GAMMAS INPUT
     15    C      IQ - NUMBER OF KNOWN LEVELS INPUT (INCLUDING THE TEST LEVEL, IF ONE)
     16    C      KAREN - NUMBER OF ITERATIONS
     17    C      DEL - TOLERANCE IN KEV OF THE GAMMAS IN THE 0-1500-KEV REGION
     18    C      BI IS THE LIMIT ON THE DEL OF THE HIGH ENERGY PEAKS
     19    C      IF THE TOLERANCES ARE NOT SPECIFIED THEY WILL BE SET TO 1.0 KEV
     20    C      FOR THE 0-1500-KEV REGION, AND 1.5 KEV FOR THE 1500 AND UP KEV REGION
     21    C      IA=1, DO TAKE; IA=0, DO CARE
     22    C      IB=1 DOES BOTH ROUTINES ONE AFTER ANOTHER (DEFAULT DOES ONLY ONE)
     23    C      IRS - NUMBER OF LEVELS FROM THE TOP IN THE TAKE PROGRAM
     24    C      IC AND ID ARE UNUSED PARAMETERS
     25    C      ALL THE PREVIOUS INFORMATION IS LISTED ON THE PROGRAM CONTROL CARD
     26    C      FOLLOWING THE CONTROL CARD ARE ALL THE INPUT GAMMAS, LISTED IN
     27    C      FORMAT(8F10.2)
     28    C      FOLLOWING THE GAMMAS ARE THE ENERGIES OF THE INPUT LEVELS, LISTED
     29    C      ONE TO A CARD IN FORMAT(F10.2), THIS ALLOWS ONE TO CHANGE THE LEVELS
     30    C      EASILY; IF THE CARE PROGRAM IS BEING RUN, THE TEST LEVEL IS
     31    C      PLACED LAST IN THE INPUT
     32    C
     33    C
     34           CALL KILL(3)
     35           DIMENSION STATE(100),DIFF(100,100),END(250),NO(100),PLEAS(100)
     36           REAL JIM(10)
     37           READ 997,ITS,IQ,KAREN,DEL,BI,IA,IB,IRS,IC,ID
     38    997    FORMAT(I3,I2,I2,2F3.2,5I2)
```

```
39                      IF(KAREN.EQ.0)KAREN=1
40                      IF(BI.EQ.0.0)BI=1.5
41                      IF(DEL.EQ.0.0)DEL=1.0
42                      IF(IRS.EQ.0)IRS=IQ
43                      READ 998,(END(I),I=1,ITS)
44                998   FORMAT(8F10.2)
45                      READ 2,(STATE(I),I=1,IQ)
46                2     FORMAT(1F10.2)
47                      ALOVE =STATE(IQ)
48                      DO 188 I=1,IQ
49                188   PLEAS(I)=STATE(I)
50                      DO 777 KLM=1,KAREN
51                      DO 187 IJK=1,IQ
52                187   STATE(IJK)=PLEAS(IJK)
53                      DO 11 KB=1,IQ
54                      IP=KB+1
55                      DO 123 KA=IP,IQ
56                      IF(STATE(KB).GE.STATE(KA))GO TO 123
57                      BAH=STATE(KA)
58                      STATE(KA)=STATE(KB)
59                      STATE(KB)=BAH
60                123   CONTINUE
61                11    CONTINUE
62                      IF(IQ.EQ.IRS)IRS=IRS-1
63                      DO 5 I=1,IQ
64                      DO 6 J=1,IQ
65                6     DIFF(J,I)=0.0
66                5     NO(I)=0
67                      IF(IA.EQ.0)GO TO 666
68                      DO 3 J=1,IRS
69                      JAMES=0
70                      DO 4 I=1,IQ
71                      DIFF(J,I)=ABS(STATE(J)-STATE(I))
72                      CALL HELP(DIFF(J,I),END,ITS,DEL,BI,GO)
73                      DIFF(J,I)=GO
74                      IF(GO.NE.0)JAMES=JAMES+1
75                4     CONTINUE
```

```
76          3     N0(J)=JAMES
77                PRINT 7
78          7     F0RMAT (1X,'PR0GRAM TEST DECAY SCHEME'//1X,'GAMMAS F0R EACH LEVEL
79          7    1BEL0W AN0THER')
80                D0 14 J=1,IRS,5
81                PRINT 8,STATE(J),STATE(J+1),STATE(J+2),STATE(J+3),STATE(J+4)
82          8     F0RMAT  (1X,5(6X,'LEVEL ',F9.2))
83                D0 12 I=1,IQ
84          12    PRINT  9,STATE(I),DIFF(J,I),DIFF(J+1,I),DIFF(J+2,I),DIFF(J+3,I),DI
85                2FF(J+4,I)
86          9     F0RMAT(1X,F7.2,1X, 5(F10.2,10X))
87                PRINT 334
88          334   F0RMAT(1X,'   '/1X,'NUMBER 0F GAMMAS'/)
89                PRINT 919,N0(J),N0(J+1),N0(J+2),N0(J+3),N0(J+4)
90          919   F0RMAT(1X,'   '///9X,5(I5,15X))
91                PRINT 333
92          333   F0RMAT(1H1,'   ')
93          14    C0NTINUE
94                IF(IB.NE.0)G0 T0 666
95                G0 T0 555
96          666   C0NTINUE
97                D0 13 KJ=1,10
98                JIM(KJ)=AL0VE-1+KJ
99                JAMES=0
100               D0 33 J=1,IQ
101               DIFF(KJ,J)=ABS(JIM(KJ)-STATE(J))
102               CALL HELP(DIFF(KJ,J),END,ITS,DEL,BI,G0)
103               DIFF(KJ,J)=G0
104               IF(G0.NE.0.0)JAMES=JAMES+1
105         33    C0NTINUE
106         13    N0(KJ)=JAMES
107               PRINT 115,AL0VE
108         115   F0RMAT(1H1,1X,'TESTING THE ',F8.2,' LEVEL'//)
109               PRINT 116,JIM(1),JIM(2),JIM(3),JIM(4),JIM(5),JIM(6),JIM(7),JIM(8),
110              1JIM(9),JIM(10)
111         116   F0RMAT(1X,8X,10F8.2)
112               PRINT 117
```

```
113          117   FORMAT  (1X, '     ')
114                DO 199 J=1,IQ
115                PRINT 118, STATE(J),DIFF(1,J),DIFF(2,J),DIFF(3,J),DIFF(4,J),DIFF(5,J),
116               1,J),DIFF(6,J),DIFF(7,J),DIFF(8,J),DIFF(9,J),DIFF(10,J)
117          118   FORMAT(1X,11F8.2)
118          199   CONTINUE
119                PRINT 129
120          129   FORMAT(1X,'NUMBER OF GAMMAS')
121                PRINT 121,NO(1),NO(2),NO(3),NO(4),NO(5),NO(6),NO(7),NO(8),NO(9),NO
122               1(10)
123          121   FORMAT(14X,10(I2,6X))
124                ALOVE=ALOVE+10.
125                PLEAS(IQ)=ALOVE
126          777   CONTINUE
127          555   END
```



```
1                  SUBROUTINE HELP(DIFF,END,ITS,DEL,BI,GO)
2                  DIMENSION END(250)
3                  DO 1 J=1,ITS
4                  IF(END(J).GE.1500.0)GO TO 10
5                  IF(ABS(END(J)-DIFF).LE.DEL)GO TO 5
6                  GO TO 1
7            10    IF(ABS(END(J)-DIFF).LE.BI)GO TO 5
8            1     CONTINUE
9                  GO =0.0
10                 RETURN
11           5     GO = END(J)
12                 RETURN
13                 END
```

```
1              C
2              C     PROGRAM VALTAVA (POWERFUL, IN FINNISH)
3              C
4              C     VALTAVA IS A PLOTTING ROUTINE DESIGNED FOR THE MSU XDS
5              C     SIGMA-7 COMPUTER.  GIVEN THE PROPER SET OF PARAMETERS IT
6              C     WILL PLOT THE DATA IN LOG FORMAT (FROM 1 TO 6 CYCLES),
7              C     DRAW A BORDER AROUND THE ENTIRE PLOT, PUT THE TIC MARKS
8              C     ON THE AXES, AND LABEL THE LOG SCALE.  IT AUTOMATICALLY
9              C     SCALES THE SPECTRA BASED ON THE MAGNITUDE OF THE HIGHEST
10             C     PEAK.  IN ADDITION, IT LABELS EACH PEAK WITH A BAR AND THE
11             C     APPROPRIATE ENERGY, AND HAS A PROVISION SUCH THAT YOU MAY
12             C     NOT WRITE OVER A PREVIOUS LABEL
13             C     TITLE CARD:    TITLE TO BE PRINTED ON THE SPECTRA IN FOR-
14             C     MAT(16X,16A4); CRUNCH (COMPRESSED) DATA DECK FOLLOWS THE
15             C     STANDARD PLOT TITLE CARD;    FOLLOWING THE DATA DECK ARE THE
16             C     ENERGY LABEL CARDS,  EACH CARD CARRIES THE APPROXIMATE
17             C     CHANNEL OF THE PEAK TO BE LABELED, AND THE ENERGY TO
18             C     APPEAR IN THIS LABEL;  FORMAT FOR THE ENERGY CARDS IS
19             C     (I4,16A4);   A MARK BILLBOARD CARD APPEARS BETWEEN SETS OF
20             C     SPECTRA AND A MARK AND END OF FILE CARD TERMINATE THE DECK.
21             C
22             C
23                   DIMENSION IPRINT(16),AN(4096)
24                   INTEGER N(4096)
25                   MARK3=0
26             999   CONTINUE
27                   READ (105,5,END=1500,ERR=1313)IPRINT
28             5     FORMAT (16X,16A4)
29                   MARKE=0
30                   MARK3=MARK3+1
31                   SX=1.
32                   SY=1.
33                   JI=3
34                   Y=0.
35                   X=MARK3*100.**43.
36                   CALL PLOT (X,Y,JI,SX,SY)
```

```
37              C
38              C       PLOTTING BORDER AND TIC MARKS
39              C
40                      CALL PLOT (0.,0.,0,1.,1.)
41                      CALL PLOT (0.,50.,2,1.,1.)
42                      CALL PLOT (0.,0.,0,1.,1.)
43                      CALL PLOT (0.,1040.,1,1.,1.)
44                      CALL PLOT (4095.,1040.,1,1.,1.)
45                      CALL PLOT (4095.,0.,1,1.,1.)
46                      CALL PLOT (0.,0.,1,1.,1.)
47                      X=0.
48                      DO 4 I=1,8
49                      JI=2
50                      X=X+500.
51                      Y=15.
52                      CALL PLOT (X,Y,JI,SX,SY)
53                      JI=1
54                      Y=-15.
55                      CALL PLOT (X,Y,JI,SX,SY)
56              4       CONTINUE
57                      CALL PLOT (4095.,0.,2,1.,1.)
58                      CALL PLOT (0.,0.,1,1.,1.)
59                      CALL PLOT (0.,1040.,1,1.,1.)
60              C
61              C       PLOT TITLE
62              C
63                      CALL PLOT (100.,995.,2,1.,1.)
64                      CALL CHAR (100.,995.,IPRINT,64,0.,0.30)
65                      CALL PLOT (0.,0.,2,1.,1.)
66                      CALL CREAD (N,NCHAN,NRUN,NERR)
67                      IF(NERR.NE.0) GO TO 1313
68                      DO 10 I=1,NCHAN
69              10      AN(I)=N(I)+1
70                      B=1.
71              C
72              C       AUTOMATIC SCALING AND DATA PLOTTING
73              C
74                      DO 11 I=1,NCHAN
75              11      IF(AN(I).GT.B)B=AN(I)
76                      EN=6.
77                      IF(B.LE.100000.)EN=5.
78                      IF(B.LE.10000.)EN=4.
79                      IF(B.LE.1000.)EN=3.
80                      IF(B.LE.100.)EN=2.
81                      DO 676 I=1,NCHAN
82              676     AN(I)=ALOG10(AN(I))*(750./EN)
83                      JI=1
84                      X=0.
85                      DO 16 I=1,NCHAN
86                      X=X+1.
87                      Y=AN(I)
88                      CALL PLOT (X,Y,JI,SX,SY)
```

```
 16     CONTINUE
C
C       SCALING AND PLOTTING LOG SCALE
C
        CALL NCHAR(-70.,0.,1,0.30,1,0.0)
        CALL PLOT (-15.,0.,2,1.,1.)
        CALL PLOT ( 15.,0.,1,1.,1.)
        Y=0.
        NEN=EN
        DO 111 I=1,NEN
        Y=(750./EN)*I
        CALL PLOT (-15.,Y,2,1.,1.)
        CALL PLOT ( 15.,Y,1,1.,1.)
        X=-100.
        CALL NCHAR (X,Y,1,0.30,1,0.0)
        CALL NCHAR (-70.,Y,0,0.30,1,0.0)
        Y=Y+28.
        CALL NCHAR (-40.,Y,I,0.25,1,0.0)
111     CONTINUE
        X=0.
C
C       LABELING PEAKS WITH ENERGIES
C
666     READ (105,55,END=1500,ERR=1313)K,IPRINT
55      FORMAT(I4,16A4)
        XK=K
        IF(XK.LT.(X+25.))XK=X+25
        X=XK
        CALL PLOT (X,750.,2,1.,1.)
        CALL PLOT (X,810.,1,1.,1.)
        X=XK+15.
        CALL PLOT (X,810.,2,1.,1.)
        CALL CHAR (X,810.,IPRINT,6,90.,0.30)
        GO TO 666
1500    MARKE=MARKE+1
        IF(MARKE.EQ.2) GO TO 1700
        X=4300.
        Y=-50.
        JI=2
        CALL PLOT (X,Y,JI,SX,SY)
        GO TO 999
1700    JI=-1
        CALL PLOT (X,Y,JI,SX,SY)
1313      END
```

```
      SUBROUTINE NCHAR (X,Y,NU,SZ,NOYES, DP )
      INTEGER PRIN(5),N(4),NUMB(13),SIGN
      DATA NUMB/'0','1','2','3','4','5','6','7','8','9',' ','-','+'/
      SIGN = NUMB(12)
      IF (NU.GT.0)  SIGN = NUMB(13)
      PRIN(1) = NUMB(11)
      N(1) = NU/1000
      N(2) = NU / 100 - 10 * N(1)
      N(3) = NU / 10 - 10 * N(2) - 100 * N(1)
      N(4) = NU - 10 * N(3) - 100 * N(2) - 1000 * N(1)
      IC = 0
      IT = 1
      DO 1 J = 2,5
      IGT = N(J-1)
      IF (IGT.LT.0)  IGT = - IGT
      IGT =  IGT + 1
      IF (IGT.GT.1)  GO TO 2
      IF (IC.EQ.1)  GO TO 2
      PRIN (J) = NUMB (11)
      IT =  IT + 1
      GO TO 1
    2 PRIN(J) = NUMB(IGT)
      IC = 1
    1 CONTINUE
      PRIN(IT) = SIGN
      IF ((NOYES.LT.2).AND.(NU.GT.0))  PRIN(IT) = NUMB(11)
      IF (IT.EQ.5)  PRIN(IT) = NUMB(1)
      KL = 1
      I  =1
      IF (NOYES.GT.0)  I = 3
      DO 4 J = I,5
      CALL CHAR (X,Y,PRIN(J), KL  , DP, SZ )
      Y = Y + SZ* 1. * SIND(DP)
    4 X = X SZ*20. * COSD(DP)
      RETURN
      END
```

```
FORTRAN
      1              C
      2              C     PROGRAM COINPLOT
      3              C
      4              C     COINPLOT WILL ACCEPT N CRUNCH DATA DECKS, AUTOMATICALLY
      5              C     SCALE THE PLOTS TO FIT ON A STANDARD 8 1/2 BY 11 IN. PAGE
      6              C     AND PLOT THE DATA ON A LOG SCALE.  IT ALSO PUTS A BORDER AND
      7              C     TIC MARKS ON EACH PLOT BOTH FOR THE ABCISSA AND ORDINATE.
      8              C     THE USEFULLNESS LIES IN THAT THE COINCIDENCE PLOTS THUS
      9              C     GENERATED CAN BE DIRECTLY REPRODUCED RATHER THAN HAVING TO
     10              C     EMPLOY THE SERVICES OF A DRAFTSMAN.
     11              C     THE INPUT CONTROL CARD CONSISTS OF THE PARAMETERS:
     12              C     BURKE,CROSS,KARE,IAM,MCHAN,BURK1,CROS1
     13              C     BURKE = THE WIDTH OF THE FINAL PLOT (X AXIS, IN INCHES)
     14              C     CROSS = THE HEIGHT OF THE FINAL PLOTS (Y AXIS, IN INCHES)
     15              C     KARE = THE NUMBER OF PLOTS PER PAGE, DEFAULT  = 3
     16              C     IAM = IF IAM=1 THEN EACH SET OF DATA DECKS REQUIRES A
     17              C     SEPARATE CONTROL CARD; IF IAM=0 (DEFAULT) THEN ONLY THE
     18              C     FIRST DATA DECK REQUIRES THE CONTROL CARD
     19              C     MCHAN = THE NUMBER OF CHANNELS TO BE PLOTTED (DEFAULT=4096)
     20              C     BURK1 = THE ORIGIN OF THE FIRST PLOT (X AXIS, IN INCHES)
     21              C     CROS1 = THE ORIGIN OF THE FIRST PLOT (Y AXIS, IN INCHES)
     22              C     FOLLOWING THE CONTROL CARD ARE THE STANDARD CRUNCH DATA
     23              C     DECKS (INCLUDING TITLE CARD); (CAUTION   IF KARE =3 E.G.
     24              C     THEN THERE MUST BE AT LEAST 3 DECKS, AND /OR MULTIPLES OF 3.
     25              C     ALSO, IF AT ANY TIME DURING A LONG PLOTTING SEQUENCE YOU
     26              C     WISH TO CHANGE THE PLOTTING CONTROL CARD, THEN IAM MUST
     27              C     BE SET TO 1 ON THE PREVIOUS SET OF DATA DECKS
     28              C
     29              C
     30                    DIMENSION IPRINT(16),AN(4096)
     31                    INTEGER N(8192)
     32                    MARK3=0
     33              C
     34              C     READ THE CONTROL CARD
     35              C
     36              987   READ(105,4567,END=1700)BURKE,CROSS,KARE,IAM,MCHAN,BURK1,CROS1
```

```
      4567  FORMAT(2F5.2,2I1,I4,2F5.2)
            IF(MCHAN.EQ.0)MCHAN=4096
            IF(KARE.EQ.0)KARE=3
            IF(BURK1.EQ.0.0)BURK1=2.
            IF(CROS1.EQ.0.0)CROS1=2.
            BURK1=BURK1*100.
            CROS1=CROS1*100.
      999   CONTINUE
      C
      C     PLOT THE BORDER
      C
            CALL PLOT (0.,0.,0,1.,1.)
            MARK3=MARK3+1
            IX=MARK3*13
            CALL PLOT (IX,0.,3,1.,1.)
            CALL PLOT(0.,1100.,1,1.,1.)
            CALL PLOT (850.,1100.,1,1.,1.)
            CALL PLOT (850.,0.,1,1.,1.)
            CALL PLOT (0.,0.,2,1.,1.)
            CALL PLOT (BURK1,CROS1,2,1.,1.)
            CALL PLOT (0.,0.,0,1.,1.)
            YQ=0.
            DO 158 JIM=1,KARE
            READ (105,5,END=1700,ERR=1313)IPRINT
      5     FORMAT (16X,16A4)
            SX=(100./MCHAN)*BURKE
            SY=(100./(1040.*KARE))*CROSS
            Y=YQ
            CALL PLOT (0.,Y,2,SX,SY)
            CALL PLOT (0.,0.,0,SX,SY)
            CHAN=MCHAN-1.
            CALL PLOT (0.,1040.,1,SX,SY)
            CALL PLOT (CHAN,1040.,1,SX,SY)
            CALL PLOT (CHAN,0.,1,SX,SY)
            CALL PLOT (0.,0.,1,SX,SY)
            X=0.
      C
      C     PLOT THE TIC MARKS FOR THE CHANNELS
      C
            J=CHAN/500.
            DO 4 I=1,J
            JI=1
            X=X+500.
            Y=0.
            CALL PLOT (X,Y,JI,SX,SY)
            Y=15.
            JI=1
            CALL PLOT (X,Y,JI,SX,SY)
            Y=-15.
            CALL PLOT (X,Y,1,SX,SY)
            CALL PLOT (X,0.,1,SX,SY)
      4     CONTINUE
            CALL PLOT (CHAN,0.,1,SX,SY)
            CALL PLOT (CHAN,1040.,1,SX,SY)
```

```
      CALL PLOT (0.,1040.,1,SX,SY)
      CALL PLOT (0.,0.,1,SX,SY)
      CALL CREAD (N,NCHAN,NRUN,NERRR)
      IF(NERRR.NE.0) GO TO 1313
C
C     AUTOMATIC SCALING AND PLOTTING DATA
C
      DO 10 I=1,NCHAN
10    AN(I)=N(I)+1
      B=1.
      DO 11 I=1,NCHAN
11    IF (AN(I).GT.B)B=AN(I)
      EN=6.
      IF(B.LE.100000.)EN=5.
      IF(B.LE.10000.)EN=4.
      IF(B.LE.1000.)EN=3.
      IF(B.LE.100.)EN=2.
      IF(B.LE.10.)EN=1.
      DO 676 I=1,NCHAN
676   AN(I)=ALOG10(AN(I))*(800./EN)
      JI=1
      X=0.
      DO 16 I=1,MCHAN
      X=X+1.
      Y=AN(I)
      CALL PLOT (X,Y,JI,SX,SY)
16    CONTINUE
      CALL PLOT (-15.,0.,2,SX,SY)
      CALL PLOT ( 15.,0.,1,SX,SY)
      Y=0.
      NEN=EN
      DO 111 I=1,NEN
      Y=(800./EN)*I
      CALL PLOT (-15.,Y,2,SX,SY)
      CALL PLOT ( 15.,Y,1,SX,SY)
111   CONTINUE
      YQ=1040.
158   CONTINUE
      CALL PLOT (0.,1040.,2,SX,SY)
      BACK=.(CR0S1+CR0SS*100.)
      FOR=BURK1+BURKE*100.+200.
      CALL PLOT (FOR,BACK,2,1.,1.)
      IF(IAM.EQ.1)GO TO 987
      GO TO 999
1700   JI=-1
      CALL PLOT (X,Y,JI,SX,SY)
1313     END
```